Université de Lille

THÈSE

Ecole Doctorale :
Sciences de la Matière, du Rayonnement et de l'Environnement

présentée par

Tanushree KANE

En vue de l'obtention du titre de

DOCTEUR EN CHIMIE
Spécialité: Molécules et Matière Condensée

Oxydation sélective et préférentielle du sulfure d'hydrogène par bouclage chimique

Selective and preferential oxidation of hydrogen sulfide by chemical looping

4 Décembre 2018

JURY

Cuong PHAM-HUU, Directeur de Recherche, CNRS, Université de Strasbourg   **Rapporteur**

Jose LOPEZ-NIETO, Professeur, CSIC, Université Polytechnique de Valence (E)   **Rapporteur**

Franck DUMEIGNIL, Professeur, UCCS, Université de Lille

Carole LAMONIER, Professeur, UCCS, Université de Lille

Axel LÖFBERG, Chargé de Recherches, CNRS   **Directeur de thèse**

Acknowledgement

RESUMÉ

Le gaz naturel et le biogaz contiennent du H_2S qui doit être éliminé avant toute utilisation. Cela se fait généralement par adsorption, par la récupération de H_2S et par conversion en soufre élémentaire dans des procédés de type Claus. L'oxydation sélective catalytique de H_2S par O_2 est une alternative, mais les catalyseurs subissent une désactivation en raison de l'accumulation d'espèces soufrées et le mélange H_2S/O_2 nuit à la sélectivité. De plus, cela ne peut pas être fait en présence de l'hydrocarbure pour des raisons de sécurité.

Un procédé innovant d'oxydation sélective de H_2S en bouclage chimique est proposé dans lequel la réaction se déroule en deux étapes : la réduction d'un solide porteur d'oxygène par H2S avec formation de S élémentaire et la régénération du porteur par O_2.

Il est démontré que V_2O_5 est une phase active prometteuse pour ce procédé. Parmi plusieurs supports testés, le TiO_2 et le SiO_2 s'avèrent les plus adéquats et il est montré que les matériaux de faible surface doivent être privilégiés. L'effet de la teneur en V_2O_5 sur le support de TiO_2 est étudié et il est montré que la distribution optimale de phase active est atteinte lorsque l'équivalent de 2 monocouches de V_2O_5 est présent. L'étude de la réactivité de ce porteur montre qu'un équilibre optimal entre V^{3+}, V^{4+} et V^{5+} est nécessaire. La présence d'espèces V^{4+} favorise la réactivité, mais seule la réduction d'espèces V^{5+} à V^{4+} est sélective, la réduction en V^{3+} entraînant la formation de SO_2.

Ce procédé est insensible à la présence de méthane, ouvrant la voie à la purification du biogaz ou du gaz naturel sans nécessiter de séparation préalable du H_2S.

RESUME

Natural gas and biogas resources contain H_2S, which needs to be removed prior to any use. This is usually done by adsorption followed by H_2S recovery and conversion through Claus type processes to produce elemental sulfur. Direct catalytic selective oxidation of the H_2S to elemental sulfur is an alternative but catalysts suffer from deactivation due to accumulation of sulfur species and H_2S/O_2 mixing usually affects selectivity. Furthermore, it cannot be done in the presence of the hydrocarbon due to safety issues.

To overcome these limitations, a Chemical Looping Selective Oxidation of H_2S (CLSOSH) process is proposed in which the reaction proceeds in two steps: a "reductant step" in which H_2S reduces the carrier and produces elemental S and an "oxidant step" in which the carrier is regenerated by O_2.

V_2O_5 was demonstrated that to be a promising active phase for CLSOSH. Several support materials were tested. TiO_2 and SiO_2 proved to be the most adequate and it was shown that low surface area materials should be privileged. The effect of V_2O_5 loading on TiO_2 support was investigated and it was shown that optimal distribution of V_2O_5 is reached when the equivalent of 2 monolayers of active phase are present. Detailed analysis of the reactivity of this carrier showed that an optimal balance between V^{3+}, V^{4+}, and V^{5+} need to be found. The presence of V^{4+} species promote reactivity but only V^{5+} to V^{4+} species reduction should be involved to reach optimal selectivity as reduction to V^{3+} lead to SO_2 formation.

CLSOSH proved to be insensitive to the presence of methane is the feed, opening the path for biogas or natural gas purification without the need of H_2S separation.

Table of Contents

Chapter I

Introduction and bibliography.

Chapter 1 – Introduction and bibliography

1.1 - H₂S and H₂S removal

About 10% of total global emissions of H_2S are due to human activity in particular from petroleum refineries, coke ovens, paper mills (using the sulfate method), and tanneries [1]–[4]. H_2S is one of the most dangerous and toxic gases emitted through the chemical process in different industries. It is harmful to human beings as well as to animals causing death at concentrations above 350 ppm.

The presence of sulfur is one of the main problems associated with fossil fuels, and it must be removed before the fuels can be used as energy sources or chemical feedstock. Sulfur is present in fuels in the form of hydrogen sulfide (H_2S) or it is chemically combined with hydrocarbons. Even after treatment, gasoline or diesel fuels still contain sulfur from a few parts per million (ppm) to several hundred ppm, generally, while natural gas contains up to 20 ppm sulfur. Depending on the type of the coal and the process, the sulfur content in coal-derived gaseous fuels may vary from several hundred ppm to more than 1 %.

Even though H_2S has a high heating value its use as a fuel is difficult as one of its combustion products is SO_2 which is harmful to the environment.

H_2S also constitutes the major problem for industrial processing. When fuels containing H_2S are used in subsequent industrial transformations, severe poisoning of any catalysts by depositing on the surface and killing the active site of the catalysts will occur.

Another disadvantage of H_2S is its reactivity with equipment and can lead into corrosion and/or sulfur deposition.

For all these reasons, it is crucial to remove H_2S from the original feedstock at the earliest stage of any process.

Chemical oxidants are often used in wastewater treatment plant to manage the toxicity and odor from hydrogen sulfide produced industrially. However, most commonly, H_2S has to be removed from the polluted stream before it can be transformed or valorized. Many commercial technologies based on wet and dry adsorption and oxidation have been used for H_2S removal from gases. These methods are used separately and some are used in combinations. Use of these methods depends on the requirement of the end gas products and the amount of gas that needs to be treated during the process.

A usual process used in H_2S removal is based on **absorption** [5], [6]. The decrease in concentration of hydrogen sulfide from percentage to ppm levels is easily attainable in these process streams. The different processes used under these categories include absorption in liquids such as alkanolamine, ammonia solution and alkaline salt solutions. Mostly in the

industries, adsorption techniques are used with different alkanolamines. Well known example is $HOCH_2CH_2NH_2$. The presence of hydroxyl group helps in the decrease in vapor pressure and increases the water solubility of alkylamine in solution. Amine present in the solution neutralizes the H_2S. This solution then passes through the absorber bed for further process. There are certain disadvantages of this process as it cannot be used for the purification of coal gas, which contains COS, CS_2, HCN, pyridine bases, thiophene, mercaptans, ammonia and traces of nitric oxide in addition to CO_2 and H_2S impurities. There is the possibility of side reactions of alkanolamine with these impurities. To overcome these problems, ammonia solution is used. H_2S can be eliminated from coal gas feedstock by absorption in aqueous ammonia at room temperature in absorption columns.

Another solution for H_2S removal is the use of weak acid anion such as carbonate or phosphate and alkaline salts solutions formed from sodium or potassium. The weak acid used as a buffer which helps in the maintaining the pH from changing too rapidly on the absorption of the gases. At room temperature, H_2S is absorbed into a solution of dilute sodium carbonate in an absorber column. H_2S is then regenerated by using the column in counter solution flow. Regenerated H_2S is then oxidized by using SO_2 and nearly 95 % of H_2S can be removed through this process. This simple economically operating process has disadvantages like oxidation of H_2S with SO_2 sometimes leads into the thiosulphate formation which gets stuck into the column and contaminates the basic salts used during the process and the disposal of the extracted sulfide as SO_2 is environmentally damaging.

Combination of sodium hydroxide (NaOH) and sodium hypochlorite (NaOCl) gives a practical approach for the H_2S removal problem. The principal reason for the use of this chemical is their oxidation capability, low cost, and availability. The reactions that occur during this process are as follows:

$$H_2S + 2NaOH \leftrightarrow Na_2S + 2H_2O \qquad\qquad Eq\ 1.1$$

$$Na_2S + 4NaOCl \leftrightarrow Na_2SO_4 + 4NaCl \qquad\qquad Eq\ 1.2$$
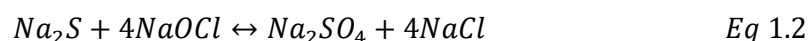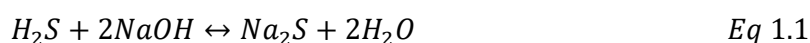
This is a continuous process and generates operating cost directly related to the amount of H_2S in the stream. This is the only economically reasonable process for gas streams with relatively low concentrations of H_2S. The disadvantage of this process is that as the reactions occur in the aqueous phase this gas phase must be transported to the liquid phase. The products of the above reactions stay dissolved in the solution until the solution is saturated. To avoid salt precipitation, the solution is periodically or continuously removed and refilled.

Different processes are also developed along with these main absorption processes. Koppers Company developed a vacuum distillation method which allowed the H_2S to be recovered rather than combusted by operating at low pressure and using steam as the stripping vapor. The further process, developed as Benfield process, in which hot potassium carbonate is used

and can remove 90 % of the H_2S from a feedstock with less evolution of the carbonyl sulfide, carbon disulfide, and mercaptans. This process is used now a day to remove CO_2, SO_2, and HCN. Various reactions are involved in the process including hydrolysis which amplifies the overall H_2S removal. This process has been modified further in recent years and it has been reported that it can reduce H_2S levels in the exit gas to < 1 ppm.

Other H_2S removal processes are based on **adsorption**. These have been extensively reviewed recently[7]. In these cases, solid substrates are used which have the capacity to physisorb (usually in high porosity materials) or chemisorb H_2S. Carbon bases supports, zeolites, metal-organic-framework or oxide materials are usually used for these purposes. The key factor for the selection of the most adequate material is the selectivity towards H_2S adsorption and its capacity in line with the volume of gas that needs to be purified. The regenerability of the solids is also a key factor which often limits the use of these technologies.

1.2 - H_2S Oxidation

When H_2S has been removed from the desired effluent, it needs to be recovered from the adsorbent or absorption solution, further transformed and, possibly, valorized. The Claus process is certainly the most ancient and proven method for transforming H_2S to elemental Sulfur nowadays.

1.2.1- Claus process

Claus process was invented in the second half of 19th century to recover elemental sulfur from gaseous hydrogen sulfide produced during fuel desulfurization. Indeed, many petroleum refining and chemical industries use this desulfurization process to convert the sulfur content of petroleum product to hydrogen sulfide. Claus process proceeds through two steps: first is thermal and second is catalytic [1].

In the first step, one third of the of the initial H_2S is burned in combustion chamber at 1000°C-1200°C.

$$H_2S + \frac{3}{2}O_2 \rightarrow SO_2 + H_2O \qquad \Delta° = -519 KJmol^{-1} \qquad Eq\ 1.3$$
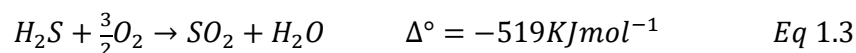
It is then followed by the catalytic reaction between SO_2 formed and the remaining H_2S.

$$SO_2 + 2H_2S \rightarrow H_2O + \frac{3}{n}S_n \qquad \Delta° = -146.5 KJmol^{-1} \qquad Eq\ 1.4$$
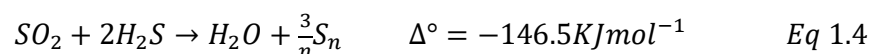
In the first step of Claus process a large number of reactions occur during the thermal combustion, yielding a large variety of products. This adds to wide variations in H_2S conversion. To acquire a suitable H_2S/SO_2 ratio, one of the most important points is the

temperature of the system. If it is low (< 925 °C), kinetic problems possibly can occur, but if it is too high (> 1600 °C), production of SOx and NOx increases and which ultimately results in corrosive or acid attack to the furnace. Formation of byproducts like COS and CS_2 in the furnace cannot be avoided because of the presence of CO_2 and hydrocarbons in the system.

In the second step, the optimal ratio for the H_2S and SO_2 react is around 2: 1 to form elemental Sulfur. Maximum yield can be achieved by using less exothermic catalytic process in the second step. After passing through the series of the reactors, the gas flows through a sulfur condenser, where liquid sulfur is condensed and collected. The residual unreacted H_2S and SO_2 is then transported to the next stage, where it is recycled in the presence of Claus catalyst. In practice, it signifies that the reactor temperature has to be maintained just above the sulfur dew point to prevent its condensation on the catalyst. However, conversion of COS and CS, by hydrolysis also occurs during this catalytic step, therefore to obtain the better conversion a temperature higher than 230 °C is essential which induces thermodynamic equilibrium limitations to the process. Several Claus units are thus necessary to achieve the highest conversion. The first converter inlet temperature is 230-250 °C to get a maximum conversion of COS and CS_2, the second one is 200-220 °C, and the third one is 190-210 °C for a maximum H_2S-SO_2 reaction. The outlet temperatures are higher, reaching 340 °C in the case of the first reactor. Lower temperature in this process leads to the deactivation of the catalysts by decomposition of sulfur.

Over time, without changing the main principle of the process, Claus process technology has evolved. The main aim of the Claus process is not only converting H_2S but also eliminating other sulfur compounds present in the refineries[8].
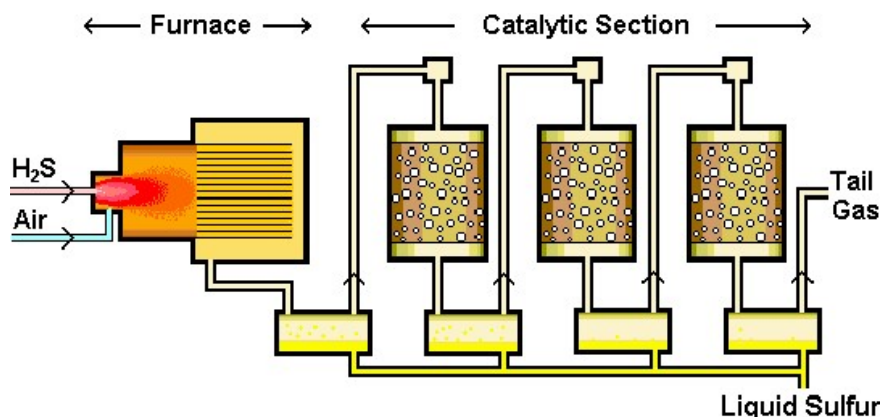
Figure 1.1: Claus process illustration [9]

As discussed before, other sulfur compounds are also formed like carbon disulfide (CS_2) and carbon oxysulfide (COS), 20 to 50 % of the pollutants in the tail-gas contribute to these compounds. Their presence in the system affects the catalysts. By hydrolyzing these gasses, H_2S gas can be regenerated which can then be selectively oxidized.

Effective catalysts are required in this process. They should be highly selective, with high surface areas and particles generating low and stable pressure drop as well as high resistance and stability in the presence of water. They should also not be too expensive as during the industrial process a large amount of catalyst is used. Catalysts that are used in this process are alumina, TiO_2, MgO, and CaO [2][8].

The recovery of sulfur in the Claus process is not complete due to the overall limitation of thermodynamic equilibrium (95-97 % of sulfur is recovered). The remaining hydrogen sulfide in the effluent must be removed by additional costly tail gas-treating (TGT) systems. The Claus process is therefore uneconomical for small plants and not suitable for the gas streams with low concentrations of H_2S.

As sulfur recovery is necessary for many small-scale plants, other processes are looked as alternatives for Claus process such as liquid redox and scavenging systems to recover the sulfur for their small-scale sour gas treating applications. But these effective systems have relatively high operating costs. Combination of Selective oxidation with tail gas treatment provides savings both for capital and operating costs over conventional treatments.

Hence, in order to meet the call of strict environmental regulations, large numbers of new methods have been developed to improve the sulfur recovery efficiency of Claus plants. Recently two dry catalytic processes were developed. Both Mobil direct oxidation process (MODOP) and Super Claus process apply one-step recovery of elemental sulfur from Claus tail gas. These processes were industrialized with the challenge to remove this remaining H_2S from the system. So the most efficient among all these processes was the dry catalytic oxidation of H_2S to elemental sulfur after hydrogenation of the sulfur-containing gas by H_2. The advantage of this selective oxidation is that it is not equilibrium limited. The two processes use, respectively, TiO_2-based or alumina-supported iron oxide/chromium oxide catalysts. Although, complete recovery of sulfur is possible, there is a certain adverse effect of these processes, such as the toxic properties of chromium oxide and the formation of SO_2 as byproducts by means of the following reactions steps. Removal process depends on a number of reactors used during the process.

$$2H_2S + \frac{1}{2}O_2 \rightarrow \frac{3}{n}S_n + H_2O \qquad\qquad Eq\ 1.5$$

$$H_2S + \frac{3}{2}O_2 \rightarrow SO_2 + H_2O \qquad\qquad Eq\ 1.6$$

$$\frac{1}{n}S_n + O_2 \rightarrow SO_2 \qquad\qquad Eq\ 1.7$$

$$\frac{3}{n}S_n + 2H_2O \rightarrow H_2S + SO_2 \qquad\qquad Eq\ 1.8$$
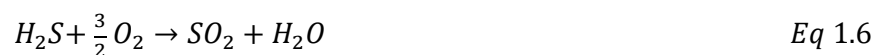
To summarize, it was evident that elemental sulfur yield depends on the catalyst performance, so selective catalysts are necessary to avoid the total oxidation of H_2S to SO_2/SO_3 and the side

reaction of the sulfur oxidation. Not only catalytic performances are responsible for the selectivity towards sulfur but also temperature and H_2S/O_2 ratio. In the literature, the preferable reaction temperature found is between 180°C and 250°C. Indeed, while working on the co-feed H_2S oxidation, temperature preferred is always above 180°C as sulfur is present in the gaseous state at this temperature.

1.3- Selective oxidation of H_2S

Selective oxidation reactions are amongst the most performed chemical reactions after polymerization in chemical industries. Oxidation reactions plays the vital role in the current chemical industrial process in the production of economically important intermediates such as alcohols, epoxides, aldehydes, ketones and organic acids, but also will contribute to the formation of new green and sustainable chemical processes. Gas-phase selective oxidation of alcohols using air or oxygen as the oxidant shows the industrially practical and environmentally benign protocol, which produces aldehydes and ketones in a solvent-free and in a continuous manner.

In the field of hydrocarbon selective oxidation, the main challenge is to limit over-oxidation to undesired product as these will always be favored by thermodynamics. These reactions also face technical difficulties as mixing of hydrocarbons and oxygen can generate explosive mixtures.

Selective oxidation of H_2S into elemental sulfur is one of the options to overcome the drawbacks of the Claus process and to achieve desired product in minimum economic losses. Overall selective oxidation performances depend on the many factors such as a reaction temperature, side reactions and byproducts, presence of other reactant and catalyst selection

$$2H_2S + \frac{1}{2}O_2 \rightarrow \frac{1}{n}S_n + H_2O \qquad\qquad Eq\ 1.9$$

Direct oxidation of H_2S to elemental sulfur is irreversible and does not have any equilibrium limitations. This is an exothermic reaction and can be carried out at low temperature (150-250 °C). Side reactions that occur during the process such as oxidation of the produced sulfur and complete oxidation of H_2S to SO_2 are responsible for the alteration of sulfur yield in a single step oxidation process. An increase of sulfur yield in such a selective oxidation process strongly depends upon the development of new active and selective catalysts. In the recent studies on the reaction on the laboratory scale many studies have been carried out in different reaction conditions [10]. Some of the main conclusions in this field are reminded hereafter.

1.3.1 - Catalysts for direct (co-feed) selective oxidation of H_2S

Catalysts plays an essential role in the selective oxidation of H_2S process. These catalysts should have high stability in presence of sulfur with high selectivity towards desired productswith sufficiently high surface area and the resistance towards water. By considering

these important properties many researchers studied the different catalysts for the process. It was observed that different rare earth metals like vanadium, magnesium, iron, cobalt, molybdenum, bismuth, and antimony on one side, and different supports like CeO_2, TiO_2, SiO_2, SiC, alumina, different clays, and HUSY were studied extensively to get the selectivity towards desired product [8], [11]–[15]. Metal oxides, oxide or carbon supports and different clays have been the most extensively studied.

In terms of activities for H_2S-selective oxidation by oxygen (H_2S/O_2 = 0.5) metal oxides active phases can be classified in the following order:

$$V_2O_5 > Mn_2O_3 > CoO > TiO_2 > Fe_2O_3 > Bi_2O_3 > Sb_6O_{13} > CuO > Al_2O_3 = MgO = Cr_2O_3.$$
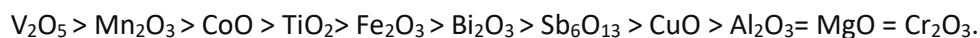
Among these, V_2O_5, MgO and Mn_2O_3 are considered the most selective catalysts. Iron and Vanadium based catalyst are widely used for this reaction and large volume of literature is available. Iron oxide is one of the oldest catalysts tested in selective oxidation of H_2S. It is also a cheap catalyst, it has relatively high activity for H_2S oxidation, but its sulfur selectivity is quite low because of requiring an excess amount of oxygen. But number of methods have been already established to modify iron oxide catalysts to obtain more selective and stable catalysts specifically by addition of other additives like antimony, tin, nickel-iron phosphates or supports such as β-SiC [16]. Terorde et al. [9] studied the selectivity of iron based systems on different supports like Al_2O_3, MgO, TiO_2, CeO_2, ZrO_2, and SiO_2. This study shows that inertness of the support towards the sulphate formation decides the best activity of the system. SiO_2 proved as a better support with iron as compared to other support.

Acidic properties of the support and its effect on the interaction with metal were studied [9], [17], [18]. Iron oxide impregnated on the alumina-intercalated Laponite clay proved as an active catalyst for selective oxidation with iron oxide mostly present in the form of isolated Fe^{3+} in an oxidic environment. Strong Lewis acid sites present on the catalyst helps in the adsorption of the H_2S on the catalyst surface which proved as a favorable step for the oxidation.

Vanadium catalysts also attracted the attention of the researcher due to its redox properties and ability to react at low temperature. Number of literature is available on the Vanadium based catalysts for this process. Studies on the different doped metal on the vanadium catalysts proved the effect of these metals on the vanadium species and hence on the activity and selectivity of the catalysts. Various Metals like Mo, La, Cu, Ce were studied in detail [10][19]–[22]. Presence of other metals like Ag, Na, Cu and Ca also have effect on the activity of the H_2S conversion to elemental sulfur. The catalytic behavior in the partial oxidation of H_2S of these catalysts strongly depends on the nature of crystalline phases. Incorporation of the V_2O_5 with the other metal enhances the activity [23].

In many other studies, selective binary oxide catalysts have been used for the reaction. Cu-V catalysts has been used to study the reaction which leads to the 98 % selectivity. This catalyst is then compared to Cu-V-Mo catalysts which proved to be better in terms of conversion but not in selectivity. Sulfate species form with this catalysts during the initial stage of the reaction. V^{5+} species present in the catalysts resulted in the formation of mostly SO_2. Partially reduced catalyst which contained V^{2+} and V^{+4} in the forms of Cu_3VS_4 and VO_2, showed high activity in selective oxidation. As stated above fully oxidized Vanadium species leads to over oxidation to SO_2 whereas partially reduced V^{2+} and V^{4+} species leads to selective oxidation to elemental sulfur[24].

In the literature, a study shows the effect of lanthanum in the vanadium catalysts. $LaVO_4$ catalysts were studied and then further promoted with Antimony. La-V-Sb catalysts worked better in a wide "temperature window" for obtaining 100 % sulfur yield. Basicity and the larger size of the La^{3+} ion in the system is responsible for the better activity. Apart from this, presence of Sb in the catalysts helps in the reduction of the vanadium oxidation state and which leads to the improved site isolation effect. This finally resulted in generating reduced species of the vanadium responsible for the better selectivity of the system [25].

Rare earth metals were used previously because of their abundance and because of their high ionic radii. A study [26] shows that bimetallic magnesium vanadium catalysts were more active and selective as compared to only vanadium oxide catalyst. Reduction of the vanadium species in V_2O_5 is much more difficult than the bimetallic rare earth vanadium species.

Jong Shik Chung et al. [27] studied the CrO_x and CrO_x supported on SiO_2 catalysts for the reaction. These Cr based catalysts proved to be active at low temperature. Amorphous Cr_2O_3 provides higher yield with stronger resistance against water than supported Cr/SiO_2. But at high temperature, above 300 °C, supported catalysts have same activity as amorphous Cr_2O_3 because the side reactions occurring on the silica support removes SO_2 which helps to increase the sulfur yield. Lattice oxygen in the chromia plays a vital role in the oxidation of H_2S, but Chromium based catalyst is better to avoid due to its toxic nature.

One of the important supports that is used widely for this reaction is alumina. Different supported and binary alumina catalysts are commonly used for the selective oxidation processes [28][29]. CuO /Al_2O_3 has been studied in detailed. Catalysts were tested at low temperature (110 °C) and during the reaction several sulfurated species, such as sulfate, sulfur, and especially sulfide species formed over the surface of the catalysts. Formation of polysulfide species over the reaction time is main product among others. Even during the regeneration of the catalysts in presence of 25 % of water at 330 °C, formation of SO_2 has never been detected. This confirmed that the formation of sulfide and even polysulfide species on the surface of the catalyst is a result of simple sulfur adsorption and the oxidation of S^{-II} to S^0. Different metal oxides still have the increasing scientific interest in the recent studies and more and more studies is happening on it for the process [30].

Recently carbon based catalysts proved to be efficient solutions for the selective oxidation [3] [14][31]–[33]. Cuong Pham-Huu et al. [14] studied the reaction over NiS_2 nanoparticles with multi-walled carbon nanotubes at ambient temperature. Carbon catalysts have some advantages over the other catalysts such as their inertness which help to avoid the sulfation problems. The high surface area of the support significantly reduces the problems of mass transfers and allows high catalytic performances compared to other conventional solid carriers. In addition to this, the complete absence of microporosity in the carbon nanotubes also makes them very attractive compared to the traditional activated charcoal support in which a large number of micropores greatly increases the diffusion phenomena. Along with these advantages, these catalysts show some disadvantages such as the formation of side product like COS and CS_2 which can poison the catalysts during the process.

Dae-Won Park et al. [17], considered structural support like aluminum pillared clay doped with vanadium. This study shows that the increase in the vanadium content on the support leads to the formation of crystalline vanadium. The activity shown by the vanadia-supported catalysts depended on the nature of the surface vanadia species as well as on the acid sites of the catalyst. The bridging V-O-support bond appears to be the most critical bond. When Vanadium species are highly dispersed on the support, more V-O-support species in strong interaction are formed. The higher the loading of vanadium is, the weaker is the interaction between vanadium species and support. In this case, aluminum pillared clay gives better surface area and helps in the better dispersion of vanadium. This helps in the improvement of the interaction of the vanadium with the aluminum pillar clays surface.

Horia Metiu et al. [34] explain the stability of the V_2O_5 supported over rutile TiO_2 in the presence of water. Density functional theory has been used to examine how the presence of bulk oxygen vacancies and of adsorbed oxygen on the surface affects the V_2O_5. The oxidation reaction carried out on the surface and the reaction mechanism is that proposed by Mars-van Krevelen. The reductant takes oxygen from the oxide surface and creates oxygen vacancies, and the gaseous oxygen in the gaseous feed heals them affects a V_2O_5 cluster [10][35].

To summarize this literature study, catalysts that are necessary for this process all show redox properties. V_2O_5 based catalysts have proved to be the best and most studied catalyst for the selective oxidation in co-feed processes. Supports have their effect on the metal dispersion and control over the particle size of the loaded metal but can also directly interact with H_2S. Choice of the support will therefore play an important role for the selectivity and activity of the process.

1.3.2 - Effect of temperature

The Temperature of the process has a strong impact on the selectivity. Mostly used temperature range for this reaction is in the 150 °C-350 °C range although some have been carried out at lower temperature.

Studies have been carried out to show the effect of temperature on the reaction and on the formation of byproducts [10] [22][36]. Various catalysts have been used for the processes. The multi-metallic oxides of TiO_2-supported vanadium oxide incorporating with Fe, Cr, and Mo have been reported to maintain the lower ignition temperatures of both reduction and oxidation compared to the catalysts containing only containing only VOx and TiO_2. This improved reoxidation property of mixed oxides helps in the selective oxidation of H_2S. With increase in the temperature of the system, selectivity towards SO_2 increases.

Low temperature study for the process has been studied on the ceria based catalysts at 150°C. Crystalline V_2O_5 is the most active phase thorough out the different reaction conditions, and vanadium and ceria have a synergistic effect [21]. Specifically, Marc J. Ledoux et al. [36], [37] studied the low temperature reaction on NiS_2/SiC catalysts with discontinuous mode i.e. separation of the reaction with reaction and regeneration cycles at 40 °C, but even though selectivity towards the sulfur is high, at low temperature accumulation of the solid sulfur on the catalysts is observed which results into its deactivation. Alessandro Trovarelli et al. [31] investigated the use of low-temperature catalytic oxidation for the removal of H_2S from tail gases from geothermal plants, in presence of water and its effect on the overall performance of the activated carbon catalyst at 60 °C. They suggested that the reaction takes place in the thin water layer formed inside the catalysts pore from the dissolved H_2S and chemisorbed O_2. With the temperature, selectivity towards the sulfur decreases whereas at such low temperature (60 °C) sulfur accumulation is observed on the catalysts with low conversion of the H_2S.

Generally, at high temperature, low selectivity towards the elemental sulfur with high conversion of H_2S is observed while the selectivity towards the SO_2 is favored.

1.3.3 - Effect of presence of other reactants like water and ammonia

Number of studies have been reported for the effect of presence of other reactants such as water or ammonia. In biogas and natural gases, inbuilt water is present which eventually affect the desulfurization process. Usually steel smelting is the process where a mixture of H_2S, NH_3, and water vapor is released. This water and ammonia can affect the process of removal of the H_2S from the overall system [2] both in terms of H_2S conversion than of formation of side products. Dae-Won Park et al. [38] proposed a study of vapor phase catalytic selective conversion of H_2S in a stream containing both ammonia and water on V_2O_5/ TiO_2 and Mo–V–O/TiO_2 catalysts. With H_2S:Water:Ammonia ratio fixed at 1:12:2 in volume percent, reaction was carried out at different temperatures but higher temperature gives more of SO_2 and less production of elemental sulfur observed in the H_2S oxidation without NH_3. In the presence of NH_3, the produced SO_2 can react to form $(NH_4)_2SO_3$

$$SO_2 + 2NH_3 + H_2O \rightarrow (NH_4)2SO_3 \hspace{3cm} \text{Eq 1.10}$$

$$(NH_4)2SO_3 + S \rightarrow (NH_4)2S_2O_3 \hspace{3cm} \text{Eq 1.11}$$
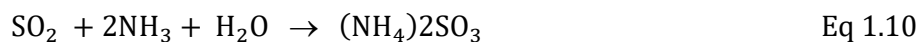
Insertion of Mo in the V-O/ TiO$_2$ proved to be better in terms of activity as compared to original system due to its increased redox property. While performing the study in presence of excess water (more than 35 vol. %) Jong Shik Chung et al. [22] explain commercial application of different vanadium catalysts in the selective oxidation of H$_2$S to elemental sulfur at low temperatures (less than 250 °C). During the reaction, they found that TiVO$_x$ was the only catalyst that could sustain its activity without deactivation at 230 °C with 85-90% selectivity towards the sulfur. Alessandro Trovarelli et al. [31] focus on the special effect of water on the overall performance of activated carbon catalyst for the direct selective oxidation of H$_2$S. It is shown that water strongly influences the reaction rate and the total amount of sulfur that can be adsorbed on the catalyst before the regeneration. As mentioned earlier, it is suggested that the reaction takes place in a thin water layer, inside the carbon pores, from the reaction of dissolved H$_2$S. Water present in the feed could then promote the deposition of sulfur on the edge of the active sites partly on the support, or mechanically remove the sulfur from the sites to the support.

1.3.4 - Effect of support

Different supports have been studied to understand their effect on the activity and selectivity of the system. Support plays an important role in the dispersion of active phase as well as on the adsorption and interaction of the reactant. Surface area, pore size and distribution along the catalysts influences the activity [2].

Many literature deals with the use of carbons as a catalyst or as an absorbent [1]. Although the reported results are partly contradictory as to the mechanism and the kinetics of H$_2$S oxidation, it appears that the porous structure and the pore size are predominant factors. Indeed, nearly all the porous solids used showed catalytic activity for H$_2$S oxidation, but their activity and selectivity depended not only on their porous structure but also on their chemical composition. Interaction of the metals with the supports can influence the activity of the process.

Piyasan Praserthdam et al. [10] explain that while performing the selective oxidation reaction of H$_2$S dispersion of the vanadium on different supports plays the important role. It has been reported that TiO$_2$-supported vanadium catalyst exhibited much better redox characteristics compared to those supported on SiO$_2$, resulting in more stable catalytic activity. Sena Yasyerli et al. [16] explain that CeO$_2$ is a good candidate for high temperature H$_2$S removal. It was also shown that a Ce-V mixed oxide catalyst containing equimolar amounts of cerium and vanadium (CeVO$_4$) gave very high sulfur yields in the selective oxidation of H$_2$S. Recent studies with cerium incorporated manganese adsorbents prepared for high temperature H$_2$S removal

indicated that the major role of cerium oxide in these adsorbents was to improve the regenerability of the adsorbent and to form elemental sulfur during the regeneration step. The H_2S oxidation reaction with molecular oxygen on sodium faujasites was investigated in a flow system within the temperature range 0-300 °C and at higher temperatures (70-300 °C). NaY is distinctly more active than NaX. Catalysts shows generation on the surface of radicals' species such as S_x, $HS_x^{\cdot-}$, $O_2^{\cdot-}$, $SO_2^{\cdot-}$, $SO_3^{\cdot-}$, and $H_2S_2^{\cdot-}$. These species take part in the reaction as intermediate compounds, and their concentrations strongly influence the reaction rate [39]. Furthermore, in a review study, G C Bond et al. [40] explains the effect of the support on the formation vanadium active species. This concept of the oxide monolayer was suggested by Russell and Stokes, when measuring the dehydrogenation activity of MoO_3/Al_2O_3 catalysts. This further explains that, in analogy to the use of metals in the form of small particles dispersed on a support, an oxide is most efficiently used when present as a layer applied as thinly as possible over the surface of a similar support. The oxide then exists as a monolayer or monomolecular dispersion and is maximally influenced by the support. This type of study further explains that the novelty of the concept of oxide monolayers stability on the surface of the support due to the formation of oxo species [41].

Detailed DFT study has been also done on samples with V_2O_5 over TiO_2 and reduced form of V_2O_5. This study concluded that the geometry of supporting surface is responsible for the dissociation energy of the vanadyl group and so the mobility of vanadyl oxygen in case of low-density (less than monolayer) vanadate particles on this surface [42].

Interaction of the active species with the support also determines the selectivity towards desired products.

In terms of the mechanism, most of the reactions have been discussed on the basis of an oxidation-reduction mechanism. Mainly these reaction based on three different mechanisms such as the Mars–van Krevelen (M–V K) mechanism or the lattice oxygen-based redox mechanism, phase cooperation and site isolation[43]. While discussing the oxygen based reactions, one needs to consider the main types of oxygen electrophilic and nucleophilic which are responsible for total and partial oxidation, respectively. Electrophilic oxygen consists of electron deficient adsorbed species such as superoxide O_2^-, oxides O^- and nucleophilic oxygen includes saturated species such as terminal oxygen groups M=O. This nucleophilic "O" oxygen species is capable of carrying out selective oxidation, for example, it was observed that catalytic activity and selectivity continued at the same level even after gas phase oxygen is cut off. But the existence of the equilibrium leads to over oxidation of the species [44].

1.3.5 – Insight on vanadium based carrier

As explained in the previous paragraphs vanadium-based catalysts have proved to be better for selective oxidation of H_2S.

These catalysts have been studied extensively in last three decades for several reactions due to the great redox capacity of vanadium. Supported vanadium oxide catalysts are very important in industrial processes. In many cases they are doped with promoters to improve their activity and/or selectivity, and supports are used to improve mechanical strength, thermal stability and lifetime [40].

One of the main issues regarding supported vanadium is the way the species are dispersed on the surface in particular when the content reaches monolayer formation [45], [46]. Different studies show that titania surface may be covered by one or more layers having precisely the lamellar structure of V_2O_5. However, many researchers proved that there are at least two forms of vanadium oxide, one of which covered the support surface as a layer of isolated or polymeric vanadate or vanadyl groups, quite unlike the surface of V_2O_5 [45]–[51]. Thus, Vanadium can be present in various forms on the support including monolayers to crystalline phase. Presence of these different phases depend on the interaction of vanadium with support as well as on the concentration of vanadium. Textural properties of the support also play an important role in the existence of different species. Oxide monolayers also appear to be quite thermally stable[40].

These allow to distinguish between surface vanadia overlayer species and crystalline V_2O_5 phases with respect to different monolayers formation on the supports.[10], [11] [52]–[56].
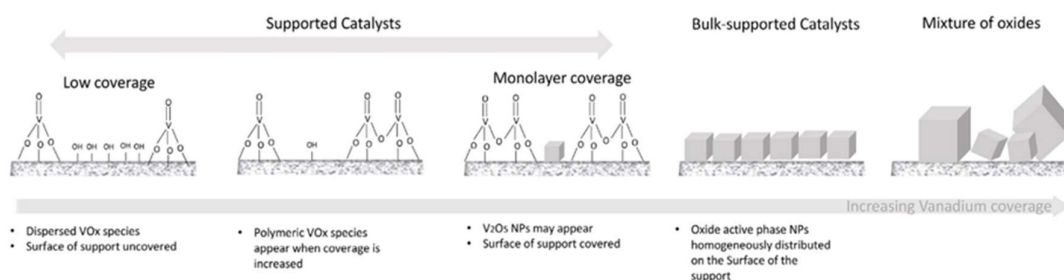
Figure 1.2 - Different approach for the dispersion, of V_2O_5 on the support [57]

Properties of surface vanadia species can be experimentally determined with several different characterization techniques both physico-chemically (Raman, IR, XPS, solid state [51]V NMR and UV-VIS DRS) and chemically (TPR, chemisorption and oxidation reactions).

1.3.6 - Redox property of vanadia based catalysts

While studying the redox properties of the vanadium based catalysts, Wachs et al. [48][58] studied different supported vanadium oxide catalysts which are active for many hydrocarbon oxidation reactions. Characterization studies have revealed that the deposited vanadium phase contains two-dimensional surface vanadium along with V_2O_5 crystallites above monolayer coverage. This monolayer coverage on vanadium was studied on the different support like Al_2O_3, TiO_2, ZrO_2, Nb_2O_5, SiO_2, and CeO_2. After calcination, V (5+) species are

observed showing the full oxidation state of Vanadium. While considering the reactivity of the Vanadium species according to the Mars-Van Krevelen redox mechanism, the oxidation of hydrocarbons proceeds by two steps:

(1) The reactant molecule initially reduces an oxidized surface site and

(2) The reduced surface site is subsequently reoxidized with gas phase molecular oxygen.

The reactivity properties of the supported vanadium catalysts were compared with the structural properties of the dehydrated surface V ($^{5+}$) species rather than the dehydrated reduced surface vanadia V ($^{4+}$) and V ($^{3+}$) species. Apart from this, the importance of the role of terminal V=O bond as well as that of bridging V-O-V bond in case of the hydrocarbon selective oxidation was shown. The surface concentration of bridging V-O-V bonds increases with surface vanadia coverage due to the increase in the ratio of polymerized to isolated surface vanadia species as illustrated in Figure 1.3.

The reduction of V_2O_5 proceeds through several stages

$$V_2O_5 \rightarrow V_6O_{13} \rightarrow VO_2 \rightarrow V_2O_3$$
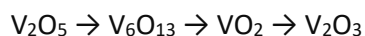
Colpaert et al. [59]also have reported the temperature dependence for the reduction of V_2O_5. It is believed that during the reaction over a V_2O_5 catalysts, lower oxides are formed which have an active part in the reaction mechanism. The enhanced mobility of the oxygen at these boundaries is thought to influences the oxidation-regeneration rate of the V_5O_5-catalyst.

For partial oxidation of H_2S, it has been suggested that high amount of vanadium present in the system generating V_2O_5 species proved as a better catalyst at the lower temperature [18]. V_2O_5 crystallites are partially reduced forming V_4O_9 which seems to be active and selective in this type of reactions [23] [60][56] [61].
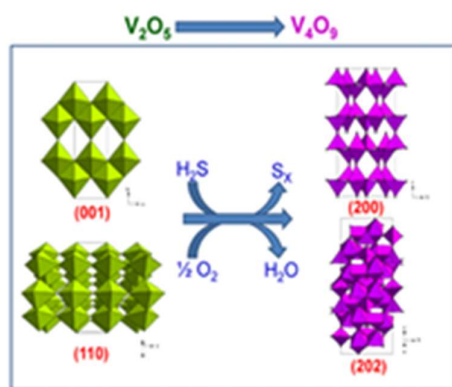
Figure 1.3: Redox property of the V_2O_5 [12]

Effect of the presence of different alkali metals (Li, Na, K) along with vanadium species on activity was also studied [12] [20] [26]. Doping vanadium oxide catalysts with alkali-metals can modify both structural and acid characteristics of catalysts, changing thus their catalytic properties. SO_2 production is observed during the first stage of the reaction but it decreases with time as after the reaction it shows more of reduced species of V_2O_5. V_4O_9 is the main crystalline phase observed in catalysts after reaction and is responsible for the selective oxidation. The presence of V^{5+}-O-V^{4+} pairs as a substitute of V^{5+}-O-V^{5+} pairs (as in V_2O_5) encourages higher selectivity to the partial oxidation product [62].

To conclude this review of catalytic systems for selective oxidation of H_2S, it can be seen that the temperature range where the researchers got the best results varies from 180 to 300 °C. It is also interesting to underline that 100% conversion and 100% selectivity can be achieved but with really low % of H_2S in the inlet (0.3%, 1% …). Focusing on the catalyst, it seems that iron, manganese, vanadium and sodium compounds are the most active. It is also reported in the literature some disadvantages using one or another catalyst [66]. The incorporation of alkali metal to pure V_2O_5, with an alkali metal/vanadium ratio of 0.04, especially the sodium-doped one, favors an increase in the catalytic activity for partial oxidation of H_2S, with high selectivity to sulfur (>98%)[12]. Titanium based catalyst shows deactivation in the presence of water vapor. Vanadium based catalyst has high activity and selectivity but the drawback is that it depends on the chemical state of vanadium. Iron based catalyst should be optimize because they required an excess amount of oxygen [67], so it is easier to reach a mix between partial and total oxidation and it gets deactivated due to the sulfidation and sulfur deposition. In presence of CH_4 and CO_2 catalysts does not shows better activity at low temperature [10]. Generally, if the catalyst show high conversion its selectivity decreases.

Use of high concentration of H_2S and O_2 is not suitable due to safety aspects considering the explosive limit of H_2S. As mentioned earlier presence of other reactants may influence the overall selective oxidation process. So, preferential oxidation of H_2S is not possible in presence of reactant like different alkanes in particular when excess oxygen is needed as this can induce severe safety issues.

Year	Ref.	Catalyst	Feed	X_{H2S} (%)	Selectivity to S (%)	Yield (%)	T(°C)
1993	[17]	Fe/SiO$_2$	1% H$_2$S/ 5% O$_2$/ 30% H$_2$O/ 64% He	97	97	94	247
2000	[26]	CeVO$_4$	1% H$_2$S/ 5% O$_2$/ 94% He	100	99	99	180
2003	[63]	V-Sb-O + Bi$_2$O$_3$ (1:3)	5% H$_2$S/ 2.5% O$_2$/ 5%NH$_3$/ 60% H$_2$O/ 27.5% He	90	100	90	260
2006	[18]	CeVO$_4$	1% H$_2$S/ 0.5% O$_2$/ 98.5% He	100	95	95	250
2011	[2]	V$_2$O$_5$-supported Fe-pillared clay	5 % H$_2$S/2.5 .% O$_2$/ 92.5 % He	100	95-97	95	280
2011	[64]	Mn/Activated Carbon	0.3% H$_2$S/ 0.3% O$_2$ (in air)/ 99.4% N$_2$	100	100	100	180
2012	[12]	Na / V$_2$O$_5$	1.2% H$_2$S/ 5% air/ 93.8% He	100	98	98	200
2012	[29]	6$_{wt}$% V$_2$O$_5$ / Al$_2$O$_3$-SiO$_2$-Fe$_2$O$_3$-MgO	5% H$_2$S/ 2.5% O$_2$/ 92.5% He	84	97	81	300
2012	[8]	Fe / SBA-15	1.2% H$_2$S/ 5% air/ 93.8% He	100	100	100	200
2013	[18]	7$_{wt}$% Fe / Al$_2$O$_3$	5% H$_2$S/ 2.5% O$_2$/ 92.5% N$_2$	100	100	100	180
2014	[21]	20V$_2$O$_5$/CeO$_2$	0.02% H$_2$S/ 0.01% O$_2$ and N$_2$	98	99	97	150
2015	[23]	Me-containing V$_2$O$_5$, (Me- Ag, Cu, Ca and Na)	H$_2$S/ air/ He with molar ratio 1.2/ 5.0/ 93.8	100	94	75	180
2016	[65]	CeO$_2$/TiO$_2$	5% H$_2$S/ 2.5% O$_2$/ 92.5% He	98	99.2	97	220
2018	[10]	3 wt % V$_2$O$_5$/ TiO$_2$	H$_2$S/ 0.015% O$_2$, 0.03% N$_2$/ 0.96 CO$_2$/ 0.97% CH$_4$	80	62	50	130

Table 1.1 Relevant work published in recent years for oxide based systems for selective oxidation of H$_2$S.

1.4 - Chemical Looping processes

In recent years, lot of studies have been done on chemical looping processes and their industrial applications. Main principle of chemical looping oxidation is that an oxygen carrier material is used as a reactant and not as a catalyst [68]. It consists of a two-step reaction where the reduction of the oxygen carrier takes place in the first step and in second step this reduced carrier get re-oxidized and simultaneously regenerated. Thus, the main difference in the principle between the co-feed and this process is the decoupling the main reaction in two steps so that the operation conditions can be optimized independently. In principle, chemical looping can be considered for all phases (gas, liquid or solid) or in heterogeneous systems. Main advantage of the chemical looping over co-feed system is the continuous regeneration of the solid during reaction and therefore there is no accumulation of by-products on the solid. This potentially allows to limit deactivation phenomena.

In the following review of literature, we will consider only solid oxygen carriers and gas phase reactants. In these cases, chemical looping generally involves the use of fluidized bed systems [69] or fixed bed switching reactors. Definitely, original reactor systems are necessary with respect to classical co-feed fixed (or fluidized) bed reactor. For the experimental studies in the laboratory scale the fixed bed reactor which is fed alternatively with the gas reactants is usually the most appropriate. Another possibility, which is better adapted for industrial applications, would be the use of a circulating bed reactor. The main principle would be transportation of the catalysts from one reactor to the other where each part of the two steps can performed separately.

It is important to note that such circulating bed reactors are commonly used in industry. One of the most recognized processes is the Fluid Catalytic Cracking (FCC) [70][71]. This process is used mainly in petroleum refineries. The primary aim of the process is to vaporize and crack low value heavy oil into different more valuable products (gasoline, diesel, olefins…) in the first reactor and regenerate the catalyst in the second one. The vaporized petrol gets in contact with a powdered catalyst in order to carry the reaction. The main issue in such conditions is the deactivation of the catalyst due to the amount of carbon deposition on the active sites from the cracking reactions. Therefore, the catalyst is circulated rapidly into a second vessel to be regenerated by air, in other words, burning the carbon by oxygen. In addition to this, working with fluidized beds helps to avoid hot spots in comparison with fixed beds, which have worse heat transfer.

Generally, chemical looping has been considered for hydrocarbon conversion. First, oxygen carrying material get reduced in presence of hydrocarbon. This reduced carrier then transfer to the air reactor which then oxidizes the metal and regenerates it. This regenerated catalyst is then reused for the combustion process in fuel reactor. Side reactions may occur during the reactions and deposits on the catalysts can occur but during the oxidation step these deposits

get oxidized so they do not accumulate contrary to co-feed catalytic processes. This is one of the important advantages of the system over conventional reaction system.

The chemical looping combustion (CLC) is one of the processes which uses such circulating oxygen carrier concept. A fuel is in contact with a solid oxide through which the required oxygen is provided to have the total combustion, ideally a mixture of CO_2 and H_2O. Steam is then condensed which allows getting pure CO_2. This pure CO_2 can then be trapped for further valorization or sequestration. After the combustion, the catalyst is transferred to a second vessel to be re-oxidized by air in order to recover the oxygen capacity. A general reaction is given as follows:

$$C_nH_2m + (2n + m)M_yO_x \rightarrow (2n + m)MyO_{x-1} + mH_2O + nCO_2 \quad \Delta°H > 0 \quad Eq\ 1.12$$

$$M_yO_{x-1} + \tfrac{1}{2}\,O_2\ (air) \rightarrow MyOx \quad \Delta° < 0 \quad\quad\quad\quad\quad Eq1.13$$
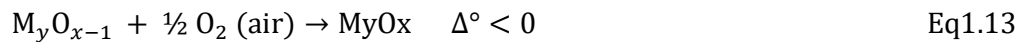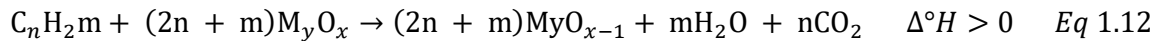
M_yO_x = oxidized oxygen carrier

M_yO_{x-1} = reduced oxygen carrier

CLC is essentially developed with the aim of reducing CO_2 emissions in fuel combustion processes.

Other breakthrough in the field of chemical looping is dry reforming of methane (DRM) to produce syngas. Chemical looping DRM has been investigated successfully at laboratory scale by using periodic feed reactor and Ni/CeO_2 based materials as oxygen carriers [72]. DRM is a highly endothermic reaction that needs to be carried out at high temperature i.e. above 600 °C.

$$CH_4 + CO_2 \rightarrow 2CO + 2H_2 \quad\quad\quad\quad\quad\quad Eq\ 1.14$$

Again, the reaction is divided into two steps. The first step consists of the reacting methane with an oxygen vector material that would get reduced and produce selectively syngas. In a second step, this reduced solid would be re-oxidized by CO_2 to regenerate oxygen vector.

$$Step\ 1 - CH_4 + Sol - O \rightarrow Sol - R + CO + 2H_2 \quad\quad Eq\ 1.15$$

$$Step\ 2 - Sol - R + CO_2 \rightarrow Sol - O + CO \quad\quad\quad Eq\ 1.16$$
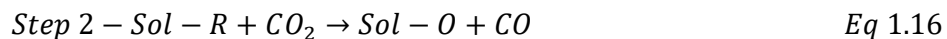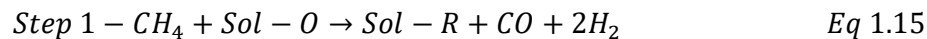
The main advantage of this process is that -if the stream from the first step is isolated -a syngas with H_2/CO ratio of 2 can be achieved which is ideal for the industrial purpose. Another advantage is that it avoids the Reverse Water Gas Shift (RWGS) reaction as there is no direct

contact between CO_2 and H_2. Finally, as the solid is periodically regenerated, deposited carbon can be removed and does not accumulate, catalysts deactivation is thus prevented.

Chemical looping has been considered for other reforming processes for syngas formation. For example, in auto thermal reforming (ATR) methane is co-feed with the steam to get the supplemental oxygen to overall perform the steam reforming of methane. Along with this, partial oxidation of methane can be done by using chemical looping process as a degree of fuel oxidation is controlled by carrier residence times or by using appropriate solid oxygen vectors which results in the formation of CO and H_2.

Another application of the chemical looping method is for selective oxidation. A famous industrial process is oxidative dehydrogenation of n-butane. R. M. Contractor et al. studied this reaction on the $(VO)_2P_2O_7$ catalysts. The vanadium phosphate was circulated between two reactors. n-butane was oxidized in one bed whereas in the other, the vanadate was re-oxidized [73]. E. Bordes et al. [74] explains the butane dehydrogenation reaction by using, a fluidized bed or a recirculating solids riser reactor (RSR) which allows to have a continuous regeneration of the catalysts. Advantage of the RSR is it can separate reduced catalysts from the product stream and treated back to in the regeneration zone for reoxidation. The catalyst is thus recirculated between the two zones and remains in a transient cyclic state. Absence of oxygen during one step helps in the selectivity [71], [75]–[77]. In this procedure, the main redox process occurs in between the V^{5+} and V^{4+} oxidation states of vanadium. Stoichiometry of the chemical system is as follows,

$$C_4H_{10} + V^{5+} \rightarrow MA + V^{5+} + 2H_2O \qquad\qquad Eq\ 1.17$$

$$O_2 + V^{4+} \rightarrow V^{5+} \qquad\qquad Eq\ 1.18$$

Minimizing as much as possible the oxidation of maleic anhydride into CO_x and H_2O

$$MA + V^{5+} \rightarrow 4CO_x + V^{4+} + H_2O \qquad\qquad Eq\ 1.19$$

This system is applicable for higher concentration of the reactant as compared to the co-feed conventional reaction system.

J. Santamaria et al. [78] worked on n-butane oxidative dehydrogenation with fluidized bed reactor with MoO_3/MgO catalysts and used two-zone fluid bed reactor (TZFBR) for the reaction which also use the concept of sequential operation at catalyst level. Such two-zone fluid bed reactor is different from the circulating fluid bed reactor (CFBR) as only one vessel is employed, and oxygen is introduced as a part of the fluidizing gas, whereas the hydrocarbon flow is introduced at an intermediate point of the catalyst bed. This allows the hydrocarbon oxidation to take place with lattice oxygen in the reducing zone of the bed. The oxygen-depleted (reduced) catalyst is then regenerated (reoxidized), after being transported by

internal circulation to the oxidizing zone at the bottom part of the reactor, where oxygen is fed.

Chemical looping concept can therefore open the field for several industrial processes optimization. **The key to such development is in the oxygen carrier**. Such oxygen carriers need to fulfill specific requirements. They should have:

- high reactivity in both the oxidation and the reduction reaction;
- show good selectivity for the desired (total or partial) oxidation;
- good stability over many of redox cycles;
- good resistance towards coking or contaminants deposition and removal;
- good mechanical resistance in circulating bed systems.

So, efforts are mostly committed to select proper oxygen vector solids for the targeted process.

1.5 - Scope of the thesis

Biogas, and in particular biomethane, is an important source of renewable carbon which is the object of increasing interest in the frame of climate issues and future limitation of the availability of fossil carbon sources.

This biogas generally contains significant amounts of H_2S (a few hundred ppm to a few %, depending on the source of the biogas). The presence of H_2S constitutes a major handicap for the recovery of biogas. In the case of thermal combustion of methane, the biogas must be purified to maximum H_2S levels of ppm in order to avoid SO_x emissions during combustion. When methane is recovered for the production of synthetic fuel or high value-added chemicals (e.g. through reforming to synthesis gas), these transformations necessarily involve catalysts whose performances may be affected by the presence of H_2S. While the development of new generations of catalysts resistant to sulfur poisoning is underway, this does not solve the problem of the presence of sulfur compounds in the end use products.

It seems sensible to develop a method of purification of the biogas prior to any intervention of valorization. Indeed, considering the low reactivity of methane, it is preferable to react preferentially H_2S in an H_2S/CH_4 mixture because any product of methane upgrading would have a greater reactivity and thus make it more difficult to treat preferably H_2S. Currently, the applied methods involve the adsorption of H_2S or the separation and transformation of H_2S into S by the Claus process as already explained. This is a well-established process but it suffers several drawbacks essentially due to thermodynamic limitation which imply multiple operations to reach full conversion of H_2S to S.

Direct selective oxidation of H_2S to S is an interesting solution to remove H_2S from gaseous effluents. This reaction can be carried out at a relatively low temperature (100-250 °C) in the presence of a catalyst and O_2. The gas phase S may be condensed at the reactor outlet and

then independently recovered. The main difficulty is to obtain a satisfactory selectivity at a very high conversion. Furthermore, the possibility of mixing reactants (H_2S and O_2) is limited for safety reasons and this can be a further limitation if the presence of other reactive species is considered (e.g. methane).

1.5.1 - Proposal

Our proposal is to perform selective oxidation of H_2S using an oxygen carrier oxide and a chemical loop system. The principle, as generally described above, is to split the process into two stages. During the first, an oxide is brought into contact with the gas containing the H_2S, the oxide is reduced, H_2S is oxidized to S + H_2O, S is transported in the gas phase (T>100-150 °C) and condensed at the reactor outlet. In the second step, the solid is re-oxidized by O_2 (air) so that regeneration of the catalysts takes place and solid regains its oxygen carrying capacity.

$$H_2S + MeO_x \rightarrow MeO_{x-1} + S^{gas} + H_2O \qquad\qquad Eq\ 1.20$$

$$MeO_x + \frac{1}{2}O_2 \rightarrow MeO_x \qquad\qquad Eq\ 1.21$$
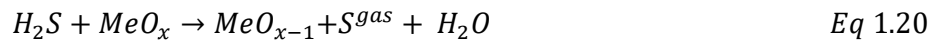
This type of reaction can be carried out in a periodic feed reactor (PFR) or in two separate reactors using a circulating bed (CBR) reactor.

The CBR configuration is the simplest to schematize in order to represent the operation of the process (Figure 1.4).
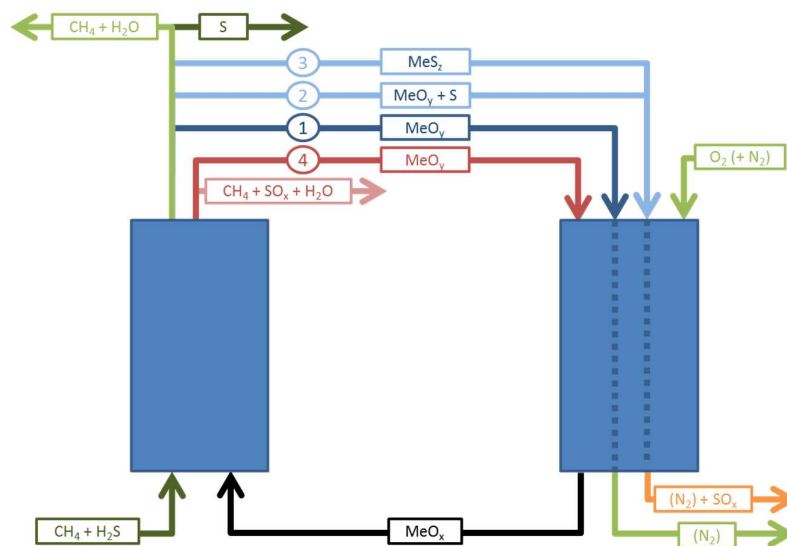
Figure 1.4 – Illustration of Chemical looping selective oxidation of H_2S for biogas valorization

The process described above is represented by route 1 where the circulating oxide exclusively acts as an oxygen carrier between the two half-reactions. Two other cases may be considered in the event that some or all of the sulfur is transported from one reactor to another, either by the presence of adsorbed S on the surface of the solid (route 2), or by the total or partial transformation of the oxide into sulfide (route 3):

$$H_2S + MeO_x \rightarrow MeO_{x-1} + S^{ads} + H_2O \qquad\qquad Eq\ 1.22$$

$$H_2S + MeO_x \rightarrow MeS_z + H_2O \qquad\qquad Eq\ 1.23$$
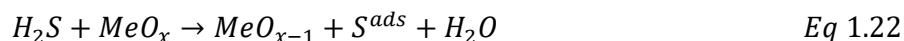
In both cases (routes 2 and 3), re-oxidation also involves the oxidation of the sulfur compound (S or sulfide) to SO_2 and/or SO_3. This hypothesis could constitute a disadvantage but could also be exploited for the direct manufacture of sulfuric acid. The absence of water vapor in this reaction step should limit the formation of this acid in the re-oxidation reactor.

The periodic re-oxidation of sulfur species on the surface of the carrier can also help to overcome the deactivation of the catalyst which is generally observed when co-feed H_2S oxidation is studied.

A last possibility is considered, namely the non-selective oxidation of H_2S in SOx directly by the solid in the first reactor. In addition to SO_x, this reaction would lead to the simultaneous formation of water (and thus probably H_2SO_4), which is difficult to separate from the effluents. It could also lead to the deactivation of the solid and the corrosion of the installations. This route should therefore be avoided as much as possible.

The first point to be optimized is therefore the selectivity of the reduction reaction of the solid by H_2S towards the <u>selective oxidation</u> of this S-molecule or, optionally, sulfide. Chemical loop operation should considerably improve this by the absence of gaseous phase oxidant. The second point to be optimized will then be to carry out this reaction under conditions allowing the <u>preferential oxidation</u> of H_2S and not the other components of the gas to be treated.

We propose to study vanadium oxide based materials as oxygen carriers for this novel chemical looping selective oxidation of H_2S (CLSOHS).

After a description of the experimental methodology (Chapter 2), reactivity of bulk vanadium oxide will be presented for this Chemical looping selective oxidation of H_2S (Chapter 3).

Then, a comparative study of supported materials will be presented (Chapter 4). A detailed analysis of a specific TiO_2 supported V_2O_5 carrier will then be proposed (Chapter 5).

Finally, the influence of several process parameter will be analyzed, included the presence of methane in the reactive feed (Chapter 6).

Chapter II

Experimental methodology

Chapter 2 – Experimental methodology

In the following chapter, the working system, experimental procedure, and calculation for the reactant conversion to the product with the raw data from mass spectrometer analyzer are explained.

2.1 - Chemical looping reactor setup

The main reaction carried out in this system is partial oxidation of H_2S gas to the solid sulfur. The originality of this work consists in doing this reaction in the periodic way, the so-called "chemical looping". There are certain specificities for this reaction which needs to mention for the better understanding of the subject as well as for the procedure and technical details.

Schematic diagram of the system is given below. It consists of four main sections. The red and blue sections allow the preparation of the reductant (H_2S) and oxidant (O_2) flows. The green section allows the preparation of three Ar flows: (i) central Argon flow is fed continuously, whereas (ii) two lateral Ar serve for replacing the reactant (reductant or oxidant) gases when these are not flowing to the reactor section (in black). The following section consists of the reactor itself and subsequent condensers and is kept at a constant flow rate thank to the permutation of H_2S or O_2 with equivalent Ar flows.
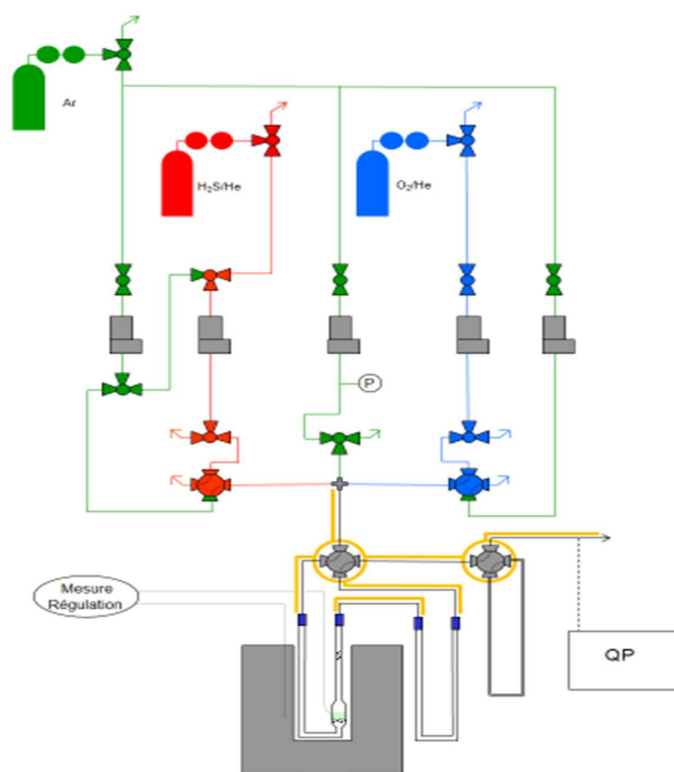
2.2 - Reactor

All the reactions are carried out in "U" shaped reactors. The "carrier", eventually diluted in Sic, is placed on a fritted disc. Temperature is regulated by oven between 150 -250 °C and monitored using thermocouples placed in contact with the external walls of the glass/quartz reactors and another into the oven.

Figure 2.2: Picture of the experimental setup

2.3 - Sulfur condensation

Sulfur is the main product desired during this reaction. It is present in the gaseous form above 150 °C so temperature of the tubing from the outlet of the reactor to the mass spectrometer is maintained above 150 °C by using heating tape to avoid accumulation of S. This accumulated sulfur usually creates problems in the partial pressure of system and affects the signal on the mass spectrometer.

In between reactor and the mass spectrometer, a two-fold condensing device is used to trap the solid sulfur formed during the reaction and avoiding it to accumulate into the analyzer. First, at the outlet of the reactor a U'' shaped glass tube is connected before the 4 way-valve and maintained at room temperature (no heating). This condenser is directly connected to the reactor and is easy to remove and cleaned after a few experiments as sulfur gets accumulated in it. This sulfur can be cleaned out by using hot toluene (above 80 °C) or by heating it above 180 °C. Second, after the reactor valve, a second spiral metal condenser is present. This one

is maintained at room temperature or less using water bath. Such double condenser system allows rapid removal of most of the S produced in the first condenser while ensuring that no S reaches the mass spectrometer. The condensers sizes and shapes have been chosen in order to minimize the deformation of the periodic feed response due to back mixing in the tubing.

2.4 - Exhaust gas purification

All gasses pass through the glass bottles filled with solid palates of NaOH for purification before being sent to the vent.

$$H_2S + NaOH \rightarrow NaSH + H_2O \qquad\qquad Eq\ 2.1$$

$$NaSH + NaOH \rightarrow Na_2S + H_2O \qquad\qquad Eq\ 2.2$$

Hydrogen sulfide reacts with sodium hydroxide to produce sodium sulfide and water. Thus, NaOH allows remaining H_2S to react with it and avoids its direct release of the poisonous gas into the environment. This reacted Na_2S and NaSH can then be discarded periodically and carefully.

2.4.1 - Safety

Various precautions to be carried out while dealing with the H_2S gas because of its poisonous nature. H_2S gas detector is always kept handy while performing the experiment. MFC's and the tubing for H_2S and H_2S/Argon should always be purged by using pure argon after every experiment, to avoid the corrosion of the tube. Due to the risk in the accumulation of the sulfur in the lines, a pressure gauge is connected to the central argon line.

2.5 - Gas flow control

The Flow of the gasses is controlled through a mass flow controllers (Brooks SLA5850). Calibration of the gas flows can be performed before each experiment to have precise flows and concentrations of specific gases. These are done manually by using bubble flow meter.

2.5.1 - Periodic feed operation

Four-way valves are used to have better flow without blindside connections which may generate diffusion responses. The principle consists of having three gas flows: a central gas flow continuously fed with argon, and two side flows which contain argon/reductant or argon/oxidant flows. On each side, the argon flow corresponds to that of the reductant or oxidant, respectively. By this way, the total flow rate at reactor inlet remains constant during periodic operation.

Two other four-way valves are used in order to isolate the reactor or the second condenser, respectively. In such way, when isolated (or in by-pass mode) the flow is never interrupted except for the short time needed for valve rotation.

These four-way valves are operated with high-pressured air actuators which can be controlled manually or connected to the computer through the software realized at the lab. Through this software, this four-way valves system gets automatized allowing more precise results than by switching valves manually. This system is able to perform reproducible experiments and saves time as long tests can imply several hundreds of valve movements (e.g. 5 hours test needs more than 200 movements of the valves).

This automatized system is also better in terms of the safety required during the experiments as H_2S and O_2 can be explosive gasses if mixed together at the temperature above 150 °C. Indeed, security features have been introduced to avoid accidental gas mixing.
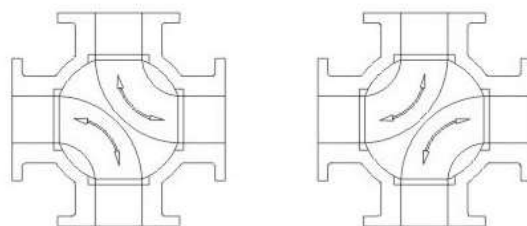
Figure 2.3 - Schematic representation of gas switching in four- way valves

Gases used during the experiments are fed in the periodic way.
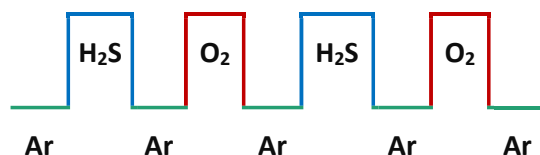
Figure 2.4 - Schematic diagram alternate flows of the reactant during periodic system.

During a typical periodic feed cycle, reduction gas (H_2S) passes through the reactor for 1 minute. To remove this gas from the reactor, inert gas (argon) is passes through the system for 2 minutes. Then, oxygen flows through the system for 1 min to oxidize the solid. To remove unreacted or excess oxygen from the system, again the flow of argon passes through the reactor for 2 minutes. This overall time required is 6 min. and the process is repeated sequentially. This is represented by the following notation 1-2-1-2.

In some case studies, this cycling the pattern changes to 0.5-2-0.5-2 where flow of the H_2S and oxygen is restricted to 0.5 min and argon keeps at 2 min. and second cycle pattern is 3-2-3-2, where H_2S and oxygen flows for 3 mins and argon flow for the 2 min. This type of study carried out to understand the different effect of exposure of the reactant to the catalysts.

During each experiment, the periodic cycles is performed with the reactor 4-way valve in by-pass position in order to calibrate the mass spectrometer response. This is done at the beginning and end of each experiment, systematically.

Different inert gases are used and have different roles in the reaction system as well as in the calculating the data.

Argon

Argon gas is used for different reasons.

First, it is used as the diluents and allows to explore a certain range of reactants concentrations and to maintain the overall flow of the gasses. To maintain constant flow during periodic operation, the reactant gases are always replaced by the same flow of Argon in the periodic feed system.

As Ar is always the major component of the gas flow, it allows keeping the same viscosity of the gas throughout the process as the change in the flow of the gases can affect the sensitivity of the mass spectrometer. Argon gas is also used during degassing between each step of the periodic reaction to avoid direct contact between reductant and oxidant. This time of neutral cycle in whole process i.e. the time of argon flow through reactor also affect the adsorption and desorption process of the catalyst. Finally, the Argon partial pressure at the outlet of the reactor is affected by the variation of total flow rate due to the reactions occurring in the reactor as the system is always at atmospheric pressure. Monitoring continuously the Ar pressure allows calculating precisely the real outlet flow rate at any moment.

Helium

Helium is used as a diluted gas in the H_2S and O_2 cylinder. This helium constitutes a reference as the ratio between He and reactant gas is constant. Thus, the He signal allows the calculation of the theoretical reactant gas inlet signal to which the experimental signal is compared to determine conversion.

2.6 - Reaction conditions

Reaction conditions used during the experiments are varied according to the requirement of the experiment and depending on the study to be carried out. The concentration of the H_2S is varied from the 1000 ppm to 4000 ppm. Different H_2S: O_2 ratios are used. Extensively, for most of the study ratio maintained at 1:5, i.e. O2 is varied from 5000 ppm to 20000 ppm. In specific

study, various ratio used such as 1: 2.5, 1: 0.5 as well. Helium gas is mixed in the reactant as a diluent, its overall concentration varies according to the change in the concentration of the reactant.

The temperature range explored is between 150 and 350 °C. Typically between 50 to 900 mg of solid is employed, eventually diluted in inert material like SiC.

Between experiments, temperature treatments of the solids are performed by exposing the solid to diluted O_2 (1%) and heating the sample to 400 °C to fully re-oxidize the carrier and remove Adsorbed sulfur species.

2.6.1 - Partial pressure analysis (online mass spectrometer)

Part of the gas stream (approx. 5 ml/min) is continuously pumped towards the mass spectrometer (Omnistar, Pfeiffer) through a two-stage pressure reduction system. This allows to obtain a linear response of to mass spectrometer signals with respect to partial pressures in the reaction setup.

In the mass analyzer, the gas is ionized through electron bombardment. A voltage is applied between anode and cathode, which accelerates the electrons generated by the filament. Then, the ions are separated by the m/z ratio by a quadrupole mass filter which consists of four parallel rods arranged in the square position. Every pair of opposite rods designated (+) or (-) is connected with the other. The functional quadrupole field deflects the ions in the X and Y directions, resulting in helical trajectories through the filter. The required mass range and desired resolution are governed by the dimensions of the filter and the selection of the operating frequency. This ion later goes through a detector (secondary electron multiplier) to increase the collected signal. Finally, a Faraday collector detector can also be used but with much less sensitivity.

The most significant m/z is used for each component but interference between different gasses have also to be taken into account as shown in Table 2.1.

The sensitivity of the online mass-spectrometer is determined relatively to Argon. He, H_2S and O_2 sensitivity are calculated during each experiment using the by-pass periodic feed sequence at the beginning and end of each test. Mass spectrometer background signals are also determined during this sequence.

Other gases are calibrated regularly using calibrated composition gas cylinders (SO_2, CO_2 …). Arbitrary sensitivity factors are used for SO_3, H_2SO_4 and S (S_8).

m/z	H2	He	H_2O	O_2	Ar	H_2S	SO_2	SO3	H_2SO_4	S_8	m/z
1	2										1
2	100										2
3											3
4		100									4
16			1	22			5				16
17			21								17
18			100								18
19			1								19
20			0.3		15						20
26									0.2		26
27									1		27
28											28
29									1		29
30											30
31									0.1		31
32				100		44	10				32
33						42	0.1		0.2		33
34						100	0.4		0.5		34
35						3					35
36					0.3	4			0.2		36
37											37
38					0.1				0.1		38
39									0.1		39
40					100				0.1		40
41									1		41
42									0.1		42
43									0.5		43
44									1		44
45									1		45
46									0.1		46
47									0.2		47
48							49		51		48
49							0.4		1		49
50							2		2		50
51									0.1		51
64							100		50	100	64
80								100	100		80
81									72		81
82									6		82
83									4		83
84									0.2		84
96										21	96
98									50		98
128										55	128
m/z	H2	He	H_2O	O_2	Ar	H_2S	SO_2	SO3	H_2SO_4	S_8	m/z

Table 2.1 Ion fraction distribution for main components

2.6.2 - Calculations
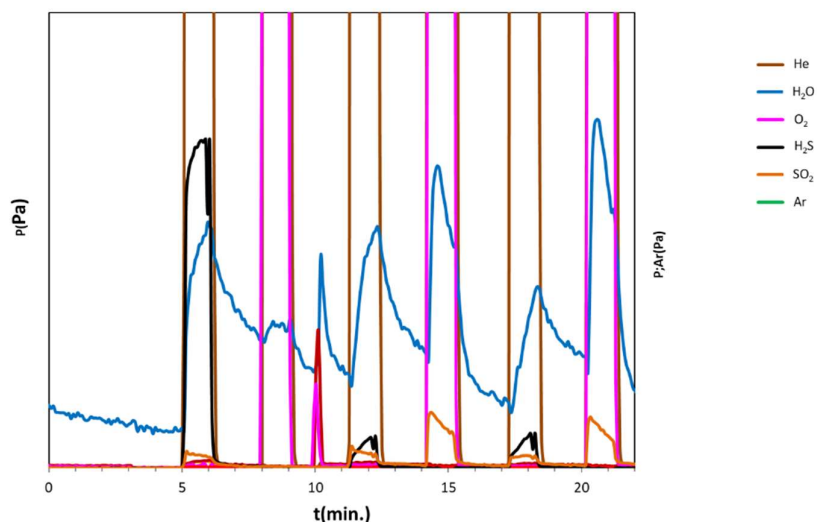
Figure 2.5 - schematic diagram reaction representation during the experiments.

After performing the reaction on the catalysts, different MS Signal obtained and after integrating each cycle.

During first and the last cycle of the reaction the reactor is closed to get the reference bypass value for the calibration of the analyzer. Figure 2.5 illustrates the partial pressures evolution on a typical experiment during the first cycles.

The so-called "Reductant step" is consists in the exposure of the carrier to H_2S (Black line). In this step H_2S diluted with Helium is passed through the reactor. The "Oxidant step" is the exposure of the oxygen (Pink) diluted with helium (brown). As explained, the first and last cycles are performed with the reactor in by-pass position. These cycles allow background definition and gas sensitivity determination for Ar, He, H_2S and O_2. In case of evolution of these parameters between the beginning and end of experiment, a linear interpolation is used to optimize quality of response.

From these gas composition evolutions with time, important information can be obtained on the reactivity of the system. At this stage of the study, **quantitative information is obtained by integrating the reactant or product during a full cycle**. Thus, the following quantitative results represent an average on a full cycle. This should be kept in mind when interpreting the results.

Further analysis of the dynamics of the gas evolution within a single step can also be considered but, at this stage of the study, is not proposed.

The main quantitative data that are retrieved are the following:

H_2S conversion X_{H2S} (%) is obtained by integrating the outlet H_2S flow and comparing this to the theoretical H_2S inlet calculated from the He tracer.

$$XH_2S(\%) = \frac{(H_2S(inlet) - H_2S(outlet))}{H_2S(inlet)} * 100$$

O_2 conversion X_{O2} (%) is obtained by integrating the outlet O_2 flow and comparing this to the theoretical O_2 inlet calculated from the He tracer.

$$XO_2(\%) = \frac{(O_2(inlet) - O_2(outlet))}{O_2(inlet)} * 100$$

$S_{SO2}R$ (%) represents SO_2 selectivity **in reductant phase** (amount of SO_2 formed in presence of H_2S and following inert gas divided by amount of converted H_2S).

$$S_{SO2}R(\%) = \frac{SO_{2(R)}}{XH_2S(\%)} * 100$$

$S_{SO2}O$ (%) represents SO_2 selectivity in oxidant phase (amount of SO_2 formed in presence of O_2 and following inert gas divided by amount of converted H_2S).

$$S_{SO2}O(\%) = \frac{SO_{2(O)}}{XH_2S(\%)} * 100$$

$S_{SO2}T$ (%) represents total SO_2 selectivity

$$S_{SO2}T = S_{SO}\ R + S_{SO}\ O$$

Selectivity to S is considered as the complement to

$$S = 100 - S_{SO2}T$$

It should be noted that S formation cannot be monitored. Thus, selectivity towards S is always an indirect information.

The amount of lattice oxygen involved in the reductant step can be calculated considering the amount of S and SO_2 produced during the reductant step and taking into account the theoretical amount of corresponding H_2O which should be produced.

By looking in more detail the evolution of partial pressures, some important phenomena can be identified. Again, Figure 2.5 is a non-optimized example given in order to describe the operation:

- As explained, H_2S conversion is obtained by comparing the integrated amount of H_2S flowing out in comparison to the by-pass response. In this illustration H_2S conversion is clearly not total.
- Presence of SO_2 in reductant phase (H_2S exposure) is indicative of unselective oxidation by the solid.
- SO_2 can be produced also during the inert step which follows the exposure to H_2S. This is indicative of oxidation of adsorbed species by the oxygen from the solid.
- SO_2 is formed during exposure to O_2, meaning that O_2 contributes to the re-oxidation of the solid **AND** of that of surface "S" species.
- The presence of water produced simultaneously during oxidant step suggests that adsorbed "S" species must be hydrogenated, so probably H_2S and not elemental S.

2.7 - Characterization methods.

Oxygen carriers have been characterized by using different techniques like X-Ray Diffraction (XRD), N_2 physisorption (BET), Raman, Temperature programmed reduction (TPR) and X-ray photoelectron spectroscopy (XPS)

Detailed information of the used characterization techniques is given below.

2.7.1 - X-ray powder diffraction (XRD)

XRD is a rapid, non-invasive analytical technique primarily used for phase identification of crystalline materials. XRD analysis was applied on the different catalysts to identify the presence of different phases in the catalysts.

The XRD patterns of the different catalysts were obtained using a D8 Advanced Bruker AXS diffractometer. The wavelength of CuKα1 X-ray radiation used was 1.5418 Å. The configuration for Bragg-Brentano diffractometer was theta-2 theta. The samples were immobilized on ceramic glass (Macor) holders. The angle (2θ) of XRD was varied between 10 and 80° with a step size of 0.02° and an integration time of 3 s.

2.7.2 - Temperature-programmed reduction (TPR)

TPR is a technique for the characterization of heterogeneous catalysts to quantify their reduction capacity. V_2O_5 and other supports oxides were tested by TPR to compare the relative changes in reduction capacity.

0.050 g of catalyst samples were treated in the TPR tests apparatus Micromeritics Autochem equipped with a quartz U-shaped microreactor. A H_2/Ar gas mixture was sent into the reactor at 50 mL/min while the reactor temperature was increased from room temperature to 800 °C at a heating rate of 5 °C/min. At the end of the analysis H_2 consumption by the active phase can be calculated. For the study of the sample with different supports reactor temperature was increased to 1000 °C

2.7.3 - Textural properties analysis via Brunauer–Emmett–Teller (BET) and Barrett-Joyner-Halenda (BJH)

The textural properties, specific surface area and pore size distribution, were studied via N_2 adsorption-desorption measurements at liquid nitrogen temperature. BET theory aims to explain the physical adsorption of gas molecules on a solid surface and serves as the basis for the measurement of the specific surface area. BJH analysis is a pore size distribution determination method, which is typically applied to nitrogen desorption data measured at 77 K on catalysts.

Two types of surface area analyzers were employed during the course of this work: the Micromeritics Flow Sorb III serial 416 and the Micromeritics TriStar-II. The first one provided the single-point surface area measurement and was capable of measuring the samples surface area from 0.01 m^2/g to over 1,000 m^2/g. Before the test, a continuous flow of N_2 passed over the sample at atmospheric pressure, and then the degassing process was performed at 150 °C for 30 min. After degassing, the samples were first cooled at liquid nitrogen temperature, and sequentially into distilled water. The surface area can be calculated based on the equation described below:

$$S_{BET} = \frac{A*L}{m_{degassing}};$$
Eq 2.3

Here A is molecular cross-sectional area, m is the mass of adsorbent, and L = 6.023*10^{-23} is the Avogadro constant.

The surface areas and porosity were obtained using Micromeritics TriStar-II device. The device contains two parts: one is the sample degas system, which contains a sample degasser (Micromeritics Vacprep 061) and a vacuum pump (PFEIFFER Duo 2.5). Another one is an analysis system, which contains the surface areas and porosity analysis equipment (Micromeritics TriStar-II) and a vacuum pump (PFEIFFER Duo 2.5).

Before sample analysis, the samples were degassed at 150 °C in vacuum for a few hours. After the samples were placed in the test chamber; the surface area and pore size distribution were calculated automatically. The total pore volume (V_{total}) was estimated from the amount adsorbed at a relative pressure of 0.99.

2.7.4 - The X-ray photoelectron spectroscopy (XPS)

This analysis was performed using a Kratos Analytical AXIS UltraDLD spectrometer. A monochromatized aluminum source (AlKα=1486.6 eV) was used for excitation. The X-ray beam diameter is around 1 mm. The analyzer was operated in constant pass energy of 40 eV using an analysis area of approximately 700×300 µm. Charge compensation was applied to compensate for the charging effect occurring during the analysis. The C 1s (2848 eV) binding energy (BE) was used as internal reference. The spectrometer BE scale was initially calibrated against the Ag 3d5/2 (368.2 eV) level. Pressure was in the 10^{-10} Torr range during the experiments. Simulation of the experimental photopeaks was carried out using Casa XPS software. Quantification took into account a nonlinear Shirley background subtraction.

2.7.5 - Raman spectroscopy

Raman spectra were recorded at room temperature with the 647.1 nm excitation line from a Spectra Physics krypton ion laser with 3 mW laser power at the sample. The beam was focused on the compounds using the macroscopic configuration. The scattered light was analyzed with an XY 800 Raman Dilor spectrometer equipped with an optical multichannel detector (liquid nitrogen-cooled charge coupled device). The spectral resolution was approximately 0.5 cm^{-1} in the investigated 200-1000 cm^{-1} range.

Chapter III

Bulk V$_2$O$_5$ reactivity in Chemical Looping Selective Oxidation of H$_2$S.

Chapter 3 – Bulk V_2O_5 reactivity in Chemical Looping Selective Oxidation of H_2S

It has been shown in Chapter 1 that Vanadium oxide and particularly V_2O_5 is active and selective for selective oxidation of H_2S in the classical cofeed way and is certainly the most investigated active phase for this reaction [10] [21][79] .

In a first attempt to implement the chemical looping concept, we explore the properties of bulk V_2O_5 without support to be used as a reference solid before considering the study of supported carriers.

Before considering any potential oxygen carrier, it is necessary to take into account some consideration regarding the thermodynamics of this process. As mentioned in Chapter 1, selective oxidation of H_2S is thermodynamically favorable and can be performed in a wide range of temperature. Obviously, total oxidation towards SO_2 in even more favorable, in particular at low temperature considering its exothermicity.

The role of a catalysts **in co-feed processes** is to promote kinetically the reaction by (i) lowering the activation energy and thus accelerating the reaction rate and (ii) orienting the reaction pathway toward the most desired product. Obviously, the catalyst does not affect the thermodynamic equilibrium of the reaction

In **chemical looping processes**, the oxygen carrier does not act as catalyst but as a reactant. It is therefore necessary to check the feasibility of each step of the redox process.

In the case of V_2O_5, the variation of Gibbs free energy of oxide reduction by H_2S should be calculated for the numerous partially reduced phases reported in the V-O phase diagram. However, even if the redox properties of V_2O_5 have been extensively studied in catalysis, the number of partially reduced phases for which thermodynamic data is available is limited. Using standard Gibbs free energy ($\Delta_fG°$) data using from "*factsage.com*" [80] website database, $\Delta_fG°$ have been calculated for V_2O_5 reduction by H_2S to several reduced oxides considering selective or total oxidation. Re-oxidation of the reduced oxides have also been considered.

The resulting data is reported in Figure 1. It can be seen that in the reaction temperature range considered for this work (150-250 °C), the reduction of V_2O_5 to VO_2, V_3O_5 or V_4O_7 is always possible. In the case of V_2O_5 reduction to VO_2 (V^{5+} to V^{4+}), the $\Delta_fG°$ for selective or total oxidation are very near meaning that the reaction kinetics will play an important role on the overall reactivity of the systems.

These calculations show that globally V_2O_5 can be considered for this process. It should nevertheless be underlined that these thermodynamic calculations are limited to well-known

and crystallized oxides. Surface vs bulk states, defects, interactions with supports and dopants are all factors which can affect these thermodynamic properties. This can modify the reactivity of the carrier both in terms of transformation rate (in either favorable or unfavorable way) as in classic co-feed catalysis but also in term of feasibility of such transformation.
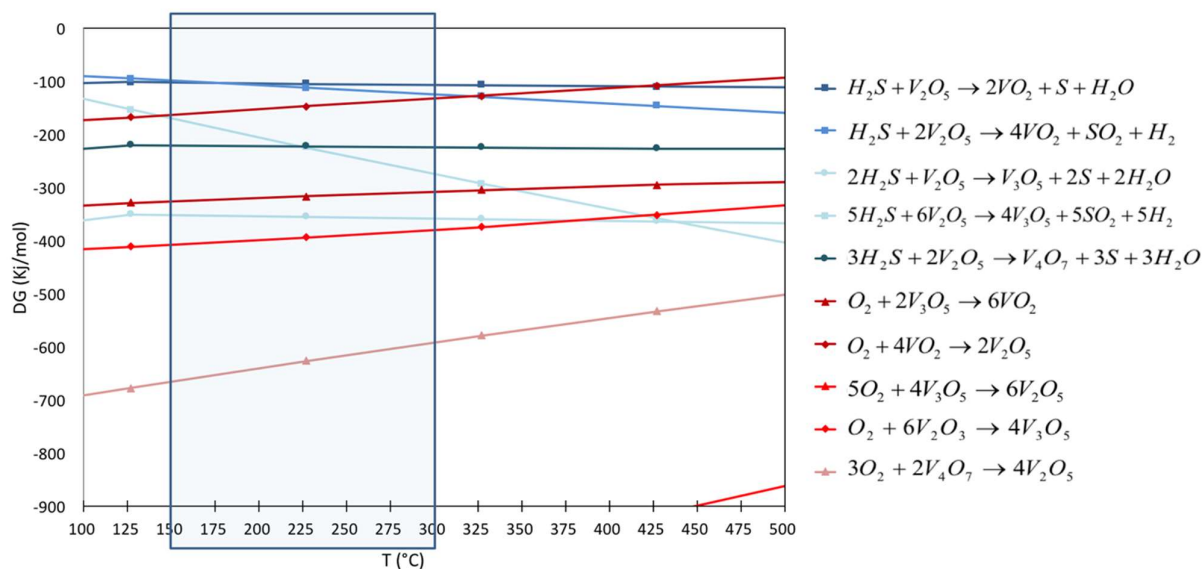
Figure 3.1: Variation of standard Gibbs free energy with temperature. Reduction of V_2O_5 by H_2S (blue), reoxidation by O_2 (red)

3.1 - Preparation and characterization of bulk V_2O_5.

Vanadium oxide prepared in the laboratory by calcining the precursor (ammonium metavanadate). Stepwise heating of the precursor has been done in presence of N_2 until 200 °C then it heated until 500 °C by 5 °C/ min in presence of O_2. Dark orange color powder obtained at the end of the calcination show the presence of V_2O_5 (V^{5+}).
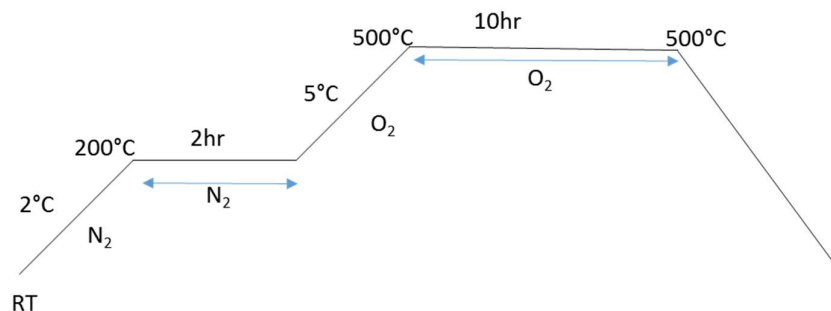
Figure 3.2: Calcination steps for the synthesis of V_2O_5

3.2- Characterization of Bulk and Surface properties

V_2O_5 sample has been characterized by different method such as BET, XRD, TPR and XPS. Table 3.1 illustrates the main characteristics of V_2O_5.

3.2.1 - BET

	Surface area (m²/gr)	Pore Volume (cm³/gr)	Pore Size (nm)	H₂ consumption (TPR) (mmol/g)	Average crystallite size (nm)	XPS	
						$V^{4+}/(V^{4+}+V^{5+})$	$V^{5+}/(V^{4+}+V^{5+})$
V_2O_5	5.5	0.03	18.4	4.62	86.7	0.095	0.9

Table 3.1: Characterization of V_2O_5.

The solid has very low surface area as (5.5 m²/g) with very low pore volume and pore size.

3.2.2 -XRD
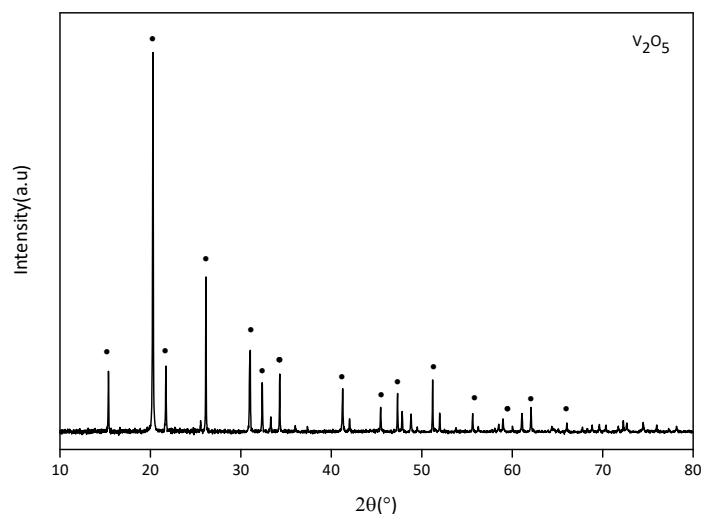
Figure 3.3: XRD study of V_2O_5 ((•) represents V_2O_5 reference peaks).

XRD of only V_2O_5 shows presence of crystalline phase of V_2O_5 Orthorhombic lattice is observed for the V_2O_5 with an intense peak 2ɵ° at 20.26 which shows typical plane of (1 0 1) (PDF 00-041-1426 JCPDF file). Average crystallite size determined by XRD is 86 nm, which is consistent with the low surface area.

3.2.3 - TPR
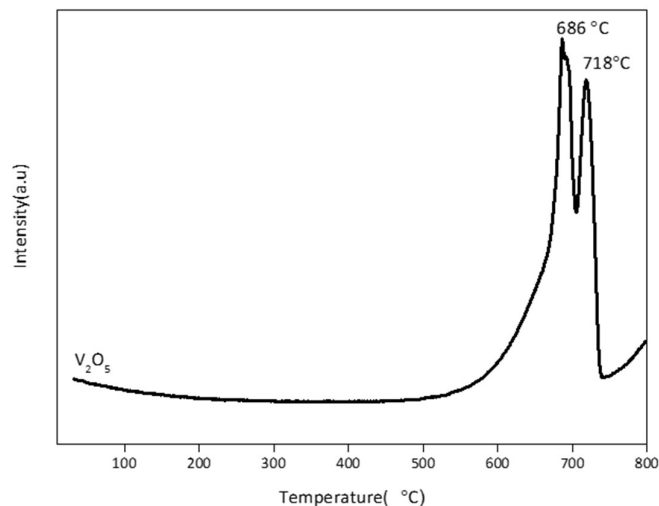
Figure 3.4: TPR study of V_2O_5 before and after reaction.

TPR study of the solid V_2O_5, exhibits two intense hydrogen consumption peaks at a 686 °C and 716 °C. Two different peaks represent the reduction of the V_2O_5

TPR profile represents the reaction between V_2O_5 and H_2,

$$V_2O_5 + H_2 \longrightarrow V_2O_{(5-x)} + x\ H_2O$$

Peak at 686 °C represents the reduction of V_2O_5 to V_6O_{13} [81]

These peaks are similar to the peaks observed in the literature for which the first peak corresponds to a reduction of V_2O_5 to V_6O_{13} which bring vanadium to an average oxidation state of $V^{+4.33}$. Reduction to V^{+4} occur in the second step. Similar TPR profile was obtained by G. Bond [40]

3.2.4 - XPS

XPS measurements were performed to obtain information about the surface elemental compositions and valence states of the carrier. Binding energy values were calibrated using the C 1s core level at 284.8 eV as the reference to eliminate possible charging effect that may occur because of surface contamination.
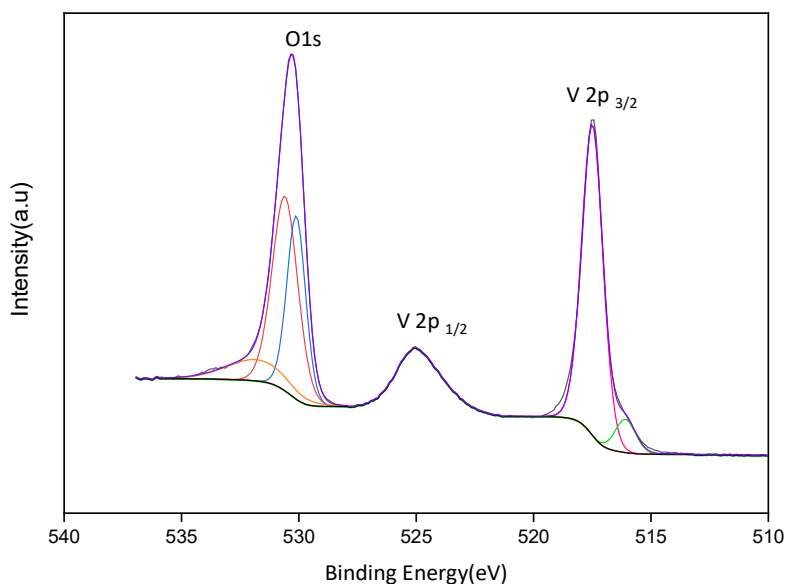
Figure 3.5: XPS study of V_2O_5 before reaction of V2p and O1s

XPS spectrum of V_2O_5 is characterized by two photopeaks at V $2p_{3/2}$ and V $2p_{1/2}$ with ΔE 7.6 eV. The chemical shift observed on the photopeak V $2p_{3/2}$ can be useful in order to distinguish the V^{4+} and V^{5+} species when the vanadium is found in two distinct phases and two different degrees of oxidation. On the other hand, the difference in energy between the O 1s and V $2p_{3/2}$ core levels may provide additional information for determining the oxidation state of vanadium. ΔE between the O 1s and V $2p_{3/2}$ is 12.9 eV, confirming the presence of V^{5+} oxidation state in the solid [82]. After deconvolution of V $2P_{3/2}$, together with the presence of V^{5+} species at 517.5 eV and V^{4+} is observed at 516 eV[40] [40], [83], [84]. In the case of photoemission from oxygen, the O 1s signal clearly shows three different surface oxygen species. Photopeak at 530.59 eV represents the oxygen associated with the Vanadium species, the one at 530.11 eV represents the mobile oxygen in the solid and photo peak at 531.79 eV corresponds to

adsorbed oxygen, hydroxyl and/or carbonate groups. These peaks are consistent with the literature for the oxygen from the V_2O_5 [83][85].

3.2.5 - Raman
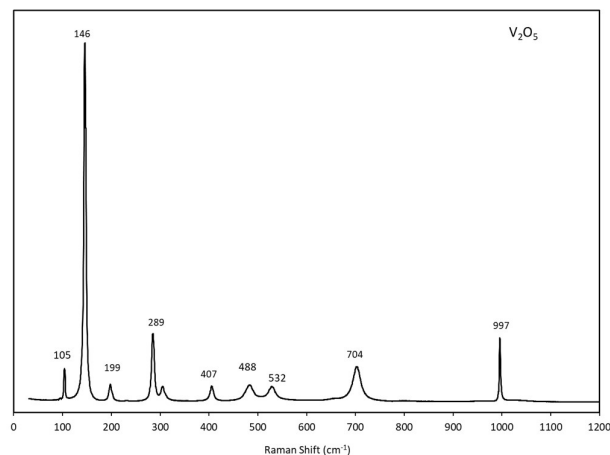
Figure 3.6: Raman study of V_2O_5 before reaction

In the Raman spectrum, the narrow peak at 997 cm^{-1}, due to the symmetric stretching vibrations of V-O groups, is characteristic of crystalline V_2O_5. Additional bands observed near 704 cm^{-1} arise from the stretching vibrations of V–O in the square octahedron of V_2O_5. The peaks at 289, 304, 488, 704, and 997 cm^{-1} are attributable to different crystalline V_2O_5 species [82].

3.3 - Chemical looping reactivity of V_2O_5 for H_2S selective oxidation.

Bulk V_2O_5 has been tested in chemical looping selective oxidation of H_2S without any further treatment after preparation. Typical experiment was carried out at 150 °C, exposing periodically for 1 minute to each reactant, with H_2S concentration of 2000 ppm and O_2 concentration of 10000 ppm. These can be considered as "reference" CLSOHS operating conditions in the overall study presented in this work.
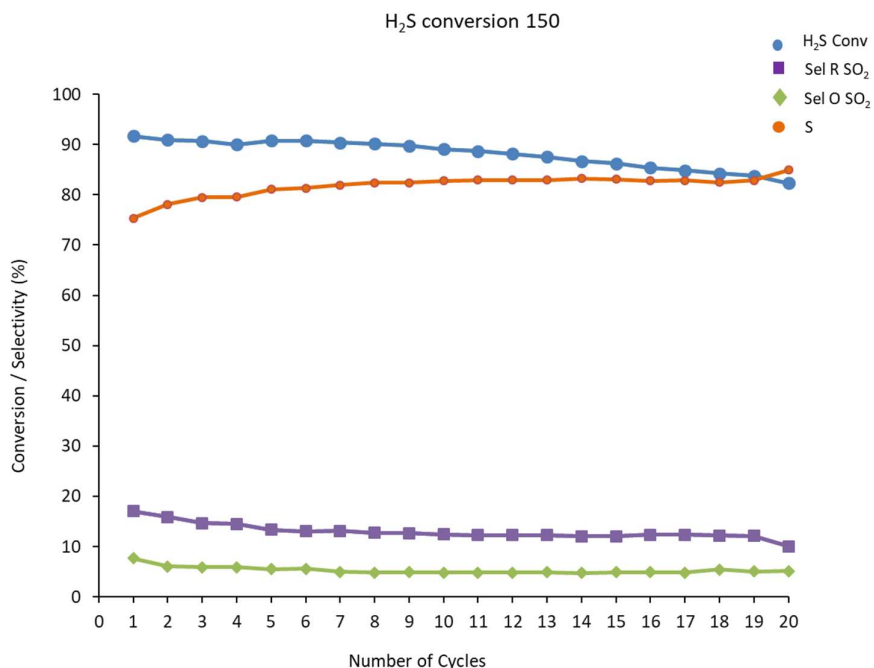
Figure 3.7: 80 mg of V_2O_5 150 °C, $H_2S:O_2$- 1:5, 2000 ppm of H_2S

Figure 3.7 illustrates the reactivity of V_2O_5 over 20 cycles. It is reminded that each point corresponds to the reactivity integrated over the cycle. Although H_2S conversion decreases by time by 8% it remains very high (above 80%) over the full experiment. In terms of selectivity, some SO_2 is formed directly during the reductant step and seems constant during the experiment. Other SO_2 is produced during the oxidation step. This one slightly decreases during the first 5-6 cycles and then reaches a reproducible value. The decrease of SO_2 formation during oxidant step induces a corresponding increase of the overall selectivity to elemental S from 72% to 85%.

These results confirm that V_2O_5 is a potential active phase for CLSOSH. Clearly, most of the SO_2 is formed during the re-oxidation step indicating that S containing species are adsorbed at the surface of the carrier during the reductant step but are not fully converted to S or SO_2. To optimize the overall selectivity to S, two factors need therefore to be improved:

- The direct oxidation to SO_2 in the reductant step should be kept as low as possible.
- The "transport" of S containing species from the reductant step to the oxidant one should be avoided.

To better understand the reactivity of V_2O_5 in CLSOHS, the reaction has been studied by varying several experimental parameters such as reactants concentrations and reaction temperature. In details, three concentrations of H_2S have been considered (1000, 2000, 4000 ppm) while the reaction ration between H_2S and O_2 was maintained at 1:5. This ratio was then varied from 1:5 to 1:2.5 and 1:0.5. This last ratio corresponds to the theoretical stoichiometric

ration for selective oxidation of H_2S. Finally, different reaction temperatures were applied for the reaction (150 and 200 °C).

3.3.1 - Effect of reactant Concentration

In this section, different H_2S concentrations have been studied in detailed at 150 °C and 200 °C. The $H_2S:O_2$ ration was kept constant at 1:5 that is with an excess of oxygen. 20 cycles were carried out each time. Between experiments in different conditions, the sample were treated at 400 °C in oxygen to remove residual sulfur species and fully regenerate the carrier.

150 °C

Evolution of the reactivity of V_2O_5 during CLSOHS cycling at 150 °C is represented in Figure 3.8. For comparison, results of the last cycles is represented in Figure 3.9. Detailed numerical values are reported in Table 3.2.
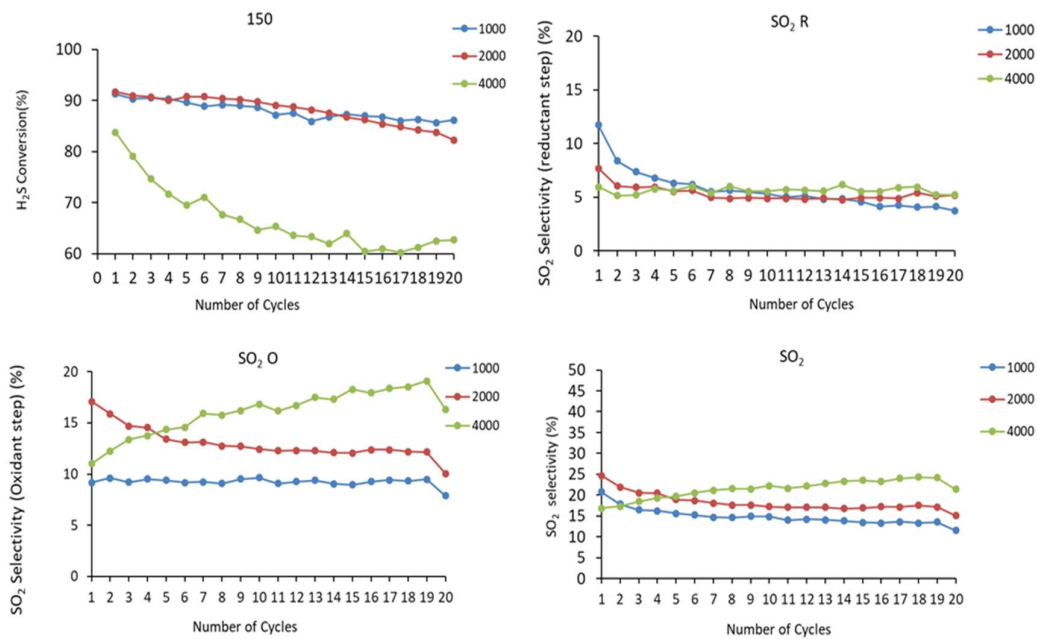
Figure 3.8: 80 mg of V_2O_5 150 °C, $H_2S:O_2$- 1:5, 4000, 2000, 1000 ppm of H_2S
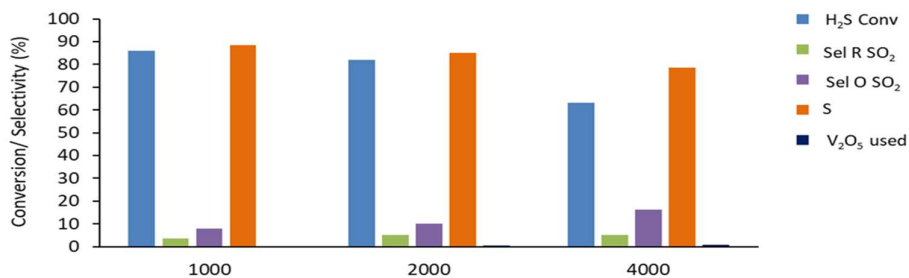
Figure 3.9: 80 mg of V_2O_5 150 °C, $H_2S:O_2$- 1:5, 4000, 2000, 1000 ppm of H_2S

At low concentration (1000 ppm), high conversion of H_2S is observed with high selectivity towards Sulfur formation. A slight decrease of conversion with cycling is observed but the formation of the SO_2 in the reductant and oxygen step is practically constant throughout the experiment, which illustrates the good regeneration of the catalysts during the reaction.

Reaction at 2000 ppm, already described in Figure 3.7, shows the high conversion of H_2S. Conversion decrease is slightly more rapid than using 1000 ppm H_2S. Almost similar formation of the SO_2 in the reductant step can be seen compared to 1000 ppm while the amount produced during oxidant step is significantly higher. At 2000 ppm the system is thus slightly less selective but this is due essentially to oxidation of adsorbed S containing species in the oxidant step.

150 °C	1000 ppm H_2S	2000 ppm H_2S	4000 ppm H_2S
H_2S feed per cycle (μmol)	4.7	8.6	16.50
Conv H_2S (%)	86	82	63
H_2S converted (μmol)	4.04	7.05	10.40
S (μmol)	3.56	5.95	8.11
SO_2R (μmol)	0.15	0.37	0.54
SO_2O (μmol)	0.33	0.73	1.74
(S/S+SO_2R) (%)	96	94	94
%O_{latt} (% V^{5+} -> V^{4+})	0.91	1.60	2.21

Table 3.2: 80 mg of V_2O_5 150 °C, H_2S:O_2- 1:5, 4000, 2000, 1000 ppm of H_2S

In the case of 4000 ppm of H_2S, initial conversion is high (80 %) but decreases significantly to reach a stable value of 60%. The selectivity towards SO_2 in the reductant step is low and remarkably similar to that observed with lower H_2S concentrations.

On the other hand, SO_2 formation in the oxidant step is much higher than others and increases steadily. This probably happens due to the excess adsorption of H_2S on the surface of the catalysts. During the reductant step, some H_2S reacts with the available V_2O_5 and remaining H_2S stay adsorbed on the surface and cover up the other remained active sites makes them unavailable for the reaction. In the next oxidant step, this adsorbed H_2S reacts with the oxygen to form SO_2 by complete oxidation. Adsorption of H_2S on the surface of the V_2O_5 plays the important role during the reaction as the surface area of the V_2O_5 is very small (5 m^2/g).

With 4000 ppm, some kind of saturation of the surface seems to occur, which reflect in the lower H_2S conversion and higher SO_2 formation in oxidant step. Interestingly, the amount of SO_2 produced during the reductant step (Table 3.2) increases rather proportionally to the amount of H_2S in the feed.

The overall amount of lattice oxygen extracted (taking into account water production) is low compared to the amount of oxygen available in this bulk V_2O_5 as it represents between 0.96 and 2.21 %. It is reminded that this value is obtained considering the amount of lattice oxygen necessary to produce S, SO_2 in reductant step and the corresponding amount of H_2O. It is then compared to the amount of lattice oxygen corresponding to total reduction of V_2O_5 (V^{5+}) to V_2O_4 (V^{4+}).

Between 1000 and 2000 ppm, the amount of lattice oxygen extracted in reductant step increases (0.91 to 1.60 %O_{latt}) nearly proportionally to that of H_2S concentration. Between 2000 and 4000 ppm of H_2S, the amount of %O_{latt} still increases but in moderate proportion (1.60 to 2.21 %O_{latt}). Therefore, although these values are low, the capacity of the carrier to provide the necessary lattice oxygen seems limited, which further explains that higher amount of SO_2 produced during oxidant step.

200 °C

In a similar way, the behavior of V_2O_5 at 200 °C and different reactant concentration is represented in Figures 3.10 and Figure 3.11 and Table 3.3.

In terms on H_2S conversion, higher values are logically obtained at such higher temperature. At 1000 ppm H_2S, stable conversion is observed throughout the 20 cycles measured. At 2000 ppm, a deactivation occurs while, at 4000 ppm a singular behavior is seen. Indeed, the activity initially decreases and then increases again.

In terms of selectivity, SO_2 formation in reductant step decreases with H_2S concentration. It should however be noticed that the net amount of SO_2 produced in this reductant step is rather similar (1µmol/cycle) whatever the H_2S concentration in the feed.

In terms of lattice oxygen consumed in the reductant step (Table 3.3), it can be seen that this one increases significantly at low H_2S concentration (0.91 to 1.55 %O_{latt}) between 150 °C and 200 °C experiments whereas such increase is less important with 2000 ppm H_2S (from 1.60 to 1.81 %O_{latt}). The trend inverts at higher concentration (from 2.21 to 3.12 %O_{latt}). This could be explained by the more effective regeneration at higher temperature considering that the O_2 concentration is also increased.

From the general trends, on can see that the reactivity of experiment at 2000 ppm at 200 °C follows that of the one made with 4000 ppm at lower temperature suggesting that, again, the available oxygen from the solid is totally consumed due to higher net amount of SO_2 produced. The regeneration of the carrier does not seem to be complete during oxidant step which induces the deactivation.
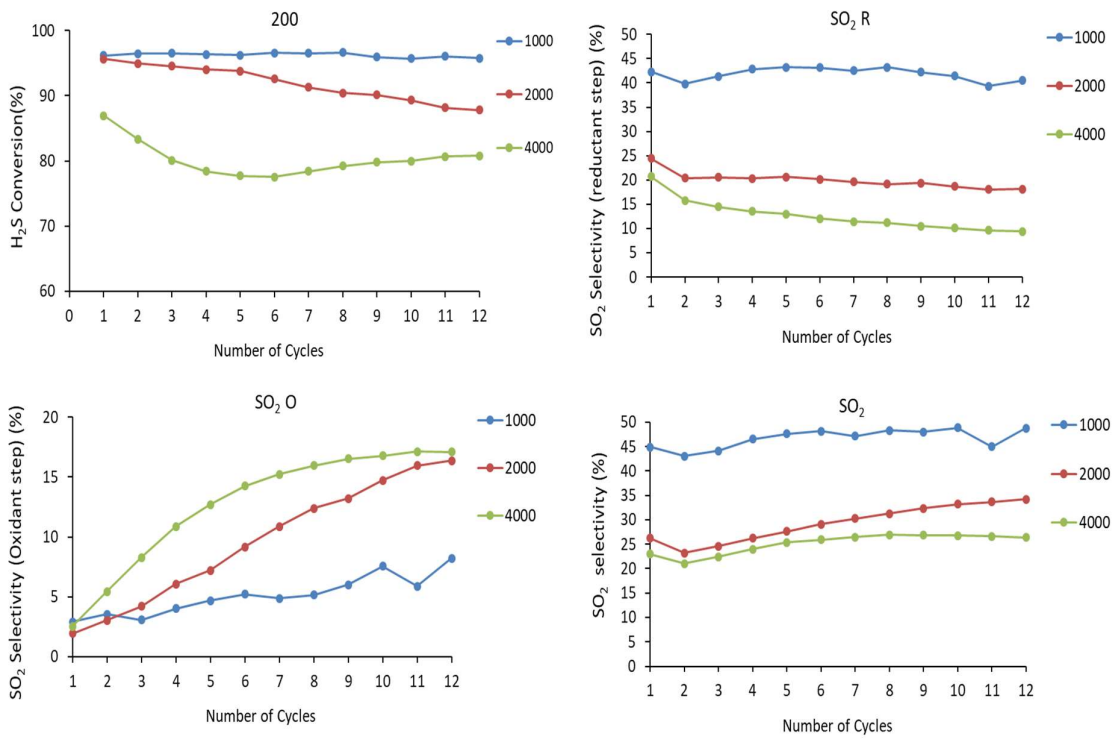
Figure 3.10: 80 mg of V_2O_5 200 °C, $H_2S:O_2$- 1:5, 4000, 2000, 1000 ppm of H_2S
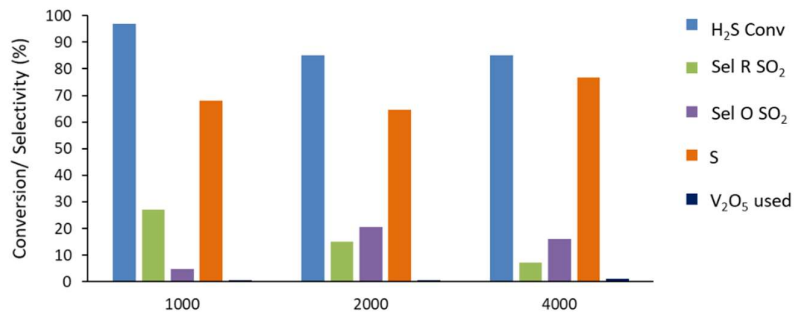
Figure 3.11: 80 mg of V_2O_5 200 °C, $H_2S:O_2$- 1:5, 4000, 2000, 1000 ppm of H_2S

200 °C	1000 ppm H$_2$S	2000 ppm H$_2$S	4000 ppm H$_2$S
H$_2$S feed per cycle (μmol)	4.7	8.6	16.50
% Conv H$_2$S	97	85	85
n converted (μmol)	4.56	7.31	14.03
S (μmol)	3.69	4.69	10.71
SO$_2$R (μmol)	1.25	1.09	1.01
SO$_2$O (μmol)	0.22	1.53	2.31
(S/S+SO$_2$) (%)	71	81	91
%O$_{latt}$ (% V^{5+} -> V^{4+})	1.55	1.81	3.12

Table 3.3: 80 mg of V$_2$O$_5$ 200 °C, H$_2$S:O$_2$- 1:5, 4000, 2000, 1000 ppm of H$_2$S

3.3.2 - Effect of Temperature

To better observe the influence of reaction temperature, the experiments performed with 200 ppm H$_2$S (and 10000 ppm O$_2$) are directly compared (Figures 3.12 and 3.13, Table 3.4).
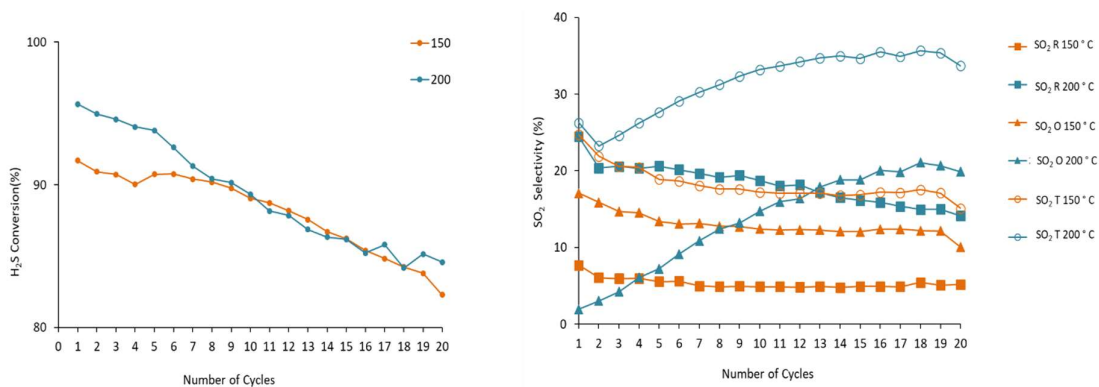
Figure 3.12: 80 mg of V$_2$O$_5$ 2000 ppm H$_2$S, H$_2$S:O$_2$-1:5 C, 2000 ppm of H$_2$S
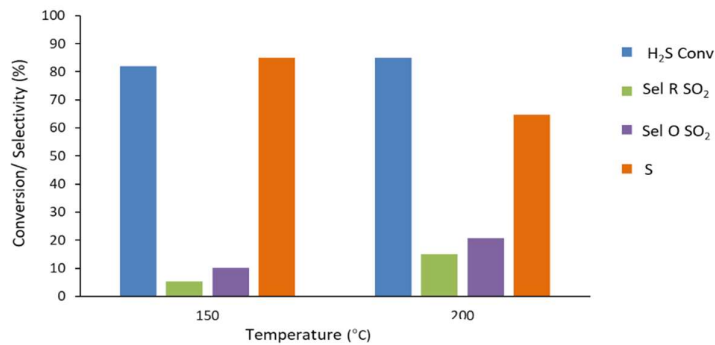
Figure 3.13: 80 mg of V$_2$O$_5$ 2000 ppm H$_2$S, H$_2$S:O$_2$- 1:5, 2000 ppm of H$_2$S

2000 ppm	150 °C	200 °C
H_2S feed per cycle (µmol)	8.6	8.6
% Conv H_2S	82	85
n converted (µmol)	7.05	7.31
S (µmol)	5.95	4.69
SO_2R (µmol)	0.37	1.09
SO_2O (µmol)	0.73	1.53
$(S/S+SO_2)$ (%)	94.19	81.21
$\%O_{latt}$ (% V^{5+} -> V^{4+})	1.60	1.81

Table 3.4: 80 mg of V_2O_5, 2000 ppm $H_2S:O_2$-1:5, 2000 ppm of H_2S

With increase in the temperature of the reaction, increase in initial H_2S conversion is observed. However, in both the cases H_2S conversion decreases and, by the end of the cycles, reach similar values for both temperatures. SO_2 formation is observed during both the reductant and oxidant cycle.

Selectivity to SO_2 at low temperature is rather constant along cycling both for SO_2 produced during reductant and oxidant steps. At high temperature, SO_2 produced during reductant step is rather constant while that produced during re-oxidation increases continuously. This indicates that although S containing species continue to be adsorbed on the surface of the carrier, the amount which is fully converted to either S or SO_2 during reductant step is decreasing along the cycles until a "stable" repetitive behavior is reached.

This is probably linked to a good balance between the amount of available lattice oxygen, the reactivity of H_2S species and the capacity to regenerate to solid. Interestingly it can be noted that at the end of the cycling the amount of lattice oxygen involved in the reaction is only slightly higher at 200 °C (1.81 $\%O_{latt}$) than at 150 °C (1.60 $\%O_{latt}$).

3.3.3 - Effect of different reactant ratio

Previous results illustrate that a delicate balance between the reactivity of the solid, that of H_2S in reductant step and that of O_2 is necessary to reach good performances.

Effect of different ratio of reactant has been studied at 150 °C by keeping the H_2S concentration at 2000 ppm and changing the oxygen concentration accordingly. Oxygen concentration changed from 10000 ppm, 5000 ppm and 1000 ppm to achieve the ratio of 1:5, 1:2.5, 1: 0.5 respectively. The 1: 0.5 ratio correspond to the stoichiometric one for selective oxidation of H_2S. Results are illustrated in Figures 3.14 and 3.15 and Table 3.5.
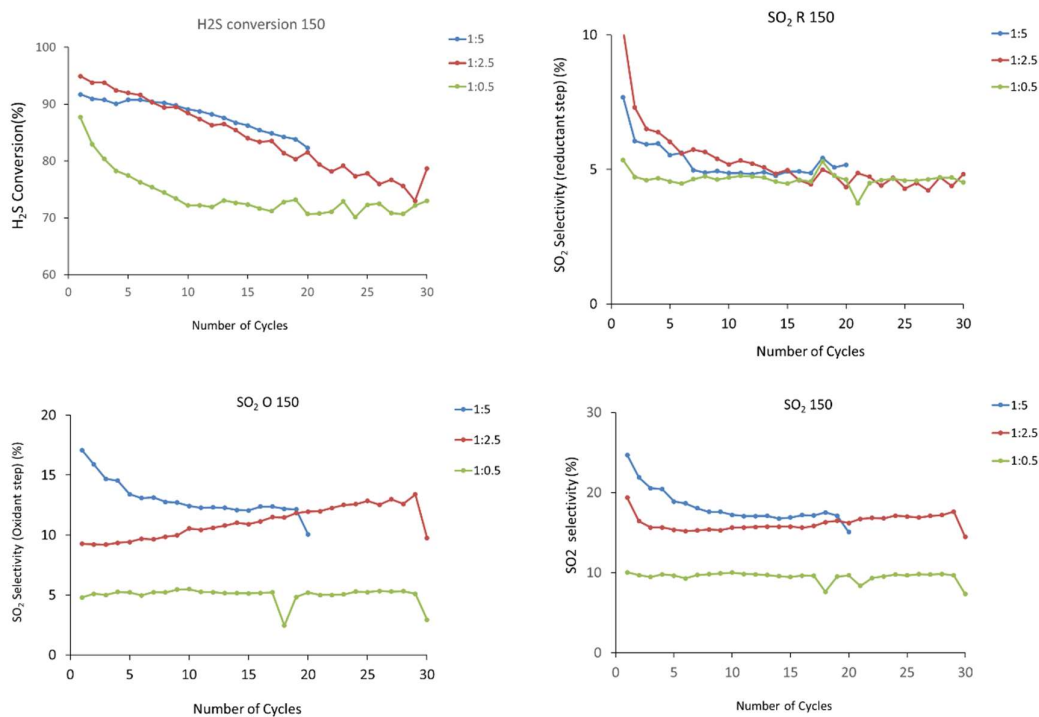
Figure 3.14: 80 mg of V$_2$O$_5$, 150 °C, 2000 ppm of H$_2$S, H$_2$S:O$_2$- 1:5,1:2.5, 1:0.5
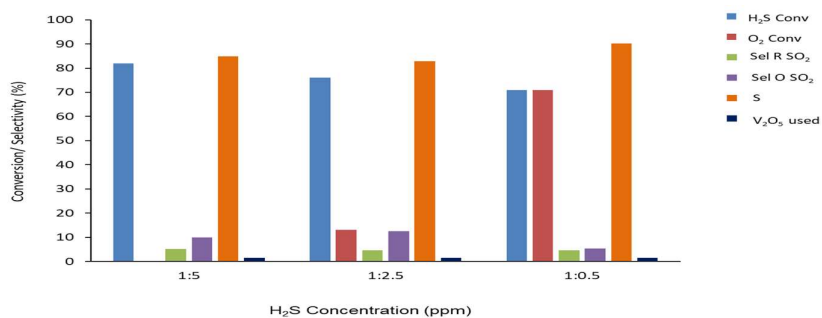
Figure 3.15: 80 mg of V$_2$O$_5$, 150 °C, 2000 ppm of H$_2$S, H$_2$S:O$_2$- 1:5,1:2.5, 1:0.5

150 °C	1:5	1:2.5	1:0.5
H$_2$S feed per cycle (µmol)	8.6	8.6	8.6
% Conv H$_2$S	82	76	71
n converted (µmol)	7.05	6.54	6.11
S (µmol)	5.95	5.39	5.48
SO$_2$R (µmol)	0.37	0.31	0.29
SO$_2$O (µmol)	0.73	0.84	0.34
(S/S+SO$_2$ R) (%)	94.19	94.6	95
%O$_{latt}$ (% V^{5+} -> V^{4+})	1.60	1.43	1.44

Table 3.5: 80 mg of V$_2$O$_5$, 150° C, 2000 ppm of H$_2$S, H$_2$S:O$_2$- 1:5, 1:2.5, 1:0.5

For each ratio H_2S conversion varies with time. In the case of the ratio, 1:2.5, the slope of conversion evolution with cycles is steeper than using 1:5 ratio. The initial slope of deactivation is even steeper using stoichiometric ratio of 1:0.5, but in this case activity reaches a stable value after approx. 10 cycles.

Except during the very first cycles of each experiment, the selectivity towards SO_2 in the reductant step is very stable and unaffected by the O_2 concentration.

The initial amount of SO_2 formation during oxidant step significantly increase with O_2 concentration during this step. However, this amount decreases during cycling in the cases of the highest O_2 concentrations whereas it is remarkably stable for the low one.

It can be noted that although the O_2 concentration decreases by a factor 10 between the ratio 1:5 to the ratio 1:0.5, the overall amount of lattice oxygen involved in the process decrease only very slightly in line with the decrease of overall conversion.

3.4 - After reaction characterization

Samples were studied before and after reaction to evaluate the structural or chemical changes in the catalysts during the reaction. Contrary to steady state reactions for which a sample can be collected after reaction, in the case of chemical looping processes, two samples should be considered by ending either after the reductant or the oxidant steps.

Reactions were carried out on distinct samples at different temperature like 150°C and 200 °C (2000 ppm of H_2S with 10000 ppm of O_2). Total 30 cycles were performed and reaction stopped after 30th cycles after H_2S step or O_2 step respectively. The reactor was then closed and cooled to room temperature. So, in total 4 samples are studied after reaction:

V_2O_5 (H_2S, 150 °C): reaction stopped after 30 cycle after H_2S step at 150 °C

V_2O_5 (H_2S, 200 °C): reaction stopped after 30 cycle after H_2S cycle at 200 °C

V_2O_5 (O_2, 150 °C): reaction stopped after 30 cycle at O_2 cycle at 150 °C

V_2O_5 (O_2, 200 °C): reaction stopped after 30 cycle after O_2 cycle at 200 °C

These samples were characterized by XRD and XPS and Raman.

3.4.1 - XRD

XRD study of the V_2O_5 solid after reaction shows mostly identical V_2O_5 diffractograms compared to the as prepared sample. Particle size do not vary significantly with respect to the original V_2O_5

Catalysts	H_2 consumption (TPR) (mmol/g)	average crystallite size (nm)	
		V_2O_5	S
V_2O_5 (H_2S, 150 °C)	3.8632	77.5	34.74
V_2O_5 (H_2S, 200 °C)	1.896	90.3	74.9
V_2O_5 (O_2, 150 °C)	2.034	83.5	32.1
V_2O_5 (O_2S, 200 °C)	3.711	90.8	65

Table 3.6: Characterization of V_2O_5 after reaction.
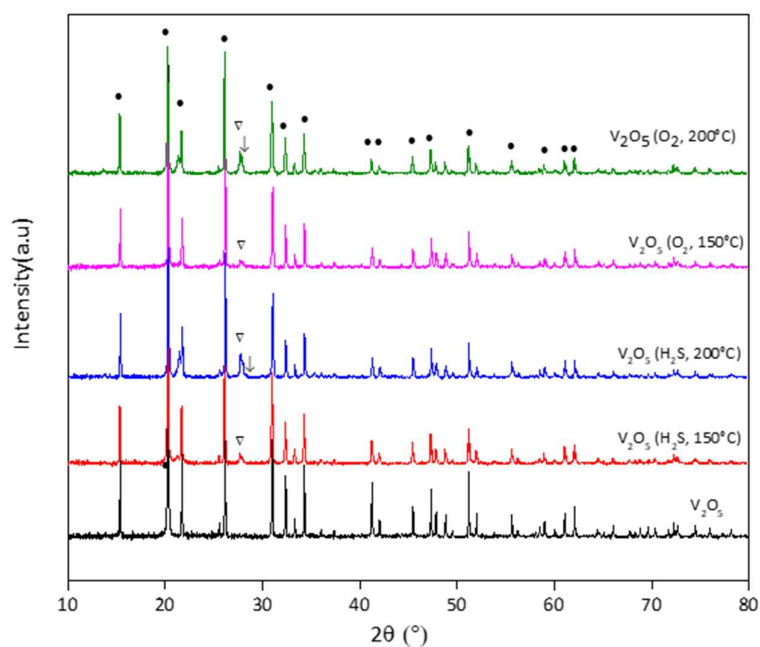
Figure 3.16: XRD study of V_2O_5 before and after reaction.
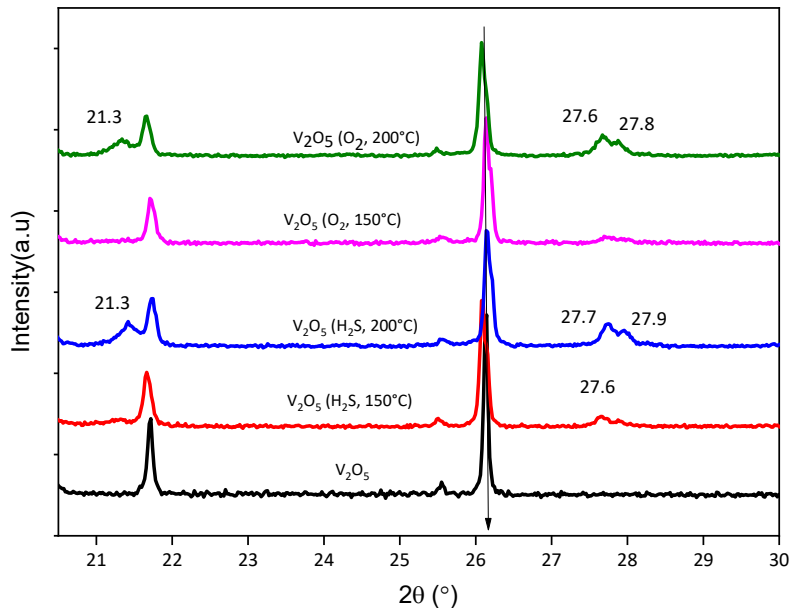
Figure 3.17: XRD study of V₂O₅ before and after reaction

A small supplementary peak at $2\Theta=27.7°$ can be observed and could be attributed to VO_2 (0 1 0) plane according to JCPDF file PDF 04-003-2035. This peak is present at various intensities on all samples after reaction and more intensely on samples collected after reaction at 200 °C.

These high reaction temperature samples also reveal a small peak at $2\Theta=21.3°$ this could be attributed to the presence of Sulfur with plane (0 2 0) in reference with the JCPDF file PDF 01-076-1100 although the presence of crystalized S particles is rather surprising.

3.4.2 - XPS

Figure 3.18 shows the XPS spectra on all samples after reaction for O1s and V2p compared to that of the sample before reaction. Figure 3.19 shows the XPS spectra on all samples after reaction for S2p
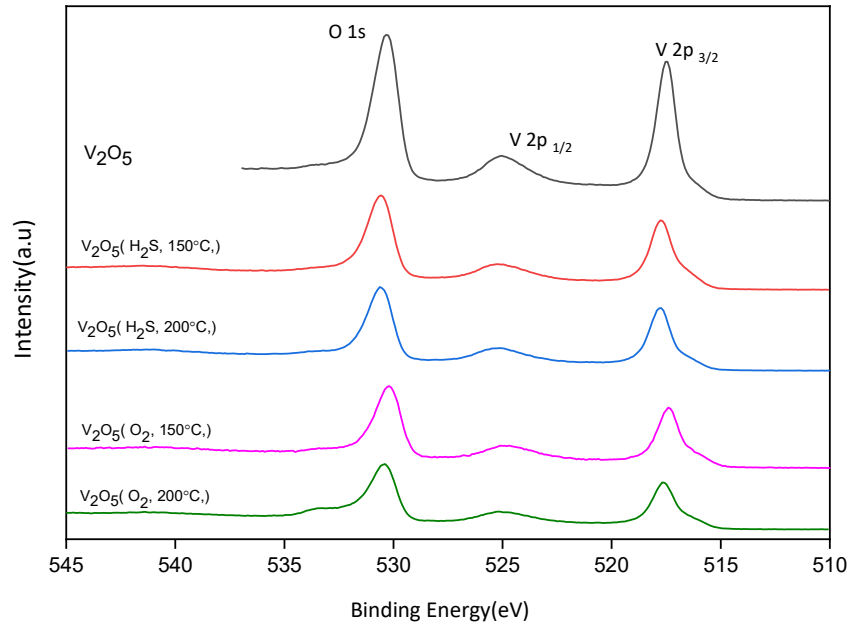
Figure 3.18: XPS study of V$_2$O$_5$ before and after reaction with V2p and O1s.
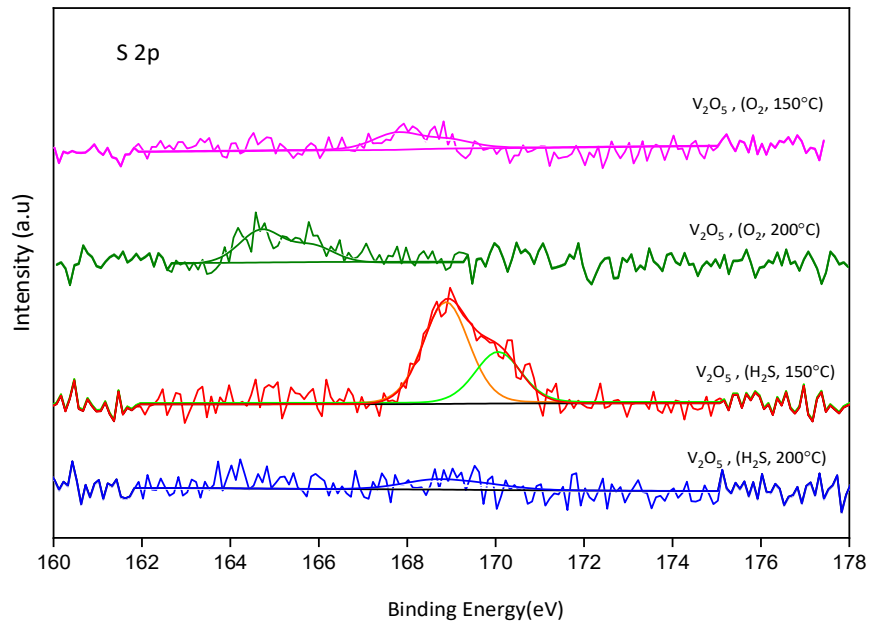
Figure 3.19: XPS study of V$_2$O$_5$ before and after reaction with S 2p

Carrier	B.E (eV) V 2P		$V^{4+}/$ $(V^{4+}+V^{5+})$	$V^{5+}/$ $(V^{4+}+V^{5+})$	V^{4+}/V^{5+}	S/V
	V^{4+}	V^{5+}				
V_2O_5	516.09	517.49	0.065	0.93	0.071	-
V_2O_5 150 °C H_2S	516.39	517.73	0.18	0.82	0.22	0.02
V_2O_5 200 °C H_2S	516.33	517.78	0.15	0.85	0.17	-
V_2O_5 150 °C O_2	515.97	517.39	0.17	0.83	0.19	
V_2O_5 200 °C O_2	516.17	517.62	0.19	0.81	0.23	-

Table 3.7: XPS study of V_2O_5 before and after reaction with S 2p

Both V^{4+} and V^{5+} are observed throughout the study. By the deconvolution of the different components, it is possible to estimate the ratios of V^{4+}/V^{5+}, which are reported in Table 3.7.

Contrary to what could be expected, no significant differences in V^{4+}/V^{5+} ratio can be observed on the samples although they were collected at different temperature and after reductant or oxidant step.

This could be explained by the fact that once the step is performed and the reactor closed, the surface oxidation state may evolve thanks to oxygen diffusion between the bulk of the solid and its surface. What seems more significant is that even after the oxidant step, V^{4+} species are present. This would indicate that the V oxidation state cycling does not occur reaching the full V^{5+} at the surface but would take place between lower average oxidation states.

Practically no sulfur can be detected on these samples with the exception of the sample collected after reductant step at 150 °C. In this case, a peak at 168.8 eV is clearly seen providing a S/V ratio of approx. 0.02. From the position of the S2p peak, sulfate seem to be formed on the surface of V_2O_5 [86].

The absence of S on the sample treated at 200 °C is also surprising considering that SO_2 is produced during oxidant step in these conditions. To allow this to happen, sulfur containing species must be present in adsorbed form on the surface after the reductant step. Again, the diffusion of oxygen from the bulk, which is enhanced by temperature, could explain that these adsorbed species continue to be oxidized by the carrier during the period the reactor is closed before cooling to room temperature.

3.4.3 - Raman
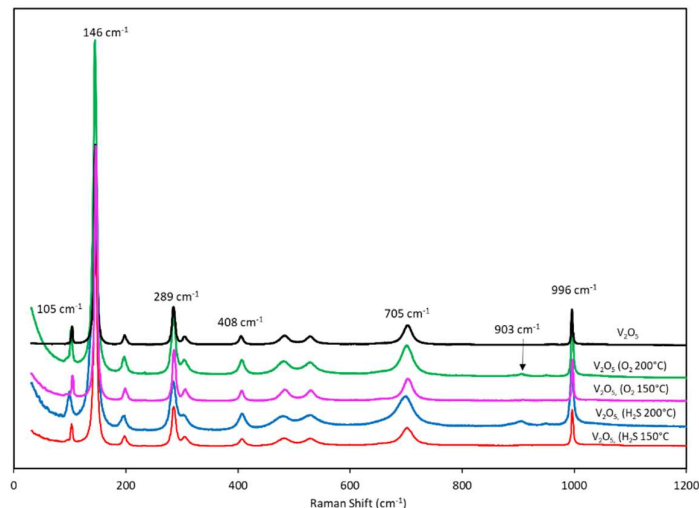
Figure 3.20: Raman study of V_2O_5 before and after reaction

After reaction, all the peaks of the bulk V_2O_5 are present at both the temperatures or at last exposed reactant. However, after reaction at 200 °C, small shoulder at 903 cm^{-1} is observed irrespective of the last reactant present. As shown by L. Kevan et al.[87], this peak can be assigned to bridge V-O-V chain vibrations of polymeric vanadium oxide species as these peaks feature in the 800-900 cm^{-1} region. Peak at 903 cm^{-1} could also show the presence of the V^{5+}-O-V^{4+} from the structure V_4O_9 as shown by J.M. López Nieto et al. [61][88].

3.5 - General discussion and conclusions

In line with the well-known activity of V_2O_5 in co-feed selective oxidation of H_2S and with the thermodynamic considerations, these results confirm that vanadium oxide materials can effectively be considered as active carriers in chemical looping process.

They also show that although reaction temperature is rather low (150-200 °C) both surface species and subsurface layers of the oxide are involved in the reactivity. Indeed, if one considers that one V_2O_5 unit will occupy approx. 0.21 nm^2 [89], taking into account the specific surface area of the solid (5.5 m^2/gr) and the amount used (80 mg), the amount of surface V_2O_5 can be estimated to 0.63 μmol for these experiments, to be compared to 440 μmol of total V_2O_5. As seen in the tables describing the reactivity, the percentage of lattice oxygen involved varies between 0.91 and 3.12 %O_{latt}, i.e. between 4 and 12 μmol, which would represent the involvement of 6 to 12 layers of V_2O_5. Clearly, this is obtained considering exclusively the reduction of V^{5+} species to V^{4+} and the numbers of layers involved would be smaller if reduction to V^{3+} is taken into account but still subsurface layers should be involved to account for the reactivity of the system.

It is interesting to observe that in all cases some SO_2 is formed during the reductant step. The amount (SO_2R) varies between 0.15 to 0.50 µmol at 150 °C and 1.01 to 1.25 µmol at 200 °C. These are in the same order of magnitude as that of surface V_2O_5 calculated above. This could suggest that the outermost oxidized vanadium species generated during re-oxidation result in unselective oxidation but, in this case, one would not expect this amount to vary significantly. On the contrary, the amount of SO_2R increases significantly with temperature and is also affected by the concentration of H_2S, in particular at 150 °C.

Another possible explanation would be that certain surface planes exposed by the solid lead to unselective oxidation, which can then proceed more deeply through subsurface layers according to temperature and H_2S pressure, while other plane would show better selectivity. Such anisotropic behavior of crystalline oxides has already been observed for several selective oxidation reactions [90], [91]. Clearly it is premature to draw further hypothesis based on these limited results.

The involvement of rather deep subsurface layers of the oxide is coherent with the presence of both V^{4+} and V^{5+} species on all samples after experiment, independently of reaction temperature of the nature of last step before recovering the sample. Indeed, if the presence of V^{4+} species could be expected after reductant step, it was more surprising after the oxidant one. However, if one considers that subsurface layers are progressively involved during cycling, it is possible that the re-oxidation does not proceed so deeply immediately at each cycle. If reduced species are still present, the solid would slowly re-equilibrate by diffusion of oxygen species from to surface towards the bulk. Inversely, deeper oxygen species from the bulk may migrate to the subsurface are in samples recovered after reductant step.

This shows that the transient nature of the process must always be kept in mind when comparing results considering that the solid continues to evolve between reaction steps, where it is submitted to external "stress", and relaxation periods.

This can also be underlined regarding the presence of sulfur species on samples after test. While this could be expected after oxidant step, very little if observed after reductant also. No S could even be detected by XPS on sample treated at 200 °C after H_2S exposure. Although, as explained, S should be present after such cycling, its absence during characterization suggest that it continues to be converted by the solid explaining that no sulfurs species or only oxidized form can be detected.

The results presented in this chapter basically confirm that V_2O_5 is a potential candidate as active phase in oxygen carriers for CLSOHS. They show that H_2S can be selectively converted to elemental S on such materials which further demonstrate to have good cyclic regeneration properties both in terms of oxygen capacity and surface sulfur species removal.

The transient nature of chemical looping processes make further hypothesis on the reaction mechanism highly speculative at this point. It can however be confirmed that not only outermost surface species are involved in the redox process. Indeed, rather deep reduction/oxidation of the solid is possible even at such low reaction temperature.

Although some SO_2 is formed during reductant cycle as discussed above, the selectivity towards elemental sulfur in this step is always very high. Indeed, most of the SO_2 formed during the experiments showed is produced during the oxidant step.

To optimize the CLSOHS process using V_2O_5 based solids, two essential aspects will therefore need to be optimized: on one hand, the "intrinsic" selectivity to S in the reductant steps will have to be increased and, on the other, the presence of S containing species remaining adsorbed on the carrier after reductant step will have to be minimized.

Chapter IV

Different supports for Chemical Looping Selective Oxidation of H$_2$S.

Chapter 4 - Different supports for Chemical Looping Selective Oxidation of H$_2$S.

Supports play an important role in catalysis. They help optimizing the dispersion of active phase thus increasing the number of active sites, but can also influence the reactivity of these sites through active-phase/support interaction. They may also play a direct role in the catalytic reaction by favoring the adsorption of reactants or by providing reactions pathways to species adsorbed on the active phase (spillover). Effect of different support on the H$_2$S catalytic selective oxidation reaction is well explained in the literature [38]. Interaction of the active phase with the support plays a vital role during the mechanism of the reaction.

It is expected that such effect should be present also for CLSOSH processes. To highlight this effect, the nature of the support is varied using V$_2$O$_5$ as active phase. At this stage, high loading of active phase is considered in order to understand if the support can induce particular properties to rather large V$_2$O$_5$ species and therefore directly compare with the results obtained on bulk material shown in the previous chapter.

4.1 - Synthesis of the Oxygen Carrier solids

Active phase was impregnated on synthesized or commercial supports. Different supports were considered for the synthesis of catalysts like TiO$_2$, CeO$_2$, ZrO$_2$, Al$_2$O$_3$ and SiO$_2$[17][29][92][18] [93]. Among these, TiO$_2$ and Al$_2$O$_3$ are commercial supports from Sigma Aldrich. Other supports were synthesised in laboratory with precipitation method using different hydrolysis additives.

As commercial support from Sigma-Aldrich shows traces of K, Na it can have strong effect on the Vanadium dispersion and its activity, before using the support for the solid preparation, it was washed in water to remove this impurity. Support was mixed with water and stirred for 3 hrs vigorously. Slurry was then centrifuged and dried at at 100 °C overnight.

Ceria support was prepared in laboratory by precipitation method using TEA. Ratio for Ce (NO$_3$): TEA was 1:4 whereas that for methanol: TEA was maintained at 1:4. Solution A was all metal nitrates (Ceria Nitrate) and water whereas solution B is TEA with methanol. Initially both solutions were stirred separately to form clear solutions. Solution A was then added to solution B dropwise with continuous stirring. Brown colored precipitate was observed in the beaker. This solution (slurry) was then stirred continuously for 24 hrs. to form a uniform slurry. After 24 hrs. stirring, water was evaporated by continuous stirring at 80 °C. The sample was then dried at 80 °C overnight. Final solid was then calcined at 500 °C for 5 hrs. in presence of air.

Zirconia support was prepared by precipitation method using ammonia solution. Required amount of $Zr(NO_3)$ was dissolved in water and stirred for 15 mins to form homogenous clear solution. 25% concentrated ammonia was then added slowly and drop wise in to this clear solution. Dark brown precipitate was then observed. This solution (slurry) was then stirred continuously for 24 hrs. to form a uniform slurry which was then filtered and washed with water several times. The sample was then dried at 80 °C overnight. Final solid then calcined at 500 °C for 10 hrs. in presence of air.

SiO_2 support was prepared in laboratory by precipitation method using ammonia solution. Required amount of TEOS was dissolved in ethanol-water mixture and stirred for 30 mins to form homogenous clear solution. 25% concentrated ammonia was then added slowly and drop wise in to this clear solution. White colored precipitate was then observed. This solution (slurry) was then stirred continuously for 2 hrs to form a uniform slurry. Obtained slurry was then filtered and washed with water several times. The final sample was then dried at 80 °C overnight. Final solid then calcined at 500 °C for 10 hrs in presence of air.

Active phase was deposited by impregnation method. Ammonium Meta vanadate was used as a precursor for synthesis process. The desired amount of precursor was dissolved in 20 mL of distilled H_2O. Then 1g of support was mixed with water and stirred. The precursor solution was then added to the solution which was stirred for 2 hrs. Continuously for aging and to make a uniform slurry. Afterwards, water was evaporated, and the remaining slurry dried at 80 °C. Finally, the sample was calcined for 10 hrs. in air at 500 °C using a ramping rate of 2°C/ min. In all cases, 25 Wt. % of V_2O_5 was used for the different supports.

4.2 - Characterization

The carriers were characterized in order to determine their physical properties such as the specific surface area, the particle size, their surface and bulk properties such as the composition, the crystallite size, the structure, etc.

4.2.1 - BET

Table 4.1 summarizes the properties of the different supports. SiO_2 and TiO_2 present the lowest surface areas among these supports and, coherently, the largest pore size. Silica surface area is rather low for such support, but the preparation method was not optimized to obtain high specific surface area materials. Commercial alumina shows the highest surface area as could be expected.

Support	Surface area (m²/g)	Pore volume (cm³/g)	Pore size (nm)
TiO_2	11.3	0.07	26.6
SiO_2	7.04	0.014	14.4
Al_2O_3	153.9	0.508	9.3
ZrO_2	22.3	0.012	3.03
CeO_2	61.6	0.099	5.46

Table 4.1: Characterization of support

Oxygen Carrier 25 Wt %	Surface area (m²/g)	Pore volume (cm³/g)	Pore size (nm)	average crystallite size (nm)	
				Support	V_2O_5
V_2O_5/TiO_2	7.2	0.058	61.5	88	51
V_2O_5/SiO_2	1.6	0.025	46	-	86.7
V_2O_5/Al_2O_3	118.8	0.365	8.98	10.4	59.1
V_2O_5/ZrO_2	21	0.025	5.24	32.5	56.9
V_2O_5/CeO_2	23.0	0.062	7.623	12.4	50.9

Table 4.2: XRD Study for different oxygen carrier

Table 4.2 summarizes the properties of the different supported 25 Wt% V_2O_5 solids obtained after impregnation

SiO_2 and TiO_2 present the lowest surface areas among other supports and, coherently, obtain high specific surface area materials. Commercial alumina shows largest pore size. Silica surface area is rather low for such support, but the preparation method was not optimized to

As expected for such high active phase loading, surface area and pore volume of the solids decrease after impregnation of V_2O_5 in case of the all support. Whereas in case of pore size it increases after loading, however, trend for the pore size is almost similar as in for the support.

Through the XRD study it was observed that the Al_2O_3, CeO_2 and ZrO_2 based solids present almost the same crystallite size of V_2O_5 (around 50-60 nm) irrespective of the crystallite size of the support. For SiO_2 based carrier, crystallite size of the V_2O_5 is 86.7 nm.

Bigger crystalline size is observed for TiO_2 support after impregnation. This is attributed to the presence of the big size particles over the support. Pore size and average crystallite of the TiO_2 with V_2O_5 is highest among all.

4.2.2 - XRD

XRD studies show the presence of V_2O_5 species on all supports irrespective of their surface area and nature. This is because of the high loading of the V_2O_5 present in the systems. In the graph •-represent the indication of V_2O_5. In every carrier,* represent the support.
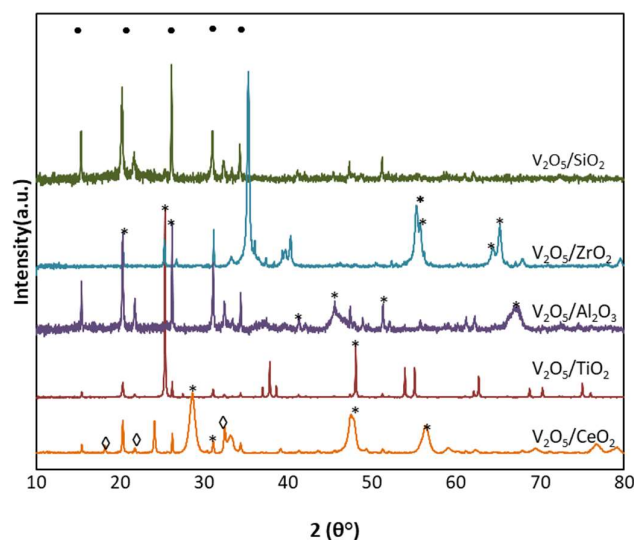
Figure 4.1: XRD Study for different oxygen carrier, ◊-CeVO₄,-Support, •-V₂O₅*

The Al_2O_3, CeO_2 and ZrO_2 based catalysts present almost the same crystallite size of the V_2O_5 around (50-60 nm) irrespective of the crystallite size of the support. Whereas in case of the SiO_2 catalysts, crystallite size of the V_2O_5 is 86 nm, that is practically identical to that of the bulk V_2O_5 studied in previous chapter.

V_2O_5 over TiO_2 illustrates the presence of the strong peak at 2Ө at 25.28 ° which represent the presence of TiO_2 peak with (1 0 1) plane of the tetrahedral structure of TiO_2, with reference to the JCPDF file (PDF 00-021-1272). Vanadium present on the support is in the orthorhombic structure of V_2O_5 (PDF 00-041-1426) and peak present at 20.7 ° illustrates the presence of the plane (0 0 1).

SiO_2 support is amorphous. During the XRD study only intense peaks of the V_2O_5 is observed on the support. There is no peak available to show the presence of the support SiO_2.

Cubic form of the Al_2O_3 is present in the solid V_2O_5-Al_2O_3, Peaks at 37.6° and 67.5° illustrates the presence of the strong peak for Al_2O_3, apart from that solid shows the intense peak for V_2O_5. With typical intense peak at 20.7 ° with (0 1 0) plane and 26.01 ° with (1 0 1) plane (PDF 04-012-3680).

Ceria-based solid illustrates the presence of the $CeVO_4$ species with strong peak at 18.12° with the plane of the (1 0 1) and 24.03° with (2 0 0) plane which corresponds to the tetragonal structure (PDF 00-012-0757). This is an evidence for the formation of the mixed oxide of Ce and V. Along with it strong intense peaks of the CeO_2 are also present. Peaks at 28.55° illustrates the presence of the CeO_2 with plane of (1 1 1) and at 33.08° represent the (2 0 0) plane with cubic structure. V_2O_5 is present on the support in the form of the orthorhombic structure with the plane of (0 0 1) at 20 3° and at 26.3° with (1 1 0) plane.

4.2.3 - TPR

Oxygen Carrier (25 Wt %)	H_2 consumption (TPR) (mmol/g)
V_2O_5/TiO_2	1.26
V_2O_5/SiO_2	2.81
V_2O_5/Al_2O_3	2.36
V_2O_5/ZrO_2	1.14
V_2O_5/CeO_2	3.50

Table 4.3: H_2 Consumption for supported oxygen carriers
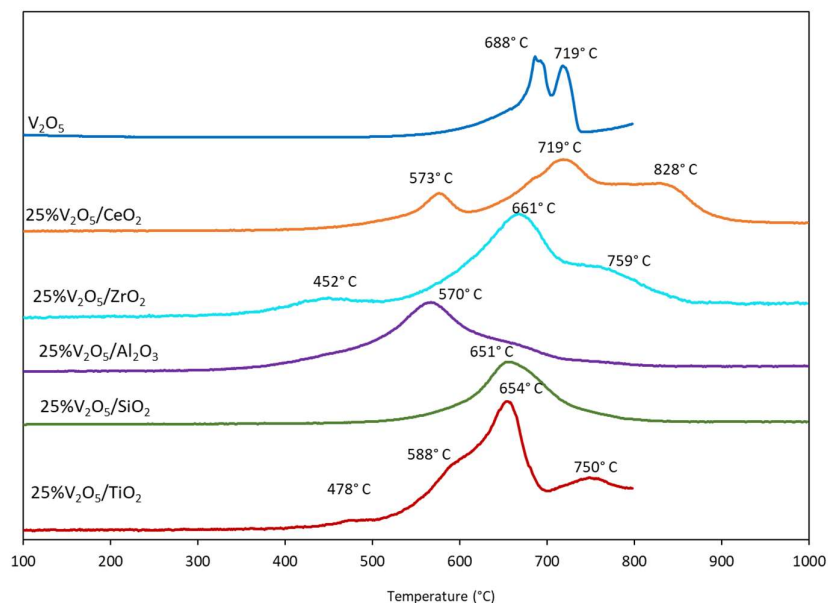
Figure 4.2: TPR study of Oxygen carrier

As shown by Wachs et al. [20] the nature and reactivity of surface vanadia species is strongly influenced by the specific nature of oxide support.

TPR study 25wt % on different supports show the presence of the several peaks at different temperatures that suggest the stepwise reduction of the V_2O_5 species which is present initially [40] but at lower temperature with respect to bulk V_2O_5. Bond et al. [94] stated that at high loading of the vanadium on TiO_2 generate paracrystalline V_2O_5 specie which show reduction at lower temperature.

On the other hand, Grzybowska et al. explained [95] that multiple reduction peaks located at 461, 661, 698 and 860 °C could be attributed to successive steps of the reduction to V_2O_3 via V_6O_{13} and V_2O_4, or/and to heterogeneity of V–O which are reduced.

The TiO_2 based solid exhibits four different peaks at 478 °C, 588 °C, 654 °C, and 750 °C represents the successive steps of the reduction of the V5+ to V4+. However, peaks at 480° C can be for the reduction of the V^{5+} or for the slightly impure TiO2 as suggested by Bond et al. [94].

Ceria based solid exhibits a peak at 573 °C which can correspond to the reduction of polyvanadate or crystalline V_2O_5 whereas peaks at high temperature at 719 °C and 828 °C corresponds to the reduction of the ceria species as shown by Shen et al. [96]. Hong He et al. [97] also attribute the reduction at the high temperature to bulk ceria, whereas Dogu et al. [98] proposed that the broad peak obtained at high temperature corresponds to the removal of oxygen from bulk of $CeVO_4$, resulting the reduction of V^{5+}.

Zirconia based solid shows a peak at 448 °C illustrating the reduction of the V_2O_5 species. Whereas the peak at high temperature represents the reduction at ZrO_2 [99].

For the alumina-based solid, in the TPR profile shows a peak present at the 570 °C attributed to the reduction of V^{5+} to V^{4+} (V_2O_4). Reduction peak for Al_2O_3 is absent in the spectrum [92]. Hugo I. de Lasa et al. [100] assigned the peak at 560 °C to the reduction of bulk V_2O_5-like surface species.

Finally, the TPR profile of SiO_2 based solid shows presence of the only one broad peak centered at 651 °C which represents the reduction of surface vanadia species.

The reduction temperature of vanadium specie supported on all supports is lower than that of bulk V_2O_5, which indicates that even if high loadings are considered the particle size and the interaction between active site and support are key factors in the reducibility of vanadium species.

4.2.4 - XPS

The V $2p_{3/2}$ and the O 1S XPS spectra were analyzed to determine the oxidation state of the vanadium impregnated on different supports.

Carrier	B.E (eV) O 1s			$V^{4+}/$ $(V^{4+}+V^{5+})$	$V^{5+}/$ $(V^{4+}+V^{5+})$	V/support	V/O
	O 1s	O 1s	O 1s				
V_2O_5/TiO_2	529.3	531.3	533	0.23	0.7	0.21	0.09
V_2O_5/SiO_2	530	-	533.1	0.10	0.9	0.18	0.44
V_2O_5/Al_2O_3	-	531.4	-	*	1	0.19	0.1
V_2O_5/ZrO_2	530.1	531.3	533	0.07	0.9	0.35	0.18
V_2O_5/CeO_2	530.3	531.4	-	0.06	0.9	2.65	0.36

Table 4.4: XPS study of the V 2p3/2 and the O 1S XPS s
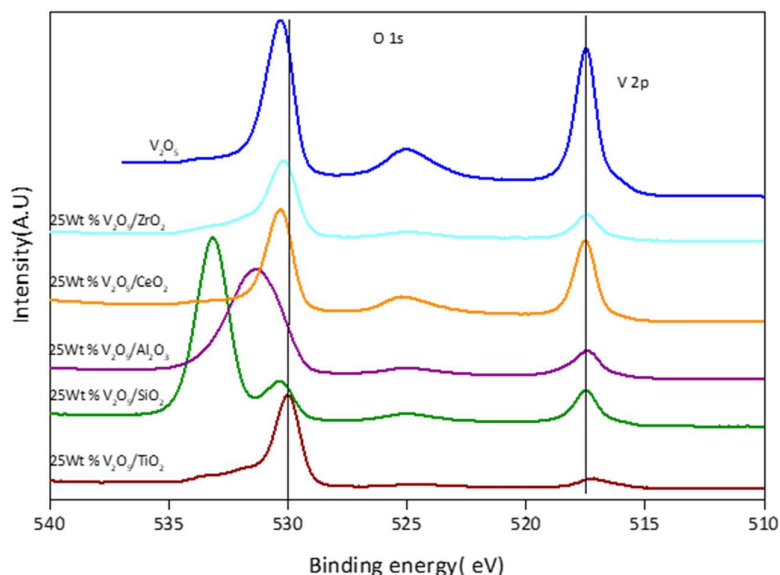
Figure 4.3: XPS study of the V $2p_{3/2}$ and the O 1S XPS

Different oxygen carrier shows the presence of different oxidation state depending on the interaction between the V_2O_5 and support. After deconvolution of the peaks for the different solids, it is evident that only V^{5+} and V^{4+} species are present in the systems. For example, in case of SiO_2 based solid, two peaks observed at binding energy 517.4 which represents the V^{5+} and peak at 516.0 illustrates the presence of the V^{4+}.

TiO_2 based solid present the highest amount of the V^{4+} compared to other solids, followed by SiO_2, ZrO_2, CeO_2 and finally Al_2O_3.

V/Support ratio increases from TiO_2 to CeO_2. Maximum ratio is observed in case of the ceria based solid (around 2.65), which correlates the presence of the big particle size of the vanadium on surface. TiO_2, SiO_2 Al_2O_3 give almost the same ratio. High ratio in ceria also represent the formation of the well-dispersed vanadium on the surface.

Regarding oxygen, three species are observed. However, explanation is not simple as the total oxygen content is not straightforward. Generally, peak at 530.4 eV is attributed to O in vanadium oxide [101]. In case of the SiO_2 catalyst, different oxygen species are present. From the deconvolution of the spectra, two components representing different chemical states are recognized. 533 eV illustrate the presence of the oxygen connected to the Si in SiO_2 [102]. So more oxygen is involved in the SiO_2 than V_2O_5. In case of TiO_2 based carrier, peak at 529.9 eV is attributed to oxygen from TiO_2 [103]. Peak at 531.3 eV exhibits the presence of the O in Ti" solid solution or Ti_2O_3 [104] while 533 eV is due to adsorbed molecular water [10]. In case of alumina based catalyst, 531.4 eV peak is attributed to the oxygen from Al_2O_3 [102].

4.2.5 - Raman
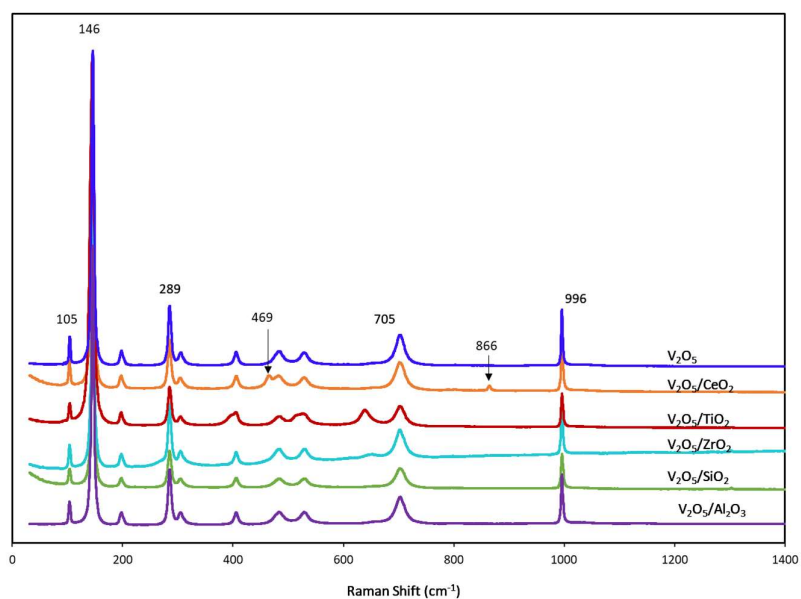
Figure 4.4: Raman study of different oxygen carrier

The narrow peak at 996 cm^{-1}, due to the symmetric stretching vibrations of V-O groups, is characteristic of crystalline V_2O_5. Additional bands observed near 705 cm^{-1} arise from the stretching vibrations of V–O in the square octahedron of V_2O_5. The peaks at 284, 304, 483, 702, and 997 cm^{-1} observed on all support are attributable to different crystalline V_2O_5 species.

For the ZrO_2 solid, peak present at 996 cm^{-1} can also coincide with the formation of the ZrV_2O_7 [99]. Nevertheless, the presence of the surface V_2O_5 can reasonably be supposed.

The peak present at 469 cm^{-1} on CeO_2 supported carrier can be attributed to the presence of the $CeVO_4$ which is also confirmed by a low intensity peak at 866 cm^{-1} [105].

For TiO_2 based carrier, the bands at 195, 400, 530, and 640 cm^{-1} are due to anatase. These coincide with the 133, 393, and 530 cm^{-1} peaks of V_2O_5 and makes it difficult to distinguish between the prominent species present for anatase and crystalline V_2O_5.

Due to the presence of the high loading of the V_2O_5 over the surface of all the supports, overall solid shows the presence of the formation of the dominant crystalline V_2O_5 in all cases.

4.3 - Reactivity of supported carriers in CLSOH

4.3.1 - Reactivity of supports

Before studying the properties of supported carriers, experiments were performed on supports without active phase. Results on the last stable cycle on TiO_2, SiO_2 and CeO_2 are summarized in Table 4.5. Al_2O_3 and ZrO_2 were not tested.

CeO_2 shows near total conversion with very high selectivity towards SO_2. This demonstrates

Support (m^2/g)	H$_2$S Conversion (%)	SO$_2$ Selectivity (%)
TiO$_2$(10)	7 (28 cy)	18 (28 cy)
SiO$_2$(7)	3 (9 cy)	13 (9 cy)
CeO$_2$(61)	98 (28 cy)	52 (28 cy)

Table 4.5: Reactivity of different support (150 °C)

that the ceria support itself plays the role of oxygen carrier.

Reactivity of the TiO_2 and SiO_2 supports are almost the same as illustrated in Figure 4.5. Low conversion of H_2S and rather low selectivity towards SO_2 are observed. However, in the case of TiO_2, SO_2 is principally formed in the reductant step, which indicates that TiO_2 can act, to some extent, as oxygen carrier. On the contrary, for SiO_2, SO_2 is most formed in the oxidant step suggesting the oxidation by dioxygen of adsorbed sulfur containing species. In terms of selectivity to S, values should be taken with caution. Indeed, as explained in Chapter 2, formation of the elemental sulfur is not observed directly but calculated by mass balance between consumed H_2S and SO_2 produced. For instance, at such low conversion, adsorption and accumulation of S species on the support cannot be excluded. For SiO_2 support, conversion of H_2S is low (around 5%), whereas for TiO_2 support, H_2S conversion reach 10% by the end of the cycling.
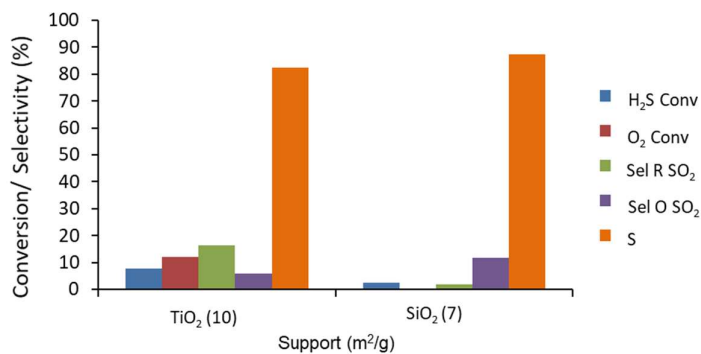
Figure 4.5: 200 mg of Support, 800 mg of SiC, 2000 ppm H_2S; 10000 ppm O_2, 150 °C

4.3.2 - Reactivity of supported V_2O_5
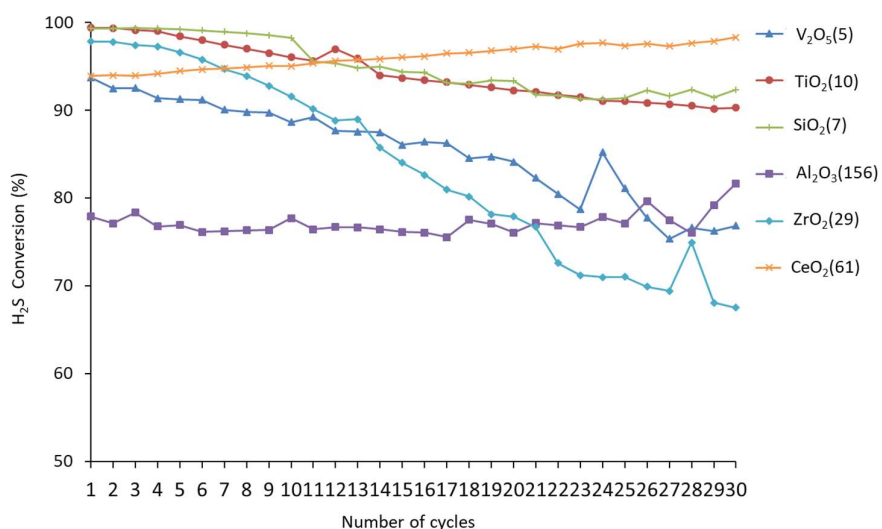
Figure 4.6: H_2S Conversion on 200 mg of V_2O_5/Support + 800 mg of SiC or 80 mg of V_2O_5 + 900 mg of SiC, 150 °C, 2000 ppm H_2S; 10000 ppm O_2

In Figure 4.6, the evolution of H_2S conversion at 150 °C with respect to number of cycles for different supported V_2O_5 solids as well as bulk V_2O_5 is shown. Experiments have been done in "standard" conditions, i.e. with 2000 ppm of H_2S, 10000 ppm of O_2 and 1 minute exposure to each reactant. Carriers were mixed to SiC to reach similar bed volume for all samples. SiC was checked to exhibit no reactivity.

H_2S conversion is very high for all solids as they all exhibit initial conversion above 90% with the exception of Al_2O_3 supported carrier (80%). The conversion evolves with cycling differently according to the nature of the support. Activity of Al_2O_3 supported carrier is stable, that on CeO_2 support increases. In other cases, the activity decreases progressively. This is particularly

the case for ZrO_2, while TiO_2 and SiO_2 show very similar evolutions from 100 to approx. 92-93% H_2S conversion.

The singular behavior of ceria, for which conversion of H_2S increases with cycles, could be due to the presence of $CeVO_4$ species in the solid which may participate to the reaction and contribute to the over-oxidation to SO_2 as seen in figure 4.7. Indeed, this solid exhibit the worst (highest) selectivity to SO_2 formation during the reductant step ($SO_2R = 10\%$). In the same time, this solid shows the highest amount of SO_2 formed during the oxidant step as can be seen in figure 4.8, and thus the worst overall selectivity to S formation.
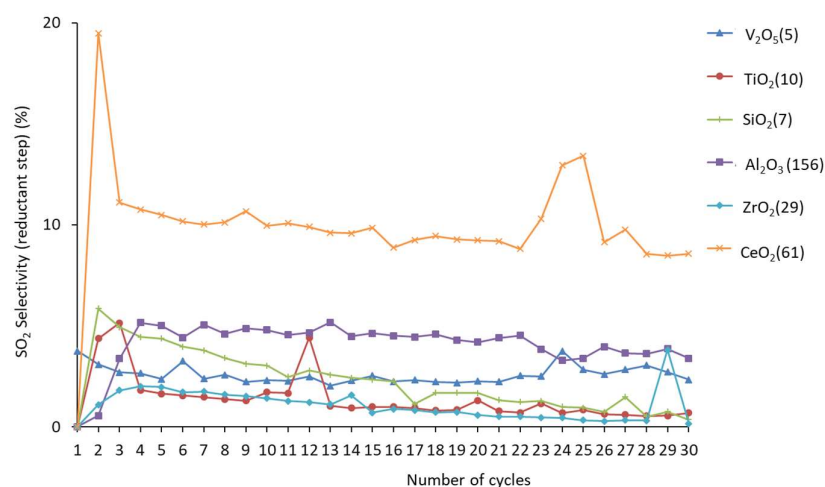
Figure 4.7: SO_2 selectivity (reductant step) on 200 mg of V_2O_5/Support + 800 mg of SiC or 80 mg of V_2O_5 + 900 mg of SiC, 150 °C, 2000 ppm H_2S; 10000 ppm O_2
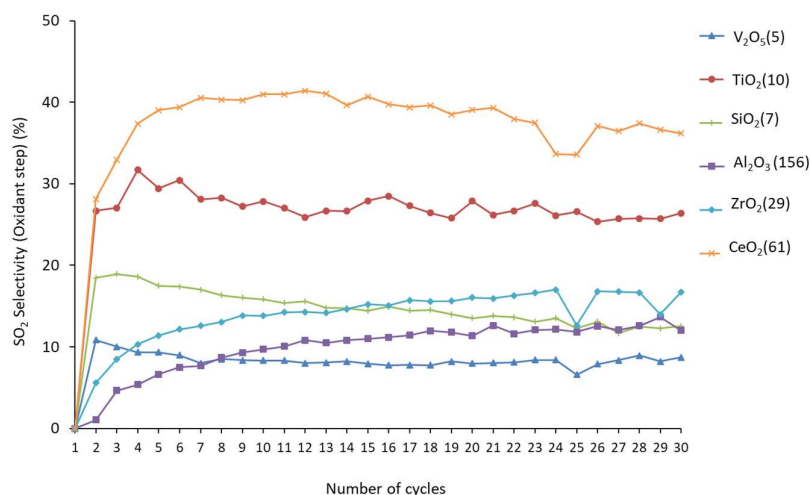
Figure 4.8: SO_2 selectivity (oxidant step) on 200 mg of V_2O_5/Support + 800 mg of SiC or 80 mg of V_2O_5 + 900 mg of SiC, 150 °C, 2000 ppm H_2S; 10000 ppm O_2
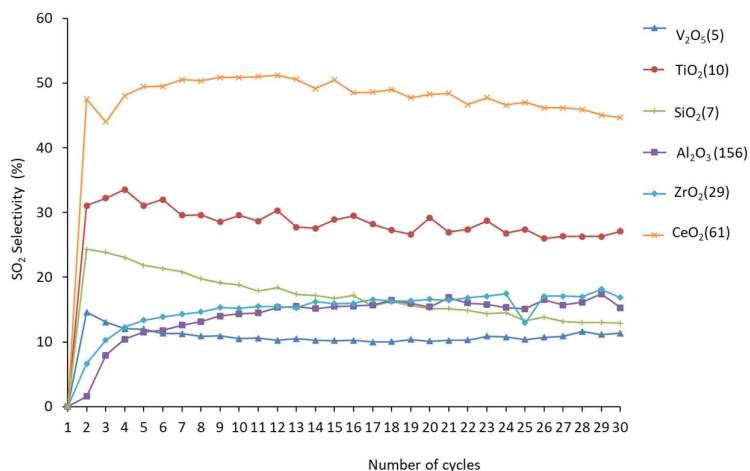
Figure 4.9: Total SO₂ selectivity on 200 mg of V₂O₅/Support + 800 mg of SiC or 80 mg of V₂O₅ + 900 mg of SiC, 150 °C, 2000 ppm H₂S; 10000 ppm O₂

Figure 4.10 summarizes the conversions and selectivity (in percentage) of the different solids (last cycles reported) while Table 4.6 provides similar data expressed in net amounts of reactant or products.
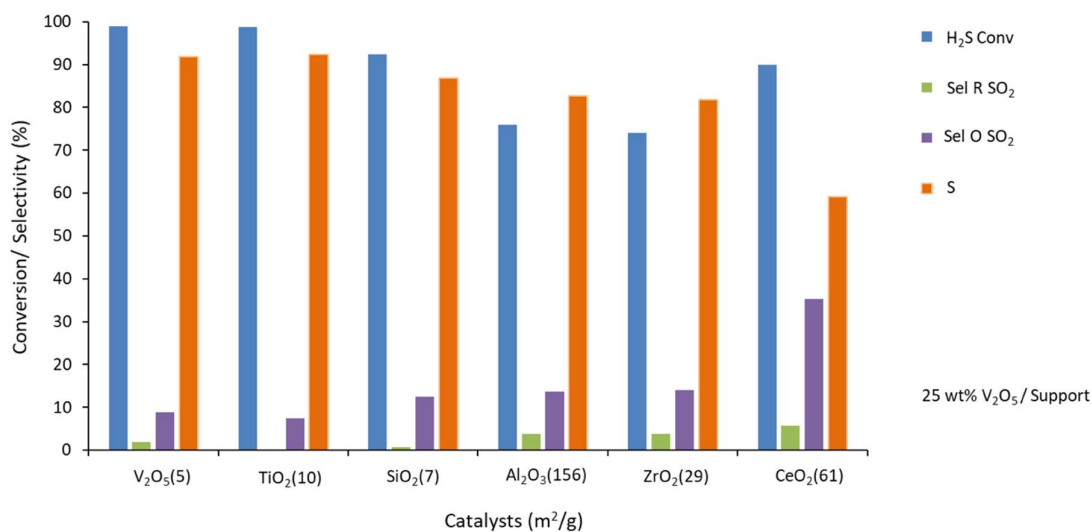
Figure 4.10: Overall reactivity (%ages,) 200 mg of V₂O₅/Support + 800 mg of SiC or 80 mg of V₂O₅ + 900 mg of SiC, 150 °C, 2000 ppm H₂S; 10000 ppm O₂

For reminder (see Chapter 3), V_2O_5 shows some formation of SO_2 during the reductant step but high selectivity towards the elemental sulfur (91%) is achieved during this step. Indeed, most SO_2 is formed during the oxidant step. As there is no support present in this case, V_2O_5

directly reacts with H_2S and 1.60 % of the lattice oxygen (considering reduction of V^{5+} to V^{4+}) is actually involved.

150 °C	V_2O_5	25wt%TiO_2	25wt%SiO_2	25wt%Al_2O_3	25wt%ZrO_2	25wt%CeO_2
H_2S feed (µmol)	8.6	8.6	8.6	8.6	8.6	8.6
% Conv H_2S	82	99	92	76	74	90
n converted (µmol)	7.05	8.74	7.94	6.94	6.36	7.92
S (µmol)	5.95	8.08	6.91	5.33	5.29	4.62
SO_2R (µmol)	0.37	0.01	0.06	0.26	0.25	0.46
SO_2O (µmol)	0.73	0.66	0.99	0.95	0.83	2.85
(S/S+SO_2R) (%)	94	99	99	95	96	91
%O_{latt} (V^{5+} to V^{4+})	1.60	2.8	2.45	2.14	2.11	2.06

Table 4.6: Overall reactivity (net amounts), 200 mg of V_2O_5/Support + 800 mg of SiC or 80 mg of V_2O_5 + 900 mg of SiC, 150 °C, 2000 ppm H_2S; 10000 ppm O_2

As mentioned above, all the supported V_2O_5 exhibit high conversions of H_2S (above 75%). Among these, TiO_2 based carrier lead to the maximum conversion of H_2S ~ 99% followed by SiO_2 and CeO_2 based carriers (90-92 %). Al_2O_3 and ZrO_2 show the lowest conversion of H_2S (≈75%) but still are in the same range as bulk V_2O_5.

SO_2 production is observed in the reductant step for Al_2O_3, ZrO_2 and CeO_2 supported V_2O_5 as for bulk V_2O_5. The amount is slightly higher for CeO_2 supported V_2O_5 which suggest a contribution of the support as active carrier coherently with the reactivity observed on the bare support.

Interestingly very low amounts of SO_2R are formed using TiO_2 and SiO_2 supports. These solids show nearly full selectivity to elemental S if one considers only the reductant step.

The amount of lattice oxygen involved in TiO_2 supported V_2O_5 is slightly higher than that of bulk V_2O_5 but is coherent with the lower amount of active phase used (80 mg for bulk and 200mg containing 25 wt% for supported samples, i.e. 50 mg V_2O_5) and the higher activity of the supported sample. For other samples, this amount decreases logically with decreasing conversion and/or increasing amount of SO_2 formed during oxidant step.

200 °C

Figures 4.11 provide the reactivity results observed at 200 °C on these solids.

With the exception of Al_2O_3 supported V_2O_5, H_2S conversion increases for all carriers. Globally, the selectivity to elemental S decreases significantly. SO_2 formed during reductant step increases for all samples, but particularly for TiO_2 and SiO_2 supported V_2O_5. At this temperature, bulk V_2O_5 actually shows the best overall selectivity.

As more lattice oxygen is required to form SO_2 than elemental S in the reductant step, the percentage of O_{latt} logically increases in line with the lower selectivity. This time, the amount of %O_{latt} involved increases more for the supported sample than for bulk V_2O_5 even considering the lower amount of active phase used. The supports seem to induce higher oxygen mobility or reactivity compared to bulk V_2O_5.
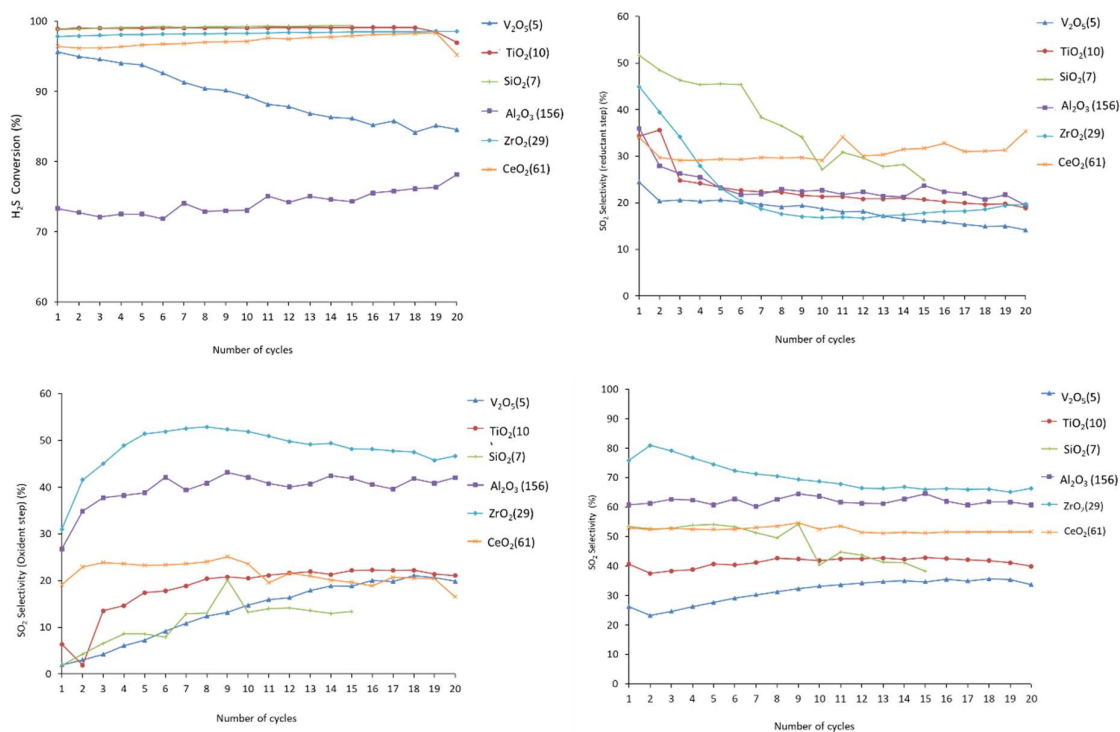
Figure 4.11: 200 mg of V_2O_5/Support + 800 mg of SiC or 80 mg of V_2O_5 + 900 mg of SiC, 200 °C, 2000 ppm H_2S; 10000 ppm O_2
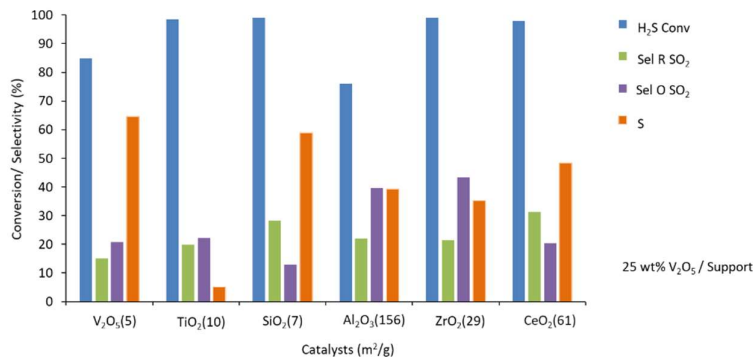
Figure 4.12: Overall reactivity (%ages,) 200 mg of V_2O_5/Support + 800 mg of SiC or 80 mg of V_2O_5 + 900 mg of SiC, 200 °C, 2000 ppm H_2S; 10000 ppm O_2

200 °C	V_2O_5	25wt%TiO_2	25wt%SiO_2	25wt%Al_2O_3	25wt%ZrO_2	25wt%CeO_2
H_2S feed (µmol)	8.6	8.6	8.6	8.6	8.6	8.6
% Conv H_2S	85	98.4	99	76	99	98
n converted (µmol)	7.31	8.71	8.51	6.54	8.51	8.62
S (µmol)	4.69	5.01	4.99	2.30	3.25	4.12
SO_2R (µmol)	1.09	1.75	2.41	1.47	1.74	2.72
SO_2O (µmol)	1.53	1.95	1.11	2.76	3.52	1.78
(S/S+SO_2R) (%)	81	74	67	61	65	60
%O_{latt} (V^{5+} to V^{4+})	1.81	3.60	4.23	2.36	2.99	4.23

Table 4.7 Overall reactivity (net amounts), 200 mg of V_2O_5/Support + 800 mg of SiC or 80 mg of V_2O_5 + 900 mg of SiC, 200 °C, 2000 ppm H_2S; 10000 ppm O_2

4.4 - General discussion and conclusions

These results show that the choice of support is crucial for the development of V_2O_5 oxygen carriers for chemical looping selective oxidation of H_2S. It will influence the reactivity of the active phase but can also play a role on the adsorption and activation of H_2S. Indeed, H_2S can form H-bond with surface OH groups of all the adsorbents. This adsorption phenomenon was studied and explained in detailed by F. Mauge [106]. Different supports like SiO_2, Al_2O_3, TiO_2, and ZrO_2 were used for the study of the adsorption of the H_2S on the surface. This is the only way of adsorption of the H_2S on SiO_2, while other supports may lead to coordination as well as dissociative adsorption which further leads to the formation of OH groups and molecular water. Specifically, on titania, coordination to surface cations is predominant. By studying Lewis acid sites, basic sites and proton-donating centers explains the adsorption on the surface.

These adsorbed species can then either remain on the surface and be oxidized during the oxidant step of chemical looping, in this case producing essentially SO_2, or be oxidized by the support if it has some redox capacity. This is clearly seen in the case of TiO_2 and, mostly, CeO_2.

Otherwise, the support mostly modifies the reactivity of V_2O_5. This is seen in TPR experiments for which, in case of all supports, the reduction temperature is significantly lowered by the presence of support even if crystallite size of V_2O_5 is in the same range as that of bulk V_2O_5 studied in previous chapter.

Due to the high reactivity of all supported carriers, it is difficult to make direct correlations between reduction temperature and H_2S oxidation properties.

On the other hand, it can be seen that the Al_2O_3 supported V_2O_5 shows the lowest initial reactivity (at 150 °C) compared to other supports. This solid also exhibits the highest V^{5+} (V^{4+} + V^{5+}) ratio as practically no V^{4+} species were detected on the calcined solid. Interestingly, all other samples show the presence of V^{4+} species and high initial activity, in particular TiO_2 supported V_2O_5 which has the highest proportion of V^{4+} species.

As mentioned, the CeO_2 supported V_2O_5 behaves singularly compared to other supports. Contrary to others, the activity increases with time but also selectivity is worse. This can be clearly attributed to the reactivity of CeO_2 but also to $CeVO_4$ species.

For other supports, the selectivity to SO_2 produced during reductant step also shows to be the highest for Al_2O_3 (Figure 4.6) suggesting that (i) partially reduced V^{4+} species at the surface enhance H_2S reactivity but also (ii) that fully oxidized surface vanadium species are less selective towards partial oxidation.

This is in line with S. Yasyerli et al. [24] who showed that fully oxidized vanadium species lead to over oxidation to SO_2 whereas partially reduced V^{2+} and V^{4+} species lead to selective oxidation to elemental sulfur in classical (co-feed) catalytic reaction. Holgado et al. [61] have also proposed that V_4O_9 phase characterized by V^{4+}-O-V^{5+} bonds is the most active, selective and stable for this reaction, thus highlighting the importance of partially reduced vanadium species.

From these results, it appears clearly that TiO_2 and SiO_2 are the most interesting supports for V_2O_5 for CLSOHS. In both cases, not only the reactivity is maintained but also selectivity during reductant step is improved. Indeed, for bulk V_2O_5, formation of some SO_2 during reductant step could not be avoided whereas this is the case for these two supports, in particular at low temperature.

To better understand the role of the support it was decided to concentrate future work on one specific support i.e. TiO_2.

Chapter V

Effect of loading of the V_2O_5 active phase on TiO_2 support

Chapter 5 - Effect of loading of the V_2O_5 active phase on TiO_2 support

TiO_2 proved to be a better support for the selective oxidation of H_2S in chemical looping as it has been seen in the previous chapter.

In this chapter, the main focus will be on the study of the effect of different V_2O_5 loadings on TiO_2 support to have a better understanding of the activity and selectivity of the process.

Initially, loading of V_2O_5 will be studied on a given TiO_2 support (10 m^2/g). In a second step, the effect of porosity and specific surface area of TiO_2 will be considered by comparing results obtained by using V_2O_5 on 10 and 45 m^2/g TiO_2.

5.1 - Solid preparation

Different loading of V_2O_5 with respect to the surface area of the support were used. With reference to the literature 0.1wt% $(V_2O_5)/m^2$g is considered to generate a single monolayer on the TiO_2 [40][45], [46][51] Thus, for TiO_2 with surface area of 10 m^2/g this would correspond to a loading of 1 wt%V_2O_5 and for, TiO_2 with surface area of 45 m^2/g this would correspond to a loading of 4.5 wt%V_2O_5. Thus, depending on the desired comparison which has to be done, V_2O_5 loading can be expressed in wt% or in terms of number of equivalent monolayers (ML).

These different V_2O_5/TiO_2 carriers were prepared by impregnation method followed by calcination. In impregnation method, oxalic acid solution has been used as an additive for the dissolution of the precursor. Ammonium meta vanadate was used as a precursor for synthesis processes. The desired amount of precursor was dissolved in 30 mL of 1M oxalic acid. Then 1g of support was added to the 20 ml of deionized water and stirred for 20 minutes. Further precursor solution added to the support solution drop wise. This solution was then stirred further for 2 hrs continuously for aging and to make a uniform slurry. Afterwards, water was evaporated and the remaining slurry dried at 80 °C. Finally, the sample was calcined for 10hrs. in air at 500 °C by ramping rate of 2 °C/ min. Different loadings of the V_2O_5 were used to prepare the carriers and are expressed in terms of number of equivalent monolayers (ML). For the TiO_2 (10m^2/g) support, solids were prepared containing 0.5wt% noted 0.5ML10, 1wt% noted 1ML10, 1.5wt% noted 1.5ML10, 2wt% noted 2ML10, 5wt% noted 5ML10, 10wt% noted 10ML10 and 15.5wt% noted 15.5ML10. Whereas for TiO_2 with 45 m^2/g, solids contained 2.25wt% V_2O_5 noted 0.5ML45, 4.5wt% noted 1ML45, 7.42wt% noted 1.65ML45, 9wt% noted 2ML45 and 22.5wt% noted 5ML45.

All the catalysts were characterized by using different technique (BET, XRD, H_2- TPR, XPS, and Raman).

This chapter is divided in two parts. First, the solids with different loadings on TiO_2 10 m^2/g are studied. Then the properties are compared with those using 45 m^2/g TiO_2. Various factors

are studied in detail as already seen in the previous chapter, in particular the concentration of the reactants, the ratio of the reactant and the temperature.

5.2 - Characterization of V_2O_5 over TiO_2 10 support

5.2.1 - BET

Surface area of the all solid oxygen carriers are similar after addition of the different loadings of the active phase. Pore size and pore volume of the solids are very small and do not show much difference.

Oxygen carrier	Surface area (m²/g)	Pore volume (cm³/g)	Pore size (nm)	H$_2$ consumption (mmol/g)	Crystallite size (nm) V$_2$O$_5$
TiO$_2$(10)	11.3	0.07	26.6	-	-
V$_2$O$_5$	5.5	0.03	18.4	4.62	86
0.5ML10				0.18	n.o.
1ML10	13.8	0.06	20.6	0.11	n.o.
1.5ML	8.5	0.03	15.1	0.14	n.o.
2ML10	9.5	0.05	22.8	0.14	n.o.
5ML10	9.4	0.04	19.2	0.53	75
10ML10	10.5	0.11	48.2	1.02	65
15ML10	9.7	0.09	30.9	0.48	96

Table 5.1: Characterization of oxygen carrier (n.o. = not observed).

5.2.2 - XRD
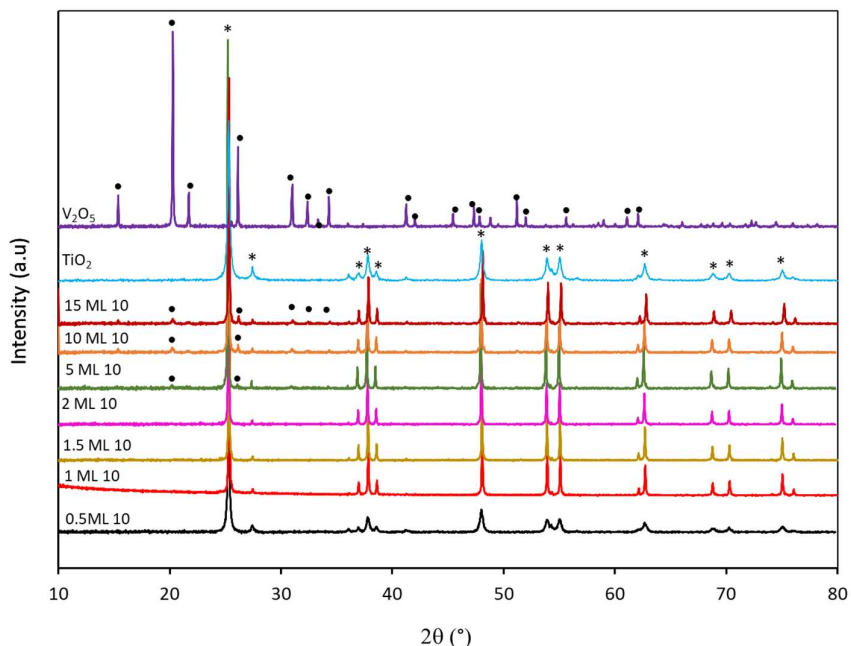
Figure 5.1: XRD study of different oxygen carrier, * support, • V$_2$O$_5$

XRD diffractograms of different samples are shown in Figure 5.1 were (•) symbol is attributed to the presence of V$_2$O$_5$ and (*) symbol to the TiO$_2$ support. The strong peak at 2Ɵ at 25.28° represent the (1 0 1) plane of the tetrahedral structure of TiO$_2$, with reference to the JCPDF file (PDF 00-021-1272).

At low monolayers below 2ML10 there is no evidence of the presence of the V$_2$O$_5$ species on the support, this can happen due to homogeneous layer formation on the support or due to the detection limit of the instrument. Crystallite size of the vanadium species does not follow the particular pattern but at the highest loading maximum crystallite size of the V$_2$O$_5$ is observed (96.3nm).

Above 2ML, presence of the V$_2$O$_5$ is evident at the position 20.7°, attributed to the plane (0 0 1) for orthorhombic structure. Peak at 26.2°, illustrates the presence of the (1 0 1) plane. Intensity of the V$_2$O$_5$ peak increases with increases in the loading of V$_2$O$_5$.

5.2.3 - XPS
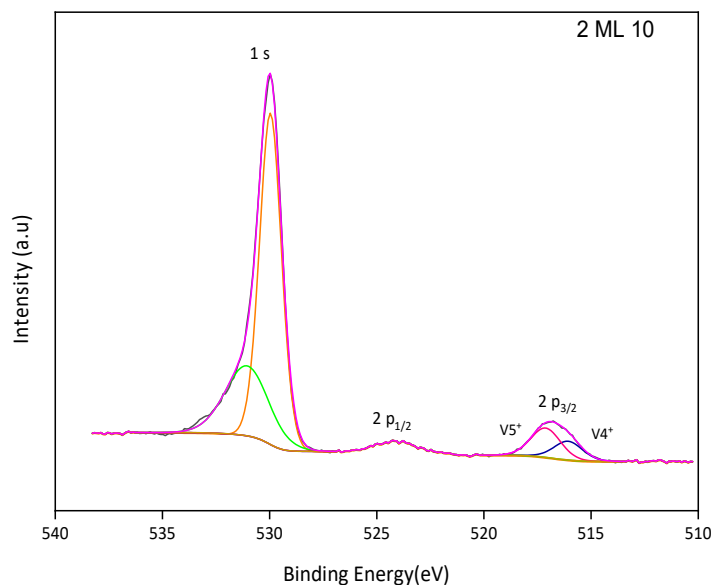
Figure 5.2: XPS pattern for O 1s and V 2p core level 2ML10

Figure 5.2 represents the XPS deconvolution pattern for 2ML10 solid. The V $2p_{3/2}$ photopeak shows two contributions at binding energies of 517.7 eV and 516.1 eV. These are close to the values usually attributed to V^{5+} and V^{4+} in V_2O_5 phase. O1s provides two peaks after deconvolution with peak at 529.9 eV attributed to oxygen from TiO_2 whereas the high binding energy peak (531.0-532.8 eV) corresponds to adsorbed oxygen, hydroxyl and/or carbonate groups which reflects the presence of anionic vacancies[85][107].

XPS spectra for all samples are shown in Figure 5.3. Similar deconvolutions calculations were performed for all samples and results are presented in Table 5.2.
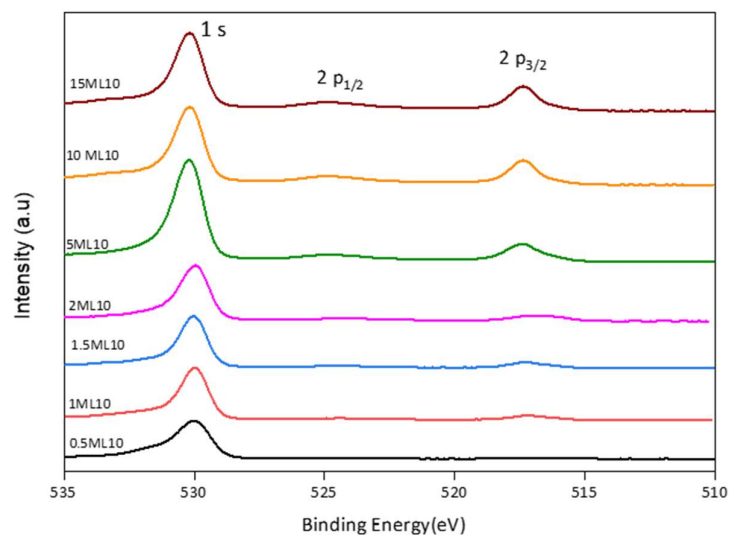
Figure 5.3: XPS pattern for O 1s and V2p core level different oxygen carrier

Oxygen Carrier	B.E (eV) V 2p		$V^{4+}/$ $(V^{4+}+V^{5+})$	$V^{5+}/$ $(V^{4+}+V^{5+})$	V^{4+}/V^{5+}	V/O	V/Ti
	V^{4+}	$V5^{+}$					
0.5ML10	*	516.7	*	1.00	*	0.01	0.04
1ML10	516.2	517.3	0.29	0.71	0.41	0.05	0.16
1.5ML10	516.0	517.3	0.24	0.76	0.31	0.07	0.16
2ML10	516.1	517.1	0.38	0.62	0.62	0.08	0.22
5ML10	516.1	517.4	0.13	0.87	0.14	0.10	0.33
10ML10	516.0	517.4	0.09	0.91	0.10	0.16	0.65
15ML10	515.9	517.0	0.11	0.89	0.12	0.16	0.64

Table 5.2: XPS study of the V 2p $_{3/2}$ and the O 1s

The V 2p 3/2 and the O 1s XPS spectra were analyzed to determine the oxidation state of the vanadium. The binding energies for the photopeak V 2p$_{3/2}$ remain almost unchanged at 517.7 eV close to the values currently attributed to V^{5+} further confirmed by the difference in energies between O 1s and V 2p$_{3/2}$ photopeaks. Presence of the V^{4+} species is clearly evident in all the samples at 516.6eV irrespective of the vanadium loading except in 0.5ML10. Presence of the V^{4+} is influenced by the change of crystalline size as well as the presence of surface vanadate species dispersed at the surface. 2ML 10 presents the highest proportion of V^{4+} species as seen by the ratio of V^{4+}/V^{5+}.

V/Ti ratio increases with the increasing loading of V_2O_5. At high loading, i.e. 10ML10 and 15ML10 V/Ti ratio is similar which indicates the presence of big crystallites of the V_2O_5.

For oxygen species, peak at 530.4 eV is attributed to O in vanadium oxide [101]. For all carrier, peak at 529.9 is attributed to oxygen from TiO_2 [103].

5.2.4 - TPR
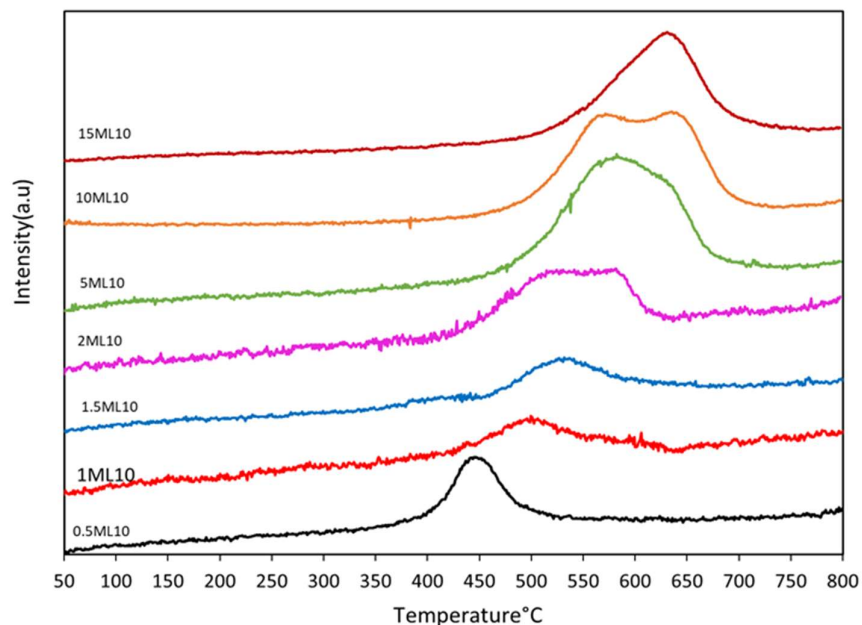
Figure 5.4: TPR study of different Oxygen carrier

With the increase in the loading of the active species, increase in the TPR peak is observed.

For the different oxygen carriers above 1.5ML two peaks of reduction are observed which indicate a stepwise reduction of V_2O_5:

$$V_2O_5 \rightarrow V_2O_4$$

$$V_2O_4 \rightarrow V_2O_3.$$
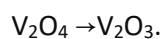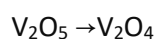
As temperature increases from the 430 °C to 630 °C with increasing Vanadium content, more prominent presence of V_2O_5 is confirmed.

Low temperature reduction peak at low ML (0.5ML10 and 1ML10) indicates the presence of the VOx species as supported by A.T Bell et al. [108] who explain that the terminal oxygen of the monomeric and polymeric species are much more labile (with respect to reduction by H_2) than the V-O-V bridging oxygen of the polymers. Bond et al. also describe [40] the different behavior for TPR profiles at different monolayers. If less than four monolayers are present, only a single TPR peak is a present, while above four monolayers an additional TPR peak at

high temperature is present, which grows in size with vanadium content. This corresponds well with the results observe in Figure 5.4.

In the case of 2ML10 a large peak is observed which can be composed of two contributions including both VOx species and V_2O_5 species.

The small peak to the surface V^{5+} reduction, this reduction peak moves to the lower temperature by decreasing the vanadium contain on the surface. 5ML indicates the broad peak at high temperature which indicates after deconvolution by two peaks at 520 °C and 630 °C. 15ML10 illustrates highest amount of the V_2O_5 and gives peak at high temperature. Loss of the doublet of the peak at vanadium content can be due to various reasons such as the low specific surface area after higher vanadium loading, the agglomeration of monomeric vanadium species by getting large V_2O_5 clusters. Nonetheless the reduction temperature is still lower than that of bulk V_2O_5 (at 686 °C and 716 °C, Figure 3.4), signifying that the particle size of V_2O_5 is a key factor in the reducibility of the vanadium species. Thus, the catalysts with small particles of V_2O_5 possess the a higher interaction with the support, favoring the reducibility than bulky ones as stated E. R-Castellan [109].

5.2.5 - Raman

The Raman spectra for different carriers are reported in Figure 5.5.
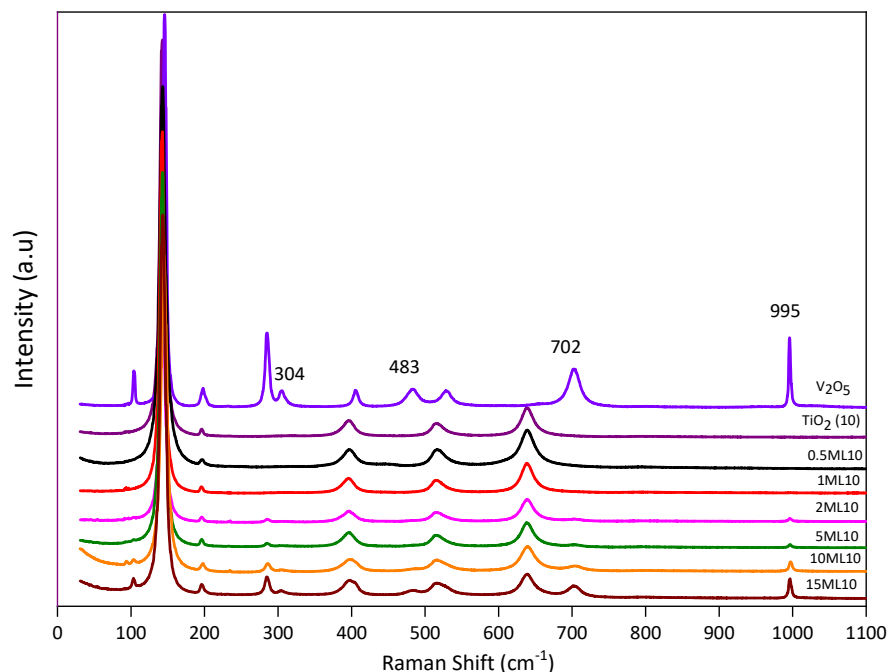
Figure 5.5 (a): Raman study of different Oxygen carrier
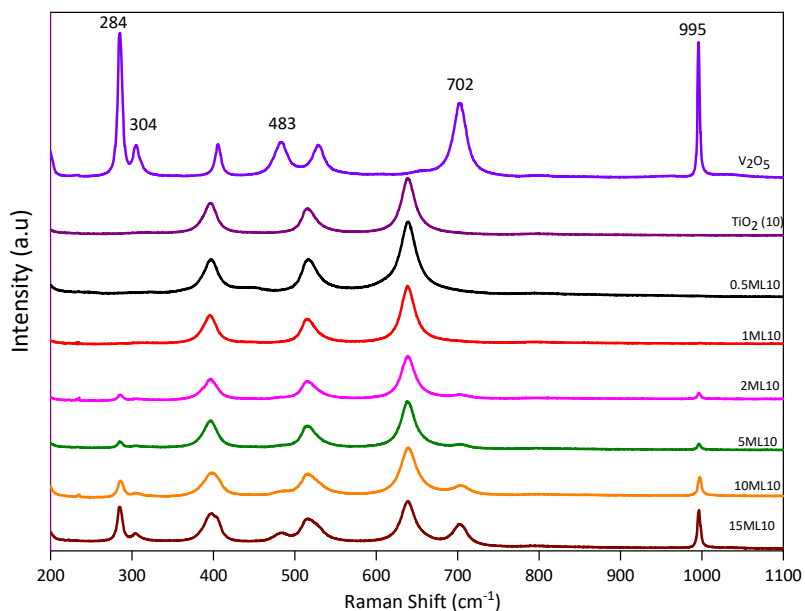
Figure 5.5 (b): Raman study of different Oxygen carrier (zoom section)

Raman study shows the presence of the different species of vanadium over the surface of the support. Presence of the vanadium is evident in the spectrum on samples containing at least 2 monolayers (2ML10 and more). Indeed, the peaks at 284, 304, 483, 702, and 997 cm^{-1} observed at higher loadings after 2ML10 are attributable to different crystalline V_2O_5 species. The most intense of these bands, located at 997 cm-^{1}, is primarily due to the symmetric stretch of V=O groups in the bulk with the symmetrical stretching mode of the terminal oxygen atom (V=O) as shows in the literature [40] [110], [111]

In the spectrum, the bands at 195, 400, 530, and 640 cm^{-1} are due to anatase. Peak present at 133, 393, and 530 cm^{-1} coincides with the peak present for the V_2O_5, making it difficult to distinguish between the prominent species present for anatase. Bond the difficulties in detecting VO_4^{3-} tetrahedra peak due to overlap with the strong TiO_2 (anatase) bands [40]. Same results are observed in the spectrum for all the solids including low loadings of V_2O_5 (0.5ML10).However, as explained in the literature, dominant isolated VO_4^{3-} tetrahedra species at 830 cm^{-1} are surprisingly absent in all the samples.

Peak in the spectrum at 284 cm^{-1} is for the deformation of V=O, whereas those at 304 and 702cm^{-1} correspond to the oxygen bridging with three vanadium atoms. Peak present at the position 485 cm^{-1} is attributed for the V–O–V structure. Peak at 485 cm^{-1} is only observed at high loading of the V_2O_5 i.e. for 10M10 and 15ML10. This peak position in the spectrum coincides with the literature as showed by E. Bordes-Richard [50].

In the literature, A. T. Bell et al. [108] observed the presence of the polymeric vanadates at 700-1100 cm^{-1} region. He further added that, as the number of vanadium centers in the polyvanadates increases, the number of terminal V=O groups per vanadium decreases to form the V-O-V bonds. This results in a shift in the frequency of the remaining V=O bonds to 997 cm^{-1}.

5.3 - Reactivity at low V$_2$O$_5$ loadings (0.5ML10, 1ML10, 1.5ML10)

The study of the reactivity of oxygen carriers in chemical looping is complex as many parameters have to be considered simultaneously. For example, when changing the active phase loading on the support, ideally the amount of carrier used during the reactivity test should be adapted accordingly in order to have the same amount of Vanadium species (or equivalent V$_2$O$_5$) involved. Unfortunately, this was not done systematically also taking into account technical limitations in terms of volume of carrier that could be inserted in the reactor. For this reason, the comparison between reactivity of carriers with different loadings of V$_2$O$_5$ is divided into this section devoted to low loadings and section 5.4 devoted to higher loading.

The reactivity of the low V$_2$O$_5$ loaded solids were tested in "standard" conditions, i.e. exposing to 1000 ppm H$_2$S for 1 minute and O$_2$ 10000 ppm (H$_2$S:O$_2$ = 1:5) for 1 minute with 2 minutes' purge of Ar inbetween the reactants. Flow was kept constant at 100 ml/min. Samples were tested at 150 °C and 200 °C.

150 °C
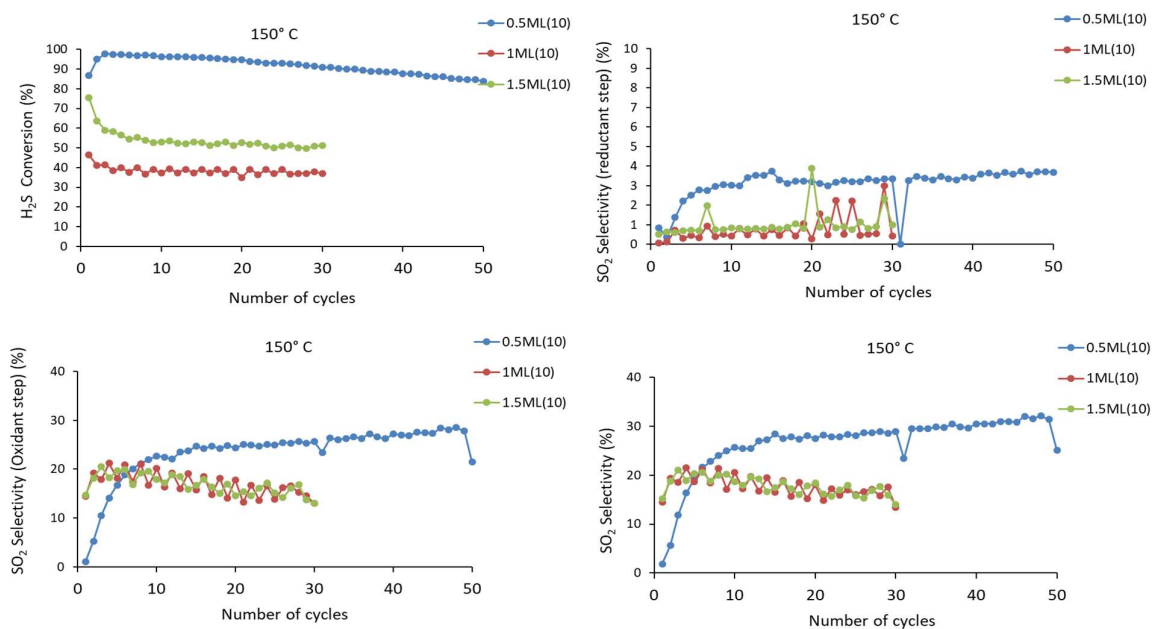
Figure 5.6: 200 mg (0.5ML 10), 100 mg (1ML10, 1.5ML10), 150 °C, H$_2$S:O$_2$ 1:5, 2000 ppm of H$_2$S
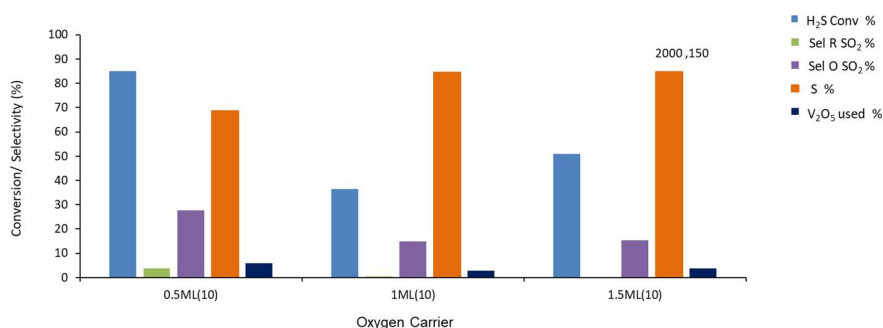
Figure 5.7: 200 mg (0.5ML 10), 100 mg (1ML10, 1.5ML10), 150 °C, $H_2S:O_2$ 1:5, 2000 ppm of H_2S

150° C	0.5ML10 (200 mg)	1ML10 (100 mg)	1.5ML10 (100 mg)
H_2S feed (µmol)	8.80	8.80	8.80
% Conv H_2S	85.0	36.5	51.0
n converted (µmol)	7.52	3.21	4.49
S (µmol)	5.12	2.70	3.79
SO_2R (µmol)	0.28	0.02	<0.01
SO_2O (µmol)	2.12	0.50	0.70
$(S/S+SO_2)$ (%)	98.5	95.0	99.0
%O_{latt} (% V^{5+} -> V^{4+})	108.2	46.8	45.7

Table 5.3: 200 mg (0.5ML 10), 100 mg (1ML10, 1.5ML10), 150 °C, $H_2S:O_2$- 1:5, 2000 ppm of H_2S

Figures 5.6 show the detailed evolution of reactivity of 0.5ML10, 1ML10 and 1.5ML10 with cycling while Figure 5.7 compares graphically the reactivity reached at the end of the experiments. The quantitative results obtained on last cycles are reported in Table 5.3.

It must be noted that the amount of carrier used for 0.5ML10 differs (200 mg) in order to take into account presence of the less V_2O_5 in the system, while 100 mg were used for 1ML10 and 1.5ML10.

For 1.5ML10, H_2S conversion is stable around 51 %. 1ML10 carrier also shows a stable behavior with an average conversion of the 35 %. It is the lowest among all samples. These samples show very similar selectivity with very low amounts of SO_2 formation during the reductant step. They also show similar ratio of lattice oxygen involved (45-46 %) if one takes as reference the reduction of V^{5+} to V^{4+} and the amount of V_2O_5 is the sample.

The difference in reactivity, both in terms of conversion and selectivity, between these samples can therefore be simply accounted for the presence of more vanadium in the reactor.

0.5ML10 shows the highest H_2S conversion but evolves along cycling from 100 to 85 %. SO_2 formation in the reductant step is higher and increases with cycling. The amount of SO_2 produced during oxidant step is also the highest and also increases with cycling.

Due to the strong dispersion of active species on the surface of the support at such low loading, it is possible that S containing species remain adsorbed on the surface after reductant cycles. If these species are not in close contact with the active phase this could make the re-oxidation process less efficient and generate an accumulation between cycles. This could explain the increase of SO_2 produced in oxidant as with increasing amounts of sulfur containing species accumulate they necessarily get in closer contact with the active phase.

For this sample, the amount of lattice oxygen involved in the reductant step is very high (108 %). As this value is calculated considering only V^{5+} reduction to V^{4+}, a value higher than 100 % indicates that the reduction to V^{3+} must occur.

200°C
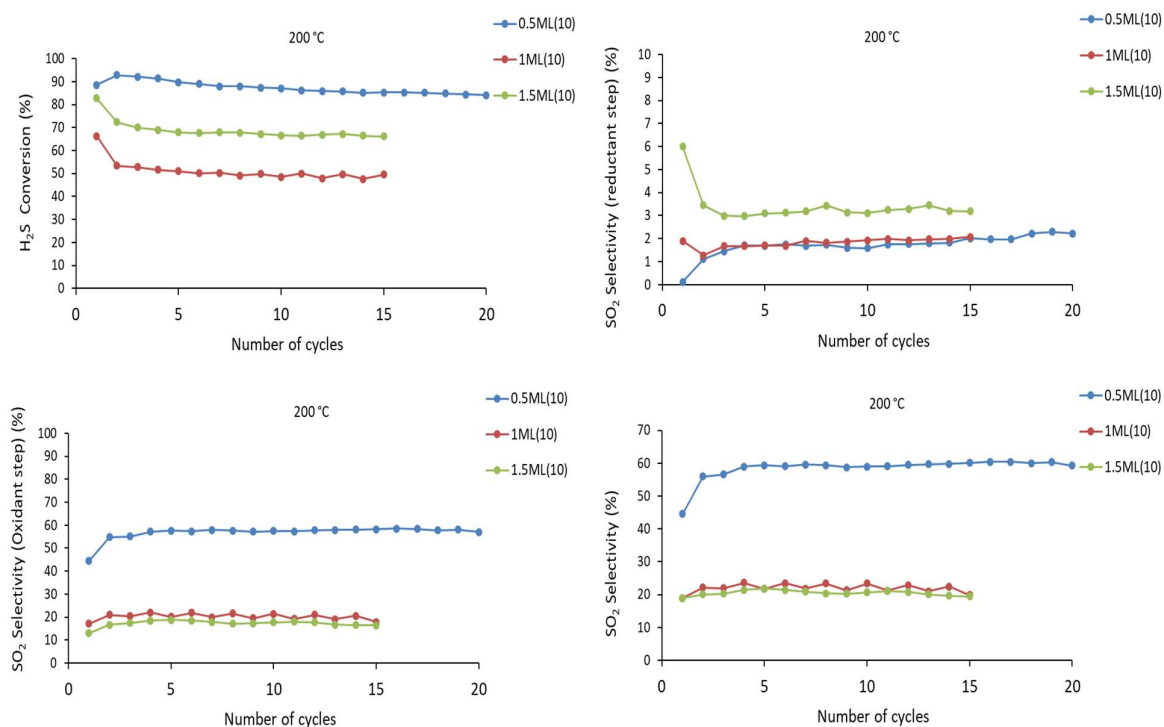
Figure 5.8: 200 mg (0.5ML 10), 100 mg (1ML10, 1.5ML10), 200 °C, $H_2S:O_2$ 1:5, 2000 ppm of H_2S
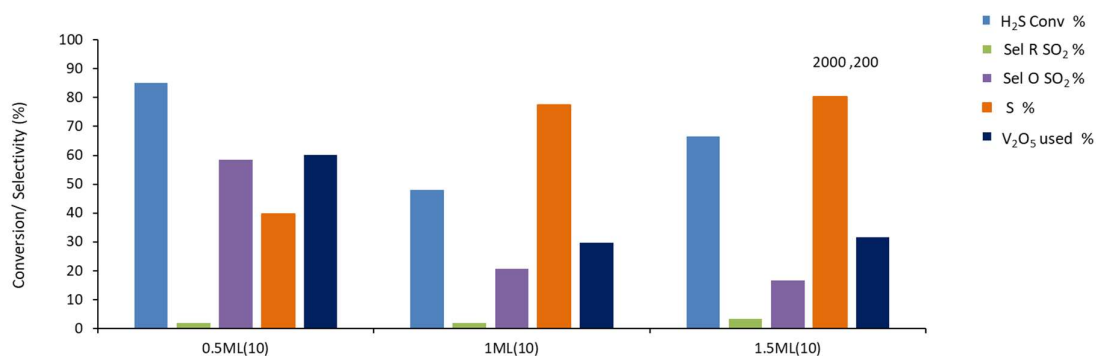
Figure 5.9: 200 mg (0.5ML 10), 100 mg (1ML10, 1.5ML10), 200 °C, $H_2S:O_2$ 1:5, 2000 ppm of H_2S

200 °C	0.5ML10 (200 mg)	1ML10 (100 mg)	1.5ML10 (100 mg)
H_2S feed (µmol)	8.5	8.0	8.6
% Conv H_2S	85.0	48.0	66.5
n converted (µmol)	7.52	4.22	5.85
S (µmol)	2.86	3.24	4.68
SO_2R (µmol)	0.15	0.08	0.18
SO_2O (µmol)	4.52	0.90	0.99
(S/S+SO_2) (%)	95.1	97.5	96.2
%O_{latt} (% V^{5+} -> V^{4+})	60.1	59.4	63.4

Table 5.4: 200 mg (0.5ML 10), 100 mg (1ML10, 1.5ML10), 200 °C, $H_2S:O_2$- 1:5, 2000 ppm of H_2S

At 200 °C, general trend observed for reaction is similar as at 150 °C for 1ML10 and 1.5ML10. Again, these solids show rather similar behaviors and the difference in reactivity can be accounted to the difference in amount of vanadium present in the reactor.

Whereas for 1ML10 and 1.5ML10 the conversion increases with temperature, for 0.5ML10 it is almost same at both the temperature at 85%. Contrary to reaction performed at 150 °C, this conversion is stable along cycling. The amount of SO_2 produced during reductant step is slightly lower. The most striking is the increase in the SO_2 formation during the oxidant step.

This means that although most of the H_2S is adsorbed on the surface of the sample (leading to high overall conversion), a large part is not fully converted to S or SO_2 in the reductant step. This reflects also in the amount of lattice oxygen involved which decreases from 108 % at 150 °C to 60 % at 200 °C.

As mentioned, the differences between the reactivity of 1ML10 and that of 1.5ML10 can be easily accounted by the highest amount of V_2O_5 present in the reactor. At these loading, the reactivity does not seem to be affected by differences in the distribution of vanadium species.

Comparing 0.5ML10 and 1ML10 provide more interesting elements as these experiments were performed with the same amount of vanadium species as proportional amount of carrier were employed.

On the other hand, using more carrier with low loading has another experimental repercussion that need to be taken into account. i.e. that the absolute value of carrier surface exposed in the reactor is double in case of 0.5ML10 with respect to 1ML10. This can have an influence on the total amount of H_2S which can adsorb on the surface in the reductant step, and thus explain the higher overall conversion of H_2S at both temperatures for 0.5ML10 compared to 1ML10. In terms of S and SO_2 formation in reductant step, 0.5ML10 and 1ML10 show very similar results at 200 °C which, at this temperature, is coherent with the fact that similar amounts of active phase are present.

In other words, at 200 °C the behavior of the different carriers do not differ significantly if one focus on the amount of active phase used. The reactivity does not seem affected by the dispersion of the active phase.

The situation is very different at lower temperature for which the amount of SO_2 formed in oxidant step at low loading 0.5ML10 is much lower than at high temperature. The overall conversion being similar, this means that the vanadium species are actually more reactive at such lower temperature. This is seen also in the amount of lattice oxygen involved which implies that reduction to V^{3+} need to be considered. One explanation could reside in the oxidant step. Indeed, the carrier re-oxidation could also be affected by the lowering of the temperature. Partially reduced V species would be present on the surface from the start of the reductant cycle and could show higher reactivity.

5.4 - Effect of different amounts of 0.5ML10 and comparison to 2ML10

As seen in the previous section, 0.5ML10 gives significantly different activity in terms of the H_2S conversion and selectivity at low temperature. This could be attributed to deeper reduction of the solid. Here we compare the reactivity of this sample using different amounts of carrier in order to be able, in the next section, to compare reactivity with higher loading samples. 200 and 900 mg of 0.5ML10 were thus tested in "standard" conditions.
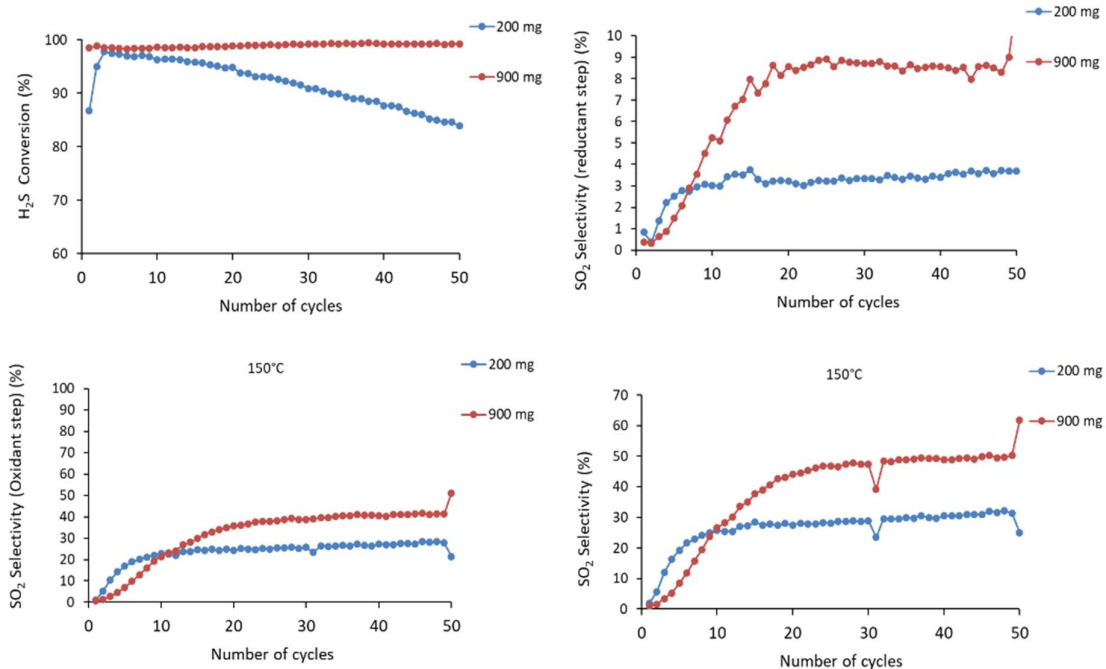
Figure 5.10.: 200 mg (0.5ML 10), 900 mg (0.5ML 10), 150 °C, H₂S:O₂ 1:5, 2000 ppm of H₂S
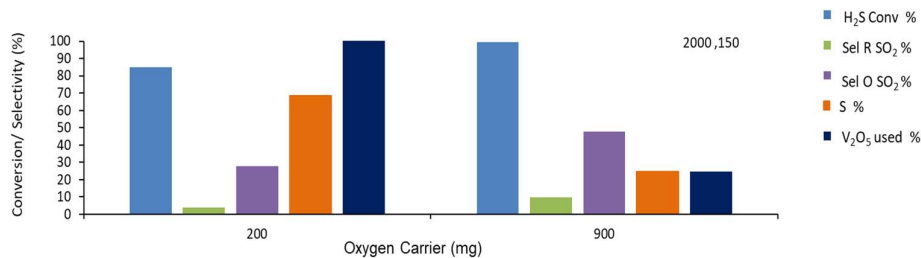
Figure 5.11.: 200 mg (0.5ML 10), 900 mg (0.5ML 10), 150 °C, H₂S:O₂ 1:5, 2000 ppm of H₂S

0.5ML10, 150° C	200 mg	900 mg
H_2S feed (µmol)	8.6	8.6
% Conv H_2S	85.0	99.0
n converted (µmol)	7.52	8.55
S (µmol)	5.12	3.47
SO_2R (µmol)	0.28	0.87
SO_2O (µmol)	2.12	4.20
$(S/S+SO_2)$ (%)	94.9	79.9
$\%O_{latt}$ (% V^{5+} -> V^{4+})	108.2	24.6

Table 5.5: 200 mg (0.5ML 10), 900 mg (0.5ML 10), 150 °C, H₂S:O₂- 1:5, 2000 ppm of H₂S

Full conversion of H_2S is observed using 900 mg of carrier, which could be expected both by the presence of more surface exposed for H_2S adsorption and by an excess of active phase. The latter can also explain the production of more SO_2 during reductant step. Interestingly however, selectivity evolves along with cycling while using 900 mg of carrier whereas it reached a stable behavior much more rapidly using 200 mg.

Most important is that the amount of SO_2 produced during oxidant step increases significantly with 900 mg of carrier. This is rather unexpected considering, again, that the active phase is in excess as compared to H_2S. Nevertheless, the increase of carrier amount also implies that more support surface is exposed to H_2S and could allow more unreacted species to accumulate on its surface as proposed earlier.

5.4.1 - Comparison between 0.5ML10 and 2ML10

In order to bridge the study between low loading carriers and that on higher ones presented in next section, it is necessary to compare 0.5ML10 and 2ML10 samples considering a similar amount of V_2O_5 in the reactor. Thus, reactivity of 900 mg 0.5ML10 (shown above) and 200 mg 2ML10 are compared.
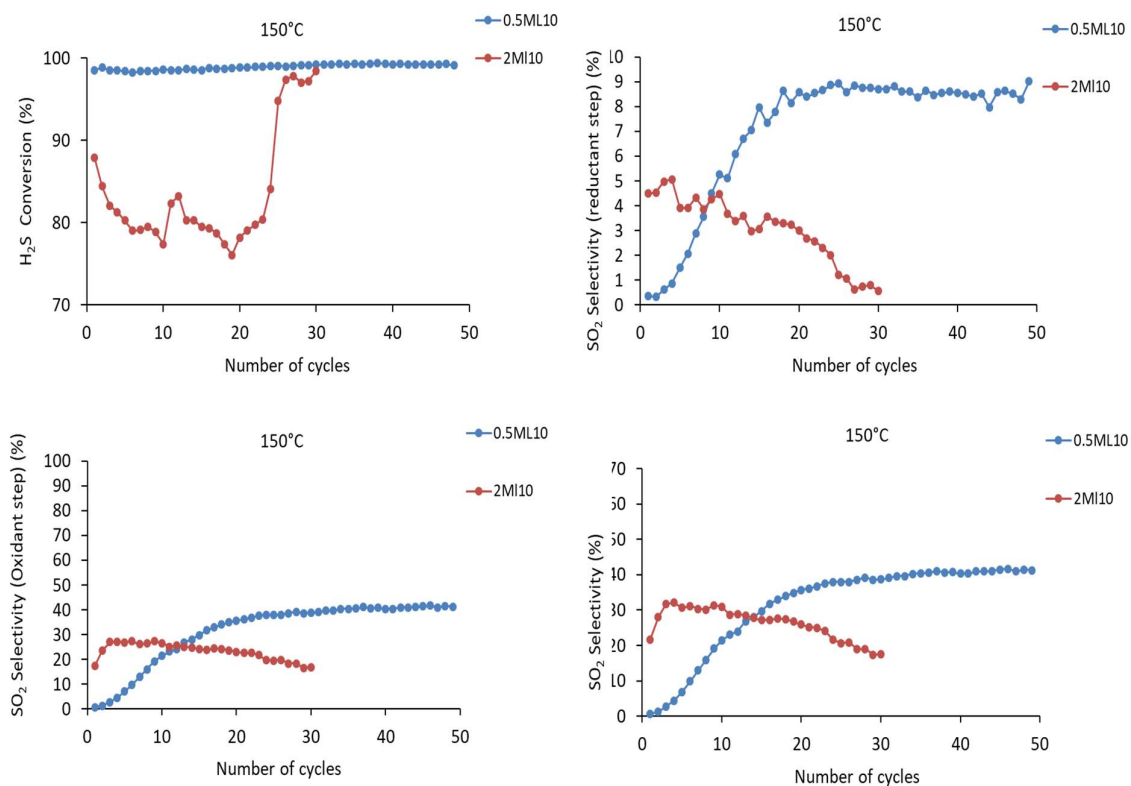
Figure 5.12: 900 mg (0.5ML 10), 200 mg (2ML 10), 150 °C, $H_2S:O_2$- 1:5, 2000 ppm of H_2S
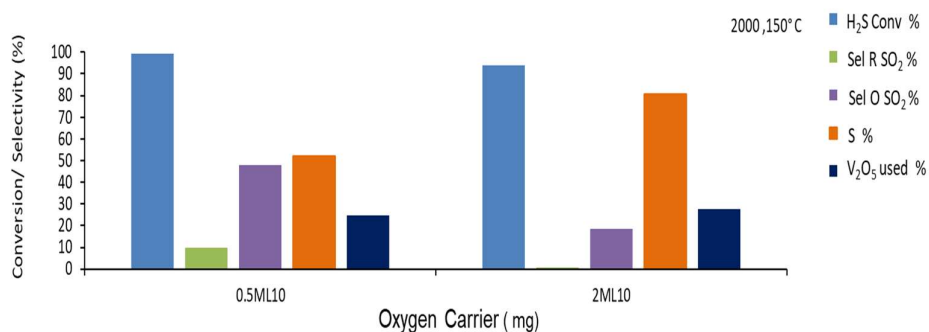
Figure 5.13: 900 mg (0.5ML 10), 200 mg (2ML 10), 150 °C, H$_2$S:O$_2$- 1:5, 2000 ppm of H$_2$S

	0.5ML10 (900 mg)	2ML10 (200 mg)
H$_2$S feed (µmol)	8.6	8.6
% Conv H$_2$S	99.0	94
n converted (µmol)	8.55	8.08
S (µmol)	3.47	6.48
SO$_2$R (µmol)	0.87	0.06
SO$_2$O (µmol)	4.20	1.54
(S/S+SO$_2$) (%)	79.9	99.1
%O$_{latt}$ (% V^{5+} -> V^{4+})	24.6	27.5

Table 5.6.: 900 mg (0.5ML 10), 200 mg (2ML 10), 150 °C, H2S:O2- 1:5, 2000 ppm of H$_2$S

2ML10 sample shows a singular behavior in terms of conversion as it initially decreases along cycling and then increases abruptly after 20-25 cycles to reach H$_2$S conversion of 94%.

Although both samples reach very high conversion, they show very different selectivity. Higher amount of SO$_2$ is formed on 0.5ML10 during reductant step indicating that highly dispersed vanadium species are less selective to elemental S. Furthermore, large amount of SO$_2$ is formed in oxidant step also suggesting, as mentioned earlier, that S species may adsorb of the support and not reach active site for oxidation within the reductant step timing. In the case of 2ML10, better coverage of the support by the active phase could be a reason why less amount of SO$_2$ is formed in oxidant step.

5.5 - Reactivity at high V$_2$O$_5$ loadings (2ML10, 5ML10, 10ML10, 15ML10)

The reactivity of the samples containing higher loadings of V$_2$O$_5$ have been studied in the standards conditions described above at 150 and 200 °C. Subsequently their reactivity was compared using different reactant concentrations.

In this case, constant amount of carrier has been used (200 mg) that means the amount of V_2O_5 placed in the reactor increases proportionally to the loading.

5.5.1 - Reactivity at 2000 ppm of H_2S, 10000 ppm of O_2

150 °C
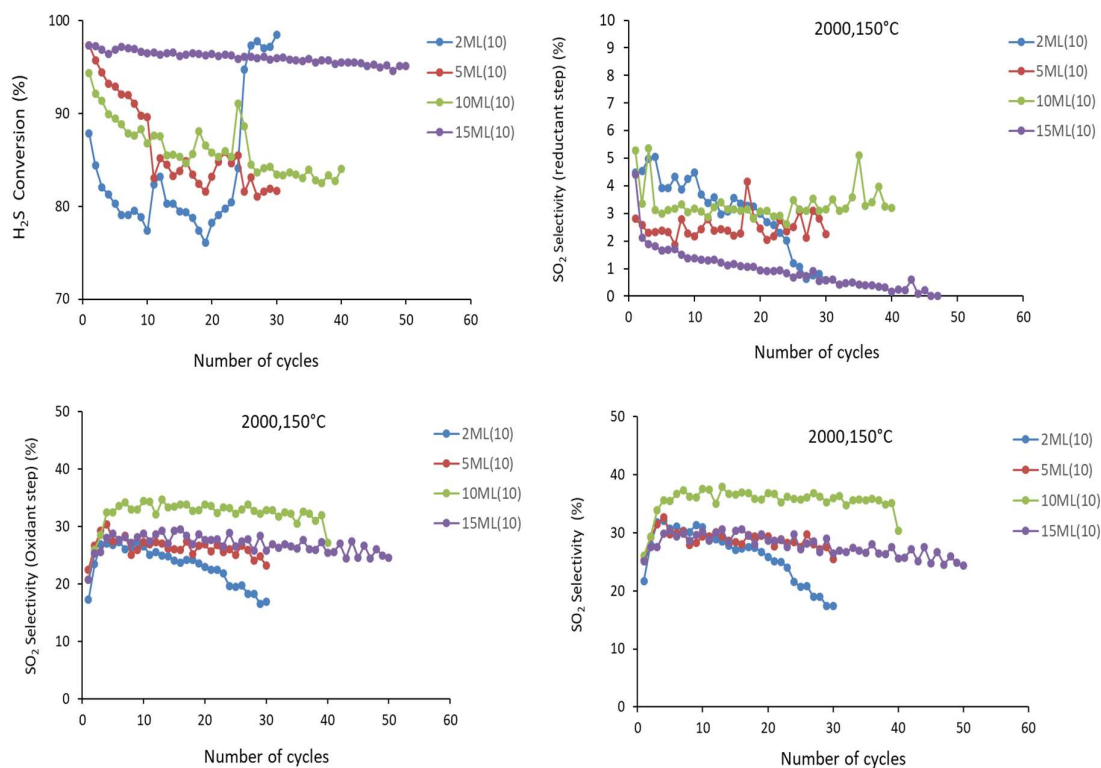
Figure 5.14.: 200 mg, 150 °C, $H_2S:O_2$ 1:5, 2000 ppm of H_2S
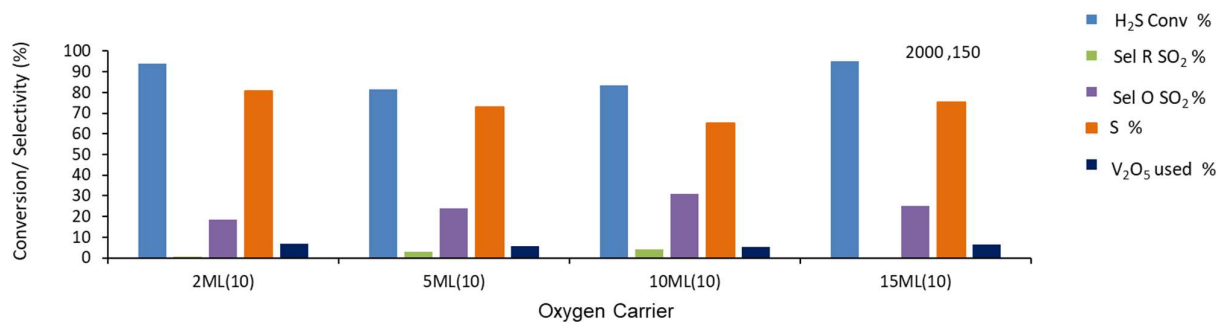
Figure 5.15.: 200 mg, 150 °C, $H_2S:O_2$ 1:5, 2000 ppm of H_2S

In terms of H_2S conversion, all samples show some evolution according to cycling. 15ML10 shows the most stable activity, although it loses approx. 4 %, while 5ML10 and 10ML10 lose 10 to 15 % of conversion. As already seen, 2ML10 shows a singular behavior as the conversion decreases for a certain number of cycles and then increase rapidly the reach a conversion comparable to that of 15ML10.

150 °C	2ML10	5ML10	10ML10	15ML10
H_2S feed (µmol)	8.6	8.6	8.6	8.6
% Conv H_2S	94.0	81.6	83.3	95.1
n converted (µmol)	8.08	7.01	7.16	8.41
S (µmol)	6.48	5.10	4.62	6.40
SO_2R (µmol)	0.06	0.22	0.28	<0.02
SO_2O (µmol)	1.55	1.70	2.26	3.78
$(S/S+SO_2)$ (%)	99.1	95.9	94.2	*99*
$\%O_{latt}$ (% V^{5+} -> V^{4+})	27.5	9.5	4.98	3.52

Table 5.7: 200 mg, 150 °C, H_2S:O_2 1:5, 2000 ppm of H_2S

The most significant differences between samples can be seen in selectivity. All samples show rather low amounts of SO_2 formed during reductant step. On the other hand, SO_2 produced during oxidant step increases considerably with loading. Again, this could be contradictory as, with increasing loading, the amount of available V_2O_5 increases also which should lead to more adsorbed S species to be converted in the reductant step.

Two phenomenon could contribute to explain this. Increase in conversion can happen possibly due to a better balanced between V^{5+}, V^{4+}, and V^{3+} at lower loading. As seen by XPS, 2ML10 shows the maximum proportion of the V^{4+} among all the solids. Presence of these partially reduced species can generate more reactive sites as compared to fully oxidized surfaces containing mostly V^{5+} species.

Another possibility is that at higher loading, V_2O_5 crystallite size is expected to increase and therefore generate less boundaries between active phase and support. In these conditions, H_2S adsorbed on the support would have less possibilities to contact with oxygen species from the active phase.
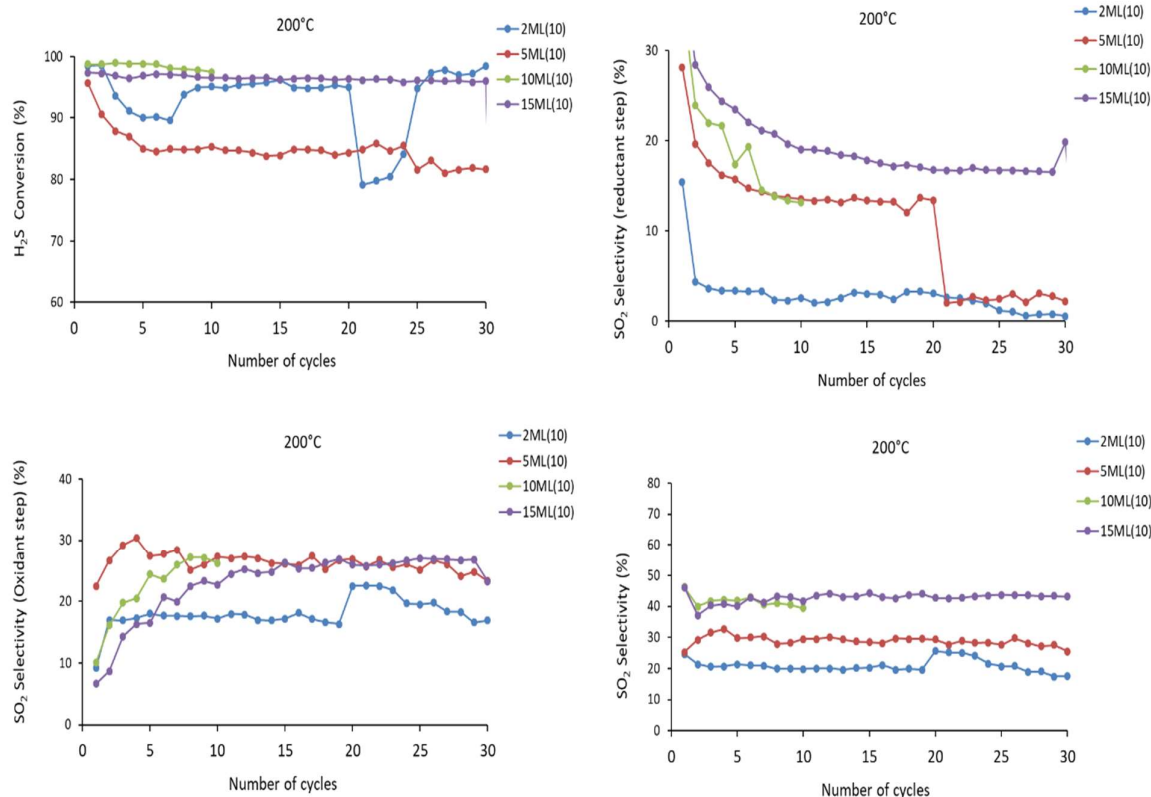
Figure 5.16: 200 mg, 200 °C, $H_2S:O_2$ 1:5, 2000 ppm of H_2S
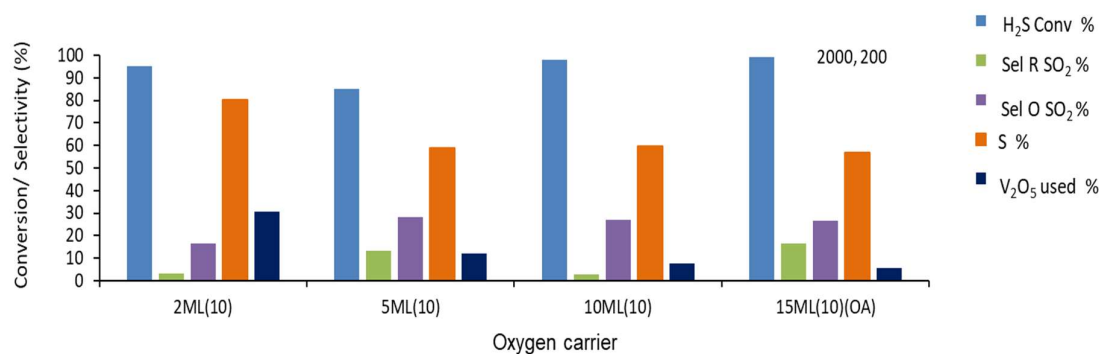
Figure 5.17: 200 mg, 200 °C, $H_2S:O_2$ 1:5, 2000 ppm of H_2S

At 200 °C, all samples show rather stable and high activity. Conversion is nearly total with the exception of 5ML10 which has a final conversion of 85 %. Samples with intermediate loading show some evolution of the selectivity, in particular regarding the amount of SO_2 produced during reductant step.

200 °C	2ML10	5ML10	10ML10	15ML10
H_2S feed (µmol)	8.6	8.6	8.6	8.6
% Conv H_2S	95.3	85.0	98.0	99.0
n converted (µmol)	8.20	7.31	8.42	8.76
S (µmol)	6.58	4.28	5.0	5.12
SO_2R (µmol)	0.27	0.97	1.13	1.39
SO_2O (µmol)	1.35	2.06	2.29	2.24
$(S/S+SO_2)$ (%)	96.0	81.5	81.6	78.6
$\%O_{latt}$ (% V^{5+} -> V^{4+})	30.6	11.9	7.6	5.5

Table 5.8: 200 mg, 200 °C, H_2S:O_2 1:5, 2000 ppm of H_2S

In terms of selectivity, the amounts of SO_2 produced during reductant step increases in all cases but more significantly for sample 5ML10, 10ML10 and 15 ML10. Indeed, the selectivity for 2ML10 remains very high (96 %) in reductant step contrary to other samples.

On the other hand, the amount of SO_2 produced in oxidant step decreases for all samples and in particular for those with the highest loadings. This could be induced by a higher mobility of adsorbed S containing species which provide more possibilities to react during the reductant step.

Although 2ML10 present a singular behavior in terms of evolution of conversion along with cycling, it is interesting to note that this sample is finally the least affected by the increase of temperature. Indeed, it only shows a slight increase of SO_2 produced during the reductant step which reflects in the percentage of lattice oxygen involved that remain in the same range (27 to 30 %).

5.5.2 - Effect of reactant concentration

The reactivity of the carriers with these high loading of V_2O_5 have been tested with 1000 ppm H_2S and 4000 ppm H_2S at both temperatures. In these case the O_2 concentrations varied accordingly to keep the H_2S:O_2 ratio constant at 1:5.

150 °C

1000 ppm of H_2S (5000 ppm of O_2)

At 150 °C using 1000 ppm H_2S concentration, all samples show high and stable conversion with the exception of the highest loading of V_2O_5 (15ML10).
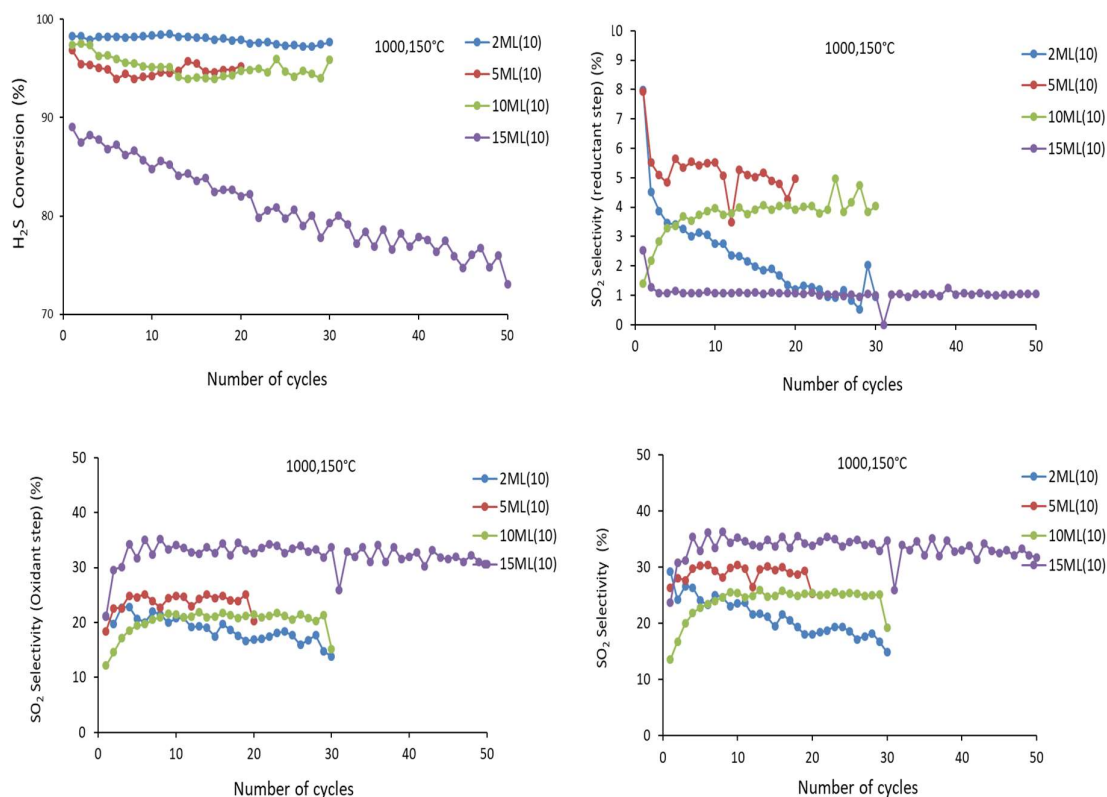
Figure 5.18.: 200 mg, 150 °C, H₂S:O₂ 1:5, 1000 ppm of H₂S
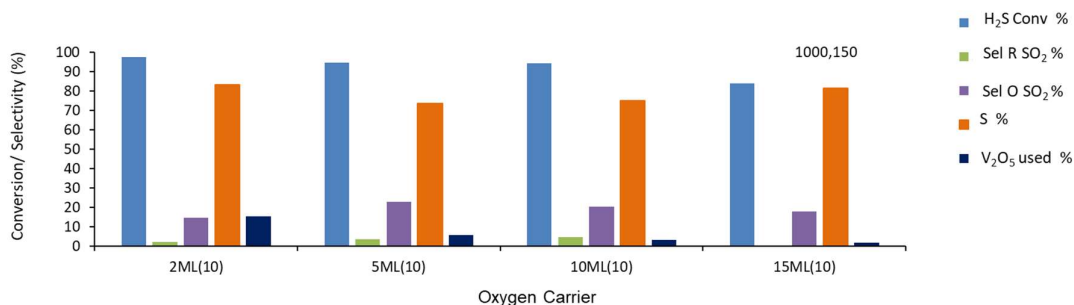
Figure 5.19.: 200 mg, 150 °C, H₂S:O₂ 1:5, 1000 ppm of H₂S

In terms of selectivity, 2ML10 sample show a decreasing amount of SO_2 produced during reductant step along cycling, while other samples show a stable behavior.

Globally performances for all samples are excellent with little SO_2 produced in both reactant steps and little effect of loading can be observed.

Especially at high loading, SO_2 produced in reductant step is surprisingly low, activity and selectivity for 2ML10 and 15ML10 is almost the same except the more lattice oxygen used for 2ML10.

150 °C, 1000 ppm	2ML10	5ML10	10ML10	15ML10
H_2S feed (µmol)	4.3	4.3	4.3	4.3
% Conv H_2S	98.0	94.0	94.0	83.9
n converted (µmol)	4.19	4.06	4.05	3.60
S (µmol)	3.48	2.97	3.02	2.92
SO_2R (µmol)	0.08	0.14	0.19	0.02
SO_2O (µmol)	0.60	0.94	0.83	0.66
$(S/S+SO_2)$ (%)	97.6	95.4	93.9	99.3
$\%O_{latt}$ (% V^{5+} -> V^{4+})	15.4	5.6	3.3	1.8

Table 5.9: 200 mg, 150 °C, H_2S:O_2 1:5, 1000 ppm of H_2S

4000 ppm of H_2S (20000 ppm of O_2)
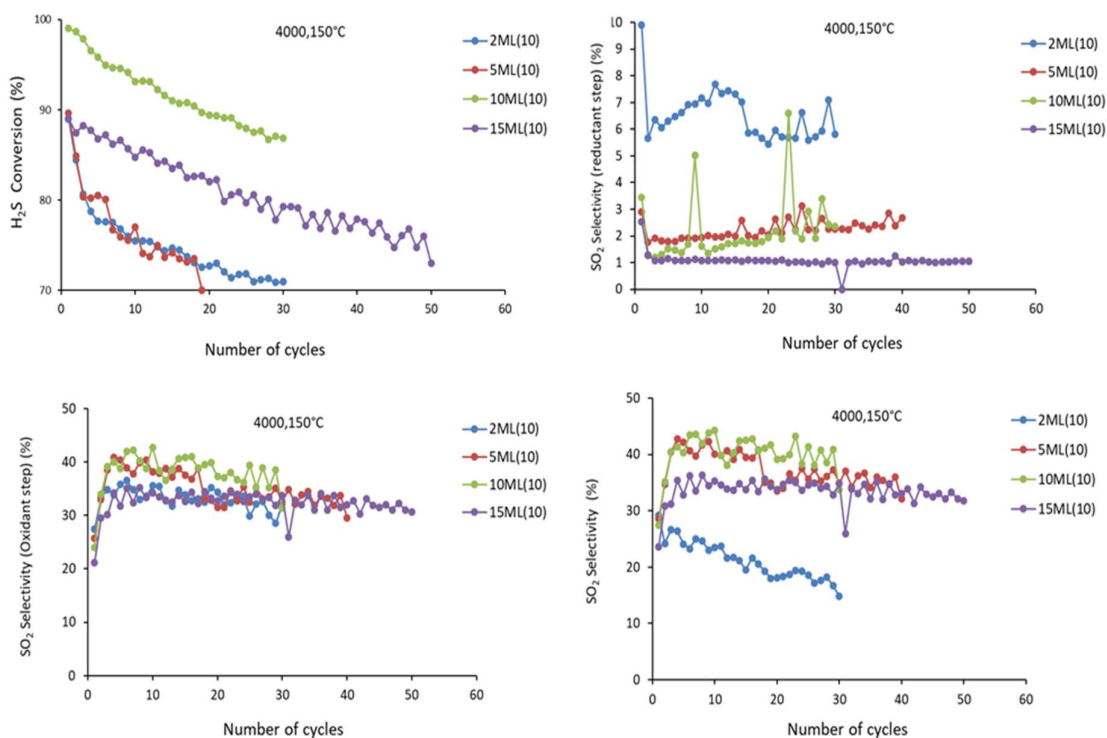
Figure 5.20.: 200 mg, 150 °C, H_2S:O_2 1:5, 4000 ppm of H_2S
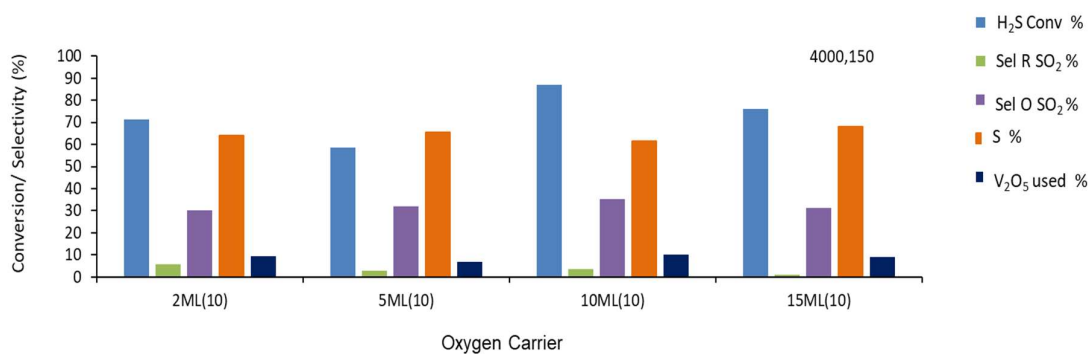
Figure 5.21.: 200 mg, 150 °C, H$_2$S:O$_2$ 1:5, 4000 ppm of H$_2$S

150 °C 4000 ppm	2ML10	5ML10	10 ML10	15ML10
H$_2$S feed (µmol)	16.5	16.5	16.5	16.5
% Conv H$_2$S	71.3	58.7	87.0	76.0
n converted (µmol)	11.76	9.69	14.35	12.5
S (µmol)	7.45	6.15	8.72	8.45
SO$_2$R (µmol)	0.70	0.28	0.49	0.13
SO$_2$O (µmol)	3.62	5.14	3.26	3.95
(S/S+SO$_2$) (%)	91.4	95.7	94.7	98.4
%O$_{latt}$ (% V^{5+} -> V^{4+})	39.5	11.5	9.3	5.3

Table 5.10: 200 mg, 150 °C, H$_2$S:O$_2$ 1:5, 4000 ppm of H$_2$S

In terms of selectivity, 2ML10 produces the largest amount of SO$_2$ in the reductant step as compared to other samples. This is surprising as this sample has the least amount of V$_2$O$_5$ available. On the other hand, it shows the largest proportion of lattice oxygen involved in the reaction.

200 °C

Experiments performed with 1000 and 4000 ppm of H$_2$S show, as in the case of 2000 ppm (Figure 5.16) a rapid stabilization of conversion and selectivity along cycling. To facilitate comparison only final reactivity are illustrated.
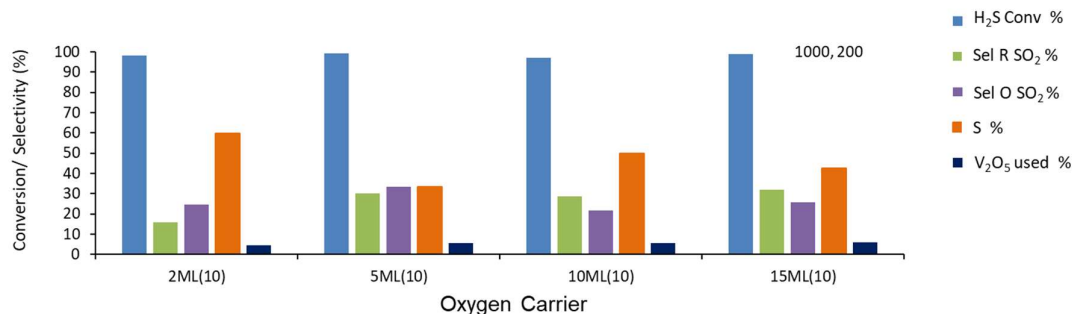
Figure 5.22: 200 mg, 200 ° C, H₂S:O₂ 1:5, 1000 ppm of H₂S

200 °C 1000 ppm	2ML10	5ML10	10ML10	15ML10
H_2S feed (µmol)	4.3	4.3	4.3	4.3
% Conv H_2S	98.0	99.4	97.0	99.0
n converted (µmol)	4.21	4.27	4.17	4.26
S (µmol)	2.49	1.40	2.03	1.78
SO_2R (µmol)	0.67	1.43	1.22	1.37
SO_2O (µmol)	1.05	1.44	0.92	1.10
(S/S+SO_2) (%)	78.9	49.4	62.6	56.6
%O_{latt} (% V^{5+} -> V^{4+})	18.6	9.4	5.2	3.5

Table 5.11: 200 mg, 200 ° C, H₂S:O₂- 1:5, 1000 ppm of H₂S

As seen with 2000 ppm H_2S, at 200 °C, the amount of SO_2 in reductant step increases significantly for all samples but more for the high loading samples. Indeed, 2ML10 shows the overall best activity both in terms of conversion and selectivity.

4000 ppm of H₂S, (20000 ppm of O₂)
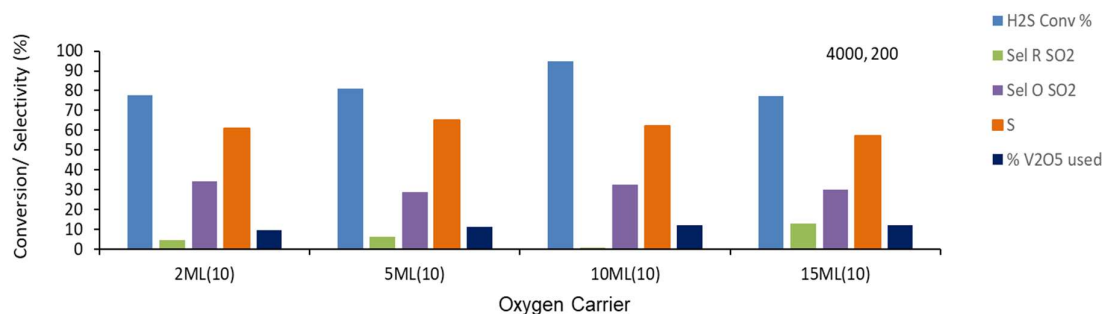
Figure 5.23: 200 mg, 200 °C, H₂S:O₂ 1:5, 4000 ppm of H₂S

200 °C 4000 ppm	2ML10	5ML10	10ML10	15ML10
H$_2$S feed (µmol)	16.5	16.5	16.5	16.5
% Conv H$_2$S	77.8	81.0	95.0	77.3
n converted (µmol)	12.84	13.36	15.67	12.76
S (µmol)	7.71	8.63	9.74	7.16
SO$_2$R (µmol)	0.62	0.84	0.78	1.66
SO$_2$O (µmol)	4.50	3.89	5.15	3.93
(S/S+SO$_2$) (%)	92.5	91.1	92.6	81.2
%O$_{latt}$ (% V^{5+} -> V^{4+})	39.6	18.4	11.0	7.2

Table 5.12: 200 mg, 200 ° C, H$_2$S:O$_2$ 1:5, 4000 ppm of H2S

Same trends can be observed as with lower concentrations. Higher amounts of SO$_2$ formed in reductant step and, most important, SO$_2$ formed in oxidant step.

Interestingly, the amount of lattice oxygen involved compared to experiment performed with same (4000 ppm) concentration at lower temperature increases significantly for all samples with the exception of 2ML10. In this case, the amount is practically identical (39.7 or 39.6%). A limit in oxygen capacity seems to be reached. The slightly higher amount of SO$_2$ produced in reductant step, consuming part of the lattice oxygen explains that less S can be formed and thus, globally some more SO$_2$ is formed in oxidant step.

5.6 - Effect of TiO$_2$ specific surface area

Specific surface area of a support is a key parameter which affect active phase dispersion but also reactivity. Porosity can also interfere with the catalytic reaction through diffusion limitations. In this section, TiO$_2$ support different surface areas (10 m^2/g and 45 m^2/g) are compared.

5.6.1 - Reactivity of bare TiO$_2$ (10) and TiO$_2$ (45) supports

In a first step, the reactivity of the bare supports (without active phase) were tested. They are noted TiO$_2$ (10) and TiO$_2$ (45) respectively.
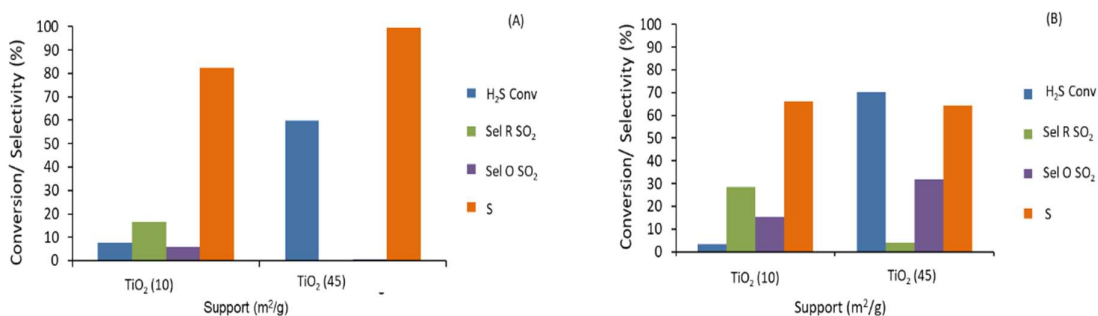
Figure 5.24: 200 mg of Support, 800 mg of SiC, 2000 ppm H_2S; 10000 ppm O_2, (A)150 °C, (B)200 °C

TiO_2 (45) leads to high conversion of H_2S (around 60%) at both temperatures compared to TiO2 (10). At low temperature, for TiO_2 (45) it was observed that SO_2 formation at reductant and oxidant step is negligible. This suggests that the conversion of the H_2S corresponds to an adsorption and accumulation of H_2S on the support. Whereas in the case of the TiO_2 (10) less H_2S conversion is observed (7.5% at 150 °C). Unlike TiO_2 (45), TiO_2 (10) shows the formation of SO_2 in both the reductant and oxidant step indicating some redox capacity in reductant step and possible regeneration in oxidant one.

At 200 °C conversion of H_2S on TiO_2 (45) increases slightly. SO_2 formation in the oxidant step increases drastically while some SO_2 appears also in the reductant step. Clearly, at such higher temperature, the oxidation of adsorbed species become possible on this support.

In Figure 5.24 it should be noted that due to the method of calculation, S selectivity is obtained by mass balance taking into account all measurable products and reactants. In particular, for TiO_2 (45), which shows no redox capacity, such high selectivity has to be considered as an artefact as accumulated H_2S will be interpreted as "S" formation.

5.6.2 - Characterization of V_2O_5 supported on TiO_2 (10) and TiO_2 (45)

To highlight the major difference between these supports, a comparative study has been carried out using solids with similar number of monolayers of active phase. For this, 2ML10 and 1.65ML45 samples have been compared. 2ML10 has 2 wt % of the active phase whereas 1.65ML45 possess 7.4 wt. % of V_2O_5.

BET

Surface area of the all solids associated with TiO_2 10 does not show difference in the surface area, pore volume, and pore size. Whereas solids associated with TiO_2 45, shows the decreases in surface area, pore volume. Pore size increases after loading. This indicate the presence of the vanadium into the pore structure. After loading 1.65ML45 is more crystalline than 2ML10.

Oxygen carrier	Surface area (m^2/g)	Pore volume (cm^3/g)	Pore size (nm)	H_2 consumption (mmol/g)	Crystallite size (nm)	
					Support	V_2O_5
TiO_2(10)	11.3	0.07	26.6	-	41	-
TiO_2(45)	46.8	0.3	24.4	-	46*,47**	-
2ML10	9.5	0.05	22.8	0.14	80.5	n.o.
1.65ML45	36.4	0.186	32	0.67	51.5	n.o.

Table 5.13: Characterization of oxygen carrier, *- Anatase, **-Rutile (n.o. = not observed).

XPS

First, 2ML10 sample was chosen as it shows the optimal reactivity as seen previously. In comparison, 1.65ML45 was chosen as it shows the most similar characteristic as 2ML10 in terms of V^{4+}/V^{5+} and V/Ti ratio as determined by XPS.

Oxygen carrier	B.E (eV) V 2p		$V^{4+}/(V^{4+}+V^{5+})$	$V^{5+}/(V^{4+}+V^{5+})$	V^{4+}/V^{5+}	V/O	V/Ti
	V^{4+}	V^{5+}					
2ML10	516.1	517.1	0.38	0.62	0.62	0.08	0.22
1.65ML45	516.2	517.4	0.24	0.76	0.32	0.07	0.20

Table 5.14: XPS of V 2p $_{3/2}$ and O 1s
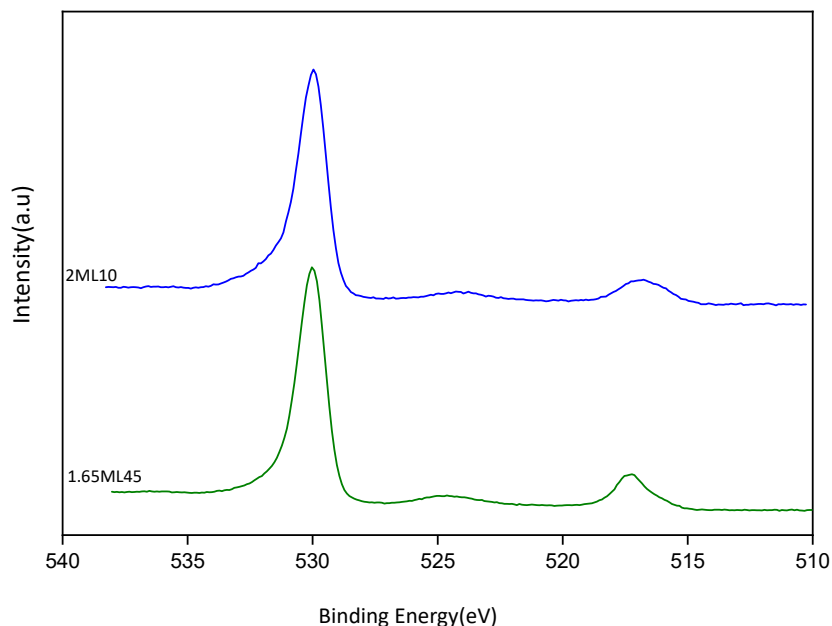
Figure 5.25: XPS of V 2p $_{3/2}$ and O 1s

The V 2p$_{3/2}$ photo peak for both the solid shows two contributions at binding energies of 517.1-517.4 eV and 516.1-516.2 eV. These are values usually attributed to V^{5+} and V^{4+} in V_2O_5 phase. Presence of separate prominent photo peaks for V^{5+} and V^{4+} observed for both solid. O1s provides two peaks after deconvolution with peak at 529.9 eV attributed to oxygen from TiO_2 whereas the high binding energy peak (531.0-532.8 eV) corresponds to adsorbed oxygen, hydroxyl and/or carbonate groups which reflects the presence of anionic vacancies [85] [107].

V/Ti ratio for 2ML10 and 1.65 ML10 show very similar values (0.22 and 0.20, respectively). Although the amount of V^{4+} species is slightly higher for the 2ML10 samples with respect to 1.65ML45 (0.38 vs 0.24 %, $V^{4+}/(V^{4+}+V^{5+})$), these characterizations suggest that the distribution of vanadium species is rather similar on these samples as could be expected considering similar number of monolayers for these solids.

In these conditions, eventual differences of reactivity between these samples should not be attributed to significant differences between active species present.

5.6.3 - Reactivity comparison between 2ML10 and 1.65ML45

Chemical looping reaction on 2ML10 and 1.65ML45 were performed in so-called "standard" conditions, i.e. exposing the carrier for 1 minute to each reactant and for 2 minutes to neutral gas between reactants and with a constant total flow rate of 100 ml/min. Reactions were

performed at different H_2S concentrations (1000 and 2000 ppm) while keeping the $H_2S:O_2$ ratio constant at 1:5. With 2000 ppm, reactivity is compared at 150 °C and 200 °C.

As explained, although samples exhibit similar content of V_2O_5 in terms of monolayers, the wt% is obviously different. Thus, to compare reactivity between samples, different amounts of carrier need to be taken in order to have approximately the same amount of V_2O_5 involved. 200 mg of 2ML10 and 60 mg of 1.65ML45 were used which correspond to 4.0 and 4.4 mg V_2O_5, respectively.

Reactivity at 150 °C

Effect of reactant concentration
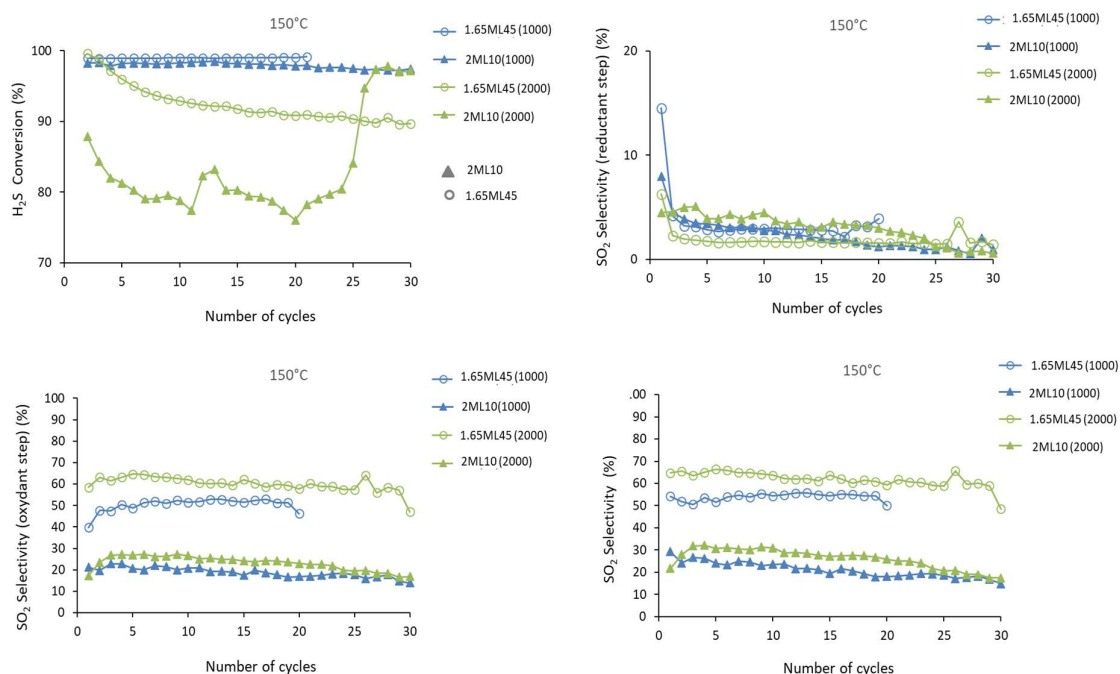
Figure 5.26: 200 mg 2ML10 or 60 mg 1.65ML45, 150 °C, $H_2S: O_2$ 1:5, 1000, 2000 ppm of H_2S
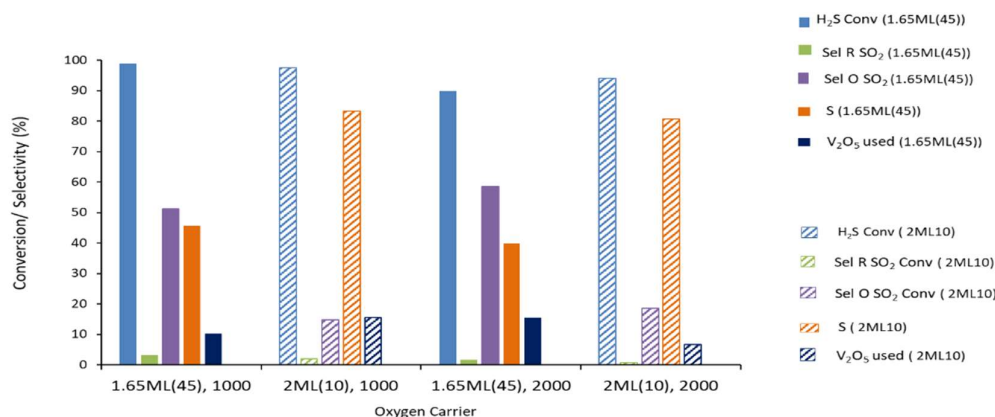
Figure 5.27: 200 mg 2ML10 or 60 mg 1.65ML45, 150 °C, H_2S: O_2 1:5, 1000, 2000 ppm of H_2S

As in previous cases, evolution of reactivity versus cycling are shown in figure 5.26 while properties recoded during last cycles are shown graphically in Figure 5.27 and quantitatively in Table 5.15

150 °C	1000 ppm		2000 ppm	
	2ML10	1.65ML45	2ML10	1.65ML45
H_2S feed (µmol)	4.3	4.3	8.6	8.6
% Conv H_2S	98.0	99.0	94.0	89.9
n converted (µmol)	4.19	4.20	8.08	7.91
S (µmol)	3.48	1.92	6.48	3.14
SO_2R (µmol)	0.08	0.14	0.06	0.13
SO_2O (µmol)	0.60	2.20	1.55	4.77
(S/S+SO_2) (%)	97.6	93.2	99.1	96.0
%O_{latt} (% V^{5+} -> V^{4+})	15.4	10.3	27.5	15.6

Table 5.15: 200 mg 2ML10 or 60 mg 1.65ML45,150 °C, H_2S: O_2 1:5, 1000, 2000 ppm of H_2S

At low H_2S concentration, both solids give same high H_2S conversion, near 100%. Conversion and selectivity are stable along cycling. The formation of SO_2 in the reductant step is very low and almost the same for both carriers and reflect in high selectivity (>93% S/(S+SO_2R) in this step. The most striking difference is the SO_2 formation in the oxidant step which is considerably more important for 1.65ML45 (2.20 µmol) than for 2ML10 (0.60 µmol). This translates in a globally lower selectivity to S for 1.65ML45 than 2ML10. This also reflect in the amount of lattice oxygen involved in the reductant step which is considerably higher for 2ML10 than for 1.65ML45.With increase in the concentration of the H_2S from 1000 to 2000 ppm, reactivity follows the same trend. In this case conversion decrease slightly with time on both carriers, while that of 2ML10 increases suddenly after 20-25 cycles as already seen

earlier. For both solids, final conversion is very high approx. >90%. The amount of SO_2 formed during reductant step is not affected by the increase in reactant concentration for both carriers. Again, the most striking difference between samples is the amount of SO_2 formed during the oxidant step. In case of 2ML10, the increase of H_2S amount injected per cycle from 4.3 to 8.6 µmol leads to an increase of only 0.95 µmol SO_2 in oxidant step, while for 1.65ML45 it increases by 2.57 µmol.

Effect of temperature with 2000 ppm of H_2S

As mentioned, the reactivity of both carriers using 2000 ppm H2S has been compared at 150 and 200 °C.

As can be seen from Figure 5.28, all samples reach very high H_2S conversion even though 2ML10 exhibit the singular behavior already mentioned. In the case of 1.65ML45 carrier, conversion decreases slightly with time but is the same at both 150 and 200 °C.
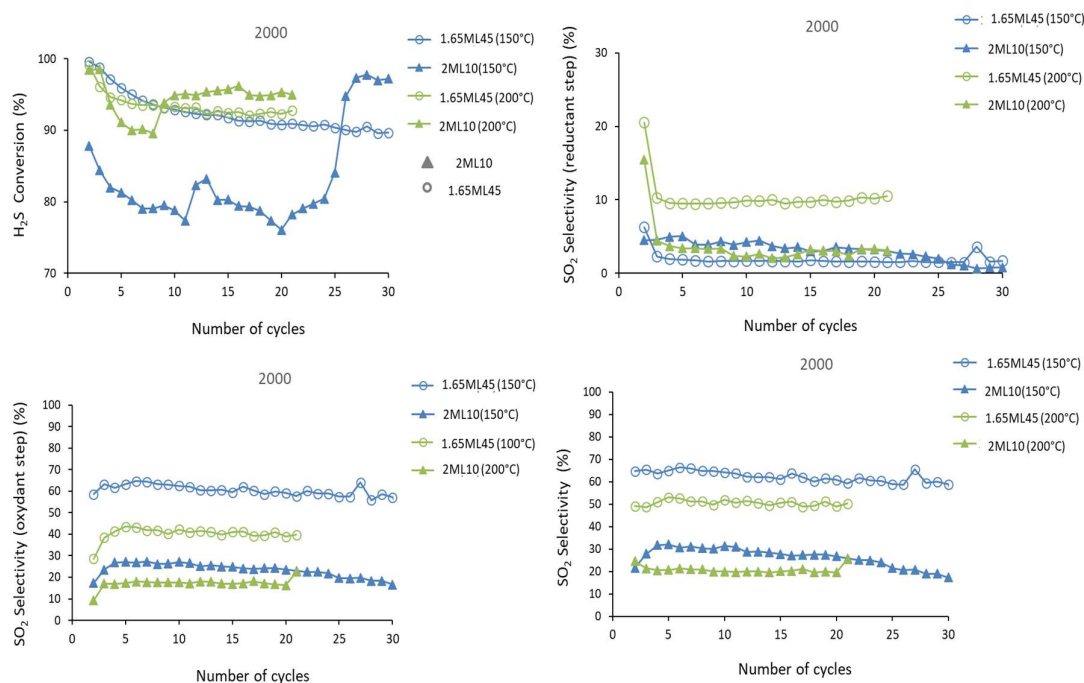
Figure 5. 28: 200 mg 2ML10 or 60 mg 1.65ML45, 150 °C, 200 °C, H_2S: O_2 1:5, 2000 ppm of H_2S
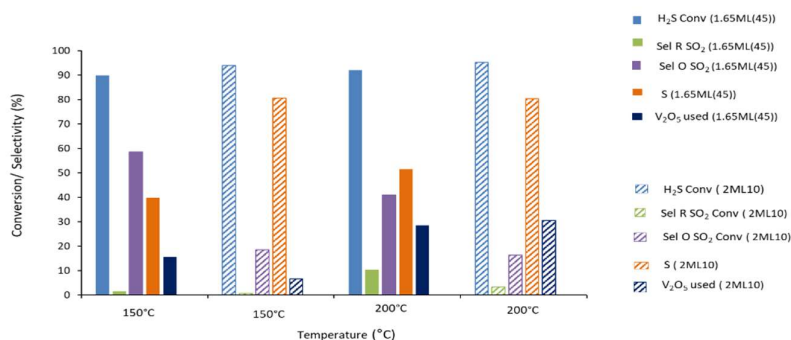
Figure 5.29: 200 mg 2ML10 or 60 mg 1.65ML45, 150 °C, 200 °C, H₂S: O₂ 1:5, 2000 ppm of H₂S

2000	150°C		200°C	
	2ML10	**1.65ML45**	**2ML10**	**1.65ML45**
H_2S feed (µmol)	8.6	8.6	8.6	8.6
% Conv H_2S	94.0	89.9	95.3	92.0
n converted (µmol)	8.08	7.91	8.20	8.10
S (µmol)	6.48	3.14	6.58	3.90
SO_2R (µmol)	0.06	0.13	0.27	0.85
SO_2O (µmol)	1.55	4.77	1.35	3.36
$(S/S+SO_2)$ (%)	99.1	96.0	96.0	82.1
%O_{latt} (% V^{5+} -> V^{4+})	27.5	15.6	30.6	28.4

Table 5.19: 200 mg 2ML10 or 60 mg 1.65ML45, ,150 °C ,200 °C, H2S: O2 1:5,2000 ppm of H2S

In terms of selectivity, increase of temperature does induce slightly higher amount of SO_2 produced in reductant step in the case of 2ML10 while this increase is more significant on 1.16ML45. Regarding SO_2 produced during oxidant step, it slightly decreases with 2ML10 and, more importantly, for 1.65ML10. At 200 °C both reach similar values of lattice oxygen involved (28-30 %) but this one is more efficiently used on 2ML10 as higher selectivity in reductant step is observed.

Clearly, the use of higher specific surface area support considerably affects the reactivity of the carrier although, at first sight, the nature of active phase is very similar.

This can be due to the porosity of the carrier as will be discussed below.

5.7 - General discussion and Conclusions

As it has already been mentioned, models regarding the nature and structure of active vanadium species in TiO_2 supports have already been proposed in the literature. In particular, it has been already well established by Wasch [58] that below monolayer coverage, only surface vanadium species in strong interaction with TiO_2 (anatase) surface are present.

Whereas above monolayer coverage small crystallites of V_2O_5 are also present on the support in addition to the monolayer of the surface vanadia species. Apart from this small V_2O_5 crystallites, somewhat distorted in comparison to bulk unsupported V_2O_5, are also available at low loadings of the V_2O_5.

G.C bond et al. [94] also shows the formation of the different structure of V_2O_5 over the anatase. For one to two monolayer surface vanadyl complexes are observed. These surface vanadyl complexes are mainly dioxo-vanadium species linked to the surface of the support by two bridging oxygens that are arranged in a disordered fashion. Above the monolayer, for two-four monolayers disordered vanadium oxides can be formed whereas above four monolayers para crystalline V_2O_5 formation is observed which is more reducible than crystalline V_2O_5.

Figure 5.30: Structural arrangements of different loadings of V_2O_5[57]

The aim of this chapter was to identify the key parameters influencing V_2O_5 reactivity when dispersed on such TiO_2 support. To do this, different loadings of the V_2O_5 over the support (10 m^2/g) were studied in detail. The influence of experimental parameters was studied the amount of carrier, reactant concentration and temperature. The carriers were characterized to understand the physico-chemical properties and correlate these with the activity and selectivity of the reaction.

Due to practical questions linked to the amount of carrier needed to perform experiments, results have been presented separately for low V_2O_5 content samples and those exhibiting equivalents of 2 monolayers or more.

As could be expected, at lower concentration presence of the V_2O_5 is not observed over the surface of the support neither by XRD or Raman. More surprisingly, other forms of surface vanadium species could not be observed either, such as mono or poly vanadates. This could be due to the sensitivity of the instrument used together with the very low content in vanadium due to the low surface area of the support.

At the lowest Vanadium species coverage (equivalent of 0.5ML of V_2O_5), the carrier proved to be the most active for H_2S conversion compared to higher loadings (1.0 and 1.5ML). On the other hand, this sample also produced the highest amount of unselective oxidation to SO_2 in

the reductant step and mass balance calculation (Table 5.3) show that more lattice oxygen is needed than that corresponding to the reduction of V^{5+} to V^{4+} species (considering all the V in V^{5+} state at the beginning). This implies that V^{3+} species need to be involved in the redox process for this carrier and could explain more formation of SO_2 in reductant step compared to higher loading catalysts if it is assumed that V^{4+} to V^{3+} transformation is less selective than V^{5+} to V^{4+} reduction with regard to S production [14][24] .

Clearly, although the overall selectivity is not the optimum, very low loadings produce very active species for H_2S conversion which, in turn, are efficiently re-oxidized in oxidant step as the activity shows good stability along cycling. However, due to the limited absolute oxygen capacity for a given amount of carrier, this sample also shows abundant production of SO_2 in oxidant step. In other words, H_2S is adsorbed on the surface of the carrier but is not fully converted to either S or SO_2 due to the limited oxygen capacity. These sulfur species are effectively oxidized in oxidant step, but some accumulation could also occur.

To overcome the limitation of oxygen capacity due to lower loading, higher amounts of carrier need to be used. This was explored in part 5.4 and it has been seen that this can significantly affect the reactivity of the system. Conversion is indeed total all along cycling but strong evolution of selectivity is observed regarding SO_2 formation both in reductant step than in oxidant one. Over-oxidation to SO_2 in reductant step can be understood if one considers that with such high amount of carrier used, the amount of V_2O_5 in the reactor is in excess with respect to that of H_2S to convert. This could enhance over-oxidation. On the other hand, this over-oxidation increases with time, suggesting that it is also linked to some evolution of the carrier. In the same time, SO_2 formed during oxidant step also increases slowly. Again, this could be a paradox considering that the solid contains well enough V_2O_5 to fully oxidized all S species in reductant step. A possible explanation could be that with high amount of carrier, the catalytic bed does not react in uniform way. In particular, a first layer of the bed could fully adsorb H_2S (as seen that 200 mg are sufficient to adsorb nearly all H_2S). In this case, this layer would be strongly reduced and produce some amount of SO_2 in reductant step. S produced could eventually be over-oxidized by flowing through the remaining of the carrier bed. Eventually, some parts of the carrier bed could be deactivated after a while does only contributing to adsorption of H_2S and not to real conversion to S or SO_2. In the time frame of the cycling, these adsorbed species would not have enough time to migrate (by desorption and re-adsorption of by surface diffusion) to active sites in order to be converted in reductant step and would finally produce SO_2 in oxidant step.

At higher Vanadium loadings, XRD and Raman characterizations show the presence of V_2O_5 species on all samples above 2ML equivalent of V_2O_5. At 2ML, the formation of "disordered vanadium oxide" growing away from the surface is also possible as evidenced by the presence of the 997cm^{-1} peak present on the spectrum for 2ML10 during the Raman study (Figure 5.5(b)). This is in agreement with the model proposed by G. C Bond.

Among these "high" loading of V_2O_5 carriers, the lowest containing 2ML shows the best properties for selective oxidation of H_2S in chemical looping mode. This can be seen both in the production of SO_2 in reductant and oxidant steps.

In reductant step, generally, all samples show good selectivity to S formation with little SO_2 production. Significant differences can nevertheless be observed in particular at higher reaction temperature. In this case, and in all H_2S concentrations, this 2ML sample shows the lowest SO_2 formation in reductant step. Simultaneously, this sample shows the highest ratio of $V^{4+}/ (V^{4+}+V^{5+})$ after synthesis. This indicates that strong interaction with the support still exist on this samples suggesting better dispersion and coverage of the support. The presence of such partially reduced species could favor H_2S dissociation on active phase surface contrary to more saturated V^{5+} species. Simultaneously, the presence of more oxygen deficient carrier could be more favorable towards partial oxidation with respect to a fully oxidized system for which more oxygen will be available.

On the other hand, when reaching higher levels of lattice oxygen extraction (38-39%) this 2ML sample shows some more SO_2 formation in reductant step. Considering that this carrier already has a large proportion of V^{4+}, the loss in selectivity could be induced by the involvement of V^{4+} to V^{3+} reduction; which would be consistent with observations made for the lower loading samples.

These results suggest that the selectivity in the reductant step needs a delicate balance between the presence and involvement of V^{5+}, V^{4+} and V^{3+} species. The redox between V^{5+} to V^{4+} seem to produce more selectively elemental S whereas deeper reduction towards V^{3+} species seem more favorable to SO_2 production. On the other hand, the presence of V^{4+} seem to enhance the reactivity of adsorbed species.

Although 2ML10 shows to be the best carrier, it shows a singular behavior with a sudden increase in reactivity after a certain number of cycles. This can be observed at both 150 and 200 °C but is more rapid at the higher temperature. This indicates that the solid evolves during cycling to reach an optimal reactivity taking into account both reduction of the solid and its re-oxidation in oxidant step. Indeed, the results shown mostly focus on reactivity in reductant step, but it should always be kept in mind that that the re-oxidation step is also crucial to regenerate active species. 2ML10 carrier will be further studied in the following chapter.

Concerning SO_2 production **in the oxidant step**, in can be clearly seen that it increases significantly with loading of V_2O_5. This can appear as a paradox because it means that more H_2S is adsorbed on the surface of the carrier and does not react to produce either S or SO_2 in reductant step while in the same time the oxygen capacity of the carrier increases. The amount of SO_2 in oxidant step is also significantly affected by temperature as differences between samples are less marked. Indeed, whereas at lower coverage the SO_2 formation in oxidant step increases at 200 °C with respect to 150 °C, at the highest loading it decreases.

As mentioned, at such high loading V_2O_5 crystallites grow on the surface of the support. However, the differences in reactivity cannot be ascribed to intrinsic properties of larger crystallites as such high amount of SO_2 produced in oxidant step where not observed on bulk V_2O_5 (Chapter 3) nor on V_2O_5 supported on TiO_2 at very high loading (25 w%, equivalent of 25ML, in Chapter 4).

A possible explanation can be found in the morphology of V_2O_5 deposited on TiO_2 above 2ML coverage. Indeed, as explained earlier, all models suggest that V_2O_5 does not grow in a uniform way by covering progressively the support but by building tower-like V_2O_5. This reflects on the V/Ti ratio which shows that even at very high loading, significant amounts of TiO_2 can still be exposed to the gas phase. In these conditions, 2ML10 sample could expose well dispersed somehow disordered V_2O_5 species on the surface of the support, leaving little distance between active particles and illustrated in Figure 5.31(a). With the increase of loading, growing of tower is favored which may leave more space between active phase particles and the reduction of number of boundaries sites between active phase and support as illustrated in Figure 5.31 (b). In these conditions, H_2S adsorbed of the surface of the support would need to migrate towards the active phase before being converted to either S or SO_2 in reductant step. As the time is limited by the cycling to 1 minute, one can imagine that species adsorbed on the support with high loading may not have sufficient time to reach active phase and be converted contrary to lower loading sample for which active phase is better dispersed. The more rapid diffusion of adsorbed species at higher temperature could, it this case, explain that less adsorbed species remain o, the support at 200 °C with respect to 150 °C. Obviously, at extremely high loading (e.g. 25 w%) the density of V_2O_5 tower on the surface would limit this phenomenon, ultimately leading to bulk V_2O_5 properties.

(a) Low loading -> 2Ml10   (b) X 5 loading -10ML10
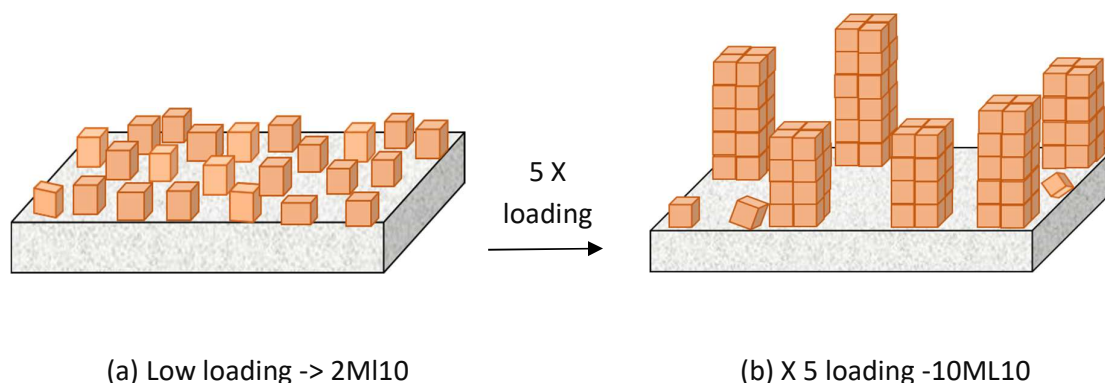
Figure 5.31: Structural arrangement of carrier at different loadings of V_2O_5

Finally, it has been seen that **textural properties** of support play an important role on the reactivity of these V_2O_5/TiO_2 carriers. Although detailed study of V_2O_5 deposited on higher

specific surface area has not been included in this work, the comparison between 2ML10 and 1.65ML45 carrier provide very useful information. For these two carriers, the characterizations show that very similar active species are present on the surface of TiO_2. On the other hand, very different reactivity has been observed with more SO_2 formed in reductant step and in oxidant step. Although some differences in the reactivity of the active phase cannot be excluded, the higher porosity of 1.65ML45 carrier could explain these differences. This is illustrated in Figure 5.31.

In an ideal system, <u>during reductant step</u>, H_2S would adsorb directly on the active phase and produce S (Route 1a in Figure 5.32 A "Reductant step") and eventually some SO_2 which would desorb and be transported out of the system in the gas flow. As seen, H_2S could also adsorb on the surface of the support and would need to migrate towards the active phase before being converted (Route 1b). Active phase would then be regenerated in the oxidant step during which residual adsorbed species would also be oxidized to produce SO_2 (Routes 1a and 1b in Figure 5.32 B "Oxidant step").

In the presence of higher porosity support, several phenomena could affect this "ideal" image. First, due to high surface area, the supports can contribute more to the adsorption of H_2S. This can generate more residual species which can contribute to SO_2 formation in oxidant step (Route 2, black, in "Reductant and Oxidant steps"). Then, S formed during reductant step can also remain trapped within the porous structure of the support (Route 3, red)). This will be considerably enhanced at lower temperature. Indeed, it should be reminded that at 150 °C, reaction takes place in conditions in which S condensation may occur (<180 °C). The real temperature of the gas in contact with the surface is probably higher than that imposed by the regulation if one considers that all these reactions are highly exothermic. This certainly contributes to avoid S accumulation at such low temperature between chemical looping steps. Higher porosity can make this process of desorption more difficult and thus generate more SO_2 when the solid is regenerated (Route 3, red, "Oxidant step"). These two phenomena contribute to an increase of SO_2 production in oxidant step.

However, more SO_2 is also produced in reductant step on 1.65ML45. This can be explained by the necessary diffusion of S produced in the inner part of the carrier towards the external surface. Due increased residence time in proximity of the carrier, S can suffer over-oxidation by subsequently entering in contact with active phase (Route 4, blue, "Reductant step"). Such phenomenon is well known in catalytic selective oxidation reaction which generally are performed on low surface area materials to avoid consecutive reactions and losses in selectivity [112]–[114] and has also been observed for H_2S oxidation [115].
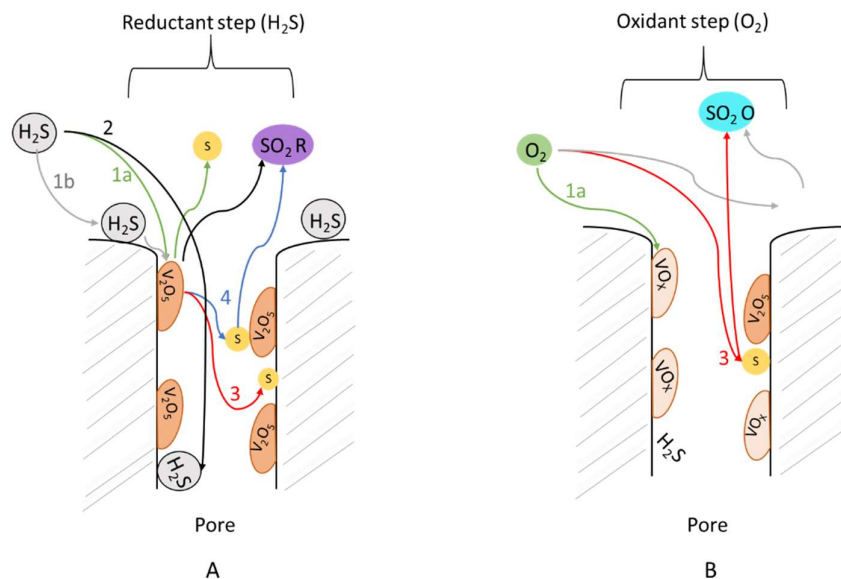
Figure 5.32: Reaction mechanism in reductant step (A) and at oxidant step (B)

These results highlight the difficulties in designing an efficient carrier system for chemical looping selective oxidation of H_2S. As globally 2ML10 showed the best results both in terms of loading with respect to available TiO_2 surface and textural properties, in the following chapter it is proposed to examine more deeply this material.

Chapter VI

"2ML10" V_2O_5/TiO_2 carrier

Chapter 6 - Detailed study of "2ML10" V_2O_5/TiO_2 carrier

In the previous chapter, it has been seen that V_2O_5 coverage above monolayer content are most favorable for CLSOSH and in particular with low surface area support.

Indeed, the carrier noted 2ML10 (2Wt% V_2O_5 on TiO_2 10 support) corresponding to 2 equivalent of V_2O_5 monolayers coverage proved as a better solid for the reaction for both activity and selectivity even in terms of the SO_2 formation in the reductant phase and sulfur formation.

In this chapter, a detailed study of this 2ML10 carrier is proposed. Several factors, like concentration of the reactant H_2S:O_2 (1:5), different ratio of reactants, reaction temperature, or different exposure times of H_2S will be presented. Furthermore, the reactivity will be studied in presence of methane.

Solids recovered after exposure to H_2S or O_2 at the end of the cycling experiments have also been characterized to better understand the structural and chemical changes in the carrier during chemical looping operation.

6.1 - "2ML10" Preparation and characterization

Preparation of different supported V_2O_5 samples are described in Chapter 5.1 including "2ML10" carrier. Detailed characterization of these materials can be found in Chapter 5.2, but to simplify the reading, the main characteristics of this carrier are reminded here.

6.1.1 - BET

Oxygen carrier	Surface area (m²/g)	Pore volume (cm³/g)	Pore size (nm)	H_2 consumption (mmol/g)	Crystallite size (nm)	
					Support	V_2O_5
2ML10	9.5	0.05	22.8	0.14	80.56	-

Table 6.1: Characterization of 2ML10 oxygen carrier.

The solid has very low surface area as (9.5 m²/g) with low pore volume and large pore size.

6.1.2 - XRD
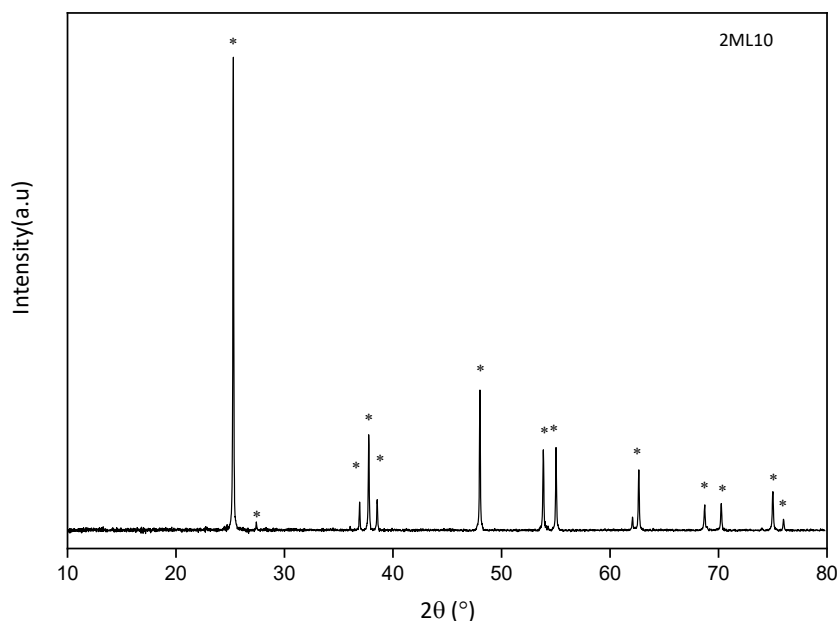
*Figure 6.1: XRD study of 2ML10, *- Support.*

XRD study of the 2ML10 illustrates the presence of mostly the TiO_2 anatase phase. 25.2° represents the presence of the intense peak for the anatase with (1 0 1) phase along with weak intense peak at 37.8°, 38.5° as per PDF 00-021-1272 file. There is no evidence of the presence of the V_2O_5 species on the support, this can happen due to homogemous layer formation on the support or as the analysis comes under the detection limit of the instrument. Uniform formation of the monolayer on the support may strongly enhance oxygen mobility and storage capacity of the solid. Crystallite size of the support is 80.5 nm, as can be seen from the intense peak of the TiO_2 anatase.

6.1.3 - TPR

Two distinct peaks at 515°C and 576°C are present in the TPR profile of 2ML10 and indicate two steps of reduction of V_2O_5 as already explained. These two peaks are composed of two contributions including both VOx species and V_2O_5 species.[40]

2ML10

Temperature (°C)
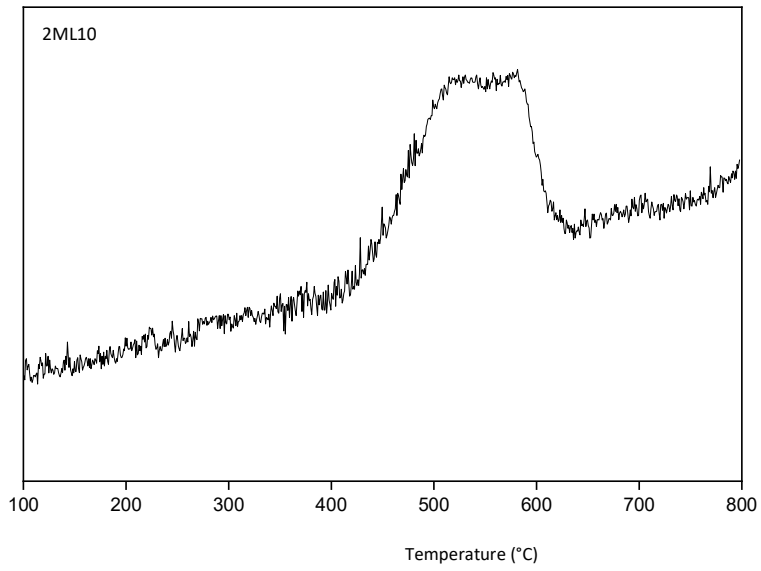
Figure 6.2: TPR study of 2ML10

6.1.4 - XPS

2 ML 10

1 s

2 p$_{1/2}$

2 p$_{3/2}$

V5$^+$ V4$^+$

Intensity (a.u)

Binding Energy(eV)
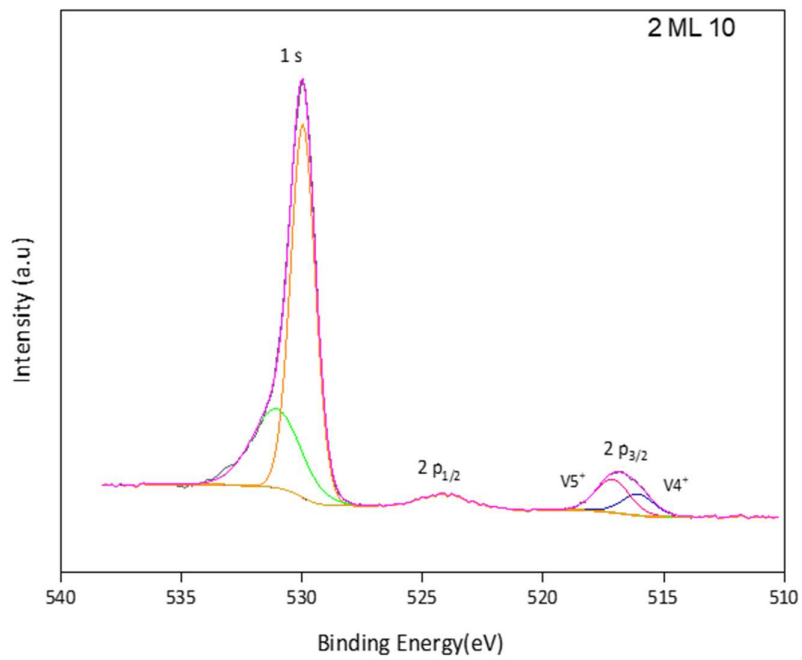
Figure 6.3: XPS pattern for O 1s and V2p core level 2ML10

Carrier	B.E (eV) V 2p		$V^{4+}/$ $(V^{4+} +V^{5+})$	$V^{5+}/$ $(V^{4+}+V^{5+})$	V^{4+}/V^{5+}	V/O	V/Ti
	V^{4+}	V^{5+}					
2ML10	516.06	517.12	0.38	0.62	0.61	0.08	0.22

Table 6.2: XPS study of the The V 2p $_{3/2}$ and the O 1s

The V $2p_{3/2}$ photopeak shows two contributions at binding energies of 517.7 eV and 516.06eV. These are close to the values usually attributed to V^{5+} and V^{4+} in V_2O_5 phase. V^{4+}/V^{5+} ratio shows the abundance of the V^{4+} species along the side of the V^{5+} species [85]. Ratio between V^{4+}/V^{5+} is 0.61.

6.2 - Chemical looping activity for 2ML10

The reactivity of "2ML10" carrier has been explored in several reaction conditions.

Compared to the "standard" reaction conditions, i.e. using 2000 ppm H_2S in reductant cycle (for 1 minute) and 10000 ppm O_2 in oxidant step (H_2S:O_2 ratio = 1:5) at 150°C, reactions have been performed by varying:

- Reactant concentration by keeping H_2S:O_2 ratio constant at 1:5.
- Reactant contact timings.
- Reactant H_2S:O_2 ratio by keeping H_2S constant at 2000 ppm.
- The influence and/or reactivity of methane on the CLSOSH process was tested.

6.2.1 - Effect of reactant concentration.

In the following results, reactivity of 2ML10 sample was studied using several reactants concentrations while keeping the H_2S:O_2 ratio constant at 1:5. 30 cycles of each system have been carried out at different temperatures (150 °C and 200 °C).

150 °C

Figure 6.4 and Table 6.3 show that better conversion is obtained with the lowest reactant concentration, i.e. 1000 ppm of H_2S. During the reaction 4.19 μmol of H_2S is converted corresponding to more than 97 % of the amount introduced during each cycle.
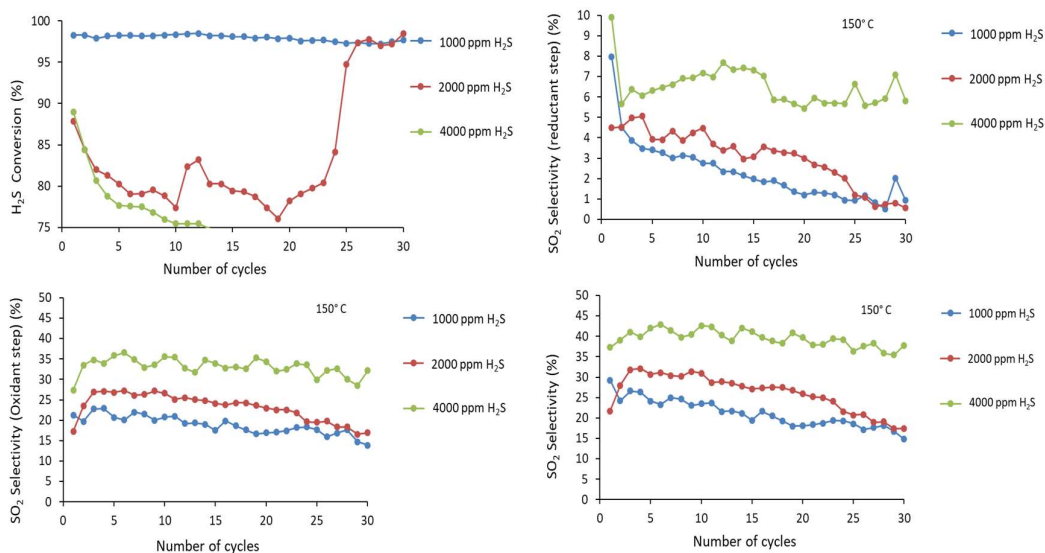
Figure 6.4: 200 mg of 2ML10, 150 °C, H₂S:O₂ 1:5
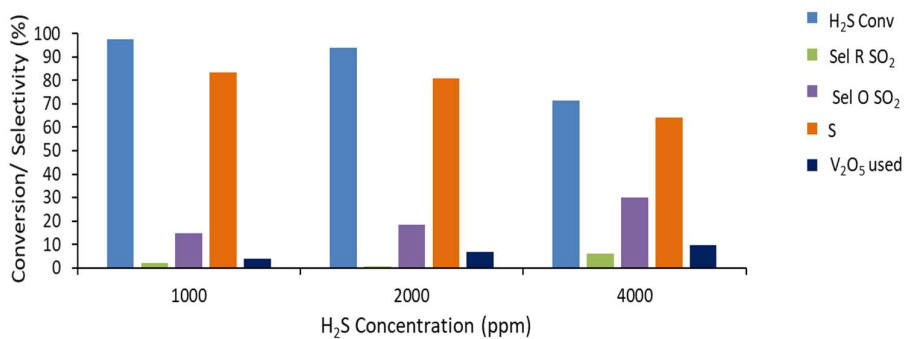
Figure 6.5: 200 mg of 2ML10, 150 °C, H₂S:O₂ 1:5

150 °C	1000 H₂S (ppm)	2000 H₂S (ppm)	4000 H₂S (ppm)
H₂S feed per cycle (µmol)	4.30	8.60	16.50
% Conv H₂S	97.5	94.0	71.3
n converted (µmol)	4.19	8.08	11.76
S (µmol)	3.48	6.47	7.45
SO₂R (µmol)	0.08	0.06	0.69
SO₂O (µmol)	0.62	1.54	3.61
(S/S+SO₂ R) (%)	97.6	99	91
%O$_{latt}$ (% V^{5+} -> V^{4+})	15.45	27.53	39.4

Table 6.3: 200 mg of 2ML10, 150 °C, H₂S:O₂ 1:5

In the case of the 2000 ppm of H_2S reaction, a singular behavior is observed. Initially the conversion decreases regularly along cycling. Then, suddenly, reactivity increases to 94 % of H_2S conversion corresponding to 8.08 µmol. Up to 2000 ppm the increase in total H_2S converted is nearly proportional to the amount of H_2S fed during the reductant step.

With 4000 ppm of H_2S, the conversion follows the same evolution than with 2000 ppm H_2S but the sudden increase is not observed. During last cycles, only 11.76 µmol of H_2S is converted.

In terms of selectivity, the reactions performed with the lowest concentration of H_2S also show the lowest selectivity (and amounts) of SO_2 produced during reductant step. In the case of 4000 ppm, this selectivity does not evolve along cycling while it actually gets better for 1000 and 2000 ppm H_2S experiments. Furthermore, the sudden increase in reactivity during 2000 ppm experiment does not affect the selectivity of the reaction.

Along with a lower conversion of H_2S, the experiment with 4000 ppm also shows the highest production of SO_2 during oxidant step. This indicates that the maximum capacity of H_2S conversion to S or SO_2 in the reductant step is exceeded in these conditions. Indeed only 7.45 µmol of S and 0.69 µmol of SO_2 are produced compared to 6.47 µmol S and 0.06 µmol SO_2 were obtained with half the amount of H_2S in the feed.

It should however be noted that the amount of lattice oxygen involved in the reductant step (taking into account formation of S, SO_2 and the corresponding necessary H_2O) is well below that corresponding to the full reduction of V_2O_5 (V^{5+}) to V_2O_4 (V^{4+}).

Another interesting observation is that although the amount of reductant (H_2S) is increased from 2000 ppm to 4000 ppm and that the available oxygen species are limited, the selectivity towards total oxidation increases. Several explanations can be proposed for such behavior. One could be that deeper reduction of the solid involve less selective species (e.g. V^{4+} to V^{3+} reduction). Another is to consider that O_2 concentration is also increased proportionally in these experiments, meaning that the re-oxidation step could bring more oxidized (and less selective) species to be regenerated.

200 °C

While working at 200 °C, similar trends for H_2S conversion are observed as at 150 °C.
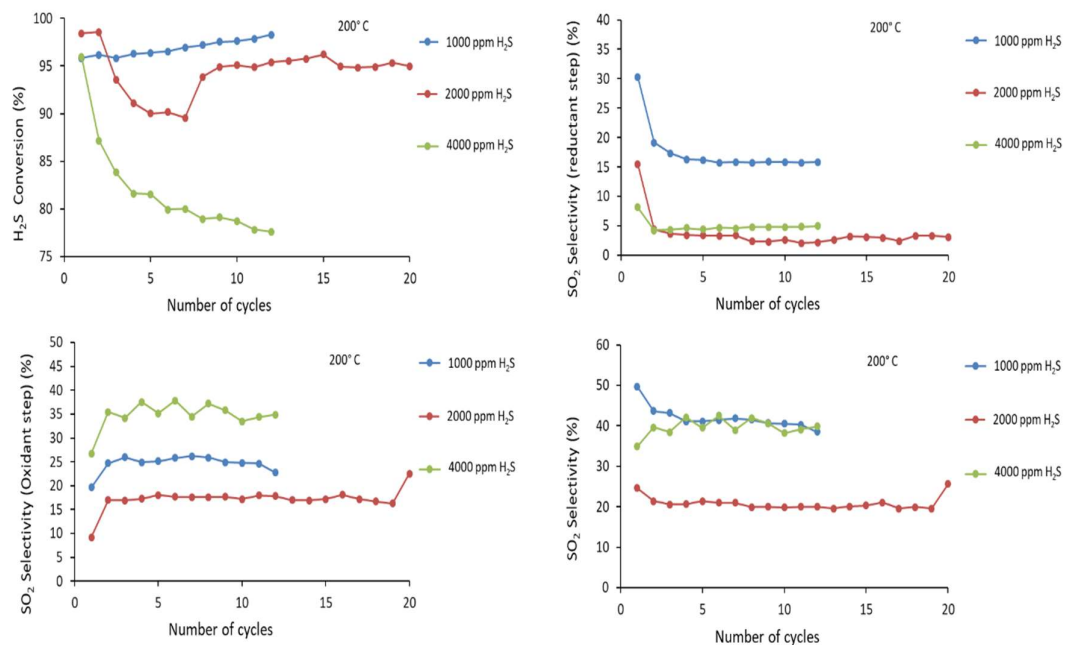
Figure 6.6: 200 mg of 2ML10, 200 °C, $H_2S:O_2$ 1:5
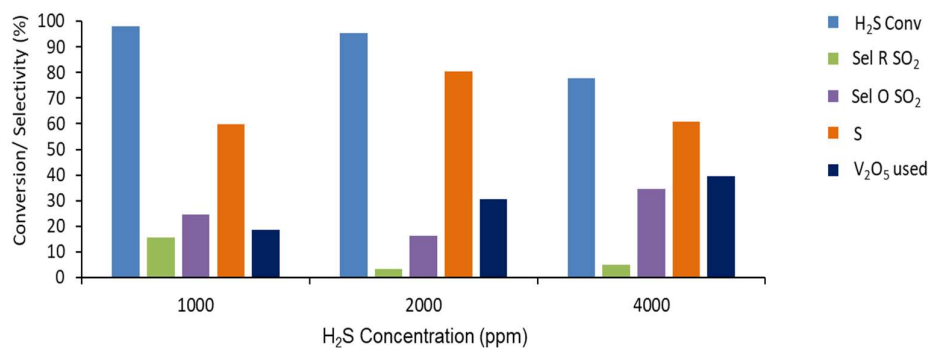
Figure 6.7: 200 mg of 2ML10, 200 °C, $H_2S:O_2$ 1:5

200 °C	1000 H_2S (ppm)	2000 H_2S (ppm)	4000 H_2S (ppm)
H_2S feed per cycle (µmol)	4.30	8.60	16.50
% Conv H_2S	98.0	95.3	77.8
n converted (µmol)	4.21	8.19	12.83
S (µmol)	2.49	6.50	7.7
SO_2R (µmol)	0.67	0.27	0.61
SO_2O (µmol)	1.05	1.34	4.5
(S/S+SO_2 R) (%)	78.9	96.0	92.5
%O_{latt} (% V^{5+} -> V^{4+})	18.5	30.5	39.5

Table 6.4: 200 mg of 2ML10, 200 °C, $H_2S:O_2$ 1:5

Although only 12 or 20 cycles were performed, one can observe the singular increase of reactivity during the 2000 ppm experiment. It occurs more rapidly than at 150 °C however.

During 1000 ppm H_2S experiment, the conversion remains high throughout the 12 cycles, while that observed during 4000 ppm decreases steadily.

Surprisingly, SO_2 formation in the reductant step does not follow the same trend as during reaction at 150 °C. Indeed, low selectivity is observed with around 0.67 µmol SO_2 formed to be compared to 4.21 µmol of H_2S converted. This is the highest value compared to other experiments.

Actually, the % of lattice oxygen involved during reductant step does not vary significantly between reactions performed at 150 or 200 °C for the three concentrations and the net amount of elemental sulfur produced is similar at these temperatures for 2000 ppm and 4000 ppm experiments. The increase of temperature mostly affects the selectivity towards elemental S in the low concentration experiment.

For the intermediate H_2S concentration (2000 ppm), temperature actually has limited effect of the reactivity of the solid as can be seen in Figure 6.8 and Table 6.5.
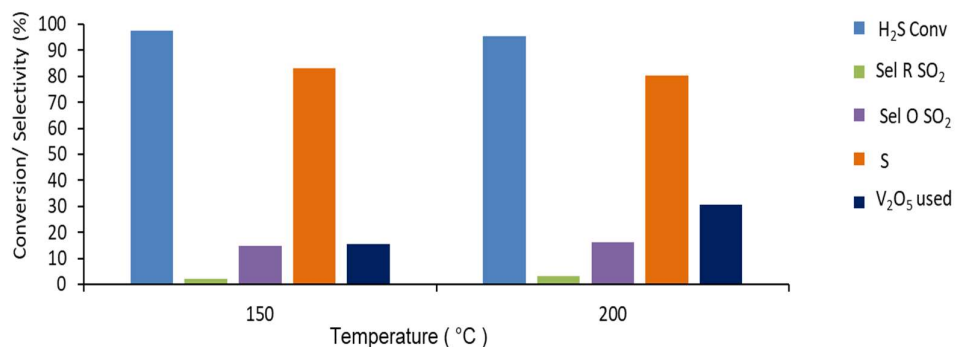
Figure 6.8: 200 mg of 2ML10, 2000 ppm of H_2S, H_2S: O_2 1:5

2000 ppm H_2S (1:5)	150 °C	200 °C
H_2S feed per cycle (µmol)	8.60	8.60
% Conv H_2S	94.0	95.3
n converted (µmol)	8.08	8.20
S (µmol)	6.47	6.50
SO_2R (µmol)	0.06	0.27
SO_2O (µmol)	1.54	1.34
(S/S+SO_2 R) (%)	99.0	96.0
%O_{latt} (% V^{5+} -> V^{4+})	27.5	30.5

Table 6.5: 200 mg of 2ML10, 2000 ppm H_2S, H_2S:O_2 1:5

6.2.2 - Effect of cycling timing

As seen, the amount of reactant to which the carrier is exposed plays an important role during the process. The amount can be varied by concentration as done above, or by varying the duration of such exposure for a given concentration. Clearly this should be done keeping the amount of solid involved constant.

For the following experiments, H_2S to O_2 ratio was maintained at 1:5 whereas the cycle pattern was changed as shown in Table 6.6. "1-2-1-2" cycling corresponds to the "standard" conditions explored until now, i.e. 1 minute exposure to each reactant with intermediate purging in Argon flow for 2 minutes between reactants.

Compared to this standard pattern, exposure to reactant was reduced by half to 0.5 minutes (0.5-2-0.5-2) or increased to 3 minutes (3-2-3-2).

Reaction were performed at 150 and 200 °C.

Cycle	H_2S exposure (min)	O_2 exposure (min)	Ar exposure (min)	Total time (min)
0.5-2-0.5-2	0.5	0.5	2	5
1-2-1-2	1	1	2	6
3-2-3-2	3	3	2	10

Table 6.6: Various cycling patterns explored

150 °C
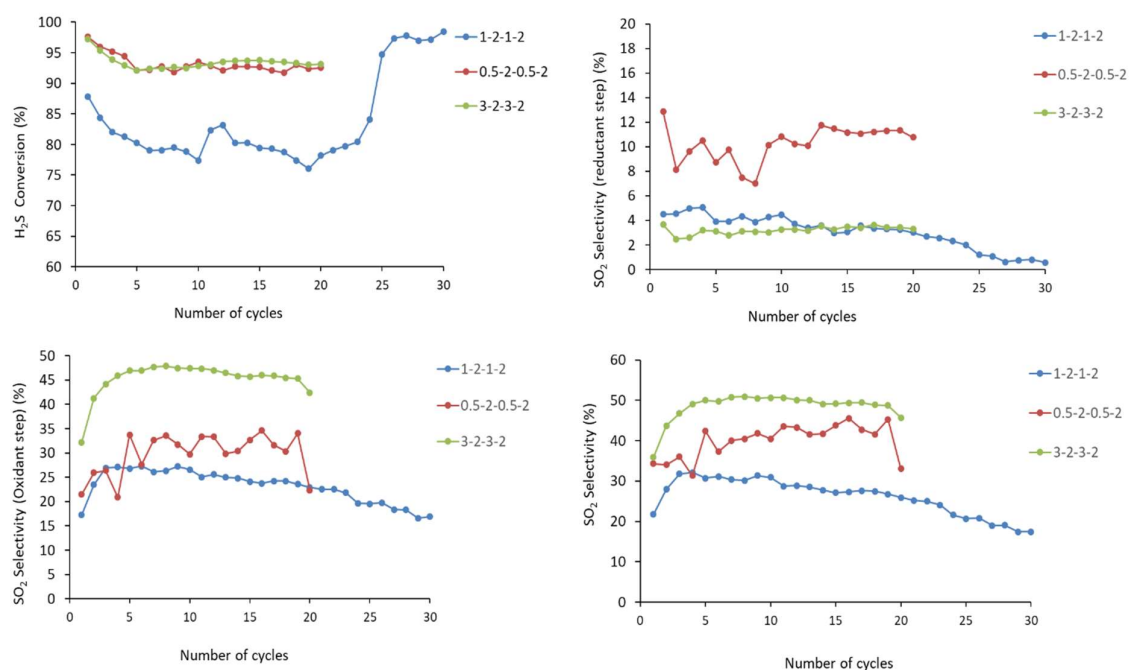
Figure 6.9: 200 mg of 2ML10, 2000 ppm of H_2S, H_2S:O_2 1:5, 0.5-2-0.5-2, 1-2-1-2, 3-2-3-2 cycle, 150 °C
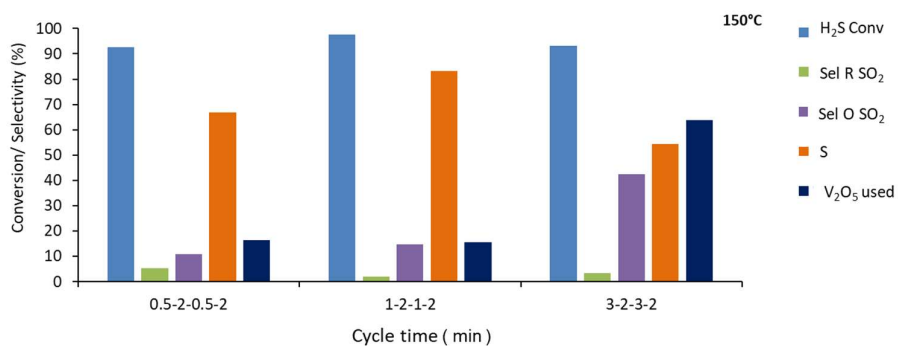
Figure 6.10: 200 mg of 2ML10, 2000 ppm of H_2S, $H_2S{:}O_2$ 1:5, 0.5-2-0.5-2, 1-2-1-2, 3-2-3-2 cycle , 150 °C

150 °C	0.5-2-0.5-2	1-2-1-2	3-2-3-2
H_2S feed per cycle (µmol)	4.3	8.60	25.9
% Conv H_2S	92.6	94.0	93.1
n converted (µmol)	3.98	8.08	24.13
S (µmol)	2.65	6.47	13.03
SO_2R (µmol)	0.43	0.06	0.80
SO_2O (µmol)	0.90	1.54	10.30
$(S/S+SO_2 R)$ (%)	86.0	99.0	94.0
%O_{latt} (% V^{5+} -> V^{4+})	16.2	27.5	59.0

Table 6.7: 200 mg of 2ML10, 150 °C ,2000 ppm of H2S, H2S:O2 1:5, 0.5-2-0.5-2, 1-2-1-2, 3-2-3-2 cycle

In the case of all three timings, the H_2S conversion is very high (>90%), especially at the end of the cycling, indeed 1-2-1-2 experiments shows the singular increase already described earlier (same experiment) but finally reach similar conversion.

The amount of S produced increase by twofold factor between experiments performed with 0.5 and 1 minute exposure to reactants. Between 1 and 3 minutes, S produced also increase but not proportionally to that of H_2S introduced per cycle. Indeed, only another twofold factor is observed whereas H_2S introduced increases of a factor 3. Actually, a large part of sulfur species is not fully converted during the reductant step and remain adsorbed on the surface

of the carrier. This leads to a huge amount of SO_2 produced during oxidant step in this last case.

Interestingly, the amount of SO_2 produced during reductant step is minimal at the intermediate reaction timing. In any case, the selectivity during reductant step is high. In these conditions, the amount of lattice oxygen involved in the reaction evolves proportionally to that of S produced. With the longest exposure time, the equivalent of 59 % of V^{5+} are reduced to V^{4+}.

200 °C

Similar experiments were performed at 200 °C. In this case, as seen in Figures 6.9, 6.10 and Table 6.7 the conversion evolves for the long exposure (3 minutes) experiment. Finally, the longer the exposure is, the lower the H_2S conversion. It must be reminded that longer exposures also mean higher amount of H_2S provided per cycle.
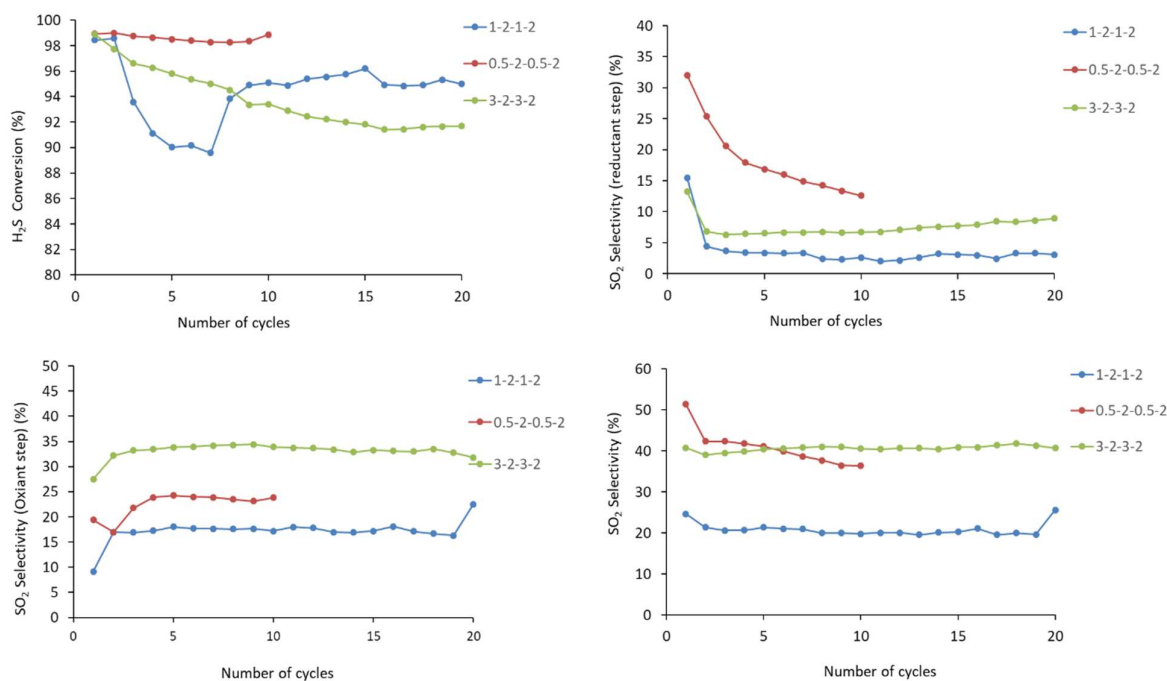
Figure 6.11: 200 mg of 2ML10, 200 °C, 2000 ppm of H_2S, H_2S:O_2 1:5, 0.5-2-0.5-2, 1-2-1-2, 3-2-3-2 cycle
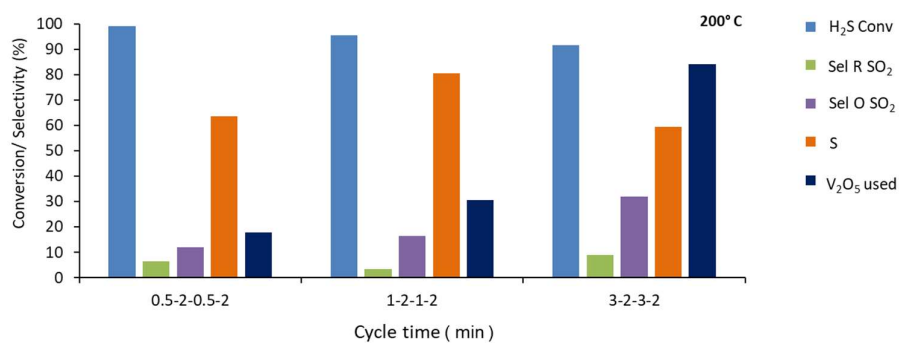
Figure 6.12: 200 mg of 2ML10, 20 0°C, 2000 ppm of H_2S, $H_2S:O_2$ 1:5, 0.5-2-0.5-2, 1-2-1-2, 3-2-3-2 cycle

For the rest, similar trends can be observed at 200 °C as at 150 °C. Huge amount of SO_2 is formed with 3 minutes exposure indicating that the maximum capacity for full conversion of H_2S is overtaken. In this case, up to the equivalent of 80 % of lattice oxygen is involved in the reductant step.

200 °C	0.5-2-0.5-2	1-2-1-2	3-2-3-2
H_2S feed per cycle (µmol)	4.3	8.60	25.9
% Conv H_2S	98.0	95.3	91.6
n converted (µmol)	4.25	8.20	23.7
S (µmol)	2.69	6.50	14.08
SO_2R (µmol)	0.54	0.27	2.12
SO_2O (µmol)	1.02	1.34	7.62
(S/S+SO_2 R) (%)	83.7	96.0	86.8
%O_{latt} (% V^{5+} -> V^{4+})	17.8	30.5	80.0

Table 6.8: 200 mg of 2ML10, 200 °C, 2000 ppm of H_2S, $H_2S:O_2$ 1:5, 0.5-2-0.5-2, 1-2-1-2, 3-2-3-2 cycle

Although H_2S is not fully converted to S or SO_2 in the longest experiment, it is interesting to note that the amount of SO_2 produced is the highest. This suggests, as already observed, that deep reduction of the carrier lead to unselective oxidation.

6.2.3 – Effect of different ratio between reactants ($H_2S:O_2$)

Effect of different ratio of reactants has been studied at 150 °C by keeping the H_2S concentration at 2000 ppm and changing the oxygen concentration accordingly from 10000

ppm to 5000 ppm, 3000 ppm, and 1000 ppm to achieve the ratio of 1:5, 1:2.5, 1:1.5, and 1:0.5 respectively.

The 1:5 ratio corresponds to the "standard" conditions studied up to this point while the 1:0.5 ratio correspond to the stoichiometric one for selective oxidation of H_2S.

150 °C

For all the ratios, the conversion of H_2S is very high (above 80 %). If one excepts the singular behavior of 1:5 experiments, other high oxygen concertation experiments show relatively stable evolution. In the case of 1:0.5, i.e. lowest oxygen concentration, the conversion decreases steadily to reach a stable conversion of 84 %.
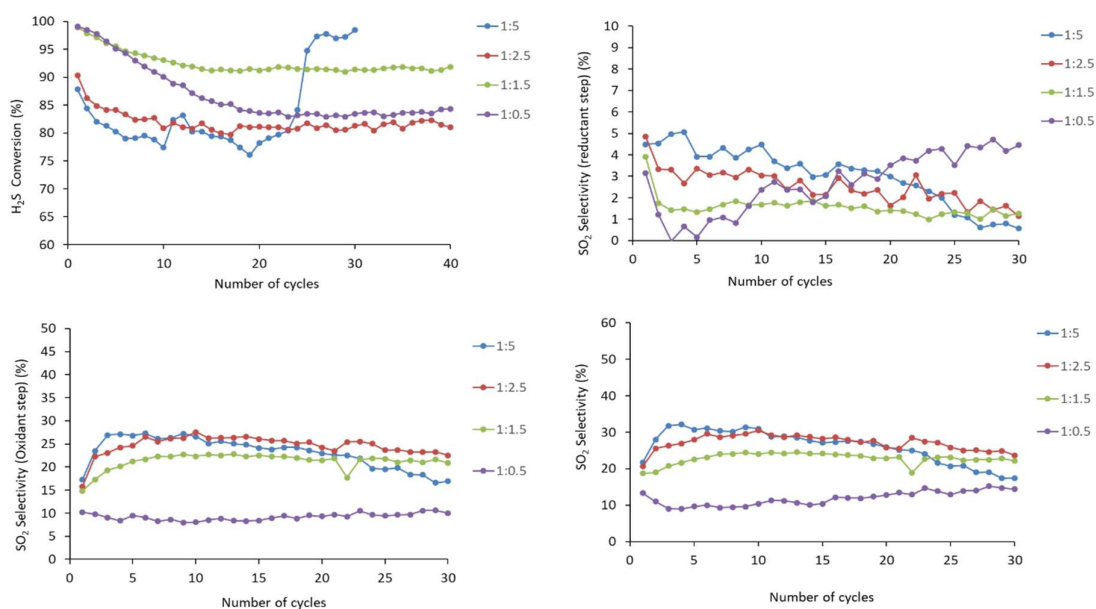
Figure 6.13: 200 mg of 2ML10, 150 °C, 2000 ppm of H_2S, H_2S:O_2 1:5, 1:2.5, 1:1.5, 1:0.5
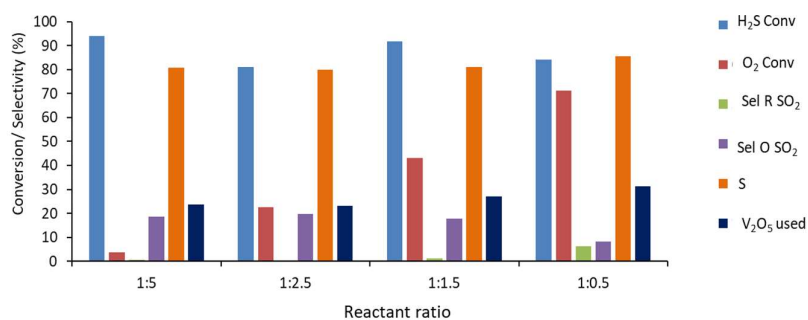
Figure 6.14: 200 mg of 2ML10, 150 °C, 2000 ppm of H_2S, H_2S:O_2 1:5, 1:2.5, 1:1.5, 1:0.5

146

150 °C	1:5	1:2.5	1:1.5	1:0.5
H_2S feed per cycle (µmol)	8.60	8.60	8.60	8.60
% Conv H_2S	94.0	81.0	91.8	84.3
n converted (µmol)	8.08	6.97	7.89	7.25
S (µmol)	6.47	5.56	6.31	6.19
SO_2R (µmol)	0.06	0.01	0.09	0.45
SO_2O (µmol)	1.54	1.41	1.50	0.60
(S/S+SO_2 R) (%)	99	99.9	98.6	93.0
%O_{latt} (% V^{5+} -> V^{4+})	27.5	23.0	27.1	31.1

Table 6.9: 200 mg of 2ML10, 2000 ppm of H_2S, 150 °C, H_2S :O_2 1:5, 1:2.5, 1:1.5, 1:0.5

While the selectivity to S for high O_2 concentration experiments increases slightly with cycling, it does not seem to be affected by the O_2 pressure. On the contrary, that of 1:0.5 evolves leading to increasing amounts of SO_2 formed during reductant step.

The experiment with the lowest O_2 concentration is also the one for which the highest amount of lattice oxygen is involved. In Figure 6.12, the O_2 conversion during oxidant step is also represented. It can be seen that it increases logically with the lowering of the inlet concentration. Most interesting is that it does not reach full conversion in the case of the lowest O_2 concentration which would correspond to that of stoichiometric selective oxidation of H_2S. At the least it should be equal to that of H_2S, or even higher consider to SO_2 formation.

This can suggest that the re-oxidation process could be limiting the reactivity of the carrier and explain the evolution of activity (decreasing H_2S conversion) if the solid is not fully re-oxidized during cycling. Previous results also suggest that the lowering of the oxidation state could generate less selective species which would be coherent with the evolution of selectivity during this low O_2 concentration experiment.

200 °C
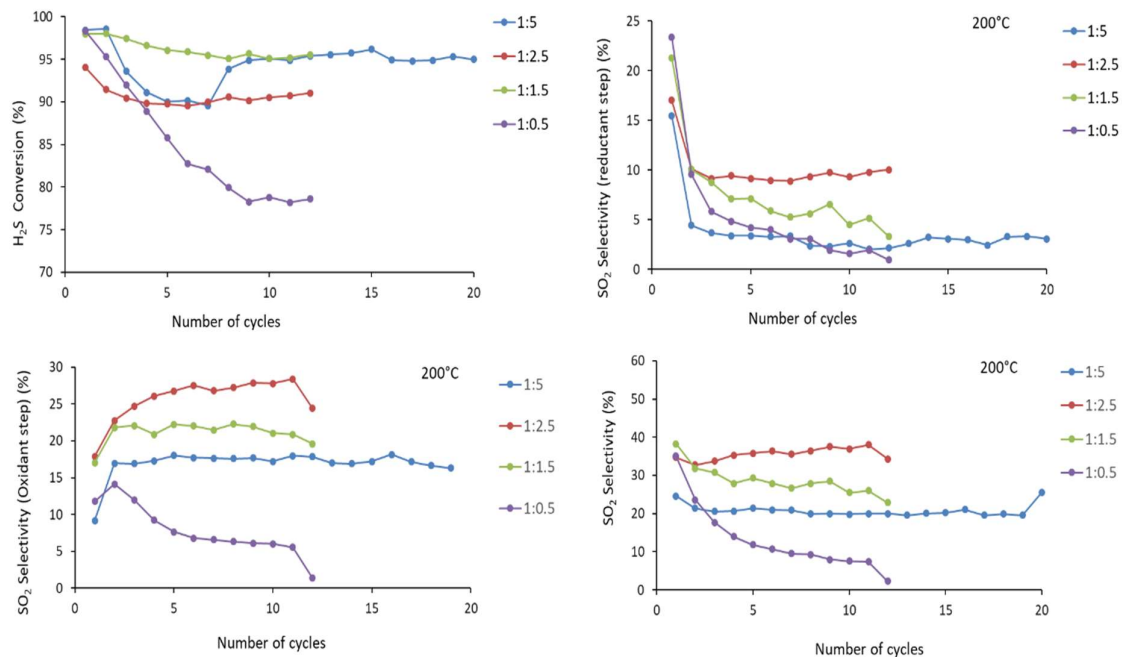
Figure 6.15: 200 mg of 2ML10, 200 °C, 2000 ppm of H₂S, H₂S :O₂ 1:5, 1:2.5, 1:1.5, 1:0.5
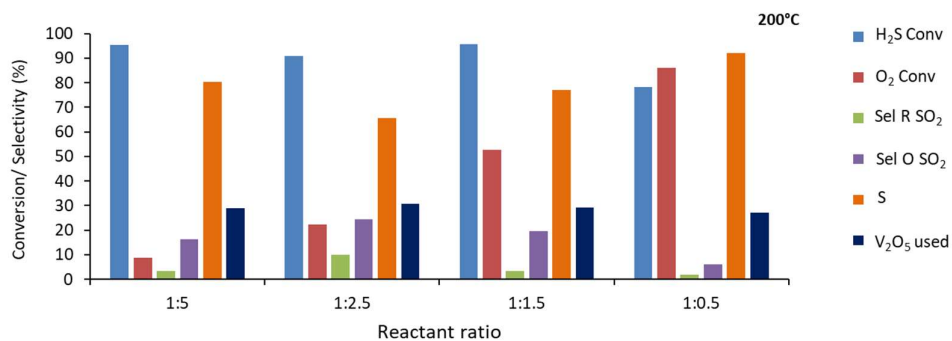
Figure 6.16 : 200 mg of 2ML10, 200 °C, 2000 ppm of H₂S, H₂S :O₂ 1:5, 1:2.5, 1:1.5, 1:0.5

200° C	1:5	1:2.5	1:1.5	1:0.5
H$_2$S feed per cycle (µmol)	8.60	8.60	8.60	8.60
% Conv H$_2$S	95.3	91.0	95.7	78.3
n converted (µmol)	8.20	7.83	8.23	6.34
S (µmol)	6.50	5.10	6.23	6.17
SO$_2$R (µmol)	0.27	0.79	0.28	0.13
SO$_2$O (µmol)	1.34	1.93	1.71	0.43
(S/S+SO$_2$ R) (%)	96.0	86.6	95.5	97.0
%O$_{latt}$ (% V^{5+} -> V^{4+})	30.5	30.8	29.3	27.1

Table 6.10: 200 mg of 2ML10, 200 °C, 2000 ppm of H$_2$S, H$_2$S :O$_2$ 1:5, 1:2.5, 1:1.5, 1:0.5

At 200 °C, for all the ratio the high and rather stable conversion of H$_2$S is observed except at the ratio 1:0.5. In this case, as at 150 °C, conversion decreases to reach 78 %.

Interestingly, reaction at low O$_2$ concentration (1:0.5) shows a better selectivity than at 150 °C. but with low conversion of the H$_2$S as SO$_2$ formation decreases both in the reductant and oxidant cycle.

To better understand the behavior of the system at such low O$_2$ concentration, the reactivity was explored at higher temperature i.e. 225 °C, 250 °C and results are compared in Figures 6.15 and 6.16 and Table 6.10.
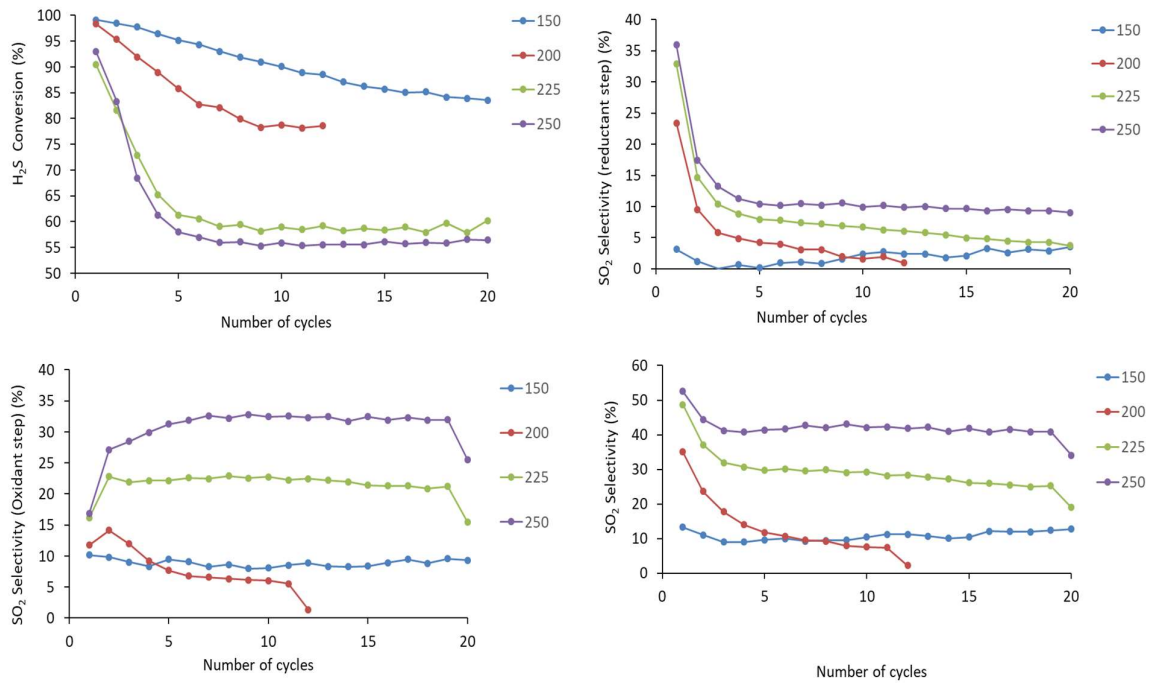
Figure 6.17: 200 mg of 2ML10, 2000 ppm H_2S, 1000 ppm O_2, $H_2S:O_2$ (1:0.5)
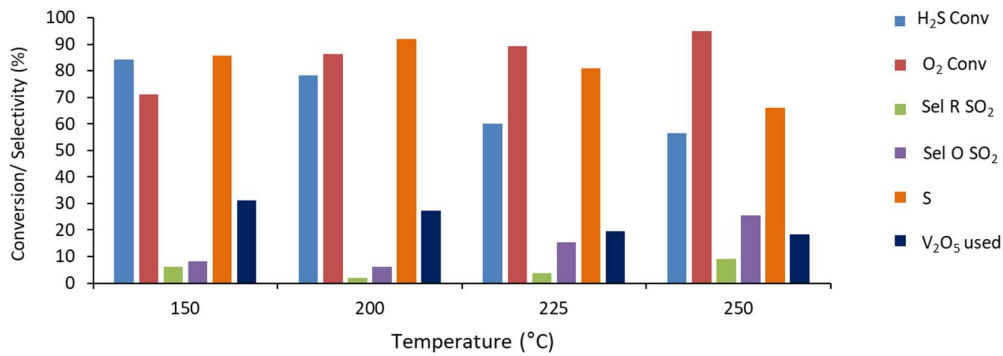
Figure 6.18: 200 mg of 2ML10, $H_2S:O_2$ (1:0.5), 2000 ppm H_2S 1000 ppm O_2

At all temperatures, the conversion decrease significantly along cycling. The speed of deactivation increases with temperature. This leads to lower conversion with increasing temperature.

Overall SO_2 formed in both reductant and oxidant steps decreases between 150 and 200 °C then increases again at higher temperature. This is particularly the case for that produced in oxidant step. This means that at higher temperature S containing species can adsorb at the

surface of the carrier (contributing to overall H_2S conversion) but would not get oxidized to produce either S or SO_2.

This reflects in the amount of lattice oxygen involved in the reaction which decreases above 200 °C. On the other hand, O_2 conversion increases with temperature and reaches values well above that of H_2S conversion at temperatures above 200 °C.

$H_2S:O_2$-1:0.5	150 °C	200 °C	225 °C	250 °C
H_2S feed per cycle (µmol)	8.60	8.60	8.6	8.6
% Conv H_2S	84.3	78.3	60.2	56.4
n converted (µmol)	7.25	6.34	5.18	4.85
S (µmol)	6.19	6.17	4.16	3.11
SO_2R (µmol)	0.45	0.13	0.19	0.44
SO_2O (µmol)	0.60	0.43	0.83	1.31
(S/S+SO_2 R) (%)	93.0	97.0	95.6	87.6
%O_{latt} (% V^{5+} -> V^{4+})	31.1	27.1	19.6	18.3

Table 6.11: 200 mg of 2ML10, $H_2S:O_2$ (1:0.5), 2000 ppm H_2S 1000 ppm O_2

At such low oxygen pressure the system clearly evolves significantly during the cyclic operation, and this leads to a decrease in overall H_2S conversion both in terms of H_2S adsorption of the carrier surface that in the actual transformation of the adsorbed species to S or SO_2 in reductant step.

However, it should be highlighted that at all temperatures, the system reaches a stable cyclic behavior indicating that a good balance between phenomena occurring at each step can effectively be reached.

6.2.4 - Effect of CH_4 presence

As explained in the chapter I, one of the potential benefits of chemical looping processes is the separation between the reductant (H_2S) and oxidant (O_2, air …) reactants. In the case of H_2S oxidation, this would allow to treat directly effluents containing H_2S in the presence of other potentially reductant species provided that the process preferentially oxidizes this compound.

As the major potential application of CLSOSH is the treatments of contaminated natural gas or biogas, it is necessary to verify the preferential and selective oxidation of H_2S with respect to methane. Reaction was therefore carried out in presence of 10 % of CH_4, with 2000 ppm of H_2S and 10000 ppm of O_2 and at different temperatures (150, 200, 250, 300 and 350 °C).

In all cases, the reaction was initially carried out without the presence of methane, immediately followed by the reaction with methane at the same temperature. Before moving to the higher temperature solid was re-oxidized at 400 °C in presence of the 10000 ppm of O_2 to ensure full regeneration of the carrier. Each time, 10 cycles were carried out without and with methane.

Results are shown in Figures 6.19 and 6.20 and Table 6.12
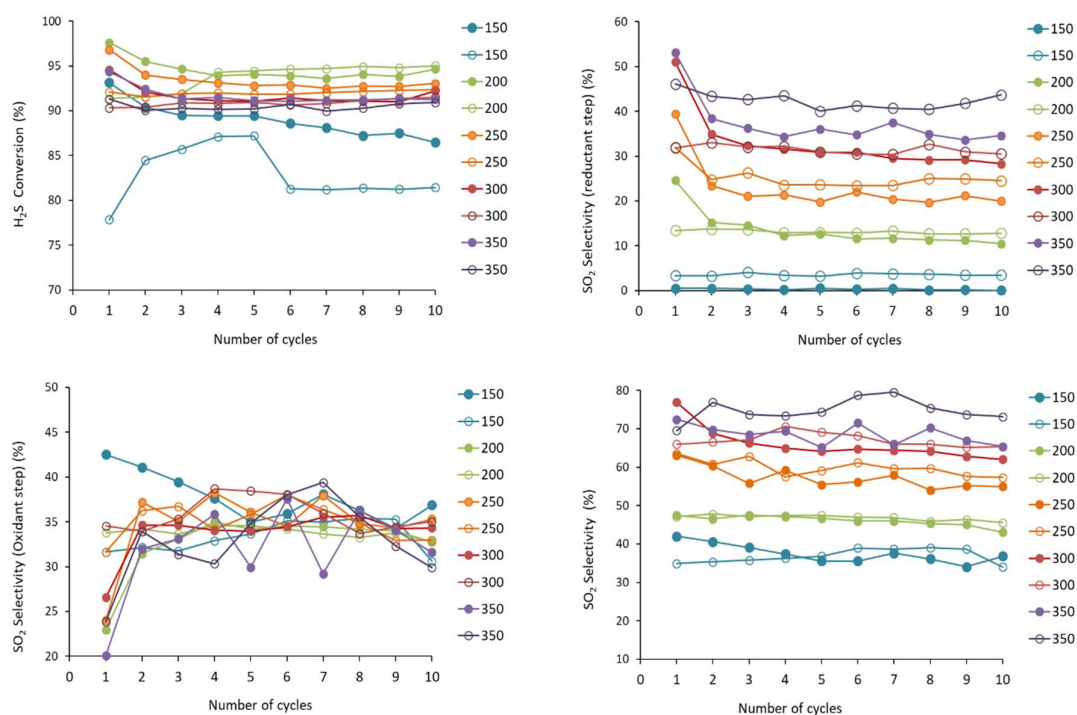
● without methane, ○ With methane

Figure 6.19: 200 mg of 2ML10, $H_2S:O_2$ (1:5), 2000 ppm, open symbols: 10% CH_4
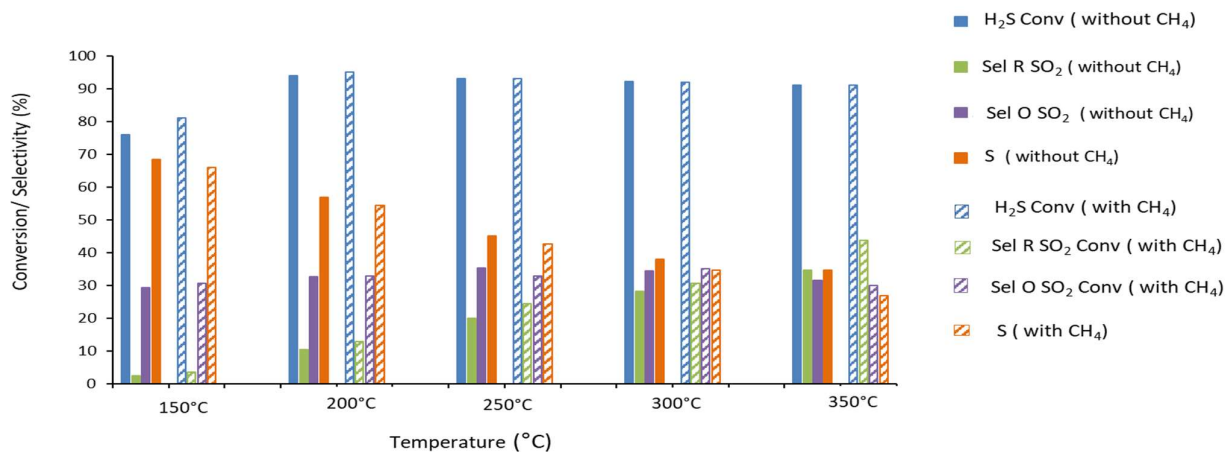
Figure 6.20: 200 mg of 2ML10, H2S:O2 (1:5), 2000 ppm, 10 % CH$_4$

2000:10000	150 °C		200 °C		250 °C		300 °C		350 °C	
	Without CH$_4$	With CH$_4$	Without CH$_4$	With CH$_4$	Without CH$_4$	With CH$_4$	Without CH$_4$	With CH$_4$	Without CH$_4$	With CH$_4$
H$_2$S feed per cycle (μmol)	8.6	8.6	8.6	8.6	8.6	8.6	8.6	8.6	8.6	8.6
% Conv H$_2$S	76.0	81.0	94.0	95.0	93.0	93.0	92.0	92.0	91.0	91.0
n converted (μmol)	6.54	6.97	8.08	8.17	8.00	8.00	7.93	7.91	7.83	7.83
S (μmol)	4.31	4.54	4.52	4.41	3.50	3.40	2.89	2.72	2.55	2.03
SO$_2$R (μmol)	0.16	0.24	0.85	1.05	1.60	1.95	2.25	2.41	2.72	3.43
SO$_2$O (μmol)	2.06	2.19	2.71	2.70	2.89	2.65	2.79	2.78	2.55	2.37
(S/S+SO$_2$ R) (%)	96.5	94.9	84.1	80.7	68.6	63.5	56.2	53.0	48.3	37.1
%O$_{latt}$ (% V^{5+} -> V^{4+})	19.8	21.8	29.3	31.3	34.4	38.3	39.8	41.1	44.3	50.9

Table 6.12: 200 mg of 2ML10, H$_2$S:O$_2$ (1:5), 2000 ppm, 10 % CH$_4$

Globally, it can be seen that the presence of 10% methane does not affect the reactivity of 2ML10 carrier both in terms of conversion and of selectivity. To the most, a very slight increase in SO$_2$ formation can be observed at the highest temperature (350 °C). It should be noted that

in all cases, no CO or CO_2 formation could be observed neither in reductant or oxidant step which would have been indicative of CH_4 conversion.

This confirms that in the temperature range of interest for CLSOSH, i.e. 150-250 °C, preferential oxidation can be performed in the presence of methane.

6.3 - After Reaction Characterization

Samples were studied before and after reaction to evaluate the structural or chemical changes in the catalysts during the reaction as seen in the chapter 3 section (3.3).

Reactions were carried out on 2ML10 samples at different temperature (150 °C and 200 °C). Four samples should thus be considered by ending either after the reductant or the oxidant steps at these two temperatures.

Furthermore, 2ML10 sample was also tested by keeping concentration constant for H_2S and by varying the concentration of oxygen. In excess of O_2 (i.e. 2000 ppm of H_2S with 10000 ppm of O_2; 1:5) and at low concentration of O_2 (i.e. 2000 ppm of H_2S with 1000 ppm of O_2; 1:0.5). So, other four samples have to be considered giving a total of eight samples are characterized after reaction:

- 2ML10 (H_2S, 150°C) : reaction stopped after 30 cycle after H_2S step at 150 °C with **10000 ppm of O_2, (H_2S:O_2- 1:5)**

- 2ML10 (H_2S,200°C): reaction stopped after 30 cycle after H_2S cycle at 200 °C with **10000 ppm of O_2 (H_2S:O_2- 1:5)**

- 2ML10 (O_2, 150°C): reaction stopped after 30 cycle at O_2 cycle at 150 °C with **10000 ppm of O_2 (H_2S:O_2- 1:5)**

- 2ML10 (O_2, 200°C): reaction stopped after 30 cycle after O_2 cycle at 200 °C with **10000 ppm of O_2 (H_2S:O_2- 1:5)**

- 2ML10 (H_2S, 150°C (0.1)) : reaction stopped after 30 cycle after H_2S step at 150 °C with **1000 ppm of O_2 (H_2S:O_2- 1:0.5)**

- 2ML10 (H_2S,200°C (0.1)): reaction stopped after 30 cycle after H_2S cycle at 200 °C with **1000 ppm of O_2 (H_2S:O_2- 1:0.5)**

- 2ML10 (O_2, 150°C (0.1)): reaction stopped after 30 cycle at O_2 cycle at 150 °C with **1000 ppm of O_2 (H_2S:O_2- 1:0.5)**

- 2ML10 (O_2, 200°C (0.1)): reaction stopped after 30 cycle after O_2 cycle at 200 °C with **1000 ppm of O_2 (H_2S:O_2- 1:0.5)**

These samples were characterized by TPR, XRD and XPS.

6.3.1 - XRD

Oxygen carrier	H$_2$S:O$_2$	H$_2$ consumption (mmol/g)	Crystallite size (nm)	
			TiO$_2$	V$_2$O$_5$
2ML10	-	0.14	80.6	-
2ML10, H$_2$S 150 °C	1:5	0.19	97.7	-
2ML10 H$_2$S 200 °C	1:5	0.16	96.9	-
2ML10 O$_2$ 150 °C	1:5	0.17	94.9	-
2ML10 O$_2$ 200 °C	1:5	0.16	90.0	-
2ML10 H$_2$S 150 °C	1:0.5	-	85.9	-
2ML10 H$_2$S 200 °C	1:0.5	-	87.3	-
2ML10 O$_2$ 150 °C	1:0.5	-	86.4	-
2ML10 O$_2$ 200 °C	1:0.5	-	91.2	-

Table 6.13: Characterization of 2ML10 carrier after reaction.
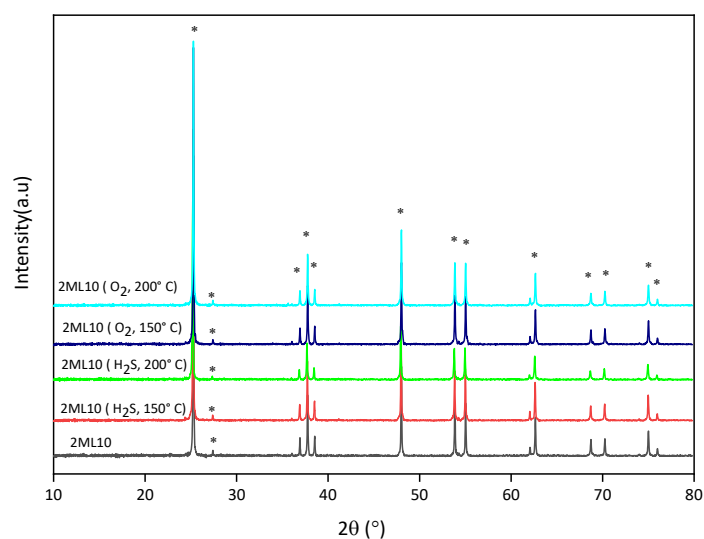
Figure 6.21: XRD study of 2ML10 (after reaction at 150 °C and 200 °C) on 2ML10 (H$_2$S:O$_2$ 1:5)

XRD pattern for the after reaction with 10000 ppm of O_2 ($H_2S:O_2$ = 1:5) does not show any significant difference in the peak position. As is the case of original 2ML10 carrier, there is no evidence of vanadium species after reaction on the solid. Reduced vanadium species peaks are also absent for all the analyzed sample. Crystallite size of the support remains constant after the reaction. XRD analysis on the carrier after reaction at 1000 ppm of O_2 ($H_2S:O_2$ = 1:0.5) does not provide any significant additional information (not reported).

6.3.2 - TPR
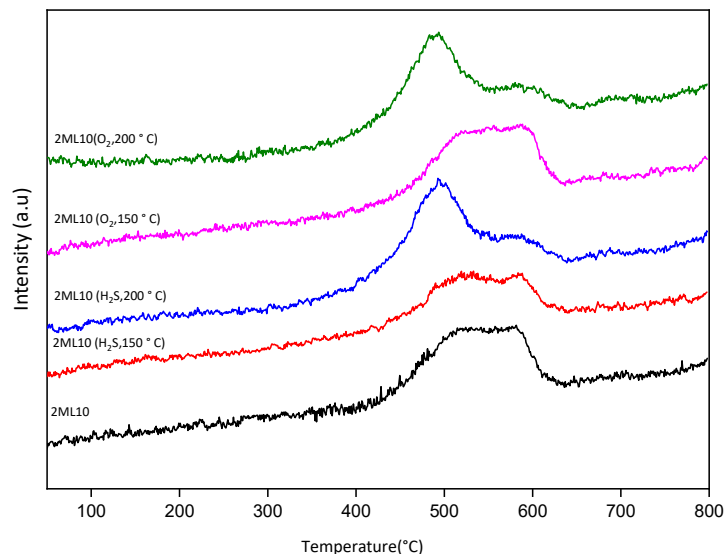
Figure 6.22: TPR study (after reaction at 150°C and 200°C) on 2ML 10 ($H_2S:O_2$ 1:5)

TPR profiles of samples treated at $H_2S:O_2$ ratio of 1:5 is shown in Figure 6.19. Interestingly, TPR performed on samples after ending cycling after H_2S exposure or O_2 exposure do not differ significantly. Major differences can be seen between samples reacted at 150 °C versus those reacted at 200 °C independently of last gas exposure. Samples treated at 150 °C show TPR very similar to that of initial 2ML10 sample, which exhibited a wide reduction peak between 450 and 600 °C. This large peak could be composed of two overlapping contributions. Samples treated at 200 °C show a reduction process starting around 400 °C with a more intense hydrogen consumption peak at 450 °C. A less intense shoulder occurs until reduction stop around 600 °C. Appearance of the second peak at high temperature suggests the presence of the distorted vanadium oxide [94].

The presence of the intense low temperature reduction peak on both samples treated at 200 °C independently of last exposure to H_2S or O_2 suggests that these species are generated during oxidant cycle at this temperature but do not intervene directly in the redox process.

6.3.3 - XPS
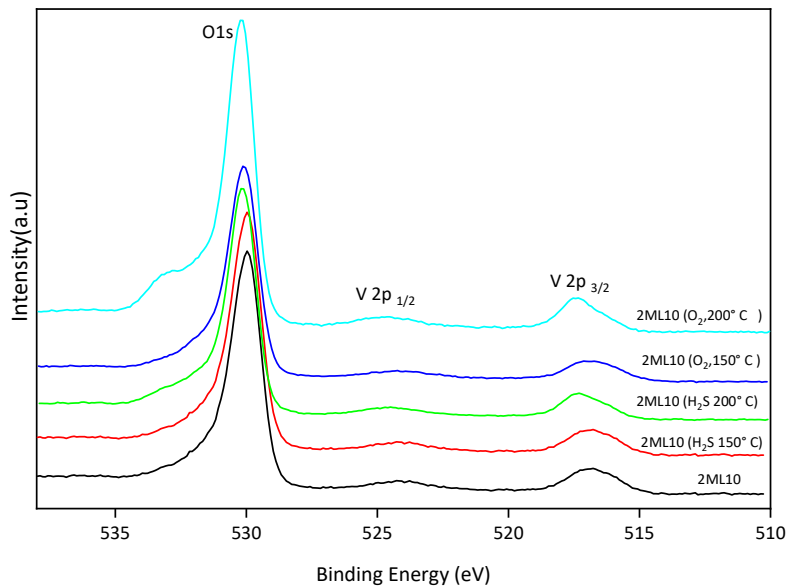
Figure 6.23: XPS pattern for O 1s and V2p core level (after reaction at 150 and 200 °C) on 2ML 10 ($H_2S:O_2$ 1:5)
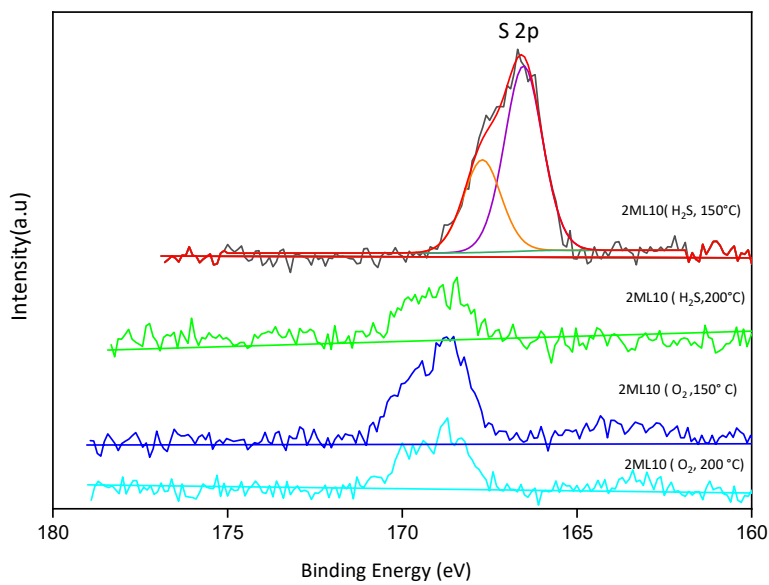
Figure 6.24: XPS pattern for S2p core level (after reaction at 150 and 200 °C) on 2ML10 ($H_2S:O_2$ 1:5)
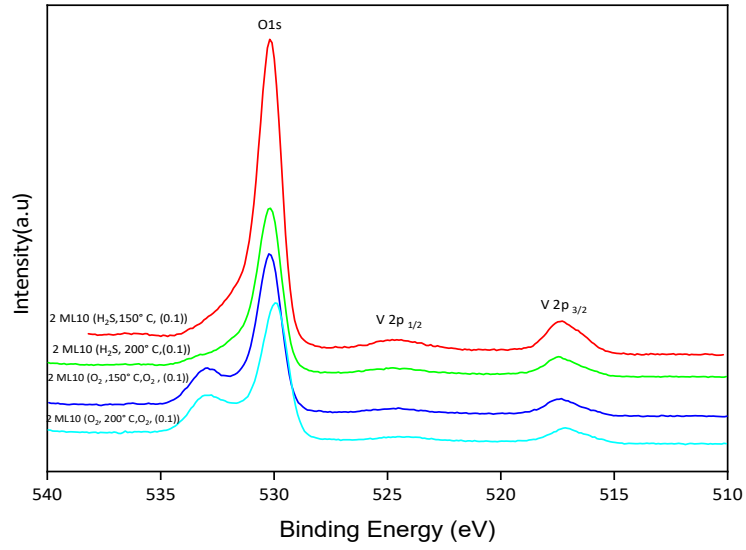
Figure 6.25: XPS pattern for O 1s and V2p$_{3/2}$ core level (after reaction at 150 °C and 200 °C) on 2ML 10 (H$_2$S:O$_2$ 1:0.5)
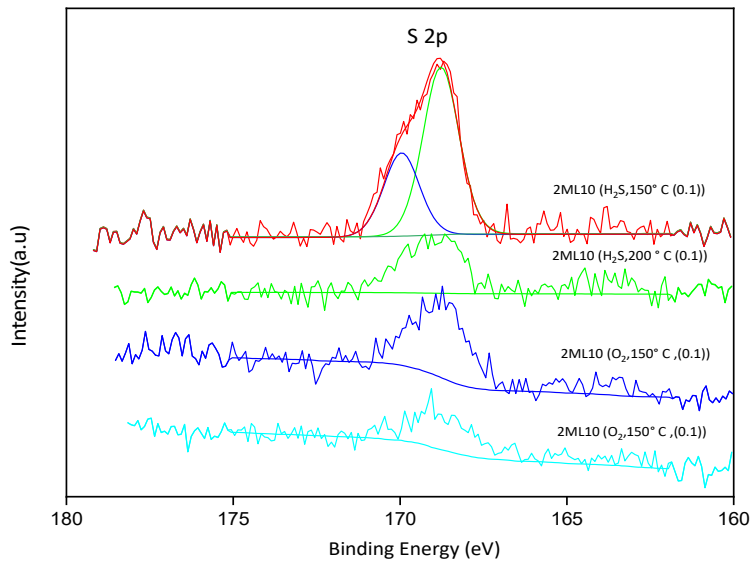
Figure 6.26: XPS patterns for S 2p core level (after reaction at 150 and 200 °C) on 2ML10 (H$_2$S:O$_2$ = 1:0.5)

Carrier	$H_2S:O_2$	B.E (eV) V 2p V^{4+}	B.E (eV) V 2p $V5^+$	$V^{4+}/$ $(V^{4+}+V^{5+})$	$V^{5+}/$ $(V^{4+}+V^{5+})$	V/O	V/Ti	S/V
2ML10	-	516.1	517.1	0.38	0.62	0.08	0.22	
2ML10, H_2S 150 °C	1:5	516.5	517.5	0.32	0.68	0.08	0.25	0.16
2ML10 H_2S 200 °C	1:5	516.2	517.4	0.30	0.70	0.08	0.23	0.08
2ML10 O_2 150 °C	1:5	516.2	517.3	*0.56*	*0.44*	0.07	0.20	0.14
2ML10 O_2 200 °C	1:5	516.2	517.0	0.22	0.78	0.06	0.20	0.07
2ML10 H_2S 150 °C	1:0.5	516.4	517.5	0.36	0.64	0.07	0.21	0.12
2ML10 H_2S 200 °C	1:0.5	516.2	517.4	0.22	0.78	0.07	0.24	0.07
2ML10 O_2 150 °C	1:0.5	516.5	517.5	0.13	0.87	0.07	0.19	0.13
2ML10 O_2 200 °C	1:0.5	515.8	517.3	0.16	0.84	0.05	0.19	0.07

Table 6.14: XPS study of 2ML10 after reaction, 1:5 and 1:0.5

XPS analysis has been performed on all 2ML10 samples after reaction stopping either after reductant or oxidant step, at the two temperatures and the two O_2 concentrations.

In all cases, only V^{4+} species are observed at 516.2 eV (±0.4 eV) and V^{5+} species around 517.3 (±0.3 eV) [85][116]. However, detection of the V^{3+} and V^{4+} is difficult as both would appear around the same peak position [82][83][104]

The proportion between V^{4+} and V^{5+} species vary according to the last exposed reactant as can be expected by the consumption of lattice oxygen for H_2S oxidation. This can be clearly seen as, in all cases, the proportion of V^{4+} species is higher after exposure to H_2S than after oxidant step. Only in one specific case (reaction at 150°C and $H_2S:O_2$ = 1:5) the V^{4+} is actually higher after oxidant step, which is quite abnormal.

As it could be seen earlier (Tables 6.9 at 150 °C and Table 6.10 at 200 °C), in all cases approx. 27 to 30 % of lattice oxygen (in terms of V^{5+} reduced to V^{4+}) is involved in the chemical looping process independently of O_2 concentration or temperature when stable cycling is reached. XPS data quantification does not reflect such intense variations between samples collected after reductant or oxidant step. For example, at 200°C and $H_2S:O_2$=1:5 proportion of V^{4+} vary between 0.30 after reductant step and 0.22 after oxidant one while a variation of 0.30 (30%)

should be observed. The limited accuracy of XPS with such low vanadium loaded samples, in particular regarding different V species quantification could account for this difference.

Interestingly, if one excepts the "abnormal" result obtained at 150°C and $H_2S:O_2$ = 1:5, the average oxidation state of V seem to be higher in all carriers collected after using the lowest oxygen pressures. Furthermore, if one looks at the proportions of species obtained after oxidants steps, it appears that the overall proportion of V^{4+} is lower after chemical looping processing than that found in the original 2ML10. In particular, up to 84-87% V^{5+} species are found at the lowest O_2 concentration experiment whereas the initial carrier contained only 62%.

Regarding O1s photopeak, after deconvolution presence of three oxygen species is observed bond with the different vanadium species or with the support. An important shoulder appears after all oxidant step, except for the sample analyzed after reaction at 150 °C and $H_2S:O_2$ = 1:5. This peak illustrates the presence of oxygen from the water or the adsorbed O_2 [117] and is only seen after the cycle stopped at oxidant step.

V/ Ti ratio do not vary significantly between samples.

Sulfur species were observed for all the samples although the intensity of the photopeak at S 2p is very low in most cases. The presence of sulfate species is prominently observed with a peak at 168.8 eV [86]. Due to the low intensity of S 2p peak, and low V content, S/V values reported in Table 6.14 have to be taken with caution. Nevertheless, XPS spectra reported in Figures 6.24 ($H_2S:O_2$ = 1:5) and 6.26 ($H_2S:O_2$ = 1:0.5) clearly show that the samples recovered after exposure to H_2S at low temperature show the most intense S photopeaks as could be expected. More surprisingly, little difference could be observed at 200 °C when comparing samples last exposed to H_2S or O_2.

6.3.4 - Raman

Unfortunately, Raman analysis could not be performed on all samples but only on those collected after reactions performed at 150 °C with the highest oxygen concentration ($H_2S:O_2$ = 1:5), i.e. the so-called "standard" conditions in which most tests were performed.

Figure 6.27 shows a zoomed portion of the spectrum in which the most significant difference between initial 2ML10 carrier and those collected after reaction is observed. Peak Present at 997 cm^{-1}, attributed to V=O in crystalline V_2O_5, loses its intensity. Whereas a new peak is observed at 903 cm^{-1} due to the presence of the V^{5+}-O-V^{4+} from the V_4O_9 structure as shown by J.M. López Nieto et al. [61][88].
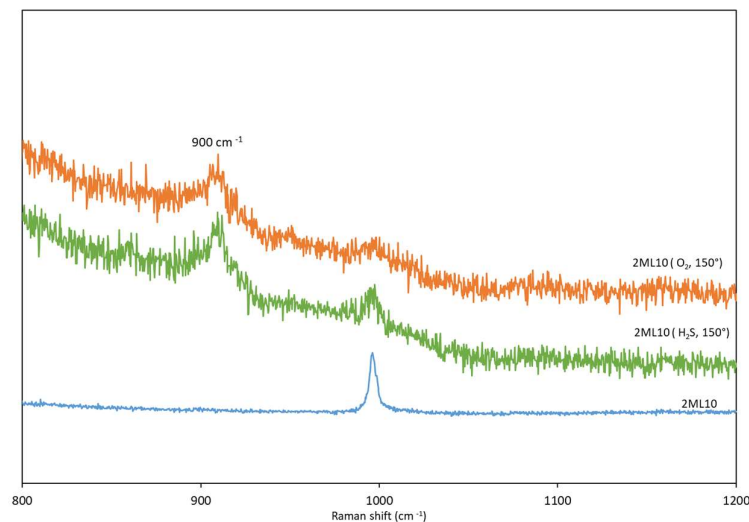
Figure: 6.27: TPR study (after reaction at 150 °C) on 2ML 10 ($H_2S:O_2$, 1:5)

6.4 - General discussion and conclusions

The objective of this chapter was to deepen our understanding of the properties of 2ML10 V_2O_5/TiO_2 carrier having observed in the previous chapter that it provided the optimal reactivity with respect to active phase loading on TiO_2 and support texture. For this, experimental conditions of chemical looping were varied in terms of reaction temperature, reactant concentration and ratio, and cycling timing.

First it should be noted that in a general way very high conversion of H_2S can be reached with this carrier in most reaction conditions. Also, even if significant evolutions along cycling is sometimes observed, in nearly all cases the system reaches a "stable" cyclic behavior after a certain number of cycles (typically 10-20 at most). In none of the experimental conditions explored did a continuous and total deactivation be observed.

This highlights the robustness of this carrier for this very constraining reaction conditions of chemical looping which imply repetitive transient solid transformations.

If rather stable activities can be reached in all experimental conditions, samples can show very different selectivity towards selective oxidation to S or unselective oxidation to SO_2.

As seen in previous chapters, whereas S production can be assumed to occur in the reductant step, SO_2 can be produced in both. In the case of SO_2 produced in oxidant step, it mostly appears when excess H_2S is provided to the system with respect to the capacity of the carrier to convert it in the reductant step. Results provided in this chapter do not bring significant new insight. The discussion will therefore mostly be focused on carrier selectivity in reductant step.

Considering SO_2 produced in reductant step, results suggest that the optimal amount of lattice oxygen available for reaction is limited to approx. 35-40 % (expressed in terms of V^{5+} to V^{4+} transformation in V_2O_5) as already observed in previous chapter. This can be seen when increasing H_2S provided in this reductant step either by increasing reactant concentration or the reductant step duration. When increasing concentration to 4000 ppm only 39 % of lattice oxygen can be extracted independently of temperature (150 or 200 °C). Furthermore, at these values of lattice oxygen involved, selectivity towards S decreases with more SO_2 formed during reductant step. This is even better seen when longer reductant time is used for which up to 80% of lattice oxygen can be extracted but with severe consequence on SO_2 formation in both reductant and oxidant step.

Considering that the initial carrier does not contain exclusively V^{5+} species at the beginning but only 62 % as shown by XPS, it is highly probable that when levels of lattice oxygen extraction of 40 % is reached, V^{4+} reduction to V^{3+} may start to occur. As this is usually concomitant with increased production of SO_2 in reductant step, it supports the hypothesis that V^{4+} to V^{3+} reduction would provide less selective oxidation of H_2S than that of V^{5+} specie reduction to V^{4+}.

On the other side, production of some SO_2 in the reductant step can also be observed when the system is potentially at higher oxidation state. This can mostly be seen when reactions are performed in conditions for which low amounts of lattice oxygen is involved, e.g. with low H_2S concentration or short reductant step timing. This is enhanced when temperature is increased in these conditions. Indeed, in most cases H_2S conversion remains very high or near to total and can increase only very limitedly whereas oxidation can proceed more efficiently. This suggests that highly oxidized carrier, or V^{5+} species present at the surface, could be less selective than partially reduced carriers.

To summarize and draw a simplified scheme of the properties of such system, it can be assumed that fully oxidize carrier (i) generate slightly less reactive carriers as observed on large crystallites or even bulk V_2O_5, and (ii) show lower selectivity due to formation of limited amounts of SO_2 in reductant step (Left case in Figures 6.28).

In presence of partially reduced carrier, conversion can reach very high levels indicating good H_2S adsorption and activation capacity.

The properties of the carriers will be mostly differentiated in terms of selectivity with lower amounts of SO_2 formed if the amplitude of V species reduction is small enough to only imply V^{5+} specie reduction to V^{4+} (Middle case in Figures 6.28). If deeper reduction occurs, involving V^{3+} species, SO_2 can again be produced and thus lowering the selectivity while reactivity remains elevated (Right case in Figures 6.28).
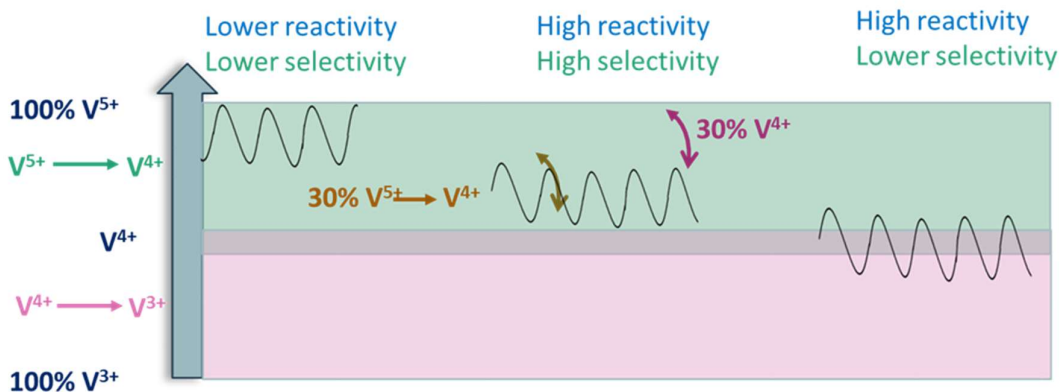
Figure 6.28: Schematic representation of reactivity according to V oxidation state

Obviously, such simplified image only describes the system once it reaches a stable cyclic behavior. A good balance between the rates of reduction during the exposure to H_2S and that of re-oxidation in O_2 is necessary to avoid continuous reduction of the carrier along cycling or, on the contrary over-oxidation and generation of unselective surface species. In this respect the process of stabilization is analogous to the reaching of steady state activity in co-feed catalysis which also involves similar rates of reduction and oxidation when Mars and Van Krevelen reaction mechanism is considered [10].

Although most experimental conditions explored lead to a relatively rapid stabilization of the carrier behavior during cycling, in some cases strong evolutions can occur. This is particularly the case of 2ML10 when tested at 150 °C and using 2000 ppm H_2S (1 minute H_2S exposure). As mentioned several times, in these conditions the carrier shows a very singular behavior with a sudden increase in reactivity after 20-25 cycles, which can be seen to occur faster at higher temperature. In all other cases, the evolution of reactivity in terms of H_2S conversion or selectivity showed to be monotonous. At this level of the study it is not possible to bring some absolute explanation for this singular behavior which affects conversion but not selectivity. Further investigation and characterization will be necessary to determine the nature of the evolution of the carrier and identify the cause of the sudden increase in reactivity. The presence of V_4O_9 as suggested by Raman characterization on this sample could provide some interesting path for further investigation.

Regarding reactivity of carriers **in the presence of methane**, it has been seen that the properties of the carrier are practically unaffected. This concern both H_2S conversion and selectivity. The absence of reactivity of methane in these conditions is not a surprise as for most catalytic reactions involving this reactant, in particular on oxide based catalysts, much higher reaction temperatures are needed. For example, in the case of V based catalysts,

temperature between 550 and 650 °C had to be used for the oxidation of methane to formaldehyde on silica supported V as shown by Loricera et al.[118] or Nguyen et al. [119]

However, it could not be excluded *a priori* that the carrier, being partially reduced by H_2S in chemical looping conditions, could not in some way interact with methane and affect the reactivity either in terms of conversion or selectivity, or eventually contaminate the carrier surface.

The confirmed absence of reactivity with respect to methane therefore opens clearly the path for the direct and preferential conversion of H_2S contained in methane streams such as natural gas or biogas.

Chapter VII

Conclusions and perspectives

Chapter 7 – Conclusions and perspectives

7.1 - Conclusions

Selective oxidation of the H_2S to elemental sulfur is a crucial reaction in industrial processes. The aim of this work was to explore the possibility of performing selective oxidation of H_2S in so-called "chemical looping" mode (CLSOSH), in particular in the frame of the valorization of methane resources such as natural gas or biogas.

The crucial point in chemical looping processes is the identification of the most appropriate oxygen carrier. Then the key factors governing reactivity and selectivity need to be understood in order to determine the conditions in which the process can be developed and its potential limitations with respect to thermodynamics, over-oxidation or more generally selectivity towards the desired product or deactivation of the carrier (e.g. by accumulation of sulfur over the surface). An important point to underline is that, as this reaction has never been studied in chemical looping mode, experimental and methodology aspects also needed to be considered.

The main strategy that was followed during this study consisted in identifying a potential active phase as carrier through literature and thermodynamic considerations. Then this carrier was tested alone in bulk form (Chapter 3). Subsequently, the most appropriate support was determined (Chapter 4). Then, the loading of active phase on this support was studied (Chapter 5). Finally, the most interesting carrier was further studied to better understand the nature of active species (Chapter 6) and the influence of several experimental parameters. Characterization of the carriers were performed for a better understanding of the solid transformations during the reaction. Finally, the process was tested in the presence of methane to check the feasibility of direct natural gas or biogas treatment which implies preferential oxidation of H_2S with respect to methane.

From the literature on co-feed catalytic selective oxidation of H_2S, V_2O_5 appeared to be a good candidate for this reaction. After checking the thermodynamic feasibility of the process on this material, it has been tested in chemical looping and proved to be highly reactive and selective towards elemental sulfur at rather low temperature (150-200 °C). It could be seen that even at such low temperature sub-surface V species are involved in the looping process and not only surface species. On the contrary, it is suspected that uppermost surface specie would be responsible for unselective SO_2 production in the reductant step (i.e. during exposure to H_2S). Depending on reaction conditions, some deactivation of the system could be observed but characterizations performed on used samples suggest that sulfur accumulation should not be responsible.

Typical oxide materials used for supporting catalysts, such as TiO_2, SiO_2, CeO_2, Al_2O_3 or ZrO_2, have been considered for supporting V_2O_5 active phase. Some of these materials show own

redox capacity which may interfere with the looping process as it is particularly the case for CeO_2. Otherwise TiO_2 and SiO_2 have been identified as the most promising supports for CLSOHS as they provide analogous or even better performances in comparison with bulk V_2O_5.

Deeper investigation on V_2O_5 supported on TiO_2 have shown that optimal performances could be reached for carrier containing the equivalent of 2 monolayers of V_2O_5 dispersed on the surface of the support. Lower loadings tend to generate very reactive but less selective active species. Furthermore, as the absolute oxygen capacity of the carrier is dependent on the amount of V_2O_5, low loadings carriers rapidly reach the limit of H_2S transformation. This allow adsorbed H_2S to be converted to SO_2 in the regeneration step. Furthermore, it also may lead to over-reduction of the vanadium species which are suspected to be less selective towards elemental S. For higher loading, the formation of tower-like V_2O_5 structures at the surface of the support seem to be detrimental to the reactivity of the carrier. Several phenomena may concur. First, larger crystallites exhibit higher proportion of V^{5+} species (with respect to V^{4+}) which seem less reactive or, in particular surface species, less selective. Second, in the case of tower-like structures, bare TiO_2 can still be exposed even at high loadings. This can participate to H_2S adsorption generating higher amounts of SO_2 produced during oxidant (regeneration) step. Finally, textural properties of the support have been proved to be very important for this process, in particular regarding selectivity towards elemental sulfur. Support with higher porosity may induce consecutive reactions in the reductant step and thus over-oxidation of product, but also accumulation of adsorbed sulfur species (e.g. elemental S produced, or unreacted H_2S). These would then be oxidized in SO_2 during regeneration steps contributing to low selectivity.

The study performed on the optimal loading of V_2O_5 (2 monolayers) on low surface area TiO_2 further confirms the importance of finding a good balance between vanadium species in different valence states. All results suggest that best selectivity in elemental sulfur is obtained when V^{5+} to V^{4+} reduction occurs, whereas V^{4+} to V^{3+} reduction seem to be more favorable to unselective oxidation. On the other hand, highly oxidized systems with high proportions of V^{5+} seem to be less reactive and slightly less selective, as already mentioned. Optimal situation can be found when approx. 30 % of V is converted from V^{5+} to V^{4+} but starting from materials which already contain significant proportions of V^{4+} (>30 %).

CLSOHS performed on most of these materials, and particularly on the optimal carrier mentioned above, show that stable repetitive cycling operation can be reached in most of the cases. Singular behaviors have been observed which need to be studied in more details. Depending of process conditions, activity in terms of conversion or selectivity towards elemental sulfur or SO_2 in either steps may vary significantly. However, total deactivation of the reaction has never been observed. Obviously, longer cycling should be considered, but at this stage it can be concluded that V_2O_5/TiO_2 systems offer very versatile and adaptive carriers for CLOSHS.

Finally, as could be expected in this reaction temperature range, the presence of methane does not interfere with the CLSOSH process in the conditions explored. No reactivity of CH_4 could be observed during the cycling even in presence of reduced active phase.

From this ever-first study of selective oxidation of H_2S in chemical looping mode, it can therefore be concluded that the technical demonstration of feasibility at laboratory scale has been provided and that a highly potential oxygen carrier system for this reaction could be proposed.

Further investigations need, obviously, to be undertaken for further development of this highly attractive process.

7.2 - Perspectives

Future work is necessary to pursue the development of chemical looping selective oxidation of H_2S. Studies need to be performed on different aspects and times scales.

Further fundamental research need to be done to better understand the dynamic behavior of active phase during cyclic operation. In the work presented here, all reactivity properties were determined considering each step as a single operation. This means that all reactants consumed and products generated were integrated over the full step to give a global reactivity. Obviously, the evolution of reactants within a single step can provide very useful information on the reactivity of the system. This kind of approach needs to have very good control of many experimental parameters, in particular reactor design and very reliable time responses through the analytical tools in order to obtain reliable transient kinetic data. For these reasons, such approach was not undertaken in the time frame of this work, but would deserve to be considered in the future.

Still on fundamental aspects, carriers have shown to evolve during chemical looping cycling. This is particularly the case for the optimal carrier which exhibited a singular non-monotonous behavior. This needs to be further investigated and detailed characterizations are particularly needed to understand these dynamic phenomena in a better way. In-situ or Operando experiments would certainly provide very interesting information but are challenging to perform due to the transient and cyclic nature of the reaction and the presence of the H_2S as the main reactant.

The lower range of the temperature can be explored on existing carrier system to have a better understanding of the accumulation of the reactant and product "S" over the surface of the carrier.

Another path for further investigations would be to explore different oxygen carrier materials. While remaining on Vanadium oxide based solids one could further explore the use of other support than TiO_2. In this respect, the work performed over the SiO_2 support provided interesting results for CLSOHS and would deserve a thorough study. Effect of various preparation methods of the carrier can also be studied to understand the presence of defects in the carrier and their effect on the reactivity of the system. Another well-known way to modify the redox properties of V_2O_5 based materials consists in doping with other elements.

Finally, other active phase could be considered starting from other active phases reported in literature to have interesting properties for selective oxidation of H_2S such as Fe_2O_3, Mn_2O_3, CoO. These would be interesting to study for CLSOHS system in particular with respect to the selectivity towards elemental Sulfur.

Along with this fundamental research, other aspects need to be considered to allow industrial development of CLSOSH.

For instance, in this work H_2S concentrations in the 1000 to 4000 ppm range have been considered as these are among the highest found in most common natural gas or biogas resources. Due to the concept of chemical looping processes, which avoid mixing between oxidant and reductant reactants, any H_2S concentration could, in principle, be considered, even pure H_2S. Exploring other ranges would be very useful on both upper and lower concentrations. For the first, very high H_2S concentrations streams, e.g. resulting from desulfuration plants, could be considered to provide a complementary route to Claus process.

In the lower range, it would be necessary to estimate the capacity of CLSOSH to perform ultimate H_2S purification to reach levels in which the stream can be utilized without further treatment, typically ppm levels. Indeed, a special attention should be paid to the reaction kinetics which may be limiting at very low concentrations.

In this work, we have shown that the presence of methane has no effect on the CLSOSH process. However, other reactants may be present in "real" hydrocarbon streams of interest and their effect on the process needs to be studied in detail.

Among others, presence of the water is inevitable either in the sources of H_2S or as product and it can affect considerably the reactivity and selectivity of the system. Indeed, many researches [120]–[122] have already studied the effect of water on the reactivity and selectivity for H_2S removal. This certainly needs to be investigated.

Presence of different hydrocarbons in the fuel depends on the sources from which it is extracted. Hydrocarbons such as alkanes, unsaturated hydrocarbons, cycloalkanes, and aromatic hydrocarbons will necessarily have higher reactivity as compared to methane. These hydrocarbons can affect the preferential oxidation of H_2S and regeneration capacity for the oxygen carrier.

Still depending on the hydrocarbon source, other S containing compound may be present, such as CS_2, COS or CH_3SH. These are generally present, if any, at very low concentrations but could constitute severe poisons to the process. Their effect should therefore be checked carefully.

Detailed study of the presence of such other reactants can also provide interesting insight for the understanding of carrier reactivity. However, as the nature and concentrations of all these potential compounds strongly depend on the source of methane, these studies will necessarily have to be done once specific hydrocarbon resources or applications are defined, possibly in collaboration with industrial partners.

References -

[1]   A. Piéplu, O. Saur, J. C. Lavalley, O. Legendre, and C. Nédez, *Claus catalysis and H_2S selective oxidation*, vol. 40, no. 4. 1998.

[2]   K. V. Bineesh, D. K. Kim, M. I. L. Kim, and D. W. Park, "Selective catalytic oxidation of H_2S over V_2O_5 supported on TiO_2-pillared clay catalysts in the presence of water and ammonia," *Appl. Clay Sci.*, vol. 175, no. 2011, pp. 183–188, 2011.

[3]   X. Wu, V. Schwartz, S. H. Overbury, and T. R. Armstrong, "Desulfurization of gaseous fuels using activated carbons as catalysts for the selective oxidation of hydrogen sulfide," *Energy and Fuels*, vol. 19, no. 1774–1782, 2005.

[4]   R. O. Beauchamp, J. S. Bus, J. A. Popp, C. J. Boreiko, D. A. Andjelkovich, and P. Leber, "A critical review of the literature on hydrogen sulfide toxicity," *CRC Crit. Rev. Toxicol.*, vol. 13, no. 1, pp. 25–97, 1984.

[5]   Diane Stirling and James H. Clark, "Adsorption and absorption of H_2S," in *The Sulfur Problem: Cleaning Up Industrial Feedstocks*, 2000, pp. 16–30.

[6]   V. Meeyoo, J. H. Lee, D. L. Trimm, and N. W. Cant, "Hydrogen sulphide emission control by combined adsorption and catalytic combustion," *Catal. Today*, vol. 44, no. 1–4, pp. 67–72, 1988.

[7]   M. S. Shah, M. Tsapatsis, and J. I. Siepmann, "Hydrogen Sulfide Capture: From Absorption in Polar Liquids to Oxide, Zeolite, and Metal-Organic Framework Adsorbents and Membranes," *Chem. Rev.*, vol. 117, no. 14, pp. 9755–9803, 2017.

[8]   Á. Reyes-Carmona *et al.*, "Iron-containing SBA-15 as catalyst for partial oxidation of hydrogen sulfide," *Catal. Today*, vol. 210, pp. 117–123, 2013.

[9]   J. S. Eow, "Recovery of Sulfur from Sour Acid Gas : A Review of the Technology," no. October, pp. 143–162, 2002.

[10]   B. Pongthawornsakun, S. Phatyenchuen, J. Panpranot, and P. Praserthdam, "The low temperature selective oxidation of H_2S to elemental sulfur on TiO_2 supported V_2O_5 catalysts," *J. Environ. Chem. Eng.*, vol. 6, no. 1, pp. 1414–1423, 2018.

[11]   K.-T. Li and T.-Y. Chien, "Effect of supports in hydrogen sulfide oxidation on vanadium-based catalysts," *Catal. Letters*, vol. 57, pp. 77–80, 1999.

[12]   M. D. Soriano, J. M. López Nieto, F. Ivars, P. Concepción, and E. Rodríguez-Castellón, "Alkali-promoted V_2O_5 catalysts for the partial oxidation of H_2S to sulphur," *Catal. Today*, vol. 192, pp. 28–35, 2012.

[13]   N. Keller, C. Pham-Huu, and M. J. Ledoux, "Continuous process for selective oxidation of H_2S over SiC-supported iron catalysts into elemental sulfur above its dewpoint," *Appl. Catal. A Gen.*, vol. 217, no. 1–2, pp. 205–217, 2001.

[14] J. M. Nhut, P. Nguyen, C. Pham-Huu, N. Keller, and M. J. Ledoux, "Carbon nanotubes as nanosized reactor for the selective oxidation of H_2S into elemental sulfur," *Catal. Today*, vol. 91–92, pp. 91–97, 2004.

[15] H. R. Mahdipoor, K. Khorsand, R. Hayati, and H. Javaherizadeh, "Effect of Reaction Furnace and Converter Temperatures on Performance of Sulfur Recovery Units (SRUs)," *J. Pet. Sci. Res.*, vol. 1, no. 1, pp. 1–3, 2012.

[16] D. D. E. Koyuncu and S. Yasyerli, "Selectivity and Stability Enhancement of Iron Oxide Catalyst by Ceria Incorporation for Selective Oxidation of H_2S to Sulfur," *Ind. Eng. Chem. Res.*, vol. 48, no. 11, pp. 5223–5229, 2009.

[17] Bineesh Kanattukara Vijayan, K. M. Il, L. G. Hwa, S. Manickam, and P. D. Won, "Catalytic performance of vanadia-doped alumina-pillared clay for selective oxidation of H_2S," *Appl. Clay Sci.*, vol. 74, pp. 127–134, 2013.

[18] X. Zhang *et al.*, "Selective oxidation of H_2S over V_2O_5 supported on CeO_2-intercalated Laponite clay catalysts," *Catal. Sci. Technol.*, vol. 3, no. 10, pp. 2778–2785, 2013.

[19] D. Park, B. Park, D. Park, and H. Woo, "Vanadium-antimony mixed oxide catalysts for the selective oxidation of H_2S containing excess water and ammonia," vol. 223, pp. 215–224, 2002.

[20] I. E. Wachs and B. M. Weckhuysen, "Structure and reactivity of surface vanadium oxide species on oxide supports," *Appl. Catal. A Gen.*, vol. 157, no. 1–2, pp. 67–90, 1997.

[21] V. Palma and D. Barba, "Low temperature catalytic oxidation of H_2S over V_2O_5 /CeO_2 catalysts," *Int. J. Hydrogen Energy*, vol. 39, pp. 21524–21530, 2014.

[22] M. Y. Shin, D. W. Park, and J. S. Chung, "Vanadium-containing catalysts for the selective oxidation of H_2S to elemental sulfur in the presence of excess water," *Catal. Today*, vol. 63, no. 2–4, pp. 405–411, 2000.

[23] M. D. Soriano, A. Vidal-Moya, E. Rodríguez-Castellón, F. V Melo, M. T. Blasco, and J. M. López Nieto, "Partial oxidation of hydrogen sulfide to sulfur over vanadium oxides bronzes," *Catal. Today*, vol. 259, no. 1, pp. 237–244, 2015.

[24] S. Yasyerli, G. Dogu, I. Ar, and T. Dogu, "Dynamic analysis of removal and selective oxidation of H_2S to elemental sulfur over Cu-V and Cu-V-Mo mixed oxides in a fixed bed reactor," *Chem. Eng. Sci.*, vol. 59, no. 19, pp. 4001–4009, 2004.

[25] K. T. Li and C. H. Huang, "Selective oxidation of hydrogen sulfide to sulfur over $LaVO_4$ catalyst: Promotional effect of antimony oxide addition," *Ind. Eng. Chem. Res.*, no. 45, pp. 7096–7100, 2006.

[26] K. T. Li and Z. H. Chi, "Selective oxidation of hydrogen sulfide on rare earth orthovanadates and magnesium vanadates," *Appl. Catal. A Gen.*, vol. 206, pp. 197–203, 2001.

[27] J. H. Uhm, Y. Shin, J. Zhidong, and J. S. Chung, "Selective oxidation of H_2S to elemental sulfur over chromium oxide catalysts," *Appl. Catal. B Environ.*, vol. 22, pp. 293–303, 1999.

[28] B. M. Reddy, M. Vijay Kumar, E. P. Reddy, and S. Mehdi, "Dispersion and thermal stability of vanadium oxide catalysts supported on titania-alumina binary oxide," *Catal. Letters*, vol. 36, pp. 187–193, 1996.

[29] R. J. A. M. Terorde, P. J. Van Den Brink, L. M. Visser, A. J. Van Dillen, and J. W. Geus, "Selective oxidation of hydrogen sulfide to elemental sulfur using iron oxide catalysts on various supports," *Catal. Today Elsevier Sci. Publ. B.V*, vol. 17, pp. 217–224, 1993.

[30] E. Laperdrix *et al.*, "Selective Oxidation of H_2S over CuO/Al_2O_3 : Identification and Role of the Sulfurated Species formed on the Catalyst during the Reaction," *J. Catal.*, vol. 189, pp. 63–69, 2000.

[31] A. Primavera, A. Trovarelli, P. Andreussi, and G. Dolcetti, "The effect of water in the low-temperature catalytic oxidation of hydrogen sulfide to sulfur over activated carbon," *Appl. Catal. A Gen.*, vol. 173, no. 2, pp. 185–192, 1998.

[32] S. Bashkova, F. S. Baker, X. Wu, T. R. Armstrong, and V. Schwartz, "Activated carbon catalyst for selective oxidation of hydrogen sulphide: On the influence of pore structure, surface characteristics, and catalytically-active nitrogen," *Carbon N. Y.*, vol. 45, no. 6, pp. 1354–1363, 2007.

[33] J. Klein and K.-D. Henning, "Catalytic oxidation of hydrogen sulphide on activated carbons," *Fuel*, vol. 63, no. 8, pp. 1064–1067, 1984.

[34] H. H. Kristoffersen, H. L. Neilson, S. K. Buratto, and H. Metiu, "Stability of V_2O_5 supported on titania in the presence of water, bulk oxygen vacancies, and adsorbed Oxygen Atoms," *J. Phys. Chem. C*, vol. 121, no. 15, pp. 8444–8451, 2017.

[35] M. Young, C. Mo, D. Won, and J. Shik, "Selective oxidation of H_2S to elemental sulfur over VOx/SiO_2 and V_2O_5 catalysts," *Appl. Catal. A Gen.*, vol. 211, pp. 213–225, 2001.

[36] N. Keller, C. Pham-Huu, C. Estournes, and M. J. Ledoux, "Low-temperature selective oxidation of hydrogen sulfide into elemental sulfur on a NiS_2 /SiC catalyst," *Catal. Letters*, vol. 61, pp. 151–155, 1999.

[37] N. Keller, C. Pham-Huu, C. Estournès, and M. J. Ledoux, "Low temperature use of SiC-supported NiS_2 -based catalysts for selective H_2S oxidation Role of SiC surface heterogeneity and nature of the active phase," *Appl. Catal. A Gen.*, vol. 234, pp. 191–205, 2002.

[38] B. G. Kim, W. D. Ju, I. Kim, H. C. Woo, and D. W. Park, "Performance of vanadium-molybdenum mixed oxide catalysts in selective oxidation of hydrogen sulfide containing excess water and ammonia," in *Solid State Ionics*, 2004, pp. 135–136.

[39] Z. Dudzik and M. Ziólek, "The specific catalytic activity of sodium faujasites in H_2S

oxidation," *J. Catal.*, vol. 51, no. 3, pp. 345–354, 1978.

[40]	G. C. Bond and S. F. Tahir, "Vanadium oxide monolayer catalysts Preparation, characterization and catalytic activity," *Applied Catalysis*, vol. 71, no. 1. pp. 1–31, 1991.

[41]	A. Khodakov, B. Olthof, A. T. Bell, and E. Iglesia, "Structure and catalytic properties of supported vanadium oxides: Support effects on oxidative dehydrogenation reactions," *J. Catal.*, vol. 181, no. 2, pp. 205–216, 1999.

[42]	V. Kovalskii and I. Zilberberg, "Effect of support on the vanadyl oxygen abstraction in supported vanadia," *Mater. Sci.*, pp. 1–21, 2018.

[43]	Z. Guo, B. Liu, Q. Zhang, W. Deng, Y. Wang, and Y. Yang, "Recent advances in heterogeneous selective oxidation catalysis for sustainable chemistry," *Chem. Soc. Rev.*, vol. 43, no. 10, pp. 3480–3524, 2014.

[44]	R. Schlögl, "Selective Oxidation: From a Still Immature Technology to the Roots of Catalysis Science," *Top. Catal.*, vol. 59, no. 17–18, pp. 1461–1476, 2016.

[45]	F. Roozeboom, P. J. Gellings, and J. Medema, "Vanadium Oxide Monolayer Catalysts," *Zeitschrift fur Phys. Chemie*, vol. 111, no. 2, pp. 215–224, 1978.

[46]	F. Roozeboom, T. Fransen, P. Mars, and P. J. Gellings, "Vanadium oxide monolayer catalysts. I. Preparation, characterization, and thermal stability," *ZAAC - J. Inorg. Gen. Chem.*, vol. 449, no. 1, pp. 25–40, 1979.

[47]	G. C. Bond, J. P. Zurita, and S. Flamerz, "Structure and reactivity of titania-supported oxides. Part 2: characterisation of various vanadium oxide on titania catalysts by x-ray photoelectron spectroscopy," *Appl. Catal.*, vol. 27, no. 2, pp. 353–362, 1986.

[48]	T. Machej, J. Haber, A. M. Turek, and I. E. Wachs, "Monolayer V_2O_5/TiO_2 and MoO_3/TiO_2 catalysts prepared by different methods," *Appl. Catal.*, vol. 70, no. 1, pp. 115–128, 1991.

[49]	P. Eversfield, T. Lange, M. Hunger, and E. Klemm, "Selective oxidation of o-xylene to phthalic anhydride on tungsten, tin, and potassium promoted VOx on TiO_2 monolayer catalysts," *Catal. Today*, 2018.

[50]	A. Löfberg, T. Giornelli, S. Paul, and E. Bordes-Richard, "Catalytic coatings for structured supports and reactors: VOx/TiO_2 catalyst coated on stainless steel in the oxidative dehydrogenation of propane," *Appl. Catal. A Gen.*, vol. 391, no. 1–2, pp. 43–51, 2011.

[51]	T. Giornelli, A. Löfberg, and E. Bordes-Richard, "Preparation and characterization of VOx/TiO_2 catalytic coatings on stainless steel plates for structured catalytic reactors," *Appl. Catal. A Gen.*, vol. 305, no. 2, pp. 197–203, 2006.

[52]	S. Surnev, M. G. Ramsey, and F. P. Netzer, "Vanadium oxide surface studies," *Progress in Surface Science*. pp. 73, 4–8, 117–165.

[53] K.-T. Li, M.-Y. Huang, and W.-D. Cheng, "Vanadium-Based Mixed-Oxide Catalysts for Selective Oxidation of Hydrogen Sulfide to Sulfur," *Ind. Eng. Chem. Res.*, vol. 35, pp. 621–626, 1996.

[54] C. L. and M. D. Ben W.-L. Jang, Roger Gläser, "Selective catalytic oxidation of H_2S to elemental sulfur over V_2O_5/Zr-pillared montmorillonite clay," *Energy Environ. Sci.*, vol. 3, pp. 302–310, 2009.

[55] N. Bahlawane and D. Lenoble, "Vanadium oxide compounds: Structure, properties, and growth from the gas phase," *Chemical Vapor Deposition*, vol. 20, no. 7–9. pp. 299–311, 2014.

[56] B. Grzybowska-Świerkosz, "Vanadia-titania catalysts for oxidation of o-xylene and other hydrocarbons," *Appl. Catal. A Gen.*, vol. 157, p. 263.310, 1997.

[57] M. O. Guerrero-Pérez, "Supported, bulk and bulk-supported vanadium oxide catalysts: A short review with an historical perspective," *Catal. Today*, vol. 285, pp. 226–233, 2017.

[58] I. E. Wachs, R. Y. Saleh, S. S. Chan, and C. C. Chersich, "The interaction of vanadium pentoxide with titania (anatase): Part I. Effect on o-xylene oxidation to phthalic anhydride," *Appl. Catal.*, vol. 15, pp. 339–352, 1985.

[59] M. N. Colpaert, P. Clauws, L. Flermans, and J. Vennik, "Thermal and low energy electron bombardment indiced oxygen loss of LOSS OF V_2O_5 single crystal : single crystals: transition into v_6o_{13}," vol. 36, pp. 513–525, 1973.

[60] T. Giornelli, A. Löfberg, and E. Bordes-Richard, "Grafting of VOx/TiO_2 catalyst on anodized aluminum plates for structured catalytic reactors," *Thin Solid Films*, vol. 479, no. 1–2, pp. 64–72, 2005.

[61] J. P. Holgado *et al.*, "Operando XAS and Raman study on the structure of a supported vanadium oxide catalyst during the oxidation of H_2S to sulphur," *Catal. Today*, vol. 155, no. 3–4, pp. 296–301, 2010.

[62] B. M. Weckhuysen and D. E. Keller, "Chemistry, spectroscopy and the role of supported vanadium oxides in heterogeneous catalysis," *Catal. Today*, vol. 78, no. 1–4 SPEC., pp. 25–46, 2003.

[63] B. G. Kim, D. W. Park, I. Kim, and H. C. Woo, "Selective oxidation of hydrogen sulfide over mixture catalysts of V-Sb-O and Bi2O3," *Catal. Today*, vol. 87, no. 1–4, pp. 11–17, 2003.

[64] H. Bin Fang, J. T. Zhao, Y. T. Fang, J. J. Huang, and Y. Wang, "Selective oxidation of hydrogen sulfide to sulfur over activated carbon-supported metal oxides," in *Fuel*, 2013, pp. 143–148.

[65] D. H. Kang, M. Il Kim, and D. W. Park, "Selective oxidation of H_2S to sulfur over CeO_2-TiO_2 catalyst," *Korean J. Chem. Eng.*, vol. 33, no. 3, pp. 838–843, 2016.

[66]   S. W. Chun, J. Y. Jang, D. W. Park, H. C. Woo, and J. S. Chung, "Selective oxidation of H $_2$S to elemental sulfur over TiO 2 /SiO 2 catalysts," vol. 16, pp. 235–243, 1998.

[67]   D. Wass *et al.*, "Contributions of Inorganic Chemistry to Energy Research Design , synthesis and characterization of vanadia-doped iron-oxide pillared," *Dalt. Trans*, vol. 40, no. 15, pp. 3938–3945, 2011.

[68]   T. Mattisson *et al.*, "Chemical-looping technologies using circulating fluidized bed systems: Status of development," *Fuel Process. Technol.*, vol. 172, no. June 2017, pp. 1–12, 2018.

[69]   Z. Guo, B. Liu, Q. Zhang, W. Deng, Y. Wang, and Y. Yang, "Recent advances in heterogeneous selective oxidation catalysis for sustainable chemistry," *Chem. Soc. Rev. Chem. Soc. Rev*, vol. 3480, no. 43, pp. 3480–3524, 2014.

[70]   A. Corma and L. Sauvanaud, "FCC testing at bench scale : New units , new processes , new feeds," *Catal. Today*, vol. 218–219, pp. 107–114, 2013.

[71]   J. Herguido, M. Mene, and J. Santamarı, "Oxidative Dehydrogenation of n -Butane in a Two-Zone Fluidized-Bed Reactor," pp. 90–97, 1999.

[72]   A. Löfberg, J. Guerrero-caballero, T. Kane, A. Rubbens, and L. Jalowiecki-duhamel, "Ni/CeO$_2$ based catalysts as oxygen vectors for the chemical looping dry reforming of methane for syngas production," "*Applied Catal. B, Environ.*, pp. 1–38, 2017.

[73]   R. M. Contractor *et al.*, "Butane oxidation to maleic anhydride over vanadium phosphate catalysts," *Catal. Today*, vol. 1, no. 1–2, pp. 49–58, 1987.

[74]   E. Bordes and R. M. Contractor, "Adaptation of the microscopic properties of redox catalysts to the type of gas-solid reactor," *Top. Catal.*, vol. 3, no. 3–4, pp. 365–375, 1996.

[75]   R. M. Contractor, H. S. Horowitz, G. M. Sisler, and E. Bordes, "The effects of steam on n-butane oxidation over VPO as studied in a riser reactor," *Catal. Today*, vol. 37, no. 1, pp. 51–57, 1997.

[76]   R. Ferna, A. Vega, and F. V Dı, "Applied Catalysis A : General Partial oxidation of n-butane to maleic anhydride over VPO in a simulated circulating fluidized bed reactor," vol. 376, pp. 76–82, 2010.

[77]   J. Gascón, C. Téllez, J. Herguido, and M. Menéndez, "Fluidized bed reactors with two-zones for maleic anhydride production: Different configurations and effect of scale," *Ind. Eng. Chem. Res.*, vol. 44, no. 24, pp. 8945–8951, 2005.

[78]   M. L. Pacheco *et al.*, "MoO$_3$ / MgO as a catalyst in the oxidative dehydrogenation of n -butane in a two-zone fluidized bed reactor," vol. 61, pp. 101–107, 2000.

[79]   M. Y. Shin, D. W. Park, and J. S. Chung, "Development of vanadium-based mixed oxide catalysts for selective oxidation of H2S to sulfur," *Appl. Catal. B Environ.*, vol. 30, no. 3–

4, pp. 409–419, 2001.

[80] C. W. Bale *et al.*, "FactSage thermochemical software and databases - recent developments," *Calphad Comput. Coupling Phase Diagrams Thermochem.*, vol. 33, no. 2, pp. 295–311, 2009.

[81] Y. H. Kim and H. I. Lee, "Redox property of vanadium oxide and its behavior in catalytic oxidation," *Bull. Korean Chem. Soc.*, vol. 20, no. 12, pp. 1457–1463, 1999.

[82] S. Surnev, M. G. Ramsey, and F. P. Netzer, "Vanadium oxide surface studies," *Prog. Surf. Sci.*, vol. 73, no. 4–8, pp. 117–165, 2003.

[83] L. M. Cornaglia and E. a Lombardo, : "E XPS studies of the surface oxidation states on equilibrated catalysts," *Appl. Catal. A*, vol. 127, pp. 125–138, 1995.

[84] J. Mendialdua, R. Casanova, and Y. Barbaux, "XPS studies of V_2O_5, V_6O_{13}, VO_2 and V_2O_3," *J. Electron Spectros. Relat. Phenomena*, vol. 71, no. 3, pp. 249–261, 1995.

[85] M. C. Biesinger, L. W. M. Lau, A. R. Gerson, and R. S. C. Smart, "Resolving surface chemical states in XPS analysis of first row transition metals, oxides and hydroxides: Sc, Ti, V, Cu and Zn," *Appl. Surf. Sci.*, vol. 257, no. 3, pp. 887–898, 2010.

[86] B. Barbaray, J. P. Contour, and G. Mouvier, "Sulfur Dioxide Oxidation Over Atmospheric Photoelectron Spectra of Sulfur Dioxide Adsorbed on V_2O_5 and Carbon," *Atmos. Environ.*, vol. 11, pp. 351–356, 1977.

[87] Z. Luan, P. A. Meloni, R. S. Czernuszewicz, and L. Kevan, "Raman Spectroscopy of Vanadium Oxide Species Immobilized at Surface Titanium Centers of Mesoporous Titanosilicate TiMCM-41 Molecular Sieves," *J. Phys. Chem. B*, vol. 5647, no. 97, pp. 9046–9051, 1997.

[88] R. Nilsson, T. Lindblad, and A. Andersson, "Ammoxidation of propene over antimony-vanadium-oxide catalysts," *Catalysis Letters*, vol. 29, no. 3–4. pp. 409–420, 1994.

[89] F. Roozeboom, T. Fransen, P. Mars, and P. J. Gellings, "Vanadium oxide monolayer catalysts. I. Preparation, characterization, and thermal stability," *ZAAC - J. Inorg. Gen. Chem.*, vol. 449, no. 1, pp. 25–40, 1979.

[90] J. M. López Nieto and B. Solsona, *Gas phase heterogeneous partial oxidation reactions*. 2018.

[91] A. W. Potts, G. R. Morrison, L. Gregoratti, S. Gunther, M. Kiskinova, and M. Marsi, "Selective oxidation of surface grains in polycrystalline tin," *Chem. Phys. Lett.*, vol. 290, no. 4–6, pp. 304–310, 1998.

[92] E. P. Reddy and R. S. Varma, "Preparation , characterization, and activity of Al_2O_3 -supported V_2O_5 catalysts," vol. 221, pp. 93–101, 2004.

[93] S. Sadasivan, "Alcoholic solvent effect on silica synthesis—NMR and DLS investigation,"

J. Sol-Gel Sci. Technol., vol. 12, pp. 5–14, 1998.

[94]   G. C. Bond *et al.*, "Structure and reactivity of titania-supported oxides. Part 1: vanadium oxide on titania in the sub- and super-monolayer regions," *Appl. Catal.*, vol. 22, no. 2, pp. 361–378, 1986.

[95]   A. Klisińska, S. Loridant, B. Grzybowska, J. Stoch, and I. Gressel, "Effect of additives on properties of V_2O_5/SiO_2 and V_2O_5/MgO catalysts. II. Structure and physicochemical properties of the catalysts and their correlations with oxidative dehydrogenation of propane and ethane," *Appl. Catal. A Gen.*, vol. 309, no. 1, pp. 17–27, 2006.

[96]   X. Gu, J. Ge, H. Zhang, A. Auroux, and J. Shen, "Structural, redox and acid-base properties of V_2O_5/CeO_2 atalysts," *Thermochim. Acta*, vol. 451, no. 1–2, pp. 84–93, 2006.

[97]   Z. Lian, F. Liu, and H. He, "Effect of preparation methods on the activity of VO_x /CeO_2 catalysts for the selective catalytic reduction of NO_x with NH_3," *Catal. Sci. Technol.*, vol. 5, no. 1, pp. 389–396, 2015.

[98]   S. Yasyerli, G. Dogu, and T. Dogu, "Selective oxidation of H_2S to elemental sulfur over Ce-V mixed oxide and CeO_2 catalysts prepared by the complexation technique," *Catal. Today*, vol. 117, no. 1–3, pp. 271–278, 2006.

[99]   F. Roozeboom, M. C. Mittelmeijer-Hazeleger, J. A. Moulijn, J. Medema, V. H. J. De Beer, and P. J. Gellings, "Vanadium oxide monolayer catalysts. 3. A Raman spectroscopic and temperature-programmed reduction study of monolayer and crystal-type vanadia on various supports," *J. Phys. Chem.*, vol. 84, no. 21, pp. 2783–2791, 1980.

[100] S. A. Al-Ghamdi and H. I. De Lasa, "Propylene production via propane oxidative dehydrogenation over VOx/γ-Al_2O3catalyst," *Fuel*, vol. 128, pp. 120–140, 2014.

[101] L. G. Gerling, C. Voz, R. Alcubilla, and J. Puigdollers, "Origin of passivation in hole-selective transition metal oxides for crystalline silicon heterojunction solar cells," *J. Mater. Res.*, vol. 32, no. 2, pp. 260–268, 2017.

[102] P. A. Zhdan, A. P. Shepelin, Z. G. Osipova, and V. D. Sokolovskii, "The extent of charge localization on oxygen ions and catalytic activity on solid state oxides in allylic oxidation of propylene," *J. Catal.*, vol. 58, no. 1, pp. 8–14, 1979.

[103] R. P. Netterfield, P. J. Martin, C. G. Pacey, W. G. Sainty, D. R. McKenzie, and G. Auchterlonie, "Ion-assisted deposition of mixed TiO_2-SiO_2 films," *J. Appl. Phys.*, vol. 66, no. 4, pp. 1805–1809, 1989.

[104] J. Mendialdua, R. Casanova, and Y. Barbaux, "XPS studies of V_2O_5, V_6O_{13}, $VO_2$and V_2O_3," *J. Electron Spectros. Relat. Phenomena*, vol. 71, no. 3, pp. 249–261, 1995.

[105] M. V. Martínez-Huerta *et al.*, "Nature of the vanadia-ceria interface in V^{5+}/CeO_2 catalysts and its relevance for the solid-state reaction toward $CeVO_4$ and catalytic properties," *J. Catal.*, vol. 225, no. 1, pp. 240–248, 2004.

[106] A. Travert, O. V. Manoilova, A. A. Tsyganenko, F. Maugé, and J. C. Lavalley, "Effect of hydrogen sulfide and methanethiol adsorption on acidic properties of metal oxides: An infrared study," *J. Phys. Chem. B*, vol. 106, no. 6, pp. 1350–1362, 2002.

[107] M. Piumetti, D. Fino, and N. Russo, "Applied Catalysis B : Environmental Mesoporous manganese oxides prepared by solution combustion synthesis as catalysts for the total oxidation of VOCs," *"Applied Catal. B, Environ.*, vol. 163, pp. 277–287, 2015.

[108] G. T. Went, L. jen Leu, and A. T. Bell, "Quantitative structural analysis of dispersed vanadia species in TiO_2(anatase)-supported V_2O_5," *J. Catal.*, vol. 134, no. 2, pp. 479–491, 1992.

[109] M. D. Soriano, J. A. Cecilia, A. Natoli, J. Jiménez-Jiménez, J. M. López Nieto, and E. Rodríguez-Castellón, "Vanadium oxide supported on porous clay heterostructure for the partial oxidation of hydrogen sulphide to sulfur," *Catal. Today*, vol. 254, pp. 36–42, 2015.

[110] G. T. Went, S. Ted Oyama, and A. T. Bell, "Laser raman spectroscopy of supported vanadium oxide catalysts," *J. Phys. Chem.*, vol. 94, no. 10, pp. 4240–4246, 1990.

[111] M. Schraml-Marth, A. Wokaun, and A. Baiker, "Grafting of V_2O_5 monolayers onto TiO_2 from alkoxide precursors: A diffuse reflectance FTIR study," *J. Catal.*, vol. 124, no. 1, pp. 86–96, 1990.

[112] J. A. Moulijn, A. E. Van Diepen, and F. Kapteijn, "Catalyst deactivation: Is it predictable? What to do?," *Appl. Catal. A Gen.*, vol. 212, no. 1–2, pp. 3–16, 2001.

[113] T. N. Mashapa, J. D. Rademan, and M. J. J. Van Vuuren, "Catalytic performance and deactivation of precipitated iron catalyst for selective oxidation of hydrogen sulfide to elemental sulfur in the waste gas streams from coal gasification," *Ind. Eng. Chem. Res.*, vol. 46, no. 19, pp. 6338–6344, 2007.

[114] H. Tian, T. Simonyi, J. Poston, and R. Siriwardane, "Effect of hydrogen sulfide on chemical looping combustion of coal-derived synthesis gas over bentonite-supported metal-oxide oxygen carriers," *Ind. Eng. Chem. Res.*, vol. 48, no. 18, pp. 8418–8430, 2009.

[115] H. M. Tasdemir, S. Yasyerli, and N. Yasyerli, "Selective catalytic oxidation of H_2S to elemental sulfur over titanium based Ti-Fe, Ti-Cr and Ti-Zr catalysts," *Int. J. Hydrogen Energy*, vol. 40, no. 32, pp. 9989–10001, 2015.

[116] E. Hryha, E. Rutqvist, and L. Nyborg, "Stoichiometric vanadium oxides studied by XPS," *Surf. Interface Anal.*, vol. 44, no. 8, pp. 1022–1025, 2012.

[117] S. Tanaka, K. Mase, M. Nagasono, and M. Kamada, "Desorption of H ions from water chemisorbed on Si(100) by O 1s excitation - An Auger electron-photoion coincidence spectroscopy study," *Surf. Sci.*, vol. 390, no. 1–3, pp. 204–208, 1997.

[118] C. V. Loricera, M. C. Alvarez-Galvan, R. Guil-Lopez, A. A. Ismail, S. A. Al-Sayari, and J. L.

G. Fierro, "Structure and Reactivity of sol–gel V/SiO$_2$ Catalysts for the Direct Conversion of Methane to Formaldehyde," *Top. Catal.*, vol. 60, no. 15–16, pp. 1129–1139, 2017.

[119] L. D. Nguyen, S. Loridant, H. Launay, A. Pigamo, J. L. Dubois, and J. M. M. Millet, "Study of new catalysts based on vanadium oxide supported on mesoporous silica for the partial oxidation of methane to formaldehyde: Catalytic properties and reaction mechanism," *J. Catal.*, vol. 237, no. 1, pp. 38–48, 2006.

[120] Y. Cho, B. Hwang, D. Park, H. Woo, and J. Chung, "Containing Ammonia and Water," vol. 19, no. 4, pp. 611–616, 2002.

[121] B. G. Kim, W. D. Ju, I. Kim, H. C. Woo, and D. W. Park, "Performance of vanadium-molybdenum mixed oxide catalysts in selective oxidation of hydrogen sulfide containing excess water and ammonia," in *Solid State Ionics*, 2004.

[122] A. Primavera, A. Trovarelli, P. Andreussi, and G. Dolcetti, "The effect of water in the low-temperature catalytic oxidation of hydrogen sulfide to sulfur over activated carbon," *Appl. Catal. A Gen.*, vol. 173, no. 2, pp. 185–192, 1998.